

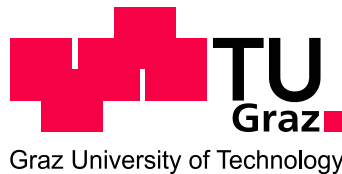
Gregor Toschkoff

Investigation of pharmaceutical tablet film coating processes using numerical simulations

DOCTORAL THESIS

For obtaining the academic degree of
Doktor der technischen Wissenschaften

Doctoral programme in Engineering Sciences
Diploma programme: Chemical and Process Engineering



Supervisor:

Univ.-Prof. Dipl.-Ing. Dr.techn. Johannes G. Khinast
Institute for Process- and Particle Technology

Graz, March 2014

“The more we learn about the world, and the deeper our learning, the more conscious, specific, and articulate will be our knowledge of what we do not know, our knowledge of our ignorance. For this, indeed, is the main source of our ignorance — the fact that our knowledge can be only finite, while our ignorance must necessarily be infinite.”

Sir Karl Popper *in* *Conjectures and Refutations: The Growth of Scientific Knowledge* (1963)

Abstract

In the pharmaceutical industry, coating of tablets is a common unit operation. In drum coating, the film is applied by spraying an film solution onto tablets moving in a rotating drum. The coating layer may fulfill different functions, from taste masking to modifying the release. One thing all tablets have in common: they will be taken by patients. In this light, it is clear that the coating has to have consistently high quality; this is ensured by strict regulations.

In order to fulfill this requirement, it is important to understand the seemingly simple process in great detail. In the literature, this strife for understanding manifests in numerous experiment studies that have been performed. Further, more recently there was a trend to extended and complemented this by the application of modern numerical simulations.

In this work, a number of approaches and simulation tools were used to study the coating process from different perspectives. The tool of choice depends on which aspects are important in the specific process. The main parts are: modeling of the air flow and spray droplets inside the drum using Computational Fluid Dynamics (CFD), and investigation of the tablet movement behavior and description of the actual spraying using Discrete Element Method (DEM). It is aimed to capture the whole coating process as closely as possible. This is done by e.g. using real geometries and processes provided by industrial partners, applying measured model parameters where possible, and using non-spherical particles based on the true biconvex tablet shape.

The results are thoroughly presented and compared to findings in literature inside the respective fields. Findings are shown at different detail levels, going from an overview of all variations to in-depth considerations. In other words, throughout this work it was aimed to contrast the global with the local view, such as highly resolved DEM results in comparison to global analytical considerations.

In sum, the presented work contains a detailed *in silico* investigation of tablet coating. A deeper mechanistic understanding of the underlying principles could be gathered, providing a valuable tool for the improvement of existing processes and especially the design of novel approaches. While tablet coating is treated here, most of it applies on arbitrary particle coating processes.

Zusammenfassung

Das Beschichten von Tabletten (und Partikeln allgemein) ist ein häufiger Produktionsschritt in der pharmazeutischen Industrie. Bei Tabletten wird der umschließende Film üblicherweise durch Besprühen in einer rotierenden Trommel erzeugt („drum coating“). Dieser Film erfüllt verschiedene Aufgaben, von der Geschmacksmaskierung bis Änderung der Wirkstoff-Freisetzung. Eines gilt jedoch immer: die Tablette ist dazu gedacht, von einem Patienten eingenommen zu werden. Daher unterliegt der Film sehr hohen Qualitätsansprüchen und entsprechend strikten Regulierungen.

Um diesen Ansprüche gerecht zu werden, muss der scheinbar einfache Prozess tiefgreifend verstanden werden. Dazu finden sich in der Literatur eine Vielzahl von experimentellen Untersuchungen. In den letzten Jahren gab es darüber hinaus einen starken Trend, diese Untersuchungen mit numerischen Simulationen zu erweitern.

In dieser Arbeit wurden mehrere Ansätze und Simulationswerkzeuge kombiniert, um den Beschichtungsprozess aus verschiedenen Perspektiven zu untersuchen. Die Hauptteile sind: Beschreibung des Luftstroms und des Sprühnebels in der Trommel mittels Computational Fluid Dynamics (CFD), und Untersuchung von Tablettenbewegung mit der Discrete Element Method (DEM). Für letztere wurden zur Beschreibung des Sprays neue Methoden implementiert. Die Bestrebung ist, den gesamten Prozess so nah an der Realität wie möglich abzubilden. Es wurden reale Geometrien und Prozessbedingungen verwendet, und die nötigen Modellparameter stammen soweit möglich aus direkten Messungen und Kalibrationen. Weiteres werden nicht-sphärische Partikel basierend auf der tatsächlichen bikonvexen Tablettenform verwendet.

Die Resultate werden gründlich präsentiert und mit den Erkenntnissen der Literatur im jeweiligen Feld in Bezug gesetzt. Ergebnisse werden in verschiedene Detailstufen betrachtet, von globalen Überblicken über Parametereinflüsse zu tiefeschürfenden Detailbetrachtungen.

Zusammenfassend erstrebt diese Arbeit, den gesamten Tablettenbeschichtungsprozess *in silico* zu erfassen und ein mechanistisches Verständnis zu generieren. Das Resultat ist ein umfangreiches Werkzeug zur Verbesserung existierender Prozesse und zur optimalen Erstellung neuer Herangehensweisen. Während hier vor allem Tabletten behandelt wird, gelten die meisten Ergebnisse für Beschichtungsprozesse beliebiger Partikel.

Table of contents

Chapter A: Introduction	13
Chapter B: Background	17
B-1 History of tablet coating (Cole et al., 2002)	17
B-2 Relevant regulatory surroundings	18
B-3 Simulation methods	19
B-4 Experimental methods	21
B-5 Considerations of the decrease of RSD over time	21
Chapter C: Mathematical Modeling of the Coating Process	27
C-1 Abstract	27
C-2 Introduction	27
C-3 Drum Coating	29
C-4 Fluidized Bed Coating	30
C-5 Application of Modeling Approaches	33
C-6 Modeling Approaches Overview	35
C-7 Analytical Modeling	36
C-8 Computational Fluid Dynamics (CFD)	46
C-9 Discrete Element Method (DEM)	47
C-10 CFD-DEM Coupling	60
C-11 Monte Carlo Method	60
C-12 Population Balance	63
C-13 Summary	65
C-14 Notation	66

Chapter D: Detailed Analysis of Air Flow and Spray Loss in a Pharmaceutical Coating Process	69
D-1 Abstract	69
D-2 Introduction	69
D-3 Materials and Methods	72
D-4 Numerical Model	76
D-5 Results and Discussion	85
D-6 Conclusions	98
D-7 Notation	99
D-8 Latin Symbols	99
Chapter E: Effect of tablet coating parameters: combining non-destructive measurements and dissolution testing	101
E-1 Abstract	101
E-2 Introduction	102
E-3 Materials and methods	104
E-4 Measurement methods	107
E-5 Results and discussion	113
E-6 Conclusion	124
Chapter F: Spray Models for Discrete Element Simulations of Particle Coating Processes	127
F-1 Abstract	127
F-2 Introduction	127
F-3 Materials and Methods	130
F-4 Results and Discussion	146
F-5 Conclusion	160

Chapter G: Design-of-Experiment based DEM simulation of an active tablet coating process.	163
G-1 Abstract	163
G-2 Introduction	163
G-3 Methods	166
G-4 Results & Discussion	174
G-5 Conclusion	188
Chapter H: Conclusion	191
Chapter I: References	193
Chapter J: List of publications	209
J-1 Publications in Peer-reviewed journals	209
J-2 Conference contributions	210
Chapter K: List of figures and tables	213
K-1 Figure captions	213
K-2 Table captions	217

Chapter A: Introduction

Among all dosage forms used to administer a drug to a patient, the tablet is still one of the most wide-spread ones, and can be considered the most typical form of drugs encountered in daily life. It falls into the class of solid oral dosage form, with all the advantages and disadvantages that come with this administration route. The international pharmacopoeia states the following formal definition:

“[...] Tablets are solid dosage forms usually obtained by single or multiple compression of powders or granules. In certain cases tablets may be obtained by moulding or extrusion techniques. They are uncoated or coated.

Tablets are normally right circular solid cylinders, the end surfaces of which are flat or convex and the edges of which may be bevelled. They may have lines or break-marks (scoring), symbols or other markings. [...]”¹

While maybe not many patients could describe tablets as elaborate as above, most patients have a clear picture of tablets in mind. This could be one of the biggest advantages of tablets: they have a high level of patient’s acceptance. They are well-known, straight-forward to take (if no problems with swallowing are present), and easy to store and transport. Further, the non-invasive route through the gastro-intestinal (GI) tract lessens the demands for sterility compared to parenteral forms such as infusions.

Passing through the GI tract is at the same time source of disadvantages. The active pharmaceutical ingredients (APIs) of the tablet run the risk to be subjected to a rough environment, and before reaching systemic circulation the API has to pass through gut walls and liver where it may be altered or inactivated (first pass effect). Other possible disadvantages are that the release profile or release location is not as intended, or that the patient’s acceptance to take the tablet is lessened by its appearance, smell, or taste.

¹ World Health Organization, *The International Pharmacopoeia forth edition, 2013*. Monographs: Dosage forms: General monographs: Tablets. <http://apps.who.int/phint/en/p/docf/>

To eliminate or alleviate many of the disadvantages, and to introduce new features, many tablet cores are coated with a functional layer. The functions of the coating include (Cole, Hogan, Aulton, & Twitchell, 2002)

- Masking of an unpleasant taste or odor of substances in the core (most likely the API)
- Protection from environmental influences such as light and oxygen, to improve stability
- Increase the elegance, for example by giving a glossy finish or by applying a color. This also helps to discern between different tablets.
- Reduce friction for a faster packing process
- Modify the drug release profile, for example in enteric coating (a coating that is resistant to gastric juice, but dissolves in the lower pH values of the small intestine) or generally any form of sustained release coating.
- Separate incompatible APIs or other substances by adding one or more of them with the coating (rather than having it in the core).

Pharmaceutical coating can be roughly divided into three main groups (Cole et al., 2002): sugar coating, film coating in drums, and film coating in fluid bed. Strictly speaking, the coating processes investigated in this work all fall into the second group, film coating of tablets. However, most findings are equally applicable for sugar coating, and to some extent also for pellet coating.

There is one thing that all coating processes have in common: at the end of the day, the resulting product will be consumed by patients. That is, persons that are in need of a certain medication, and further are likely to be in a delicate state of health. A coated tablet that does not work as intended could have serious impact on patient health and safety. Therefore, the coated tablets have to consistently fulfill the criteria for their critical quality attributes. To guarantee this, strict governmental regulations are in place (see section A-1.2 for further information).

To comply with this demand for consistent high quality, a very detailed understanding of the process is needed. To this end, a large number of experimental work has been done (e.g. (Brock, Zeitler, Funke, Knop, & Kleinebudde, 2012; Dubey et al., 2012; Just, Toschkoff, Funke, Djuric, Khinast, et al., 2013; Mauritz, Morrisby, Hutton, Legge, & Kaminski, 2010; Muliadi & Sojka,

2010; Shen, 2011)). In recent years, computer simulations have established themselves as an additional tool for the investigation of coating. It should be noted that simulations are most useful if they are not seen as a substitute for experiment, but as a complement. Also, simulation approaches normally rely on experiments for parameterization and validation. In the pharmaceutical industry, their application is still relatively new, and often a considerable initial effort is needed. However, once simulations are set up, they bring a number of benefits to the table. For example, even if they do not describe 100% of reality due to model assumptions, they are valuable to reduce the number of (often resource-intensive) experiments. A large amount of data is easily accessible, and many characteristics that are readily available in the simulation would be hard or even impossible to measure. A further advantage is that single parameters can be changed to (almost) arbitrary values, without unwanted interactions. To give an example, one could simulate a coating process with rotation speeds from zero to thousand revolutions per minute, just to see at which point the resulting tablet movement starts to be prohibitive, without thinking about the technical limitations of the apparatus, damage to tablets, or explanations to superiors on why the new coating drum already is in somewhat less than prime condition. For this matter, one could as easily describe a coating process performed on the moon.

In this work, computer simulation is used to study different coating processes, at some points also complemented with experiments. The mainly applied numerical methods are computational fluid dynamics (CFD) and discrete element method (DEM). Depending on the process, different quality criteria, such as uniformity of coating or dissolution characteristics, are important; this is explained at the corresponding positions in the single chapters.

The work is organized as follows. First, background on the surrounding pharmaceutical and regulatory landscape, as well as the simulation methods is given. Second, investigations of different aspects and processes are presented. This second part is the largest, and presented in the form of manuscripts, both already published and in the process of submission. Finally, a conclusion is given.

The manuscripts included in the second part are:

- Toschkoff, G., & Khinast, J. G. (2013). Mathematical modeling of the coating process. *Int J Pharm.*

- Toschkoff, G., Suzzi, D., Tritthart, W., Reiter, F., Schlingmann, M., & Khinast, J. G. (2012). Detailed Analysis of Air Flow and Spray Loss in a Pharmaceutical Coating Process. *Aiche J.*, 58(2), 399–411.
- Toschkoff, G., Schinwald, C., Markl, D., Koller, D. M., Scheideler, M., Leitner, M., & Khinast, J. G. (2013). Effect of Tablet Coating Parameters: Combining Non-Destructive Measurements and Dissolution Testing. Submitted to *Eur J Pharm Biopharm.*
- Toschkoff, G., Just, S., Funke, A., Djuric, D., Knop, K., Kleinebudde, P., Scharrer, G., Khinast, J. G. (2013). Spray models for discrete element simulations of particle coating processes. *Chem Eng Sci*, 101, 603–614.
- Toschkoff, G., Just, S., Funke, A., Djuric, D., Knop, K., Kleinebudde, P., Scharrer, G., Khinast, J. G. (2014). Design-of-Experiment based DEM simulation of an active tablet coating process, in preparation.

A complete list publications connected to this work (i.e., where the author of this work contributed as main author or co-author) is given in Chapter I: .

A-1 Background

A-1.1 History of tablet coating (Cole et al., 2002)

The oldest form of pharmaceutical coating is sugar coating, which was already well-known in the confectionery industry before its application in the pharmaceutical industry. Most commonly, open bowl-shaped copper pans were used (today, stainless steel is the material of choice). The process generally was strongly depending on the skill and knowledge of individual operators, and could take days. In the beginning, batch sizes were (150 – 200) kg. Later, newly developed, improved pans such as the Pelligrini pan raised the limit to (500 – 600) kg per batch. The coating liquid was applied by hand using ladles, and the temperature and amount of drying air were critical for the outcome. It is understandable that sugar coating was more and more rarely applied due to the high dependence on operator skill, and also due to the difficult identification of the product. If a clear identification is needed, one has to resort to individually printing the tablets, which is desirable to avoid. Other options of coating were investigated; however, with the advent of film coating those routes lost attractiveness.

The first commercially available film coated tablet was produced by Abbott in 1954. The basis for film coating was laid by the development of new materials, such as the cellulose derivatives. Among them, the most important was hydroxypropyl methylcellulose (HPMC), which was applied using organic solvents at a concentration of (2 – 4) %w/v and molecular weight fractions relating to a viscosity of about 50 mPas. Abbott chose a fluidized bed (Wurster) coating process, which was further developed other companies, with plants reaching capacities of 1000 million tablets per year.

However, with a trend towards aqueous film coating (as opposed to organic coating) and side-vented coating pans, fluidized bed coating of tablets is seldom seen nowadays. Between 1954 and 1975, organic solvents were still widely in use. The alternative of a HPMC of lower molecular weight and about (3 – 15) mPas was not applied because organic solvents were cheap, and it was believed that the lower viscosity coating liquid would produce weaker films. This has changed drastically due to a number of reasons, most notably a steep increase in the cost of organic solvents, stricter regulations due to environmental concerns connected with the used organic liquids, and the development of new

coating systems. In addition, aqueous coating is not flammable, making it less hazardous to work with.

When aqueous coating started to prevail, it was mostly done in the existing equipment, which was to a large part pans open at the front (and rear), with the drying air moving inside the coating drum. A huge quality improvement was achieved by the introduction of perforated pans (where the air stream goes through the tablet bed) that are used nowadays.

A-1.2 Relevant regulatory surroundings

To guarantee the production of secure and effective drugs, the pharmaceutical industry is heavily regulated. It is outside the scope of this work to describe the frameworks and guidelines; descriptions are limited to those rules that directly pertain to the research. In the case of the tablet coating process, two central critical quality attributes are of central interest here: inter-tablet uniformity and intra-tablet uniformity. In the following, the corresponding regulatory surrounding is depicted.

A-1.2.1 Inter-tablet uniformity

Generally, it is desirable to minimize the variation of coating mass between tablets of a batch. In some applications, a relatively high variation may not be a reason to reject the produced film tablets, as long as the desired function of the film is fulfilled; in others it is crucial. In this work, a large part of the investigations are related to an active coating process, where the coating contains an API. The variation of API is of course subject to strict regulations, and for active coating this directly relates to the variation of coating mass.

In effect, this means that the accepted amount of variation in coating mass here is regulated by monograph 905 “Uniformity of dosage forms” of the U.S. Pharmacopoeia, harmonized with the European and Japanese counterparts (Directorate for the Quality of Medicines of the Council of Europe, 2011; Ministry of Health Labour and Welfare, 2011; U. S. Pharmacopoeial Convention, 2011b). It discriminates between content uniformity and weight variation criteria; here, the content uniformity applies. To determine whether a batch has passed or not, a sample of size n_{sample} is drawn. The API content of the individual tablets is determined, and an acceptance value AV is calculated according to:

$$AV = |M - \bar{X}| + ks, \quad (1)$$

where X is the sample mean of the individual contents expressed as a percentage of the label claim. M is a reference value described below. s is the sample standard deviation again in terms of percentage of the label claim. k is the acceptability constant, with a value of $k = 2.4$ for $n_{\text{sample}} = 10$ and $k = 2$ for $n_{\text{sample}} = 30$. The reference value M depends on how far the mean deviates from the label claim. In active coating, this basically depends on whether the spraying is stopped after the correct time. The simulations, on the other hand, are set up such that the mean value over all tablets of a batch gives exactly the desired value. Therefore, for the sake of this work, it can be assumed that the reference value M is equal to X . The “sample” in simulations consists of all tables, but for a worst-case analysis, k is set to 2.4. With this, the equation above simplifies to

$$AV = 2.4 \times s \quad (2)$$

The acceptance value AV has to be below the maximum allowed acceptance value of 15.0, meaning that the sample standard deviation s has to be below 6.25 %.

A-1.2.2 Intra-tablet uniformity

A certain level of uniformity of the coating layer around a tablet (intra-tablet uniformity) is needed for many applications, but it gains importance when the coating has a protective function or serves for a controlled release. A common example is most likely enteric coating. Here, the coating layer protects the tablet from dissolution in the gastric environment. It has shown that even small areas of missing coating mean insufficient protection (cf. Chapter D:). Whether a coated tablet has the desired dissolution behavior or not is tested according to regulations in the pharmacopoeias, in the case of tablets especially using Apparatus 2 (U. S. Pharmacopoeial Convention, 2011a). From a statistical point of view, the specific rules of this “USP 2” implement a complex dependency of the outcome on the coating quality of single tablets (Cox, Wells, Furman, Savage, & King, 1982). In any case, this necessitates that the corresponding coating process consistently yields tablets that have a minimum coating thickness all over the tablet.

A-1.3 Simulation methods

The largest part of this work is concerned with the application of computer simulations on the investigation of coating processes. Here, two main approaches

are applied: computational fluid dynamics (CFD) and discrete element method (DEM). Which one is chosen depends on the nature of the investigation.

A-1.3.1 Computational Fluid Dynamics

Computational fluid dynamics (CFD) is a method to simulate the flow of general fluids (that is, gasses or liquids). This applies to the air flow inside the coater including the movement of the spray inside said air, the drying of the spray, the impact of the spray on the tablet, and the formation of the film due to this. In all of this, the actual movement of the tablets is not included; the tablet bed has to be approximated in some form. Knowledge on the air flow is crucial if the drying air is in intense contact with the spray. This is especially true for non-perforated drums; one such process was treated in this work. In the case of a perforated drum and an arrangement of air inlet and outlet such that the drying air mostly goes through the tablet bed and does not interfere with the spray. Here, knowledge of the air stream is of lesser importance, and a CFD simulation was seen as less useful. In general, CFD is well known and routinely applied in many fields such as automotive, aeronautic, or chemical engineering. It is therefore not described in detail here.

A-1.3.2 Discrete Element Method

DEM simulation has little to no capability to include the air stream, but can capture the movement of the tablets. In short, properties such as the position and velocities of the tablets, are calculated and potentially saved for each single tablet during a certain time span. At this point, the simulated time span normally has to be less than the total process duration. Typical values are some minutes of simulated process versus a total duration of some hours. However, this is not as strict a limitation as it may seem: a few minutes of detailed knowledge yield enough material for in-depth considerations and meaningful predictions, as shown in Chapter F. A “basic” DEM simulation gives detailed data on the tablets, but misses one important component: the spray that applies the coating, and with it the “coating” part itself. One aim of this work was to develop means to include the spray in the framework of the DEM simulation. The results are presented in Chapter E: and applied throughout the work. The DEM is not as wide-spread and as well-known as CFD, but sees a steady increase in application, and the underlying principles can be considered common knowledge in this field. Therefore, for further details, it is referenced to the available literature, e.g. (Cundall & Strack, 1979; Ketterhagen, am Ende, & Hancock, 2009a; Toschkoff & Khinast, 2013; Yamane, Sato, Tanaka, & Tsuji, 1995).

A-1.3.3 Coupled CFD-DEM simulation

In this work, either CFD (description of fluid behavior without particles) or DEM (description of particle-particle interaction) is applied, which is reasonable for the processes given here. Other situations may necessitate to describe the interaction between particles and fluid as well. For this, in the last year approaches to couple CFD and DEM were developed, giving the ability to consider air stream and tablet movement, and its interaction, in one simulation (Deen, Annaland, der Hoef, & Kuipers, 2007; Jajcevic, Siegmann, Radeke, & Khinast, 2013). While the development quickly proceeds, coupled CFD-DEM simulation of drum tablet coating is still not a straight-forward application and subject to limitations. In the foreseeable future, this will change, but for the applications in this work, it did not promise much additional information, and was therefore not included in the scope of this work.

A-1.4 Experimental methods

While the majority of this work uses numerical methods, it should be mentioned here that one chapter (Chapter D:) treats experiments as well. Using a lab-scale coating drum, small batches of tablets are produced and investigated with respect to coating uniformity and dissolution, following the guidelines described in A-1.2.2 .

A-2 Considerations of the decrease of RSD over time

In literature, it is described that the standard deviation increases proportional to the square root of time. The mean coating mass increases linearly with time, meaning that the coefficient of variation of the coating mass ($c_{v,inter}$) decreases as the inverse of the square root of time:

$$c_{v,inter} \propto 1/\sqrt{t}. \quad (3)$$

To draw a picture of what the underlying mechanic of this behavior is, a simple statistical model of the coating process was set up using Matlab (The MathWorks, Inc., USA). It is based on the decomposition of the coating process into a unit coating phase that may be repeated, and a mixing phase.

When the coating process begins, the tablets are sprayed as they move down the tablet bed. To a large extent, those sprayed tablets move along the coating wall and re-emerge at the top again to roll down to the beginning of the spray zone again. Up to this point, the majority of tablet has no coating, while a number of tablets were in the spray zone once. This is defined as the unit coating phase. The

length of the first phase corresponds to the first peak in the bed cycle time, cf. section F-4.4 . After this point, the already coated tablets will visit the spray zone a second time, more or less repeating the behavior of the unit coating phase a second time. Without axial mixing, this pattern would repeat indefinitely, leading to a smaller part of heavily coated tablets that happened to start in the axial plane of a spray zone, and a larger part of uncoated tablets that were unlucky and started between two spray nozzles. With axial mixing, this coherent behavior is broken up, and after a coherence time span, a different, randomly chosen set of tablets experiences the unit coating.

This picture of the process was now represented by the statistical simulation. A schematic is given in Figure 1. The tablets are simply represented by a vector of length n_{tab} , where the number at position i gives the amount of coating of the i th tablet. The unit coating consists of increasing the value of the first n_{spray} tablets one after the other by one (this represents the coating mass). This is repeated n_{coh} times. After that, the first n_{spray} tablets have the same value for the coating. At this point, it is assumed that axial mixing becomes noticeable. To simulate this, the positions of the tablets are mixed semi-randomly in the following fashion. The tablets on positions 1 to $1+n_{\text{mix}}$ are randomly mixed. After that, the tablets $1+p$ to $1+p+n_{\text{mix}}$ are randomly mixed, and so on. Generally, the tablets in the interval $[1+(n_p-1)*p, n_p*p]$ are mixed, with $p < n_{\text{mix}}$, and n_p increased by one until the end of the vector is reached. Figuratively, the mixing region is pushed along the vector, shuffling the tablets as it moves along. In this way, tablets are randomly mixed especially with neighboring regions, but it is extremely unlikely for them to move over longer distances, such as is to be expected from the axial mixing.

After this mixing step, the spraying starts again; this is repeated until the desired runs (correlating to the desired coating time) is reached.

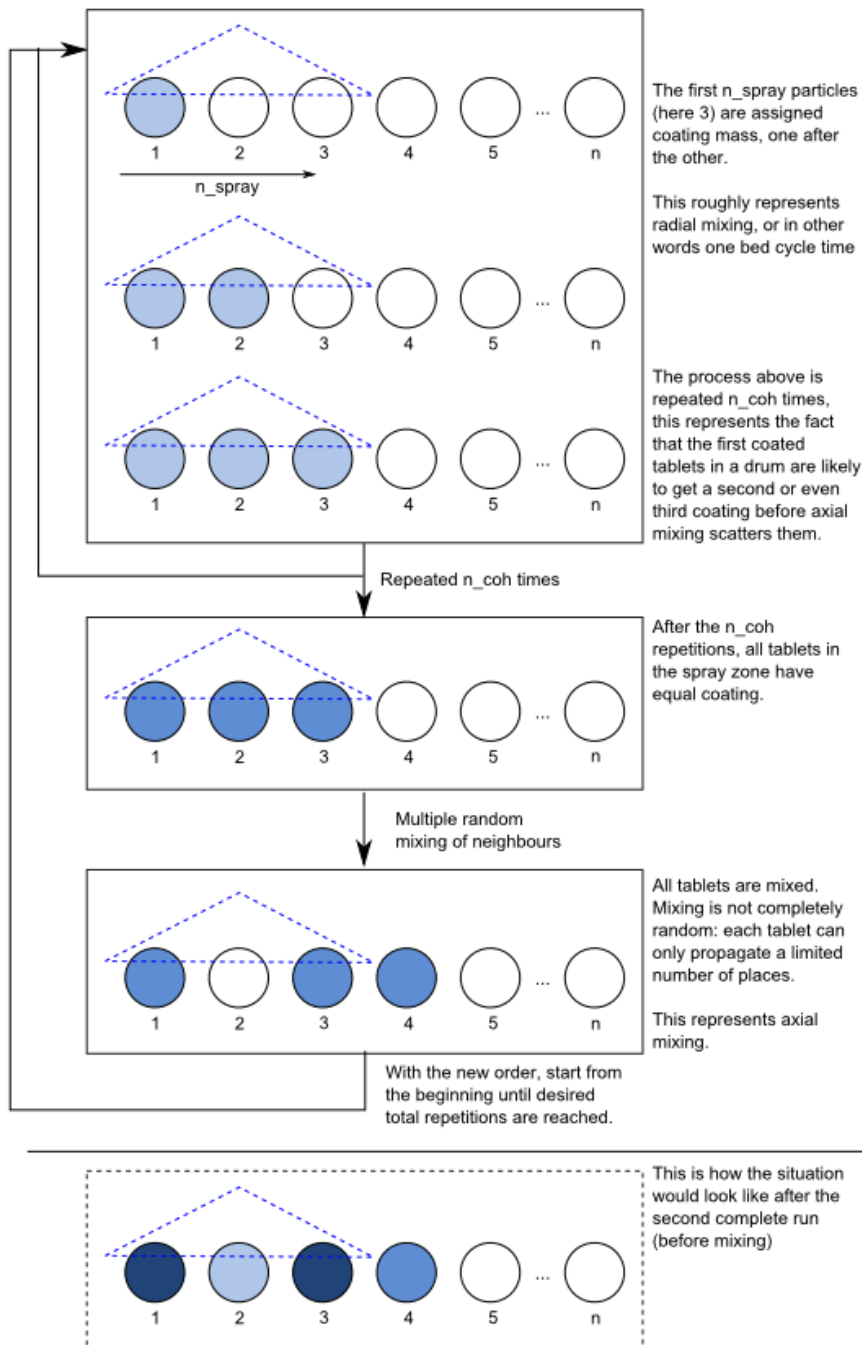


Figure 1: Schematic description of the representation of coating in a simplified statistical model based on consecutive single tablet coating and mixing.

During the whole process, the standard deviation (σ) and relative standard deviation (i.e., coefficient of variation $c_{v,inter}$) are calculated. Over the whole process, those values are saved at regular intervals; at the beginning, they are written out after each coating event of a single tablet in addition. The resulting curves are shown in Figure 2 ($c_{v,inter}$) and Figure 3 (σ). The additional curves denote the functional dependency on time (Eq. (3)) predicted in literature and also found throughout this work. On the left-hand side in both figures, the data for the whole process is shown. The data points agree well with the analytic curve. On the right hand side, each data point corresponds to a single additionally coated tablet. In Figure 2 (b) it can be seen that for the first seven tablets (up to a time of 1.5 s), the data points perfectly follow the $t^{-0.5}$ -law (dash-dotted red curve labelled t_{start}). The reason is that up to this point, successive tablets were coated without a tablet being coated twice. However, after the seventh coating, the same tablets are coated a second time, and the coefficient of variation almost keeps constant. After further seven coatings, in the settings used here the mixing step is performed, and c_v is decreasing again in the expected manner. The corresponding behavior is seen for the standard deviation (Figure 3).

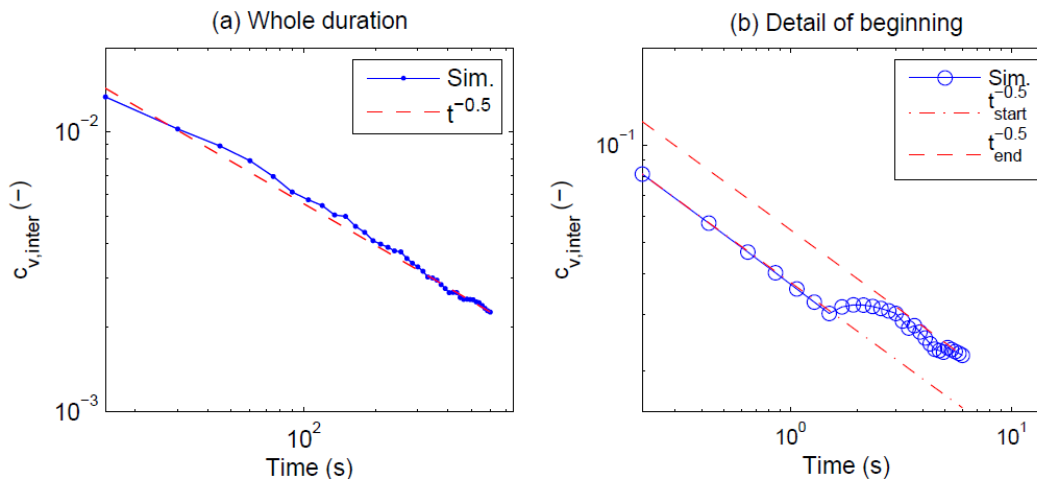


Figure 2: Decrease of the coefficient of variation of coating time over time, gathered from statistical simulations. (a): whole time range, (b): Detail showing the first 28 coating events.

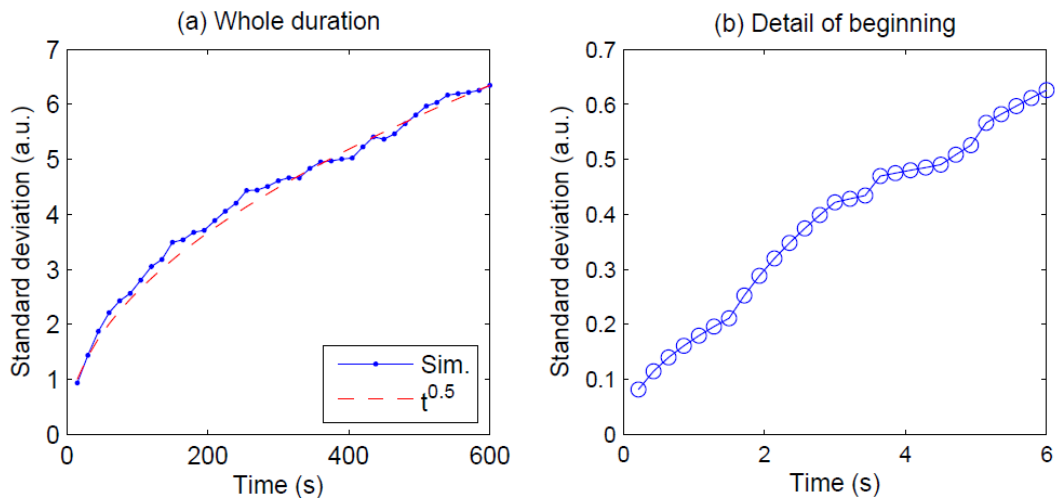


Figure 3: Increase of the standard deviation of coating mass over time, gathered from statistical simulations. A: whole time range, b: Detail showing the first 28 coating events.

At the end of the statistical simulation run, each tablet has been assigned a certain coating mass (in arbitrary units). Figure 4 shows a histogram of this distribution. It shows that it roughly resembles a Gaussian shape, as was to be expected due to the random nature of the underlying model.

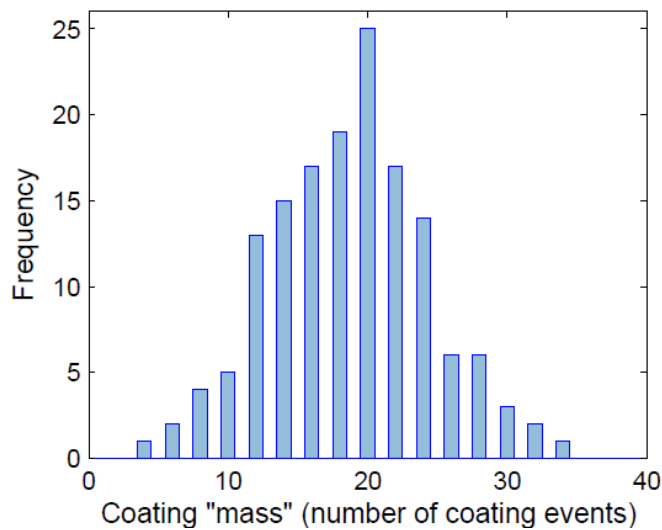


Figure 4: Distribution of coating mass, collected from the simplified statistical coating algorithm. The coating mass is given in terms of the number of spray events.

Summarizing, a simple statistical model was formulated and parameterized based on knowledge from DEM simulations. It showed that the model can predict central properties such as the decrease of the coefficient of variations in accordance with expectations. Of course, this alone cannot validate the model, but it hints that the proposed view of the principle nature of the coating process is plausible, and can help to gain a deeper mechanistic understanding.

Chapter B: Mathematical Modeling of the Coating Process

Published as: Toschkoff, G., Khinast, J.G., Mathematical modeling of the coating process. Int J Pharmaceut (2013), <http://dx.doi.org/10.1016/j.ijpharm.2013.08.022>

B-1 Abstract

Coating of tablets is a common unit operation in the pharmaceutical industry. In most cases, the final product must meet strict quality requirements; to meet them; a detailed understanding of the coating process is required. To this end, numerous experiment studies have been performed. However, to acquire a mechanistic understanding, experimental data must be interpreted in the light of mathematical models. In recent years, a combination of analytical modeling and computational simulations enabled deeper insights into the nature of the coating process.

This paper presents an overview of modeling and simulation approaches of the coating process, covering various relevant aspects from scale-up considerations to coating mass uniformity investigations and models for drop atomization. The most important analytical and computational concepts are presented and the findings are compared.

B-1.1 Keywords:

Film coating, Tablet coating, Discrete Element Method (DEM), Computational Fluid Dynamics (CFD), Modeling, Pharmaceutical Engineering.

B-2 Introduction

Coating of tablets or particles is one of the oldest and most common unit operations in the pharmaceutical industry. Generally speaking, coating is a repeated exposure of particles (tablets, granules, etc.) to a spray, containing solute and solvent. As a particle moves through the spray zone, it receives a

partial coating with a local distribution and amount depending on the local conditions on the particle's way through the spray zone. The liquid coating spreads to some extent over the particle and, in some cases, penetrates it. It also may be transferred to other particles. After being sprayed, the particle moves into a region where the partial coating is solidified, typically via evaporation of the solvent facilitated by heated drying air. This cycle of spraying and drying is repeated multiple times until the desired coating mass and/or uniformity are reached, shown schematically in Figure 5 (Turton, 2008).

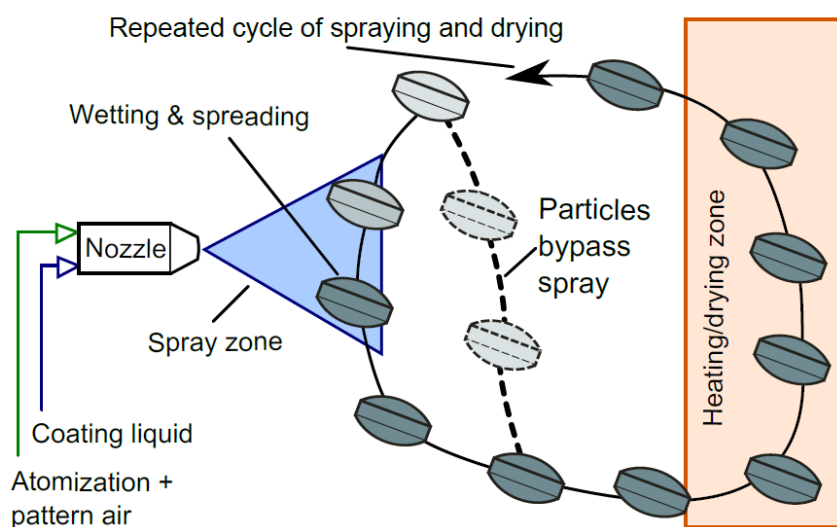


Figure 5: General principle of a particle coating process. This cycle (Coating in the spray zone – transportation and drying - re-enter the spray) appears in most types of coating apparatus. Modified from (Turton, 2008).

Although coating systems are quite diverse, the underlying principle of most of the modern systems is the same. Differences primarily relate to the way particles move between spray and drying zones and the way of removing the solvent. Since most solid dosage forms are coated using either a fluidized bed or a rotation drum, they were the focus of this work, with an emphasis on drum coating of tablets, for which an extensive body of literature exists. However, because the underlying principle is similar, findings are generally applicable to coating of particles in general.

B-3 Drum Coating

Drum coating of tablets is a very common coating method in the pharmaceutical industry. Tablet cores are placed in a rotating drum, where the rotation promotes their radial and axial mixing (Figure 6).

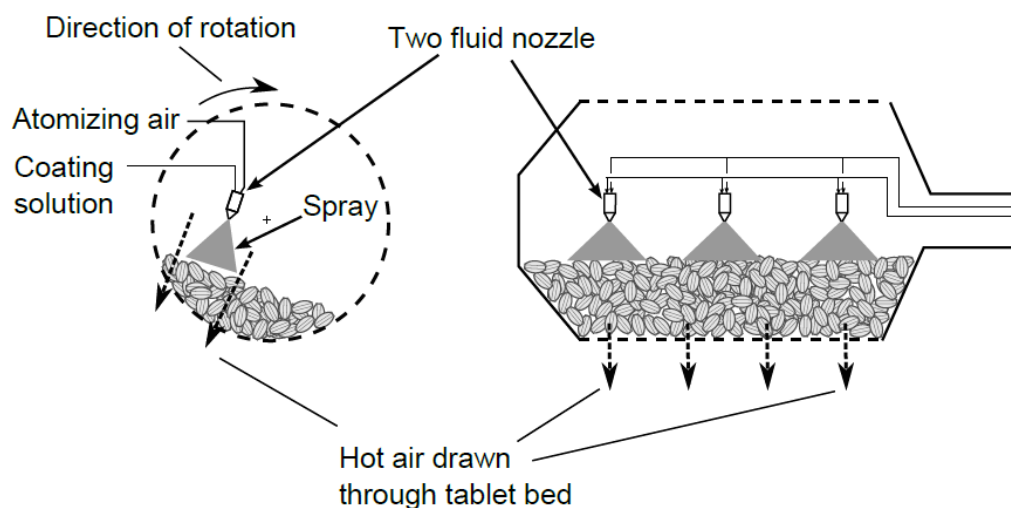


Figure 6: Schematic representation of a typical drum coating apparatus. Modified from (Turton and Cheng, 2005)

Typically, axial mixing is slower, and is often facilitated by installing baffles in the drum (Muliadi & Sojka, 2010). Drum coaters are available in different designs, distinguished mainly by the drying air flow through the drum and by the baffle arrangement. However, all of them operate similarly, with particles cascading down the top of the bed and some passing through the spray zone. The spray zone is formed by one or more spray nozzles mounted atop and spraying down onto the tablet bed.

For the coating quality, dominant factors are the movement of the tablet and locally the tablet-drop interaction. The relative effect of droplet size, impact and frequency, liquid spreading, drying and the ensuing solid-state transformations determine the morphology and quality of the coating (Bolleddula, Berchielli, & Aliseda, 2010; Suzzi, Radl, & Khinast, 2010).

During a pan-coating process, operational parameters can be divided into two groups: pan-and-tablet-related and spray-related (Pandey et al., 2006c; Porter, 2012; Ruotsalainen et al., 2002).

Important pan and tablet parameters are:

- pan diameter and depth
- pan speed
- pan load
- core shape, size, and mass
- baffle setup
- number of spray nozzles
- pan perforation
- mechanic tablet properties (e.g. hardness, friability, friction coefficient)

Important spray-related parameters are:

- spray rate
- inlet air flow rate
- inlet/outlet air temperature
- inlet/outlet air humidity
- atomizing air
- solution properties
- nozzle-to-bed distance
- coating time

To achieve a deeper understanding of the coating process, experimental investigations studied the influence of process parameters on the outcome (Müller and Kleinebudde, 2007a; Patel et al., 2009; Sandadi et al., 2004). Both inter- and intra-tablet uniformities were measured (Tobiska and Kleinebudde, 2003), with a trend towards novel non-destructive techniques, such as Terahertz-Pulse Imaging (Brock et al., 2012; Ho et al., 2007) or Optical Coherence Tomography (Koller, Hanneschläger, Leitner, & Khinast, 2011; Mauritz et al., 2010; Zhong et al., 2011).

A general review of pharmaceutical tablet spray coating was provided by (Muliadi & Sojka, 2010), with some coverage of analytical models.

B-4 Fluidized Bed Coating

Another coating unit operation is fluidized bed coating. However, for the coating of larger particles (such as tablets), which is the main focus of this review,

fluidized bed coating is much less common than drum coating. Therefore, a detailed description of this complex process is out of the scope of this work. A description of the concept and some modeling aspects are given; for an in-depth treatment, the reader is referred to the literature (e.g., Teunou and Poncelet, 2002).

In fluid bed coating, particles are introduced into a closed area (cell) and suspended by (heated) air introduced from below. A coating liquid is sprayed onto the particles from a nozzle. A schematic is shown in Figure 7.

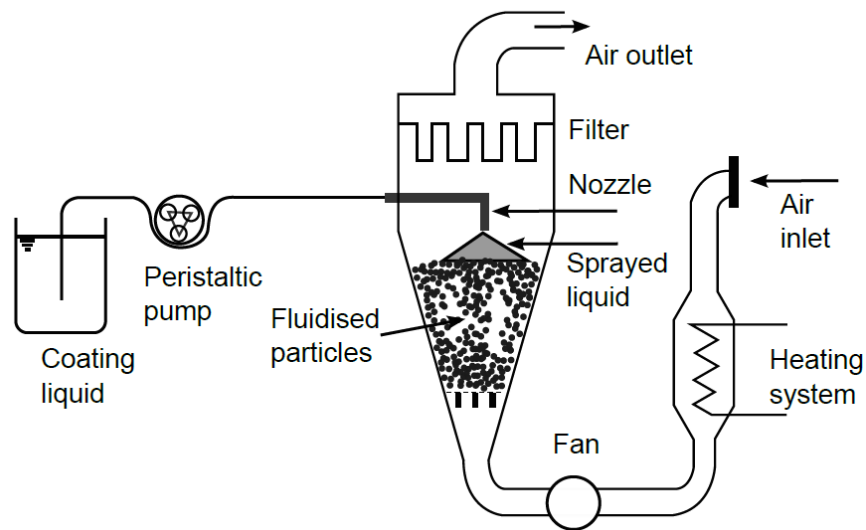


Figure 7: Schematic representation of a top spray fluid bed granulator or coater. Modified from (Teunou & Poncelet, 2002)

If properly set up, the air flow mixes and dries the particles. Several fluid bed coating varieties exist, distinguished by the choice of the nozzle position and flow setup. Examples are shown in Figure 8.

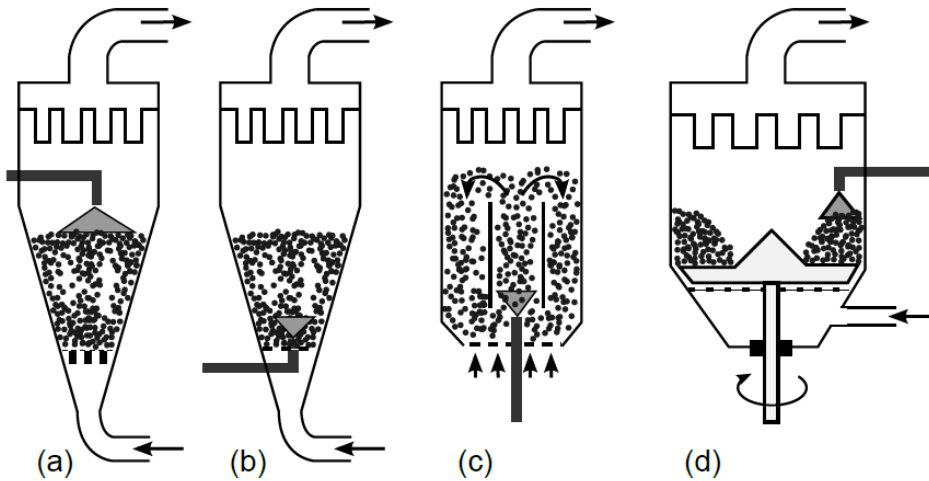


Figure 8: Different forms of fluid bed coating: (a) top spray or granulator, (b) bottom spray, (c) “Wurster” type, (d) side spray with rotating disk. From (Teunou & Poncelet, 2002)

All of them subject particles to a cycle of coating and drying events to accumulate coating layers. One of the challenges is that particles, especially small ones, tend to agglomerate. The advantages of fluidized bed coating include fast heat and mass transfer, temperature homogeneity and easy flow rate control. In addition, it is well-suited for smaller particles, which are impractical or impossible to coat in a drum.

Depending on the air velocity, different forms or configurations emerge. At low velocities, instable channeling or slugging is observed. A stable fluid bed is formed for values between the minimum fluidization velocity v_{mf} , and the terminal velocity v_t . The velocity v_{mf} mainly depends on the particle diameter d_p , the particle density ρ_p and the fluid density ρ_g and viscosity μ (Teunou & Poncelet, 2002):

$$v_{mf} = \begin{cases} \frac{(\rho_p - \rho_g)^{0.934} g^{0.934} d_p^{1.8}}{111\mu^{0.87} \rho_g^{0.066}} & \text{for } d_p < 100\mu\text{m}, \\ \frac{\mu}{\rho_g d_p} \left[(11135.7 + 0.0408Ar)^{1/2} - 33.7 \right] & \text{for } d_p > 100\mu\text{m}. \end{cases} \quad (4)$$

The Archimedes number Ar is given as

$$Ar = \frac{\rho_s d_v^3 (\rho_p - \rho_g) g}{\mu^2}, \quad (5)$$

where d_v is the diameter of an equivalent sphere. For air velocities above the terminal velocity v_t , particles are carried with the gas stream, and transportation rather than fluidization takes place. It can be estimated as (Teunou & Poncelet, 2002)

$$v_t = \left[\frac{4gd_p(\rho_p - \rho_g)}{3\rho_g C_D} \right]^{1/2}, \quad (6)$$

with the drag coefficient C_D given by corresponding correlations (Ganser, 1993; Tran-Cong, Gay, & Michaelides, 2004).

B-5 Application of Modeling Approaches

The two central quality criteria of the coating process are intra- and inter-particle uniformities of the finished product. Intra-tablet uniformity describes a variation in the coating thickness on one tablet. Inter-tablet uniformity describes the differences in the total coating mass between individual tablets. For pharmaceutical tablets, depending on the coating functionality, an entire batch can be rejected if either or both criteria are not within an acceptable limit. Therefore, a large part of the modeling effort is directed towards the prediction and optimization of these uniformities. In addition, modeling is successfully applied to scale-up of processes, thermodynamic considerations of drying, as well as to the determination of particle velocities or collision frequency, intensity, particle stress and abrasion.

B-5.1 Inter-Tablet Coating Variability

Inter-particle coating variability is one of the biggest concerns regarding coating. Uniformity can be quantified via the coefficient of variation (or relative standard deviation) of the coating mass over all tables, $c_{v,inter}$. It is calculated from the coating masses of the particles according to

$$c_{v,inter} = \frac{1}{m_c} \sqrt{\frac{1}{N_p} \sum_{i=1}^{N_p} (m_{c,i} - \bar{m}_c)^2}, \quad (7)$$

where N_p is the number of particles, $m_{c,i}$ is the coating mass of particle i and \bar{m}_c is the average coating mass of all particles. Eq. (7) is valid if the coating mass of

each particle is known. Experimentally, $c_{v,inter}$ is normally estimated from a large enough sample of particles, in which case N_P in the equation above is replaced by (N_P-1) and \bar{m}_c is estimated by the sample mean.

Some simulation methods can be used to directly determine the coating mass of each tablet and the quantities related to it. Other modeling techniques do not calculate the coating mass directly but, rather, establish the mass uniformity based on other quantities. Common quantities that are used to describe the properties of a coating process are (Kalbag and Wassgren, 2009):

- Residence time $T_{R,i}$: the total time particle i spends in the spray zone. At the end of the coating process, each tablet has a single value for its residence time, which is often assumed to be proportional to the coating mass it received. Averaging over all particles gives the average residence time $\overline{T_R}$, a single value for the entire coating process.
- Circulation time $T_{circ,i}$: the total time tablet i is outside the spray zone. Similar to the residence time above, an average circulation time $\overline{T_{circ}}$ can be defined.
- Fractional residence time $f_{R,i}$: dimensionless quantity defined as the tablets' residence time divided by the total operating time of the coating process, T_0 , also introduced in (X. Y. Liu, Xu, & Zhang, 2011). It can be used as a performance indicator. At the end of the coating process, each tablet has a different single-value $f_{R,i}$. Averaging over all tablets gives the average fractional residence time $\overline{f_R}$.
- Single visit residence time t_{SVRT} : the residence time per pass, i.e., the duration of a single visit to the spray zone. In one coating process, each tablet has multiple SVRTs, one for each spray zone visit. t_{SVRT} of all tablets for all visits is typically gathered in a single distribution. The mean value $\overline{t_{SVRT}}$ of the distribution states the average time the particle spends in the spray zone, which is important for the coating quality. If t_{SVRT} is too high, particles are over-wetted and may not dry on time. Unwanted liquid bridges may form, promoting defects such as picking (Muliadi & Sojka, 2010). If it is too low, the coating received in one pass may not be sufficient to form an intact partial coating layer per pass.

- Single cycle time t_{SCT} : the time between two subsequent visits to the spray zone of the same tablet. As for t_{SVRT} above, the distribution of t_{SCT} is calculated.
- Coating fraction α : ratio of the (average) number of particles in the spray $\overline{n_p}$ to the total number of particles N_p .

The quantities defined above are not independent from each other. Fractional residence time can be calculated from the average of t_{SVRT} and t_{SCT} as:

$$f_{R,i} = \frac{\overline{t_{SVRT}}}{\overline{t_{SVRT}} + \overline{t_{SCT}}} \quad (8)$$

The average fractional residence time $\overline{f_R}$ is equal to the fraction of tablets located within the spray zone. The average number of tablets located in the spray zone $\overline{n_p}$ multiplied by the total coating time T_0 is equal to the total number of tablets N_p multiplied by the average residence time $\overline{T_R}$:

$$\overline{n_p} T_0 = N_p \overline{T_R}. \quad (9)$$

From this, it follows that the fractional residence time is given as

$$\overline{f_R} = \overline{n_p} / N_p = \alpha. \quad (10)$$

B-6 Modeling Approaches Overview

Due to the complexity of the coating process, it is impossible to model the entire process in detail. Instead, depending on the objectives, specific modeling approaches are chosen. They differ in their scope (e.g., coating of a single tablet versus the movement of all tablets) and complexity (e.g., a single analytical expression versus a full velocity field). In this work, they are organized according to the underlying theoretical framework:

- General analytical modeling
- Computational Fluid Dynamics simulations
- Discrete-Element-Method-based simulations

- Particle movement and mixing
- Inter-tablet variability
- Intra-tablet variability
- Monte Carlo and Population Balance

The main focus of this overview is the theoretical and computational modeling. However, many models require measured values as input or experimental data for validation. Therefore, the literature regarding experimental work was cited when relevant. A more comprehensive list of experimental studies can be found in (Sahni & Chaudhuri, 2012).

B-7 Analytical Modeling

Analytical modeling refers to methods that do not depend on the numerical computations but rather describe how to calculate characteristic properties from analytical expressions. These expressions are either derived from first principles based on simplifying assumptions or based on knowledge from an experiment and/or simulation.

B-7.1 Coating Distribution

The very basic but useful “prediction” of film thickness is performed by dividing the total volume of the applied coating liquid by the total surface area, taking spray loss into account for more accuracy (Rowe, 1996). For a biconvex tablet, the surface area S can be calculated from tablet diameter d_{tab} , band height h_{band} , cap height h_{cap} and cap radius R_{cap} according to:

$$S = \pi d_{\text{tab}} h_{\text{band}} + 4\pi R_{\text{cap}} h_{\text{cap}}. \quad (11)$$

This, of course, does not take the inter-particle coating variation, i.e., the variation of the coating mass between different tablets as defined in Eq. (7), into account. A number of sophisticated computational methods described below were recently used to investigate the $C_{v,\text{inter}}$. An often used analytic expression for $c_{v,\text{inter}}$ can be stated based on renewal theory in terms of the coating mass distributions per pass and tablet circulation time (Mann, Rubinovitch, & Crosby, 1979; Mann, 1983):

$$c_{v,inter} = \sqrt{\frac{\mu_{ct}}{T_0} \left[\left(\frac{\sigma_{cpp}}{\mu_{cpp}} \right)^2 + \left(\frac{\sigma_{ct}}{\mu_{ct}} \right)^2 \right]} \quad (12)$$

where μ_{cpp} and σ_{cpp} are the mean and standard deviation of the coating-per-pass distribution; μ_{ct} and σ_{ct} are the corresponding values for the cycle time distribution and T_0 is the total coating time. This central equation is illustrated in Figure 9.

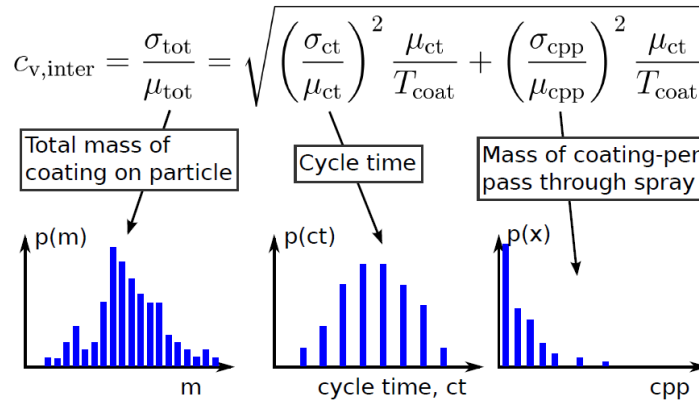


Figure 9: Schematic explanation of the dependence of the total coefficient of variation on the distribution of cycle time and coating per pass. After (Turton, 2008).

Hall found that the dependence of $c_{v,inter}$ on the coating time predicted in the equation was verified in several types of coating apparatus (Hall, 1990). In a Wurster coating process, the variation in coating per pass affected the total $c_{v,inter}$ significantly more than the variation in the circulation time (Shelukar et al., 2000). Similar results were reported in (Cheng and Turton, 2000a). Recently it has been pointed out by Freireich (Freireich & Li, 2012) that Eq. (12) could be improved. In the original derivation, it is assumed that spray times (time particles spend in the spray zone) and cycle times (time needed for a total cycle) are independent; however, strictly speaking the spray times and bed times (time between two spray events) should be considered independent. A corrected formulation introducing the coating fraction α is proposed:

$$c_{v,inter} = \sqrt{\frac{\mu_{ct}}{T_0} \left[(1-2\alpha) \left(\frac{\sigma_{cpp}}{\mu_{cpp}} \right)^2 + \left(\frac{\sigma_{ct}}{\mu_{ct}} \right)^2 \right]}. \quad (13)$$

It can be seen that the correction is small for a small coating fraction; this is typically the case.

In Eq. (12) or (13), the circulation time distribution and the mass-per-pass distribution are required as input. One (intricate) way to assess the circulation time distribution is to use magnetic tracer particles and a detection coil (Cheng and Turton, 2000b; Mann and Crosby, 1975; Waldie and Wilkinson, 1986) or radioactive particles with Position Emission Particle Tracking (PEPT) (Parker, Dijkstra, Martin, & Seville, 1997; W. Chan, Seville, Parker, & Baeyens, 2010). A method to determine the distribution of the mass per pass (which is not commonly measured) is to inject colored coating for a defined time (Subramanian, Turton, Shelukar, & Flemmer, 2003).

B-7.2 Scale-Up / Scale-Down

One application for modeling is to give guidance in scale-up: a given coating process is working on a relatively small scale, what parameter settings will ensure that the same process works on a bigger scale? This question typically arises after a process was developed on lab scale, and is to be scaled up for the routine production (industry scale). The opposite direction is scale-down, applicable when e.g. a product was mass-produced, but is now needed in smaller quantities than usual.

Scaling laws based on the equipment geometry and flow rates for coating processes in both fluid bed and pan coating were described by Turton and Cheng (2005). For fluid bed operations, the variables were air flow, product uniformity, air dew-point, distributor plate design, particle attrition, atomizing air pressure, coating time and batch charge. Scale-up laws for relative spray rate, relative coating time and air velocity were given. For drum coating, the coating and drying cycles, air conditioning, rotation rates, batch charge and the nozzle location were investigated. A formula for the coating time that takes nozzle setup into account was provided.

Rules for scale-up were formulated by considering geometric, dynamic and kinematic similarities (Levin, 2005) Geometric similarity primarily means that the shape of the drum is proportional, the baffle-aided mixing is similar and the

fill ratio is constant. Dynamic similarity aims at maintaining similar forces acting in the coater across the scales. For the particle movement in a rotating drum, the two governing forces are inertial and gravitational force. With regard to that, two approaches were developed. First, keeping the dimensionless Froude number constant (Ding et al., 2001; Orpe and Khakhar, 2001; Pandey et al., 2006c), with the Froude number being the ratio of the inertial to gravitational forces:

$$\text{Fr} = \frac{\omega^2 D}{g} = \text{const}, \quad (14)$$

with ω the magnitude of the drum rotation velocity, and D the drum diameter. Second, keeping the circumferential (“linear”) velocity of the coater constant:

$$\omega D = \text{const}. \quad (15)$$

Turton and Cheng (2005) reported that, in practice, using the Froude-number scale-up criterion often resulted in product abrasion, suggesting that the second approach may be more appropriate.

Kinematic similarity finally ensures that the velocities of the tablets remain constant across the scales, at least where they have a great impact on the coating process (e.g., the velocity in the spray zone). Different approaches were proposed. Pandey et al. (2006b) suggested to ensure similar tablet velocities on top of the tablet bed since this affected the time the tablets spend in the spray zone and thus the coating process. They also suggested maintaining a constant ratio of characteristic drying time of the spray drops to the time the tablets spent on the bed surface:

$$t_{\text{dry}} / t_{\text{surface}} = \text{const}. \quad (16)$$

In addition to the dynamic and kinematic similarity, the ratio of air flow rate and spray rate (commonly called the drying capacity) should be kept constant. Am Ende and Berchielli (2005) further assumed that the tablet bed temperature is equal to the outlet temperature and the heat loss can be neglected. Thus, keeping the inlet temperature constant across scales results in constant exhaust temperature.

The cycle time (the time span between two coating events of one tablet (Kalbag, Wassgren, Sumana Penumetcha, & Pérez-Ramos, 2008)) is longer for bigger scales. Pandey et al. (2006c) argued that since this effect offers tablets more time to dry, more coating solution can be sprayed. The spray rate \dot{V} can be scaled

based on the number of tablets in the spray zone, n_p , and the total number of tablets, N_p :

$$\dot{V} \frac{n_p}{N_p} = \text{const.} \quad (17)$$

Note that Eq. (17) does not take into account the additional effects of increasing the spray rate, such as local over-wetting near the spray zone or a change in the coating formation.

Normally, it is desirable to achieve a constant weight gain per tablet on all scales. In this case, the coating time T_0 is connected to the spray rate \dot{V} and drum load L :

$$T_0 \frac{\dot{V}}{L} = \text{const.} \quad (18)$$

An overview of the scale-up of pan coating was presented in (Pandey, Turton, et al., 2006). Four parameters that influence the coating process were selected for closer investigation: the pan load, the pan speed, the total spray rate and the inlet air flow. The presented scale-up rules were applied for scale-down: two processes optimized in a 52-inch drum were downsized to run in a 24-inch drum. The resulting tablets had a similar appearance and dissolution profiles on both scales. Further investigations showed that the pan speed had the biggest effect on the coating uniformity, while coating efficiency and opacity were mostly influenced by the drying capacity. For all scale-up considerations, the mechanical stress of the particles that may vary between the scales must be considered. Müller and Kleinebudde (2006) investigated the abrasion of tablets at different scales (Bohle BFC 5 and BFC 40). Under otherwise identical conditions, the number of impacts of tablets onto the coating drum increased with the square of the pan diameter, resulting in approximately 4.36 times more frequent impacts on the lab scale compared to the pilot scale to arrive at the same coating. In addition, Müller and Kleinebudde compared the scale-up of two-component laboratory and production spray nozzles (Müller and Kleinebudde, 2007b) and presented a scale-up approach to achieving similar droplet sizes, velocities and densities. The droplet size was scaled by adjusting the atomization air pressure and the droplet velocity by adjusting the nozzle-to-bed distance. A comprehensive overview of the scale-up of film coating is given in (Porter, 2012).

B-7.3 Velocity Scaling

With respect to a coating process in a rotating drum, it is useful to know the velocity of the particles at different surface locations as a function of the process parameters, especially at the location of the spray nozzle. Attempts have been made to determine scaling laws for the velocity that can generally be applied to a range of parameter settings.

Orpe and Khakhar (2001) collected experimental data for spherical particles in rotating cylinders of short axial length for different rotation speeds and particles sizes. Various continuum theories were applied to the experimental data, and the applicability of the theories was confirmed by comparing the outcome. Scaling analysis indicated that the Froude number and the size ratio (particle size to cylinder size ratio) influenced the flow the most. An exception was the dynamic angle of repose: it increased nearly linearly with rotation speed but did not scale with the Froude number.

Müller and Kleinebudde (2007a) gathered experimental data for tablet velocities in pan coaters ranging from lab- to production scales. They fitted the data to a mathematical model described in (Alexander et al., 2002; Pandey et al., 2006b) to arrive at

$$v = kD\omega^{0.67} \left(g / d_p \right)^{0.17} \phi^{1.8}, \quad (19)$$

where v is the velocity of particles, k is a constant, D is the pan diameter, ω is the pan rotation speed, and d_p is the particle size, and ϕ is the filling degree of the drum. The equation was a good fit across all tested coating pan sizes. From Eq. (19) it also follows that tablets are likely to move faster through the spray zone when the size of the coating drum is increased. To quantify this increase, the ratio of the velocities ξ_v between two pan coaters of different size is defined. Assuming constant peripheral speeds and the same spray zone when going from one pan size to another, ξ_v is given as the ratio of the volumes of the larger pan (V_{pan2}) and the smaller pan (V_{pan1}): $\xi_v = V_{\text{pan2}} / V_{\text{pan1}}$.

This was subsequently used as a correction factor for the scale-up of the spray rate \dot{V} depending on the spray width w (Müller and Kleinebudde, 2007b; Turton and Cheng, 2005):

$$\dot{V}_{\text{pan1}} = \xi_v \dot{V}_{\text{pan2}} \frac{W_{\text{pan2}}}{W_{\text{pan1}}} \quad (20)$$

B-7.4 Thermodynamic Models

Film coating can essentially be considered an adiabatic evaporative cooling process. Evaporation of the coating solution from the tablets depends on a combination of the drying-air flow rate in the drum (impacting mass and heat transfer between tablet and air), the system temperature, and the moisture content of the air. These driving forces in turn are governed by apparatus design and operating parameters. In general, parameters (such as spray rate or inlet air temperature) cannot be set independent of each other, and a change in one parameter will most likely influence the process in multiple ways.

Am Ende and Berchielli (2005) presented a semi-empirical thermodynamic film coating model to predict the temperature and relative humidity of the exhaust air. Mass and energy balances were formulated for a control volume of the tablet bed. The change of enthalpy due to sensible heating and the latent heat of solvent evaporation (water and/or organic components) was taken into account. Heat loss to the surroundings was included as an empirical heat loss factor f_{HL} that was fitted to match experimental data. The air flow from the spray nozzle was neglected. One important parameter that is usually monitored in a coating process and which is used for process control is the exhaust air temperature. This temperature is given by:

$$T_{\text{air,out}} = \frac{\dot{m}_{\text{air,in}} C_{p,\text{air}} T_{\text{air,in}} + x_S \dot{m}_{\text{coat}} C_{p,S} T_{\text{coat}} - x_S \dot{m}_{\text{coat}} L_{\text{vap},S} + f_{\text{HL}} T_{\text{RT}}}{\dot{m}_{\text{air,in}} C_{p,\text{air}} + x_S \dot{m}_{\text{coat}} C_{p,S} + f_{\text{HL}}} \quad (21)$$

where $T_{\text{air,out}}$, $T_{\text{air,in}}$, T_{coat} and T_{RT} are the temperatures of the exhaust and inlet air, coating liquid and the room temperature, respectively. $\dot{m}_{\text{air,in}}$ and \dot{m}_{coat} are the mass flow rates of the inlet air and coating solution, $C_{p,\text{air}}$ and $C_{p,S}$ are the specific heat capacities of air and solvent, respectively. x_S is the solvent fraction in the coating solution. The latent heat of vaporization of the solvent is given as $L_{\text{vap},S}$. For more than one solvent component, a combination of single-component values is taken. Equation (21) can be used as a scientific basis for a Quality-by-Design investigation of the scale-up of a tablet coating process (Prpich et al., 2010).

Page et al. (2006a) developed another model to predict air and product temperatures, product moisture, and air humidity in a film-coating process. In their work, a Bohle lab-coater was divided into spraying and drying zones, and balance equations for air humidity, air enthalpy, product moisture, and product enthalpy are formulated for each zone were formulated. In addition, mass and heat transfer were considered. In summary, a set of first-order ordinary differential equations was set up and solved numerically. Most of the required model input parameters were calculated or measured. A separate publication (Page, Baumann, & Kleinebudde, 2006b) describes how the remaining parameters were determined experimentally and how the model was applied.

B-7.5 Modeling of spray characteristics

In the treatment of the coating spray itself, analytical models are often used to predict drop generation and impact. With that regard, the following non-dimensional numbers are relevant:

$$\begin{aligned} \text{Weber number } We &= \frac{\rho D v^2}{\sigma} \\ \text{Drop Reynolds number } Re &= \frac{\rho D v}{\mu} \\ \text{Ohnesorge number. } Oh &= \frac{\mu}{\sqrt{\rho \sigma D}} \end{aligned} \quad (22)$$

with ρ the density, D the characteristic length (here: diameter), v the characteristic velocity, and μ the viscosity.

B-7.5.1 Drop impact and spreading

Bolleddula et al.(2010) studied the effect of droplets hitting a dry surface in the context of pharmaceutical spray coating. They addressed the dynamics of highly viscous Newtonian and complex rheological liquids over a range of Oh , We , and Re numbers. The experimental data showed reasonable agreement with models for the ratio of the maximum spread and initial diameter. An important result was that the relation

$$Oh_{\text{crit}} = 57.7 Re^{-5/4},$$

which predicts the onset of splashing, see Figure 10 (Suzzi et al., 2010).

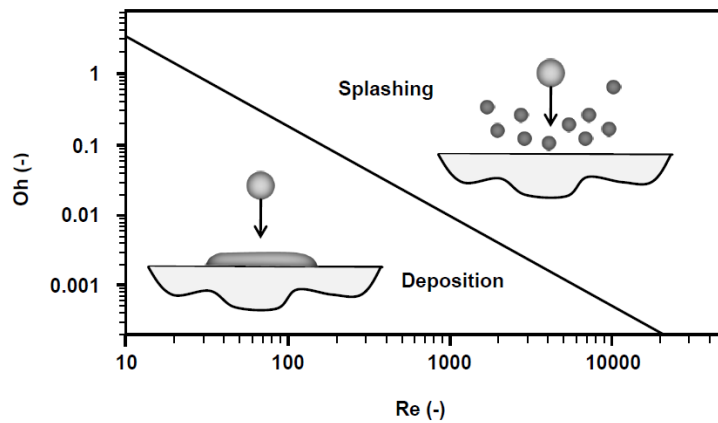


Figure 10: Deposition model of impacting droplets: critical curve. From (Suzzi et al., 2010)

Alleborn and Rasziller (2004) modeled the spreading and sorption of droplets into a porous substrate. Based on a lubrication-flow approximation and the Frumkin-Deryaguin model, they derived equations describing the time evolution of a droplet situated on a substrate. This includes both, the change of the droplet shape (profile) above the substrate, and the movement of the wetting front inside it. The limiting cases of a very thin porous layer were in accordance to corresponding experimental data.

Rafai et al. (2004) studied the time evolution of a spreading droplet for non-Newtonian liquids (that is, liquids that show shear-rate dependence in their viscosity, and exhibiting normal stresses). They find for the spreading radius R as a function of time:

$$R(t) \sim V_{\text{drop}}^{3/10} \left(\frac{\sigma}{\mu} \right)^{1/10} t^{1/10}, \quad (23)$$

where t is the time, V_{drop} is the drop volume, σ is the surface tension and μ is the viscosity. Surprisingly, this is in accordance with the well understood wetting of Newtonian fluids on smooth solid substrates ($R(t) \sim t^{1/10}$, Tanner's law). For the practical prediction of spreading rates, they also propose to replace the viscosity with effective viscosity values to account for shear-thinning or normal stress effects in fluids.

B-7.5.2 Drop generation

To predict the droplet's mean diameter produced via pneumatic atomization, Müller and Kleinebudde (2007b) reported an expression for the Sauter mean diameter (SMD) d_{32} (adapted from (Nukiyama & Tanasawa, 1939)):

$$d_{32} = \frac{585 \times 10^3}{v_{\text{rel}}} \left(\frac{\sigma}{\rho} \right)^{0.5} + 1683 \mu^{0.45} (\sigma \rho)^{-0.225} \left(\frac{1000}{J} \right)^{1.5}, \quad (24)$$

with v_{rel} being the relative air velocity at the nozzle exit, σ the surface tension, ρ the liquid density, μ the liquid viscosity and J the air-to-liquid volume ratio.

In a study of batch and continuous fluid-bed coating, Teunou and Poncelet (2002) used a correlation for the (mean) droplet size d_g suggested by Masters (1979):

$$d_d = \frac{585 \times 10^3 \sqrt[3]{\sigma}}{v_{\text{rel}} \sqrt{p}} + 597 \left(\frac{\mu}{\sqrt{\sigma \rho}} \right)^{0.45} \left(\frac{1000 \dot{Q}_{\text{liq}}}{\dot{Q}_{\text{air}}} \right)^{1.5}, \quad (25)$$

where \dot{Q}_{liq} is the liquid volumetric flow rate, \dot{Q}_{air} is the air volumetric flow rate. The relative velocity v_{rel} can be seen as approximately equal to the outlet air velocity.

Varga et al. (2003) experimentally investigated the breakup and atomization of a liquid jet and found a mechanism based on interfacial and Rayleigh-Taylor instability. A model based on the Rayleigh-Taylor initial breakup yields a practical expression for SMD:

$$d_{32} \approx \frac{0.68 \gamma^{1/2} (\rho_l v_g)^{1/4} \sigma^{1/2}}{\rho_g^{3/4} [v_g (1 + \sqrt{\rho_g / \rho_l}) - v_l] v_g^{1/4}}, \quad (26)$$

with v_l and v_g being the velocities and ρ_l and ρ_g the densities of liquid and gas, respectively; ν is the kinematic viscosity and γ a proportionality factor. Eq. (26) implies that the SMD is proportional to $v_g^{1/4}$, which was confirmed by the experimental data. More recently, Aliseda et al. (2008) extended this study to a theoretical and experimental investigation of the atomization dynamics of non-Newtonian liquids and of the performance of two-component spray nozzles, typically applied in pharmaceutical tablet coating. A Phase-Doppler Anemometry was used to characterize the spray, and the rheology of six fluids, including two

Opadry II water-based suspensions, was analyzed. An atomization model for the Sauter mean diameter d_{32} based on (Varga et al., 2003) was developed:

$$\frac{d_{32}}{d_l} = C_1 (1 + m_r) \left(\frac{b_g}{D_l} \right)^{1/2} \left(\frac{\rho_l / \rho_g}{\text{Re}_{b_g}} \right)^{1/4} \frac{1}{\sqrt{\text{We}_{D_l}}} \left\{ 1 + C_2 \left(\frac{D_l}{b_g} \right)^{1/6} \left(\frac{\text{Re}_{b_g}}{\rho_l / \rho_g} \right)^{1/12} \text{We}_{D_l}^{1/6} \text{Oh}^2 \right\} \quad (27)$$

where d_l is the liquid orifice diameter, b_g gives the size of the air outlet at the nozzle tip, and C_1 and C_2 are model constants. The mass loading effect m_r was adapted from (Mansour & Chigier, 1995). The dimensionless numbers Re , Oh , and We have been defined above in Eq. (22). Note that Weber and Ohnesorge numbers are based on the liquid orifice diameter, as denoted by the subscript l . Eq. (27) implicitly indicates the dependency of d_{32} on the gas velocity as $v_g^{-5/4}$ and surface tension as $\sigma^{1/2}$. A comparison with the data showed that the model could reasonably predict the Sauter Mean Diameter at a distance from the nozzle. In addition, it was found that the pattern air plays a negligible role in the drop formation.

B-8 Computational Fluid Dynamics (CFD)

Computational Fluid Dynamics (CFD) is a method used to simulate the flow behavior of a fluid (i.e., liquid or gas). Apart from the velocity field of a fluid, modern CFD software enables one to e.g. include different phases, considering heat- and mass transfer between phases, or describe porous regions. Relevant to coating is especially the possibility to track the movement of particles in the flow (Euler-Lagrange approach). The particle movement is influenced by the liquid flow, which in turn is affected by particles (two-way coupling). This can be used beneficially to model the coating spray. In a Design-of-Experiment (DoE) study, Wang et al. (2012) simulated drying of a single spray droplet as it traveled through a volume of air. They showed the influence of the initial drop diameter on the velocity and size loss over the traveled distance. Toschkoff et al. (2012) simulated the air flow and spray movement in a non-perforated coating drum using an Euler-Lagrange approach and following the trajectories of single droplets in the air stream. Mass and energy transfer from and to the droplet was considered, and spray loss of five spray nozzle setups was compared. Suzzi et al. (2009) used CFD simulations to investigate the film formation on spherical and

biconvex tablets under different conditions. An approach involving the Euler-Lagrange Discrete Droplet Method was applied to simulate the spray flow in the surrounding air. Film formation and evolution on the surface of the sprayed tablet was simulated in a quasi-two-dimensional model. The coating solution was a glycerol-water mixture of different concentrations/viscosities. The influence of the air temperature, the drop velocity, the drop diameter and the coating liquid viscosity on the coating thickness and the local distribution was investigated. The results showed how the intra-tablet coating uniformity was affected by changes in the process parameters. Continuum models (Euler-Euler approach) were also used to describe the particulate motion. Ding et al. (2001) used an Eulerian approach to simulate rotating drums and derived non-dimensional equations to determine scaling relationships for rotating drums. They established that the controlling factors were the Froude number, pseudo-Reynolds number, pseudo-Euler number, drum geometry ratios, drum inclination, drum fill fraction, particle size distribution and physical properties of the particles and the drum wall (coefficient of restitution, elastic modulus).

It should be noted that in the Euler-Lagrange model, the particles themselves can only have limited interaction (such as coalescing droplets), but no sophisticated models for particle collisions are included. For the full description of particle movement and collision in a fluid stream, a coupled DEM-CFD has to be applied. Applications of this coupling in coating processes of larger scale is relatively novel, work in this field is shown in section B-9.4 .

B-9 Discrete Element Method (DEM)

Recently, the Discrete Element Method (DEM) became a valuable tool for analyzing particulate processes in the pharmaceutical industry (Adam, Suzzi, Radeke, & Khinast, 2011; Ketterhagen, am Ende, & Hancock, 2009b). It is particularly well-suited to simulate the coating of tablets (or similar particles) for two reasons. First, the movement of tablets in a coater is governed mostly by gravitational and inertial body forces in combination with particle-particle and particle-wall collisions. Additional forces due to the air flow or cohesion can often be neglected or can be accounted for by DEM-CFD coupling (see below). Second, although the number of tablets (in the order of 10^5 - 10^6) involved in the coating process is high enough for granular behavior, in many cases it is low enough to be processed with the available computational hardware. A default DEM simulation provides limited data, such as the tablet position or velocity. To obtain additional attributes (e.g., coating uniformity), it must be established which tablets are in

the spray region (i.e., being coated) at a given time and which are not. For this, different approaches have been suggested.

One of the first DEM applications for tablet coating was proposed by Yamane et al. (1995), who used at most 600 spherical tablets due to computational constraints at that time. The influence of the rotation speed, the fill level and the size of the spherical tablets was investigated in terms of the RSD of residence time and the average circulation time. For tablets in the spray zone that were partially covered with coating from other tablets, only a fraction of the exposed surface was taken into account in this early work.

Reducing the three-dimensional geometry to a two-dimensional problem is only valid under certain conditions. Pohlman et al. (2006) demonstrated the effects of end-walls in rotating drums of various length and found that the influence of the walls on the overall flow is insignificant if the axial length is greater than the diameter. In this case, the flow in the coater center can be approximated by the flow in an infinitely long drum. For a length smaller than the diameter, the effect of the wall could not be neglected.

Another important concern is how to treat the shape of particles/tablets. In the literature, spherical particles are used or tablet shapes are approximated by the number of different-sized spheres that are “glued” together (Favier, Abbaspour-Fard, Kremmer, & Raji, 1999). It is known that the particle shape is a crucial factor for numerical simulations (Abedi & Mirghasemi, 2011). For example, standard round convex tablets have higher velocities in the cascading layer than spheres of the same volume and equivalent diameter (Pandey & Turton, 2005). Recently, models were developed that represent the bi-convex tablet shape more correctly by using intersecting spheres. The top/bottom is described using two partial spheres and the edge as a part of a relatively large sphere or a cylinder. Contact detection algorithms for such spheres along with a comparison to “glued” spheres are presented in (Kodam et al., 2009; Kruggel-Emden et al., 2008; Y. Song et al., 2006). Experimental validation of static packing density and dynamic angle of friction can be found in (M. Kodam, Curtis, Hancock, & Wassgren, 2012), showing good agreement for the investigated tablet shape contact model. Large-scale simulations of these approaches are still beyond current computational capacity and have not yet been reported in the literature. However, this will change in the near future with the increase in CPU power and the advent of new approaches such as running DEM simulations on graphics processors (Radeke, Glasser, & Khinast, 2010).

An overview of the different DEM simulation studies is given in Table 1. As an indicator, the number of particles in the simulation and their shape is stated. It should be noted that this does not reflect the simulation time; this depends on additional factors such as number of variations or the simulated time span.

Table 1: Development of the number of simulated particles and the particle shapes in DEM simulations over the recent years for selected references.

Year	Number of particles	Shape of particles	Type	Reference
1995	600	spherical	Rotating drum	(Yamane et al., 1995)
1999	200	irregular (18-30 glued spheres)	Proof of principle	(Favier et al., 1999)
2000	8880	Spherical	Granulator, liquid bridge model	(Muguruma, Tanaka, & Tsuji, 2000)
2002	11168	Spherical	V-mixer	(Kuo et al., 2002)
2002	2000	Spherical	Angle of repose	(Y. C. Zhou, Xu, Yu, & Zulli, 2002)
2005	1500	Spherical	Angle of repose	(Li, Xu, & Thornton, 2005)
2006	10000	Spherical	Rotating drum	(Pandey, Song, et al., 2006)
2009	7500 - 22500	Spherical	Rotating drum	(Kalbag et al., 2008; Kalbag & Wassgren, 2009)
2011	150	True biconvex tablet shape	Rotating drum, cylindrical packing	(M. Kodam et al., 2012)
2011	2516 / 1163	Spherical / 6 glued sphere	Hopper discharge	(González-Montellano, Ramírez, Gallego, & Ayuga, 2011)
2011	7830	Spherical	Rotating drum	(Ahmadian, Hassanpour, & Ghadiri, 2011)
2011	1168	Irregular (~15-20 glued spheres)	Rotating drum	(Freireich, Ketterhagen, & Wassgren, 2011; Ketterhagen, 2011)
2011	40,000-60,000	Spherical	Rotating drum	(Dubey et al., 2011)
2011	40,000	Spherical	Rotating drum	(Sahni & Chaudhuri, 2011)
2012	26,362	Irregular (1-7 glued spheres)	Rotating drum	(Suzzi et al., 2012)
2013	12,446	Spherical	Rotating drum	(Toschkoff et al., 2013)

B-9.1 Material Input Parameters

The outcome of a DEM simulation depends on the choice of the material properties used for the collision models, including stiffness and coefficients of restitution and friction for walls and particles. The stiffness is commonly described by the elastic modulus; for simulation purposes it is either estimated from available literature values or measured for the used material (e.g., four-point bending techniques (Podczeczek, Drake, Newton, & Haririan, 2006) or compression analysis (González-Montellano et al., 2011)). Measurements can also be performed via rebound tests for particle-wall (Gorham & Kharaz, 2000) and double-pendulum tests for particle values (Wong, Daniel, & Rongong, 2009), or by measuring the yield stress for single granule compaction (Ahmadian et al., 2011). The coefficient of restitution (CoR), defined as the ratio of relative velocities before and after the collision, is used to quantify the elasticity (or plasticity) of a collision. Pandey et al. performed experiments using high-speed video-imaging of a rebounding particle to determine the coefficient of restitution (Pandey et al., 2006b).

Friction coefficients are required for all material pairings occurring in a system. A straight-forward approach to measure friction is to fix an ensemble of particles onto a carrier, and measure the force needed to drag the array over wall or particle materials. In this way, Li et al. (2005) determined the friction of glass and steel spheres moving over Perspex® or steel walls. They reported a constant friction coefficient for these material pairings, as presumed by conventional friction theory. González-Montellano et al. (2011) measured particle-wall friction according to the technique by (Couroyer et al., 1999). Another possibility is to measure the bulk coefficient of friction using a Schulze ring shear cell (or other shear testers) and adjust the particle-particle coefficient in simulations to achieve the same bulk coefficient of friction (Ahmadian et al., 2011). Just et al. (2013) show the measurement of the mechanical parameters Young's modulus, coefficient of restitution (CoR), and of friction coefficients of coated and uncoated tablets (gastrointestinal therapeutic systems). In addition to the direct measurement, revised bulk friction coefficients were determined. This was done by comparing the dynamic angle of repose of the tablets in a drum coater from both, experiment and DEM simulation.

With regard to the macroscopic flow of a granular material, DEM simulations are sensitive to certain parameters such as friction (Remy, Canty, Khinast, & Glasser, 2010), while others (e.g., CoR and especially stiffness) can be changed without significantly influencing the outcome (Freireich, Litster, & Wassgren, 2009). Kuo

et al. reported that changes in the stiffness within a reasonable range had no major impact (Kuo et al., 2002). Similarly, Ketterhagen found that the elastic modulus could be increased by two orders of magnitude without significantly changing the outcome (Ketterhagen, 2011). For pan coating, the coefficient of sliding friction had a pronounced effect on the inter-tablet variation and the flow profile (Kalbag & Wassgren, 2009). Zhou et al. showed that the static angle of repose of glass beads depended on the sliding and rolling friction and was unaffected by density, Poisson's ratio, CoR and elastic modulus (Y. C. Zhou et al., 2002). In addition, it was found that the dynamic angle of repose was greatly influenced by friction coefficients (Pandey et al., 2006b). Ketterhagen et al. performed measurements of the rolling resistance for different tablets (Ketterhagen, Bharadwaj, & Hancock, 2010). An experimental investigation of the kinetic friction of tablets based on a pin-on-disk setup was presented in (Hancock, Mojica, St John-Green, Elliott, & Bharadwaj, 2010). While it is important to measure the parameters in question, a sensitivity study showed that DEM simulations were surprisingly robust (Freireich et al., 2009). Such macroscopic properties as velocity and solid fraction fields were especially insensitive to the stiffness and coefficients of restitution of the particles.

B-9.2 Inter-Tablet Coating Variability.

As pointed out above, the inter-particle variability $C_{v,inter}$ as defined in Eq. (7) is of major interest for many processes. Experimentally, $C_{v,inter}$ is normally investigated by performing a coating run, taking tablet samples during or after the run, and determining their coating mass. One challenge is to find a method for coating mass determination that is both accurate and fast. For meaningful results, the sample size should be large. In DEM simulations, one also has to find a way to model the spray, that is, to quantify the amount of coating a tablet receives. However, once this is done, the simulation yields the coating mass of all tablets at all times. From this large amount of data, the $C_{v,inter}$ can be determined with very high resolution. This is one of the reasons why the DEM has seen widespread application in this field. Investigations differ in the type of apparatus used, and to some extent in the way the spray is modeled (Toschkoff et al., 2013). Most include at least variations in the rotation speed and fill level of the coating drum.

Dubey et al. (2011) investigated the effect of rotation speed, fill level and spray patterns on mixing and coating uniformity. Three speeds (4, 6, 8 rpm), 100% and 67% loads and four spray patterns were studied. The residence time of tablets in the spray zone was gathered to quantify coating in a post-processing step. For one parameter setting, the DEM residence time results were compared to the

coating thickness measurements using laser-induced breakdown spectroscopy. The results showed that both followed a similar distribution. The spray pattern had a significant effect, indicating the importance of axial mixing. Although the coating uniformity increased with the rotation speed, for the investigated range the effect was weak. Remarkably, higher fill levels led to better uniformity, probably due to a poor mixing performance at lower fill levels. The difference between the fill levels was smaller for high rotation speed. In two related works, Sahni et al. (Sahni & Chaudhuri, 2011; Sahni, Yau, & Chaudhuri, 2011) studied the mixing and coating of spherical particles in a lab-scale spheroid pan coater without baffles via experiment and simulation. They aimed at calculating the total number of particles passing through the spray zone and the frequency distribution of the residence time. Variation parameters were the pan tilt, the rotation speed (10, 20, 30 rpm) and the fill level (21, 37, 48%). In addition, for the experimental coating runs, spray fluid concentration and spray flow rate were altered. White- and red-colored lactose spheres were loaded following certain patterns, and to quantify mixing, video imaging and thief samplers were used. Coating was simulated by recording the spray zone residence time in post-processing. Experimental and DEM results for mixing showed reasonable agreement. For coating, no comparison of the results was made.

A combination of experiments, computer simulations and accompanying analytical treatment is described in (Kalbag et al., 2008). Overall, spherical particles were used. Experiments were performed by placing a single tracer particle in the pan coater and recording the spray zone with a digital camera. Simulations were based on DEM, and a solid fraction-based algorithm was used to determine which spheres were in the spray zone. Although the algorithm did not allow for partial tablet exposure, a more accurate and computationally intense ray-tracing-based algorithm produced similar results. Different coater fill levels and rotation speeds were investigated. The ranges were 3.6-7.2 kg and 8-16 rpm for the experiments and 3.6-10.8 kg and 8-32 rpm for the simulations. The results were presented in terms of appearance frequency, average fractional residence time and related quantities. Appearance frequency is the number of times a tablet appears in the spray zone during one revolution of the drum. Both experiments and simulations confirmed well-known analytical models. The DEM simulations showed that the distribution of the single-visit residence time (t_{SVRT}) became narrower with the increasing pan speed. This means that at high rotation speed tablets tend to spend the same (short) time in the spray zone and at low rotation speeds some tablets spend a longer time in the spray zone with wider distribution, which negatively affects the coating uniformity. Both the average

and the variation of t_{SVRT} distribution decreased with the increasing rotation speed for all loads, as is commonly reported (Chang & Leonzio, 1995; Denis et al., 2003; Sandadi et al., 2004). The results for different loads followed no simple trend. On the one hand, smaller loads with a higher sprayed-to-total-tablets ratio yielded better uniformity. On the other hand, as Dubey et al. (2011) indicated, larger loads resulted in better mixing which in turn promoted uniformity as well. As such, the worst uniformity results were obtained at medium loads (~6 kg). However, this was most noticeable for low pan speeds and less so or not at all at high speeds.

The average fractional residence time was insensitive to the pan speed, inversely proportional to the load and constant over coating time. This also follows from Eq. (10) above. The standard deviation of residence time (i.e., the coating uniformity) was in good approximation proportional to the square root of time, which was expected for randomly mixed systems (Cheng and Turton, 2000b). By assuming that the mean residence time increases linearly with the coating time, the relative standard deviation (i.e., standard deviation divided by the mean) was inversely proportional to the square root of the coating time, as commonly reported in the literature.

From the DEM data it also followed that the appearance frequency was linearly proportional to the ratio of sprayed to total tablets and that it decreased with $\frac{1}{4}$ power of the Froude number, as predicted in (Alexander et al., 2002) for speeds higher than the transition speed. Higher friction coefficients (both for tablet-tablet and tablet-steel contacts) also increased the dimensionless appearance frequency, defined as the number of appearances a tablet makes in the spray zone during one pan revolution.

DEM simulations for a cycled continuous coating apparatus were performed by Suzzi et al. (2012). Three tablet shapes (round, oval, bi-convex) were modeled using the glued-sphere approach, each with three fill levels (15, 18, 21 kg). Friction coefficients and the coefficient of restitution were based on measurements. Coating was modeled based on the residence time in a cylindrical spray zone. In all cases, an increase in the coater's fill ratio led to slower mixing and to an increase in the relative standard deviation (RSD, here denoted by c_v) of the fractional residence time. While round and oval tablets showed similar trends, bi-convex tablets were less affected by the fill level. The time evolution of the relative standard deviation of binary mixing, $c_{v, \text{mix}}$, was modeled as a function of the number of revolutions N_{rev} by the exponential law:

$$c_{v,\text{mix}}^2 = c_{v,r}^2 + \exp(-k_{\text{mix}} N_{\text{rev}}). \quad (28)$$

where $c_{v,r}$ is the RSD of a random binary mixture and k_{mix} is the mixing constant that is determined via fitting and subsequently used to quantify mixing performance. The tablet flow was investigated in terms of translational and rotational velocities and granular temperature (i.e., local variation in velocity).

Pandey et al. compared a MATLAB-based DEM code with video imaging results using a tracer particle (Pandey et al., 2006b). Polystyrene spheres were placed a narrow rotating drum, amounting to a fractional fill volume ϕ (defined as volume of bed / pan volume) between 0.1 (4700 spheres) and 0.17 (7500 spheres). Also the pan speed varied (6, 9 and 12 rpm). The dependence of the dynamic angle of repose on the above-mentioned parameters and on the friction coefficients was investigated. The measured velocity profiles in the spray zone showed qualitative agreement with the simulations. The maximum velocity was found to be close to the mid-point of the cascading bed surface. Based on the data, the scaling law for surface velocities described by Alexander et al. (2002) was extended to include the effect of pan loading, resulting in the above-mentioned Eq. (19).

New insights into the mechanics of inter-tablet coating variability were gained by combining experiments, DEM simulations and an idealized analytical model in (Kalbag and Wassgren, 2009). A periodic random coating model was proposed: to simulate one coating event (one trial), a number of n_p tablets were randomly selected from all N_p tablets, to which a defined coating mass was applied. The random selection and coating application was repeated τ times (that is, τ trials were done). The inter-tablet uniformity $c_{v,\text{rand}}$ for this random coating process was derived as a function on the number of trials τ :

$$c_{v,\text{rand}}(\tau) = \sqrt{\frac{1}{\tau} \left(\frac{1}{n_p / N_p} - 1 \right)}. \quad (29)$$

The numbers of trials τ is basically a measure for the coating time. Therefore, Eq. (29) shows that even from this basic model it follows that the coefficient of variation is inversely proportional to the square of coating time, a behavior that is often described in literature. With some assumptions (e.g., uniform mass flux in the spray zone), an equation for a non-ideal (realistic) coating process is derived as:

$$c_{v,inter}(t) \approx k \sqrt{\frac{2\pi}{\omega} \frac{l}{w} \left(\frac{D}{d_p}\right)^{1-a}} \phi^{1-b} Fr^c. \quad (30)$$

where ω is the rotation speed, l is the coater length, w is the span-wise spray zone width, D is the pan diameter, d_p is the particle diameter, ϕ is the fill fraction and Fr is the Froude number, defined in Eq.(14). Constants k , a , b and c were determined by fitting to the experiments. Based on the literature data (Alexander, et al., 2002; Pandey, Katakdaunde, & Turton, 2006; Pandey, Song, et al., 2006), the following equation was derived:

$$c_{v,inter}(t) \approx 4.5 \sqrt{\frac{2\pi}{\omega} \frac{l}{w} \phi^{0.68} Fr^{-0.10}}. \quad (31)$$

Furthermore, a generic set of equations was proposed to determine which settings result in a coating mass distribution with a given mean and maximum spread. As such, the coefficient of variation of the coating mass distribution can be decreased as follows:

- by decreasing the effective spray coating mass flow rate,
- by increase the number of tablets in the spray zone,
- by increasing the mixing efficiency,
- by decreasing the total number of tablets.

B-9.3 Intra-Tablet Coating Variability

DEM has been used less frequently for studying intra-tablet uniformity than inter-tablet uniformity. A comprehensive analysis for tablets of six different shapes was performed by Ketterhagen (2011). The tablets were modeled as glued spheres, and the pan speed (16-28 rpm) and loading (1-2 kg) varied. To identify which tablets were coated, the spray zone was defined and further divided into rectangular bins. Only the uppermost tablet in each bin was considered. The bin size was a critical parameter calculated from the tablet length L_p , width W_p and thickness T_p according to $b = 1.5 \sqrt[3]{L_p W_p T_p}$.

This way, inter-and intra-tablet uniformities were obtained. For the inter-tablet uniformity, the single visit residence time t_{SVRT} and the circulation time between

appearances t_{SCT} were determined. Comparing them to the experimental results for the bi-convex tablet shape showed very good agreement. For the intra-tablet uniformity, the orientation of tablets in the spray zone was taken into account. The orientation index OI was introduced to quantify the randomness of tablet orientation and thus provides a measure for the intra-tablet uniformity. A relationship between OI and the tablet shape (expressed via sphericity or aspect ratio) was studied (Figure 11). The main result was that the more a tablet deviates from spherical shape, the lower the intra-tablet uniformity will be, which could be helpful for designing a new product. A closer investigation of the most non-uniform shape (almond shape) showed that decreasing the pan load and increasing the rotation speed led to increased inter-tablet uniformity, although the effect was relatively minor.

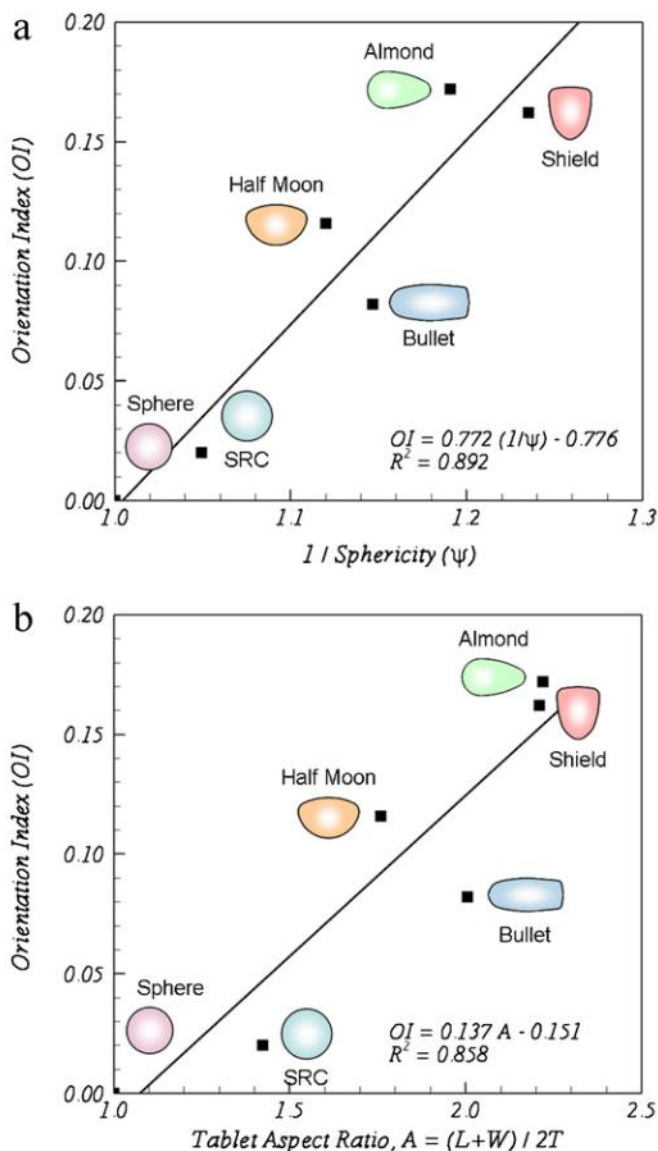


Figure 11: Relationship of the tablet orientation indices predicted based on the DEM data and the tablet sphericity (a) or aspect ratio (b). Taken from (Ketterhagen, 2011).

B-9.4 Liquid Forces and Liquid Transfer

When a newly-sprayed tablet collides with another tablet, mainly two additional effects could affect the outcome: a transfer of the still-wet coating may occur, and new (cohesive) forces due to the liquid may influence the flow behavior (Lekhal, Conway, Glasser, & Khinast, 2006; Radl, Kalvoda, Glasser, & Khinast, 2010) .

Depending on how fast the tablets are dried in a given coating process, the effect may have serious impact on the coating quality (although in many applications drying is sufficiently fast that these effects can be neglected).

A model that accounts for liquid transfer in DEM simulations was presented by Shi and McCarthy (2008). Moisture levels were tracked for each particle, with the simplification that liquid was evenly distributed on the surface. The model was based on liquid bridges that form between two particles and includes cohesive and viscous forces and the redistribution of liquid by the liquid-bridge rupture. By applying it to a simplified coating process, it was established that $c_{v,inter}$ was inversely proportional to the square root of the coating time. When the capillary force was smaller than the particle weight, the c_v showed a clear tendency to approach zero as the coating time increased, while for capillary forces greater than the particle weight, the c_v was predicted to converge to a non-zero value with increasing time.

Nase et al. (2001) studied the effect of (predominantly capillary) cohesion in granular materials and proposed a model for cohesion forces in DEM simulations using tabulated values. The static and dynamic angles in hopper discharge and rotating pan setups were studied via experiments and simulations and were in good agreement. Two dimensionless numbers for characterization were proposed: the Granular Bond Number Bo_g (the maximum capillary-force-to-the-particle-weight ratio) and the Collision Number Co (the maximum cohesive-force-to-the collisional-force ratio).

Muguruma et al. (2000) included water adhesion into a DEM simulation to investigate particle movement in a rotating fluidized bed granulator. The adhesion force was calculated based on the liquid bridge formation between the particles. The liquid bridge model ignored viscosity effects and liquid transfer and assumed that particles had a uniformly distributed coating and that the contact angle was zero. It showed that the adhesion greatly affected the particle flow. Although high-speed particle tracking velocimetry confirmed the trends for velocity profiles, the results differed quantitatively.

Song and Turton (2007) studied the influence of liquid bridges on colliding tablets. A linear relationship between normal force and normal displacement was assumed, with different stiffness for loading and unloading. Tangential forces were estimated using an incremental slipping friction model. Additionally, the adhesive and viscous forces were modeled based on the work of Muguruma et al. (2000) and Nase et al. (2001). To determine the required parameters, tablets

were covered in a thin film of liquids of different viscosities, and high-speed videos of tablet-tablet collisions were made.

B-10 CFD-DEM Coupling

Fluidized bed coaters are in a sense more difficult to simulate than drum coaters, and as mentioned cannot be treated in detail in the scope of this work. In a fluidized bed, the movement of fluid and particles and especially their interaction play a major role, and thus the air flow cannot be neglected as is often justified for drum coating. Detailed results can only be achieved via a combination of CFD and DEM methods, which for most processes is at the limit of current computational power. Much effort has been made to fully couple CFD and DEM (Fries, Antonyuk, Heinrich, & Palzer, 2011; Z. Y. Zhou, Yu, Nakagawa, & Luding, 2009). However, larger-scale applications for coating prediction are still scarce (Jajcevic, Radeke, Scharrer, & Khinast, 2012; Jajcevic et al., 2013). A few models included DEM to account for the fluid flow. Terashita et al. (2000) used DEM simulations to study a new draft-tube design in a fluidized bed coater. An additional drag force was applied to particles to model the fluid flow.

B-11 Monte Carlo Method

The Monte-Carlo (MC) method can be seen as a class of stochastic computational techniques based on repeated random sampling to obtain results. The random sampling is done according to certain probability distributions. In a sense, the MC does not directly model a system as a whole, but rather samples a larger number of random configurations of the system to describe it. The MC method itself is generally applicable and used in different fields. To be applied in coating simulations, it depends on input that describes the general nature of the system (such as the behavior of tablets or the nature of the spraying process). From this, the MC method is able to predict the expected outcome of a process for different settings of the underlying model parameters.

The needed input data can come from theoretical models, simulation tools and/or experimental data. To be accessible to MC, most coating systems are divided into at least two regions: the spray zone and the rest of the system, where mixing and drying occur. The process is strongly governed by the nature of these zones, the time the particles stay in the two zones and the particle propagation from one zone to the other. These underlying principles are investigated experimentally and/or theoretically, and the gained knowledge is used to build a

Monte Carlo model. Once the model is set up, it is able to predict the (long-term) outcome of a coating process.

In an early work going in the direction of drum coating but not including a spray, MC was applied to simulate mixing in rotating drums (Cahn & Fuerstenau, 1969). More recently, Kohavet al. (1995) used it to investigate six models to predict mixing by axial dispersion in a rotary kiln. The simulation suggested less dispersion than observed in the experiments. Pandey et al. (2006a) investigated the influence of different parameters (coating time, spray shape and area, pan loading, pan speed, particle diameter and spray flux) on the inter-tablet uniformity $c_{v,inter}$, Eq.(7), in a drum coating process. Two main inputs were required for a MC simulation: first, information on the tablet movement (e.g., location and velocity of tablets, circulation time distribution and projected surface area), which was gathered using video-imaging of the coating process, and, second, spray dynamics, including the spray area and shape, and spray flux distribution, which was collected from measurements. It was established that $c_{v,inter}$ was inversely proportional to the square root of the coating time t_c :

$$c_{v,inter} \sim 1/\sqrt{t_c} . \quad (32)$$

Variability decreased with increasing pan speed, increased axial spray zone dimension, decreased particles size and a uniform spray distribution compared to a center-heavy one. Verification experiments confirmed the trends for the fill level and the pan speed, but the $c_{v,inter}$ values from simulation were significantly lower than that in the experiments. Based on the MC simulation and a statistical analysis of experimental results, the dependence of $c_{v,inter}$ on the investigated parameters is proposed:

$$c_{v,inter} = k \frac{d_p^{1.2} N_p^{0.5}}{\omega^{0.4} t_c^{0.5}} , \quad (33)$$

where d_p is the particle diameter, N_p is the number of particles, ω is the pan speed and k is a constant.

Nakamura et al. (1998) used MC to describe a tumbling fluidized bed. In their model, a random walk of seed particles was simulated by taking into account the rotation speed and fitting to the experimental data. Particles reaching the designated spray zone received coating. For this model, the distribution of the number of visits to the spray zone followed a normal distribution. The results showed that the coating mass uniformity increased with longer coating time and with high mixing rates. The simulation confirmed the quantitative trends

determined based on the experimental data (Abe, Yamada, Hirose, & Nakamura, 1998): while the effect of the particle size on coating uniformity was not the same, the effects of the other operation conditions were reproduced.

KuShaari et al. (2006) proposed a MC model for calculating the coating uniformity in a bottom-spray fluidized bed with a Wurster tube. The movement of particles was modeled as a random walk so that the velocity distributions matched the data from the high-speed image analysis in (Subramanian et al., 2003). Spherical particles in the simulation involved the same surface area of standard round convex tablets as the one used in experiments. When the particles entered the spray zone, they received coating based on the local spray flux. Additionally, the voidage profile between the particle and the nozzle was considered and used to account for partial covering of the particles. The results were in agreement with the model of Cheng and Turton (2000b). Predictions were made for the coating uniformity resulting from different gas velocities and gap heights.

Choi and Meisen (1997) presented a model for a fluidized bed, including one-dimensional continuity and momentum equations for gas and solids in the spout and mass balance equations for the applied sulfur coating. Two different models are applied: a simple but quick model, and a more advanced model incorporating hydrodynamics and inertial impaction. The latter partitioned the fluidized bed into three zones: spout, annulus and fountain. The underlying assumption was that the particles in the spout and annulus region can be modeled as a plug flow, while particles in the fountain are assumed perfectly mixed. The amount of coating a particle received was calculated based on the residence time of the particle in the spout region. The models were used to estimate the distribution of the coating material over the particles.

Jogkellar et al. (2007) proposed a MC model to predict coating mass variability in a pan coater. It was assumed that the number of tablets in the coating zone was constant and the residence time in the spray zone was the same. Kandela et al. (2010) used MC simulations together with video imaging experiments to study the effect of the pan load (10 kg and 12 kg), the speed (4-12 rpm) and the tablet shape. Inter- and intra-tablet uniformities were some of the quality attributes considered. The tablet shape was quantified as sphericity, expressed as the ratio of the surface area of an equivalent sphere to the surface area of the tablet. The two inputs for MC were spatial movements of the tablet (from video imaging) and spatial distribution of the spray flux (analytical approximation).

Freireich and Wassgren (2010) investigated intra-particle coating variability ($c_{v,intra}$) for spherical particles using analysis and MC simulations, including a DEM case study. Basically, the spheres were sprayed from a certain direction, leaving a partial coating on roughly one half of the sphere. This was repeated multiple times using different orientations of the particle. The $c_{v,intra}$ was then calculated as the ratio of the film height standard deviation (calculated over the whole surface) to the mean film height. They showed that as long as the particle was convex, uniformly random orientations in the spray zone led to $c_{v,intra}$ proportional to the inverse square root of the number of coating events, eventually approximating zero (perfectly uniform coating). If a particle has a preferred orientation, as it does for many tablet shapes (Ketterhagen, 2011), $c_{v,intra}$ will approach a non-zero value even for an infinite number of coatings. More recently, Freireich et al. (2011a) applied the above-mentioned model to DEM data in (Ketterhagen, 2011) and found that qualitatively $c_{v,intra}$ was smaller for tablet shapes with a greater degree of symmetry. In all cases, the coating thickness on the edge was lower than on the top/bottom, with differences of up to 30%.

B-12 Population Balance

An approach that is connected to the MC method (described above) is using Population Balance Equations (PBEs). PBEs are used to describe how “populations” of separate particles develop in certain properties, such as coating mass, with time. Mathematically, they are a set of integro-partial differential equations; the connection to the MC method is that it can be applied for the solution of the PBEs, and that both heavily depend on input data describing the system.

In the application to coating processes, the amount of coating a particle gets is commonly calculated from the time it spends in the spray compartment. The used models then define compartments/regions the particles can be located in, and describe the particles flow between the compartments. In the most straightforward models, two compartments are defined, representing the spray zone and the circulation region.

One of the first two-compartment models was proposed by Sherony (1981), with particles coated in one compartment and dried in the other. The probability that a particle moves from one compartment to the other was proportional to the number of particles with the same weight in that compartment. Based on this basic model and assumptions, $c_{v,inter}$ is approximated as:

$$c_{v,inter} = 1.25 \sqrt{\frac{(1-\beta)\mu_{ct}}{t_c}}, \quad (34)$$

where β is the volume fraction of the solids in the spray region and μ_{ct} is defined according to Eq. 9. The relative standard deviation $c_{v,inter}$ is proportional to $1/\sqrt{t_c}$; this is in line with the results found using DEM as presented in section B-9.2 (see also Eq. (29)). A similar two-component model was proposed by Wnukowski and Setterwall (1989) for a top spray fluidizer bed coater with the same square-root dependency for t_c . In their work, they developed an analytical transformation of population density functions and a numerical solution for the population balance equations. The model assumed two well-mixed zones. In general, a population balance model using two well-mixed compartments needs input data for the fraction of particles that are in the active zone and for the circulation rate of particles between the well-mixed zones. Both are difficult to estimate experimentally. An extended model included a third compartment to account for more complex flow phenomena (Maronga & Wnukowski, 1997). Liu and Litster (1993) used a population balance model to predict the (inter-particle) coating mass distribution for a continuous spouted bed coater. When a size-dependent growth term was used, the results of the population balance simulation were in good agreement with experimental data, which was not the case for size-independent growth term model predictions. For no obvious reason, larger particles were coated preferentially. The simulations also predicted a more uniform coating mass distribution for batch operation of the spouted bed granulator than for continuous operation (that is, where large particles are continuously removed from the top of the granulator).

Eldredge and Drown (1999) developed a compartment model for a continuous fluidized bed coater and calciner, including spraying, attrition and fines removal. A surface renewal two-compartmental population balance model for pan coating based on the model in (Sherony, 1981) was proposed by Denis (2003). The compartments are a perfectly mixed domain (i.e., the cascading upper layer where tablets are coated), and a plug flow region (the bulk of the bed). The three parameters used were the size of the spray zone, the spray rate and the turnover time of tablets in the bed. The study showed that although the coating distribution was asymmetric, it could roughly be approximated by normal distribution for longer coating times. The predicted coating mass distribution was in agreement with the experimental data. From the experiments it also followed that the turnover time was inversely proportional to the rotational speed and that it depended on the fill level. More recently, Freireich et al. (2011b)

developed a sophisticated population balance model that used input data from DEM simulations of particle movement. It was proposed for a mixer-coater, but the principle is valid for other particle processes as long as the underlying assumptions hold. From the DEM data, the SVRT distribution was extracted for each region (spray zone and bed zone). A sub-compartment model was then generated to reproduce the SVRD distribution, based on which a system of population balance equations was formulated. This way, only a small fraction of the entire process had to be simulated via the computationally-intense DEM method, from which the PB model took over to calculate the long-term estimates. This combined approach can help to decrease computation time for large systems and/or longer simulation times.

B-13 Summary

Coating of particles (pellets, tablets, etc.) is an important process step in many industries. This is especially true in a pharmaceutical setting. Typically, the coating layer is crucial for the proper functionality of the end product. As a consequence, high quality, reliability and efficiency are expected of the coating process. To achieve this goal, significant research efforts have been devoted to this topic, which are still ongoing. For a deeper understanding of the process, it is helpful to combine the knowledge from:

1. Experimental investigations, which provide data of the process and the properties of the involved particles and substances. Experiments are the most direct approach, and closest to reality.
2. Computational simulations, which offer highly resolved data. For example, the velocities of all particles are virtually impossible to gather by experiment, but readily available from simulation.
3. Mathematical modeling to understand the underlying principles, often based on input data gathered from experiment and simulation. The result is often an analytical expression that may be based on an approximation, but is still immensely useful to provide a quick estimate of process characteristics.

This work gives an overview of recent work related to the latter two, modeling and simulation. Where it makes sense, experimental work has been included as well.

In summary, from all presented approaches, the analytical models (simple expressions predicting coating quality) are the fastest and easiest to apply, but also the least detailed ones. Even with a significant increase in computational power such simplifications will always have their merits. A higher level of information is provided by Monte Carlo and/or population balance models. These models are still abstract to a degree, but yield much more information. The resolution is sometimes limited, but for many applications it is high enough, making those approaches a good trade-off between accuracy and required computational resources. Finally, methods such as CFD and/or DEM aim to directly capture the physical system. For many systems, this is nowadays possible, and with the continuously increasing computational power, larger systems and higher resolutions will become possible soon. These simulations may also be used for generating or parametrizing analytical models that are straightforward to apply.

The collected knowledge available in the referenced literature provides helpful insights and a deep understanding of the underlying mechanics, and can serve as a valuable tool for the process design and optimization.

Acknowledgements

The Research Center Pharmaceutical Engineering is a K1 Competence Center initiated by the Federal Ministry of Transport, Innovation & Technology (BMVIT) and the Federal Ministry of Economy, Family & Youth (BMWFJ). We acknowledge funding by the Austrian Research Promotion Agency (FFG), Land Steiermark and the Styrian Business Promotion Agency (SFG).

B-14 Notation

B-14.1 Latin symbols

Symbol	Meaning	Unit
b	bin size	m
C_p	specific heat capacity at constant pressure	J/(kg K)
c_v	Coefficient of Variation (relative standard deviation)	-
d	Diameter	m
D	Drum diameter	m
f	fractional time	-
g	gravitational acceleration	m/s ²
L	Drum load	kg
L_{vap}	latent heat of evaporation	J/kg
m	mass	kg

n	number	-
N	total number	-
Q	volumetric flow rate	m^3/s
T, t	time	s
v	velocity	m/s
V	Volume	m^3
w	spray width	m
x	fraction	-

B-14.2 Dimensionless numbers

Ar	Archimedes number
Fr	Froude number
We	Weber number
Re	Reynolds number (here: for a sphere)
Oh	Ohnesorge number
Co	Collision number
Bo_g	granular Bond number

B-14.3 Greek Symbols

Symbol	Meaning	Unit
α	coating fraction (ratio of particles in the spray to total particles)	-
μ	without subscript: dynamic viscosity with subscript: mean of the variable denoted by the subscript	Pa s
ν	kinematic viscosity	m^2/s
\dot{v}	Spray rate	g/min
π	Ludolph's number	-
ρ	density	kg/m^3
σ	without subscript: surface tension with subscript: standard deviation of the variable denoted by the subscript	N/m
τ	Number of trials	-
ϕ	Filling degree of the drum, fractional fill volume	-
ω	Rotation velocity (of the drum)	rad/s, often also rpm

B-14.4 Subscript

0	Relating to the total process or the initial state
air	relating to the surrounding air/gas.
c	coating
circ	Circulation in the tablet bed (as opposed to "in the spray zone")

ct	cycle time
d	relating to the drop
g	relating to the gas/fluid
in	inlet
inter	between particles
intra	over a single particle
l or liq	relating to the liquid
cpp	coating per pass
mf	minimum fluidization
p	particle (for consistency also used for the special case “tablet”)
R	residence
rel	relative
RT	room temperature
S	solvent
SCT	Single Cycle Time
SVRT	Single Visit Residence Time
t	terminal
v	velocity
32	denoting a diameter as Sauter mean diameter

B-14.5 Superscript

\bar{x}	mean of variable x
\dot{x}	rate of change over time of variable x

Chapter C: Detailed Analysis of Air Flow and Spray Loss in a Pharmaceutical Coating Process

Published as: Toschkoff, G., Suzzi, D., Tritthart, W., Reiter, F., Schlingmann, M., & Khinast, J. G. (2012). Detailed Analysis of Air Flow and Spray Loss in a Pharmaceutical Coating Process. *Aiche Journal*, 58(2), 399–411.

C-1 Abstract

In the pharmaceutical industry, more than half of all tablets receive a film coating. A commonly used technique is drum coating, where a film solution is applied to the moving tablets by a spray nozzle. Important process parameters include the amount and temperature of drying air, as well as spray nozzle position. Among other influences, the proper adjustment of these parameters has a great impact on spray loss, defined as the fraction of spray liquid that does not form a film on the tablets. Often, the lack of scientific data hinders a process setup based on engineering principles, resulting in operational conditions based on trial-and-error approaches. Here we show how a coating system can be numerically modeled by means of computational fluid dynamics (CFD) techniques. Furthermore, we present how different parameters affect the efficiency of the process, leading to a deeper understanding of the coating device.

C-1.1 Keywords

Multi-phase flow, Computational fluid dynamics, pharmaceuticals, tablet coating, spray loss

C-2 Introduction

For many pharmaceutical products, the application of a coating layer to tablets or granules is an important step in the production process. According to the IMS Midas Database for 2007 (IMS Health Care, USA), for more than 50% of all tablet products, applying a coating is part of the production process. The purpose of coating application can be roughly divided into two categories: functional and non-functional. Functional coatings are used for taste or odor masking, to change the dissolution behavior or to add additional active ingredients. A non-functional

coating is, e.g., a colored outer layer whose sole purpose is the increase of visual attractiveness and recognition value.

In all of these cases, both intra-tablet and inter-tablet uniformity of the film is of great importance (Tobiska & Kleinebudde, 2003). *Intra*-tablet uniformity is a measure of the variation of film thickness on a single tablet, whereas *inter*-tablet variation is the difference in film mass and quality between different tablets. If, for example, the purpose of the film is to protect the API from gastric juices, a single tablet with insufficient film thickness or quality can lead to the rejection of the whole batch.

In the course of the coating process, a tablet normally passes through a spray zone multiple times, where each time a partial coating layer is applied. For a single tablet, the time between two coating events, as well as the local film distribution in a single coating event, can differ considerably. If the variation between two events is large, a large number of partial coatings have to be applied to reduce statistical variance and to get a uniform coating layer. This way, the varying and poorly controlled conditions for a single event can be statistically compensated by the high number of tablet passes under the spray region. However, this results in a drastic increase in process time and, as a consequence, a decrease in efficiency. Therefore, it is highly desirable to understand and control the coating process as well as possible.

In this study, we focus on pan coaters, where tablet cores are placed in a rotating drum, and a film-building liquid is applied to the moving tablets by means of one or more spray nozzles. In every real, non-idealized tablet coating process, there is a certain percentage of liquid that does not end up forming a film on the surface of the tablets. This so-called spray loss is known as a critical issue for many surface treatment applications, for example in the paint, coating and metallurgical industry (Davis, 2004) and is encountered in the pharmaceutical industry as well, e.g., in particle and tablet coating (Rähse, 2009) or fluidized bed devices (Schreiber, Vogt, Werther, & Brunner, 2002). A corresponding quantitative indicator is the spray yield, i.e., the ratio of the deposited spray material mass to the total mass introduced. For pan coating, the spray loss can be divided into two components:

- the liquid that ends up forming a film on the coating apparatus, and
- the non-depositing droplets that are removed with the drying air.

The problem associated with the first component lies in the increased efforts necessary during the cleaning process. The second component consists of partially or totally dried spray droplets, which are contained in the exhaust air and in most cases have to be removed by means of a filtering system before the drying air can be allowed into the environment. Eventually, the filters have to be cleaned or disposed, introducing an additional time- and cost-consuming component to the process. Thus, minimization of spray loss represents an important factor for the enhancement of efficiency and profitability of the coating process

Another important topic in aqueous tablet coating is the water content of the air inside the coater. In many cases, the tablet cores are sensitive to water, and humidity should be kept as low as possible. The acceptable range of water content cannot be stated in general, and largely depends on the properties of the tablet cores and the film forming liquid. While it is possible that problems arise from too dry tablet surfaces, normally the more significant concern is an over-wetting of tablets (as this may lead to hydrolysis of the API in the final formulation). However, the spray coating process as such demands the application of a water- (or solvent-) based liquid. As a result, it is desirable that the water (or solvent) is removed fast and efficiently by the drying air, in this way maximizing the spray rate that can be used without over-wetting the tablet bed. Thus, the drying capacity of the system should be maximized.

To a large extent, coating quality and especially spray losses depend on the quality of the spray produced by the nozzle. The most important parameters in this context are size and velocity distribution of the spray droplets. Also, as stated above, a significant amount of drying air has to be introduced, creating a pronounced air movement throughout the device. The behavior of the spray droplets after leaving the nozzle, and with it the amount of spray loss, depends to a large part on this air stream inside the coater.

Traditionally, the optimization of pharmaceutical processes is often based on empirical analysis. Although many input variables can be monitored in an experimental setup (Ruotsalainen et al., 2002), an analysis of the spray's behavior in the coating process by experimental measurements is hard to accomplish, especially for a production-scale coating apparatus. An alternative approach that sees increased use nowadays is the application of modern computational simulation tools. They allow overcoming some of the limitations of experimental measurements, thus offering the opportunity to get a deeper understanding of the process. So far, computational investigations of coating

processes have mainly concentrated on two aspects: the statistics of the tablet movement (Freireich & Wassgren, 2010; Mueller & Kleinebudde, 2007b), and the local film formation on the tablet surface (Kalbag & Wassgren, 2009; Suzzi et al., 2010). To our knowledge, apart from a work on the influence of different parameters on the spray shapes in a lab coater (Muliadi & Sojka, 2009), no work has been published focusing on the description of the drying air stream inside the coater and its influence on the spray.

The aim of this work is a novel application of computational fluid dynamics (CFD) to study the air stream inside an industrial-scale pan coater and its impact on the spray behavior inside the coater. The effects of air flow, spray nozzle position and orientation on spray loss and product quality were investigated. The following steps were performed:

- Determination of the size- and velocity distributions of the spray droplets by means of PDA measurements;
- Implementation of the spray in the CFD simulations in accordance with the measurements;
- Modeling of the deposition on the tablet bed, the coating process, the evaporation of the spray and the wall film in order to estimate the effects of the drying gas flow;
- Post-processing of the simulation data to arrive at both qualitative and quantitative conclusions.

In the next section, the setup of the investigated pan coating system is described. First, the geometry of the pan coater is reported, followed by the definition of the operating conditions. Next, the experimental characterization of the spray is presented and the adopted numerical methods are then described, followed by the results of our numerical investigations. Finally, a detailed discussion of the results and a conclusion is presented.

C-3 Materials and Methods

In the following, the coating system used for the investigations is described. Process parameters are presented, the positions of the tablet bed and the spray nozzle are provided, and the spray characterization by the application of PDA measurements is described.

C-3.1 Characterization of the coating system

A drum coater with a non-perforated rotating drum (Nicomac Coating System classic 350, Nicomac srl, Italy) was investigated. Figure 12 shows a schematic drawing of the coating process.

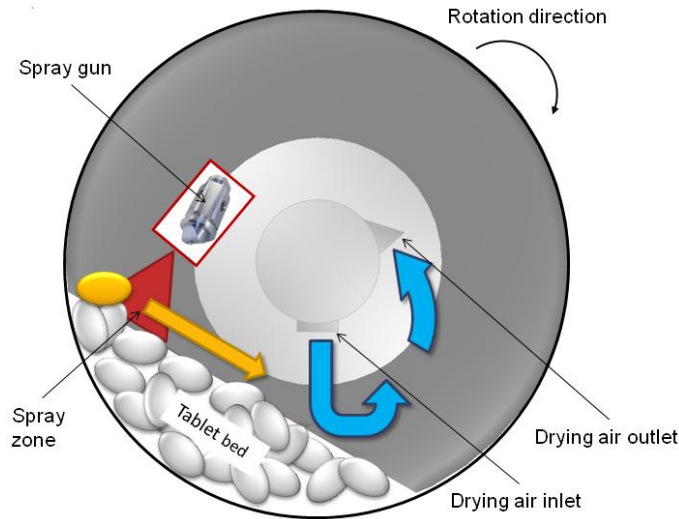


Figure 12: Schematic representation of a coating process in a drum coater. A tablet emerging on the top enters the spray zone and the drying air zone before re-entering the bed.

Along the rotational axis of the coating drum, separate channels for incoming and outgoing drying air are located inside a metallic cylinder. At the upper left of the cylinder, the spray gun system is mounted. The drying air enters the drum at the bottom of the cylinder and the exhaust air is removed at the upper right location. The parameters characterizing the coating process are listed in Table 2. These values were used to define the boundary conditions of the simulation. The stated horizontal angle of the tablet bed was estimated visually, and was subject to change during the process as the growing coating layer alters the friction between tablets and coater.

Table 2: Parameters defining the coating process.

Coater parameter	Value
Drum diameter at the front/back	0.6 m
Drum diameter in the middle	1.5 m

Drum length	1.6 m
Tablet bed horizontal angle	~ 30°
Inlet air flow	1500 m ³ /h
Inlet air temperature	60 °C
Outlet pressure relative to atmosphere	- 20 Pa
Tablet bed weight	300 kg
Tablet bed temperature	35 °C
Rotation velocity	6 rpm

In the process, the film solution is applied via two-component air-liquid nozzles (Schlick model 930 Form 7-1 S35 ABC, Schlick Atomizing Technologies, Germany). A peristaltic pump is used to transport the liquid through the hole located at the center of the nozzle tip. The spray atomization is assured by pressurized air (termed *atomizing air*) that flows through a circular opening surrounding the tip at a high velocity relative to the liquid velocity. Following the manufacturer recommendations, a second air stream (termed *pattern air*) from two additional outlets at the nozzle front is activated as well. This is done to alter the spray pattern from a circular to an elliptical cross-section with increased mass flow uniformity.

C-3.2 PDA measurement of spray properties

Measurements of the spray characteristics were performed using the phase-Doppler anemometry (PDA) technique (Hirleman, 1996). It is capable of simultaneously measuring the particle diameter, velocity and mass flux of spray droplets (Zaidi, Altunbas, & Azzopardi, 1998). Owing to the high spatial resolution and ease of use, spray characterization using PDA systems has found widespread application (Kim & Kim, 2009; Payri, Tormos, Salvador, & Araneo, 2008). In early systems, the two best-known sources of error have been Gaussian beam effects and slit effects. Both can be greatly reduced by using a dual-mode PDA, where a standard PDA is combined with a planar PDA system (Tropea et al., 1996). Therefore, in this work a dual-mode PDA system (DANTEC DualPDA, Dantec Dynamics A/S, Denmark) was used for the characterization of the spray

under realistic operating conditions. The measuring system consisted of a laser generating unit, a transmitter unit emitting the laser, a detector (58N81) and a processor connected to a personal computer (Flow and Particle Processor BSA 60). The two laser beams of 514.5 nm and 488 nm wavelengths were generated by an Argon-Ion laser and introduced into the transmission unit via fiber optic cables. The scattered light was measured and pre-processed by the DualPDA system. The raw data, including the diameters and velocities of every single measured droplet, was transferred to a personal computer. In a post-processing step, histograms were created, giving the frequency distribution of the measured quantities across all droplets of a single measurement.

For the PDA measurements, the same spray gun as in the Nicomac coating system was used. As the spraying liquid, a preparation of a methacrylic acid copolymer dispersion (Eudragit L30D-55, Evonik Röhm GmbH, Germany) was used (EVONIK Röhm GmbH, 2007). Water was added to the commercial form, i.e., an aqueous dispersion with 30% dry substance, until a percentage by weight of approx. 20% of dry substance was reached. The viscosity of the final dispersion at room temperature was 1.7 mPa s. For the nozzle operation, the atomizing air and pattern air pressure was 1.2 bar. The liquid flow rate was 60 g/min. The values were chosen according to nozzle manufacturer recommendations and practical experience from an industrial coating process.

Figure 13 shows the central part of the experimental setup. The laser beams enter from the left, and the bright area near $y=-40$ shows the measurement location, i.e., the crossover region of the four laser beams inside the spray. The spray nozzle is located in the foreground on the right-hand side; in the background the receiver unit can be seen. The distance of the measurement point from the nozzle exit was 0.2 m, approximating the distance from nozzle to the tablet bed recommended by the manufacturer. Measurements were done for nine different positions from -80 mm to 80 mm with an interval of 20 mm along the horizontal spray axis, as shown in Figure 13. From the data sets for all positions, a mean value was calculated.

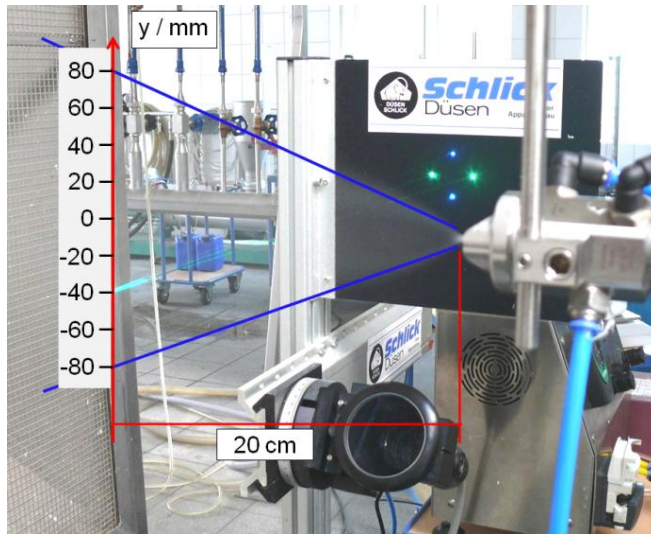


Figure 13: Picture of the experimental setup, showing the spray gun on the right and the receiver unit at the bottom. The laser beams are entering from the left, the beam crossing area (measurement zone) can be seen at position -40.

C-4 Numerical Model

For the numerical simulation of the dynamics of the air flow and the coating spray, the CFD (Computational Fluid Dynamics) code AVL FIRE (AVL LIST GMBH, Austria) was used. The model of the coating process included three subsystems:

- the air flow inside the coater
- the motion of spray droplets in the air stream
- the deposition of spray on surfaces as a wall film

Additionally, multi-phase evaporation of the coating liquid from the spray droplets, as well as from the wall film, was considered.

In our work, the common Reynolds-Averaged Navier-Stokes (RANS) approach was used to resolve the gas flow. This included the Reynolds-averaged forms of the conservation equations for mass, momentum, energy, as well as gas species. For closure of the equations, a standard κ - ε model of the turbulent flow (V. C. Patel, Rodi, & Scheuerer, 1985; Wilcox, 1998) was applied. The numerical solution of the problem was carried out in two steps. First, the air flow without spray was calculated until a converged state, i.e., a dynamic equilibrium, was

reached. Then, a transient calculation was started, using the converged steady-state as initialization. The spray was “introduced” into the air stream for a predefined time. To reduce calculation time, the spray droplets were simulated as parcels. A single parcel represents a certain number of identical droplets (the concept is explained in detail in the section on the spray module below). For each time step of the CFD calculation, the trajectory of the spray parcels was computed for a series of sub-steps. The necessary size of the sub-steps was determined automatically by the software based on the size of the CFD step and the parcel velocity. We were using a two-way coupling between continuous and solid phase. The application of numerical methods for the treatment of the droplet motion, the film formation and the evaporation is described in the next sections.

C-4.1 Mesh Generation

Based on the geometry of the coater described above, a hybrid computational grid was generated, consisting of approximately 1.5 million cells of both tetragonal and hexagonal shape. As the coater pan was nearly symmetric with respect to a mirror plane normal to the rotational axis, only one half of the coater was considered, and symmetry boundary conditions were applied at the mirror plane. In Figure 14, a three-dimensional representation of the simulation regime (i.e., the back half of the coater) is shown.

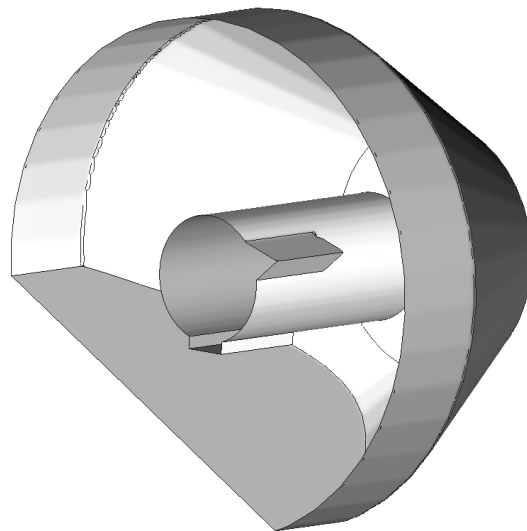


Figure 14: Three-dimensional graphic of the back half of the coating drum. The cylinder along the rotation axis in the middle holds the air inlet and outlet. The tablet bed is approximated by a moving (straight) wall at the lower left.

The cell size is automatically refined, i.e., near critical regions, such as the tablet bed wall or the air inlet, the size of the cells is decreased and, therefore, resolution is increased. Position and angle of the wall are taken from observations of an industrial coating process (see Table 2). The observations also showed that the tablet bed in the used coating pan is relatively flat for moderate to high fill levels. For the simulation, the tablet bed could therefore be represented by a moving wall with reasonable accuracy. However, for a coating apparatus with pronounced baffles, or for low fill levels, this assumption would not work.

While it is not feasible to resolve every single tablet at the tablet bed surface, a model for the treatment of the surface roughness has been applied, which takes the effects of roughness into account by an additional term in the wall function, directly modifying velocity at the wall. The surface roughness model needed the mean height of the roughness, i.e., the typical difference between high and low areas on the surface. As an estimate, half the height of a tablet was chosen.

C-4.2 Spray module

In general, an aqueous coating solution consists of several components, including a suspended polymer in water, as well as additional additives in smaller quantities (e.g., talcum). Here, it was assumed that for the droplet movement and deposition, the exact composition has little influence, as long as macroscopic properties, such as density and viscosity, were modeled realistically. Therefore, for simplicity the spray was assumed to consist of only two substances, 80% water and 20% glycerol, the latter representing the film-forming polymer and additional components, similar to the approach suggested by Aliseda *et al.* (Aliseda *et al.*, 2008). The physical properties of glycerol were taken from the manufacturer's specifications (The Dow Chemical Company, 2009).

The motion of the spray droplets was tracked using a Lagrange Discrete Droplet Method (DDM), based on the model of Dukowitz (Dukowicz, 1980). Due to a large number of droplets in the spray, it was not feasible to evaluate the encountered equations for every single droplet. Instead, we used the common statistical approach, where a group of identical droplets is represented by a single parcel. The amount of droplets in a parcel was calculated according to the given spray rate. In this way, the calculation time was greatly reduced without altering the statistical results. For each CFD time step, the Lagrange DDM equations were evaluated at a series of sub-steps for each parcel.

The movement of droplets is governed by Newton's equation:

$$m_d \frac{d\mathbf{u}_d}{dt} = \mathbf{F}_d + \mathbf{F}_G + \mathbf{F}_p, \quad (35)$$

with \mathbf{u}_d being the droplet velocity. The drag force \mathbf{F}_d is given as

$$\mathbf{F}_d = \frac{1}{2} \rho_g A_d C_D |\mathbf{u}_{rel}| \cdot \mathbf{u}_{rel} \quad (36)$$

A_d is the projected area of the droplet, \mathbf{u}_{rel} is the relative droplet velocity, and C_D is the drag coefficient. The force \mathbf{F}_G is a combination of gravity and buoyancy force, i.e.,

$$\mathbf{F}_G = V_d (\rho_d - \rho_g) \mathbf{g}, \quad (37)$$

and \mathbf{F}_p is the pressure force:

$$\mathbf{F}_p = V_d \nabla p. \quad (38)$$

Equation (35) was solved by direct time integration for each Lagrangian sub-step. The DDM incorporated a two-way coupling between the continuous and disperse phase, i.e., the influence of the air flow on droplet motion as well as that of the droplets on the surrounding air was considered.

C-4.2.1 Mass and heat balance

The mass balance equation for a droplet is given as

$$\frac{dm_d}{dt} = -\dot{m}_E, \quad (39)$$

where m_d is the mass of the droplet. The only source term on the right hand side is the mass source for evaporation \dot{m}_E , other sources like droplet break-up by secondary atomization or droplet collision were neglected.

It was assumed that the temperature T_d inside a droplet is uniform. The droplet temperature decreases due to convective and latent heat loss, depending on the

heat and mass transfer rate to the gas phase. The heat balance equation in the droplet is given by:

$$m_d \bar{c}_{p,d} \frac{dT_d}{dt} = -\Delta h(T_d) \dot{m}_E + \dot{Q}, \quad (40)$$

with $\bar{c}_{p,d}$ being the average of the specific heat capacity of all components of the droplets, Δh is the latent heat of evaporation, and \dot{Q} the heat transfer rate between gas phase and droplets. Values with an over bar are evaluated at a reference temperature and reference gas composition, i.e., at a location sufficiently far away from the droplet surface.

For the evaporation of spray droplets, a multi-component model based on the work of Abramzon and Sirignani was used (Abramzon & Sirignano, 1989), with the extension of Brenn et al. (Brenn, Deviprasath, Durst, & Fink, 2007), allowing for separate evaporation of the liquid species. In this model, the mass transfer from the liquid to the gas phase was calculated separately for each component. The total evaporated mass was then the sum of the amount evaporated for each species $\dot{m}_{E,j}$. For the heat transfer, at the beginning mean values based on the liquid composition were calculated; the calculation then proceeded equivalent to a single-component model using the mean values. The evaporation model approach is based on the film theory, according to which the rate of evaporation \dot{m}_E is calculated from the Sherwood and Nusselt numbers for mass and heat transfer, respectively. In the case of an evaporating droplet, corrected values of the Sherwood and Nusselt numbers, Sh^* and Nu^* are used. This is explained in detail below.

The mass transfer rate \dot{m}_E in the mass and energy balances are:

$$\dot{m}_{E,j} = \pi \bar{\rho}_g \bar{D}_{g,j} d Sh_j^* \ln(1 + B_{M,j}), \text{ with } \dot{m}_E = \sum \dot{m}_{E,j} \quad (41)$$

$$\dot{m}_E = \pi \frac{\bar{\lambda}_g}{\bar{c}_{p,d}} d Nu^* \ln(1 + B_T). \quad (42)$$

The terms denoted with an overbar (i.e., thermal conductivity $\bar{\lambda}_g$, specific heat $\bar{c}_{p,d}$, gas density $\bar{\rho}_g$ and binary diffusion coefficient $\bar{D}_{g,j}$ of species j in the gas phase) were evaluated at the reference point (Piccioli, 2006). d was the droplet

diameter. In the equation (41) above, the Spalding mass transfer number $B_{M,j}$ was defined as:

$$B_{M,j} = \frac{w_{j,s} - w_{j,\infty}}{1 - w_{j,s}}. \quad (43)$$

Here, $w_{j,s}$ is the mass fraction of species j at the surface of the drop, to be calculated from the vapor pressure at the droplet temperature, and $w_{j,\infty}$ is the gas phase mass fraction in the bulk.

The Spalding heat transfer number B_T in equation (42) is given as

$$B_T = (1 + B_M)^\Phi - 1, \quad (44)$$

$$\Phi = \frac{\bar{c}_{p,d}}{\bar{c}_{p,g}} \frac{Sh}{Nu Le}, \quad (45)$$

with $\bar{c}_{p,g}$ the gas phase specific heat capacity at the reference point and $\bar{c}_{p,d}$ the specific heat of the droplet liquid. The Lewis number Le is given as

$$Le = \frac{\rho c_p d}{\lambda}. \quad (46)$$

To calculate the temperature of the droplets from (40), the mass transfer rate \dot{m}_E defined above, and the heat transfer rate \dot{Q} between droplet and surrounding gas are needed. \dot{Q} was defined as:

$$\dot{Q} = \dot{m}_E \left[\frac{\bar{c}_{p,d}(T_\infty - T_d)}{B_T} - \Delta h(T_d) \right]. \quad (47)$$

However, to calculate the heat transfer rate, the mass transfer rate has to be known, and vice versa. Therefore, for each time-step, a consistent solution had to be found by iteration.

To account for the relative motion of spray droplets and gas phase, the Nusselt number Nu and the Sherwood number Sh_j for component j were calculated

from the Reynolds (Re), Prandtl (Pr) and Schmidt (Sc) numbers, according to empiric relations (Ranz & Marshall, 1952a, 1952b):

$$Nu = 2 + 0.552 Re^{1/2} Pr^{1/3}, \quad (48)$$

$$Sh_j = 2 + 0.552 Re^{1/2} Sc_j^{1/3}. \quad (49)$$

The values of Nu and Sh_j above are correct for a non-evaporating droplet. As mentioned, the model is based on film theory, where heat and mass transfer is described by gas films of constant thickness. Therefore the evaporation from the droplets was modeled with the aid of a virtual constant film. The thickness of the film was adjusted from classic film theory, this was taken into account by calculating the corrected Nusselt number Nu^* and Sherwood number Sh_j^* from the corresponding non-evaporating values as defined in (48) and (49), and a correction function:

$$Nu^* = 2 + \frac{(Nu - 2)}{F_T}, \quad (50)$$

$$Sh_j^* = 2 + \frac{(Sh_j - 2)}{F_{M,j}}. \quad (51)$$

The temperature correction function F_T and mass correction functions $F_{M,j}$ have the same form, and are given as:

$$F_T = (1 + B_T)^{0.7} \frac{\ln(1 + B_T)}{B_T}, \quad (52)$$

$$F_M = (1 + B_M)^{0.7} \frac{\ln(1 + B_M)}{B_M}, \quad (53)$$

In equation (43), the mass fractions $w_{j,s}$ of the different liquid components j were needed. They were calculated from the mole fractions of each component at the droplet surface, given as

$$\chi_{j,s} = \chi_{j,d} \gamma_j \frac{P_{v,j}}{p} \quad (54)$$

Here, $\chi_{j,d}$ is the mole fraction inside the droplet, $P_{v,j}$ is the vapor pressure of species j and p is the total pressure. The activity coefficients γ_j for the water-glycerol mixture were calculated using a group contribution method, i.e., the UNIFAC method (Agrdria et al., 1997; Attarakih, Abu Fara, & Sayed, 2001).

C-4.3 Wall film model

When modeling film formation on the walls of the coater (including the tablet bed), one can assume that the film thickness is much smaller than the wave length of variation in pressure along the walls. Therefore, one can assume that the film surface in each cell was parallel to the wall surface. Numerically, this meant that the simulation of the wall film was done in two dimensions, i.e., in the plane of the wall surface. The advantage of a two-dimensional model was that no additional computational grid has to be generated for the film treatment. The thickness of the film was only entered as a scalar value for each existing cell, i.e., the wall film thickness inside a single cell was constant. Thus, particular care was exercised to ensure that the computational grid of the coater close to the walls was sufficiently fine to ensure an excellent representation of the variation in film thickness. The time evolution of the wall film is governed by the film transport equation:

$$\frac{\partial \delta}{\partial t} + \frac{\partial u_1}{\partial x_1} + \frac{\partial u_2}{\partial x_2} = \frac{1}{\rho} s_m, \quad (55)$$

with δ being the thickness, and ρ the density of the wall film, s_m is the area-specific source term. To solve equation (55), the source term s_m and the mean velocity components u_1 and u_2 have to be calculated.

The mean velocity components were calculated from analytical velocity models, taking into account forces due to gravity, pressure gradients and in-plane shear. Due to the low film thickness and thus small mass, inertial effects could be neglected, leading to a series of steady-state velocity profiles for each time step, greatly reducing the computational cost of solving the transport equation.

The source term consisted of film mass deposited by the spray as described in section C-4.4 below, and film mass lost by evaporation. The evaporation mass flux $\dot{m}_{E,j}$ from the film is described by Fick's law of unidirectional diffusion (Stefan diffusion):

$$\dot{m}_{E,j} = \left(\frac{\rho_g (D + D_t)}{1 - w_{S,j}} \right) \left(\frac{\partial w_j}{\partial y} \right)_s \quad (56)$$

Here, ρ_g is the density of the gas phase, D and D_t the molecular and turbulent diffusion coefficients, and w_j is the mass fraction of component j at the surface. The partial derivative $\partial w_j / \partial y$ is the concentration gradient of the mass fraction normal to the surface. The density ρ_g is calculated from the ideal gas law. For the diffusion coefficient D , empirical correlations were used, and $w_{S,j}$ could be calculated from the saturation pressure. This left the gradient of the mass fraction and the turbulent diffusion coefficient as unknown quantities. Here, they were modeled by using the boundary analogy of momentum and mass transfer, i.e., the turbulent concentration profile and the turbulent diffusion process near to the liquid surface were modeled by using the analogy to the turbulent velocity profile²⁵.

C-4.4 Spray Impingement

The model for spray impingement was based on the work of Mundo et al. (Mundo, Sommerfeld, & Tropea, 1995). When a spray parcel hit a surface, it is either deposited on the wall or it splashes back, i.e., the incident droplet breaks into smaller droplets. It has been established that this process occurs depending on the dimensionless Reynolds number Re and Ohnesorge number Oh :

$$Re = \frac{\rho_L v_d d}{\mu_L} \quad (57)$$

$$Oh = \frac{\mu_L}{\sqrt{\rho_L \sigma_L d}} \quad (58)$$

where ρ_L is the liquid density, v_d the droplet velocity, d the droplet diameter, and μ_L the liquid dynamic viscosity.

Mundo showed that when plotting the experimental data for Oh as a function of Re , the regimes of splashing and deposition are separated by a critical curve given as

$$Oh_{\text{critical}} = 57.7 Re^{-1.25}. \quad (59)$$

The critical curve is shown in Figure 15. For the region over the critical curve, the droplets splash on impact. In this case, only a fraction of mass was transferred to the wall film. The rest did not deposit but formed newly generated droplet parcels. For the region under the critical curve, the complete liquid mass of the droplet parcel was transferred to the wall film.

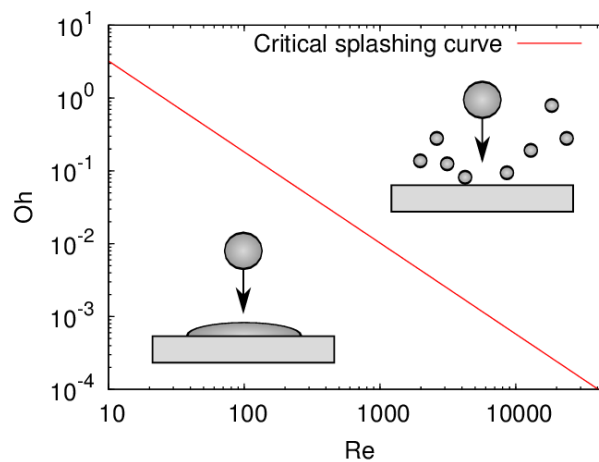


Figure 15: Ohnesorge number Oh as a function of Reynolds number Re . The splashing region and the deposition region are separated by the critical splashing curve.

C-5 Results and Discussion

In the first part of this section, the outcome of Phase-Doppler anemometry (PDA) measurements is presented. As mentioned above, the aim of these measurements was to provide the basis for realistic spray simulations. After that, the results concerning the air flow inside the coater and the spray simulations are described. Finally, indicators quantifying the process quality and the amount of spray loss are given for different nozzle configurations.

C-5.1 Spray Characterization by PDA Measurements

One of the most important quantities that influence the quality of the tablet film, and the coating process in general, is the size distribution of the spray droplets. For this reason, we first concentrated on the experimental characterization of the coating spray.

For good coating results, droplets should be roughly in the range of 10 μm to 60 μm . The measured distribution of the spray droplet diameter for standard operating parameters, i.e., atomizing air and pattern air pressure of 1.2 bar and a liquid flow rate of 60 g/min, is shown in Figure 16. The shape of the distribution (an approximate Gaussian shape with a tail to higher droplet diameters) was typical for this kind of nozzle. It could be seen that nearly all droplets had a diameter smaller than 60 μm . A droplet diameter smaller than 10 μm was considered undesirable due to the large area-to-volume ratio: these particles could be already partially or completely dried before reaching a tablet surface, therefore forming a film of lesser quality, or not contributing to film formation at all. In Figure 16, approximately 38% of droplets, which is 4% of the total droplet mass, have a diameter smaller than 10 μm .

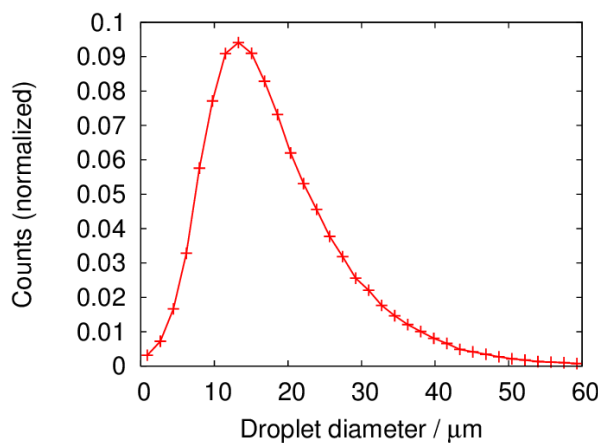


Figure 16: Number-weighted spray droplet size distribution in μm , as a mean of all positions in the PDA spray measurement at a distance of 20 cm.

C-5.2 Numerical Implementation of the Spray

While the output of the PDA measurements provided a distribution of the diameter and the velocity at a distance of 20 cm from the nozzle outlet, in the numerical simulation the spray was initialized by specifying the diameter and mass distribution of the spray parcels at the nozzle outlet. To ensure a correct

correlation between measurement and simulation parameters the droplets were initialized according to the measured droplet diameter distribution. At a distance of 20 cm, diameter and velocity of the simulated spray were then compared to the experimental data.

It should be noted that coalescence was not taken into account, as for the two-component nozzle it can be expected that droplet interaction was negligible. A concern, however, was the correct velocity distribution at the tablet bed. In the real nozzle, atomizing and pattern air introduced a driving air flow. It was found that in the numerical simulation, these air flows can be omitted if a higher parcel starting velocity is chosen. After leaving the nozzle, the parcels were quickly decelerated by the drag force; in turn they accelerated the surrounding air and generated the required air stream. By using a velocity of $v = 180$ m/s it could be shown that the simulated spray is in good agreement with the PDA measurements. A comparison of the velocities at the tablet bed for the simulation and the experiment is shown in Figure 17. It can be seen that the deviation between measurement and simulation was well inside acceptable boundaries, given the simplifying model assumptions. It is interesting to note that both the PDA measurement and the CFD simulation show a kink near the maximum of the curve, the origin of which was not conclusively known.

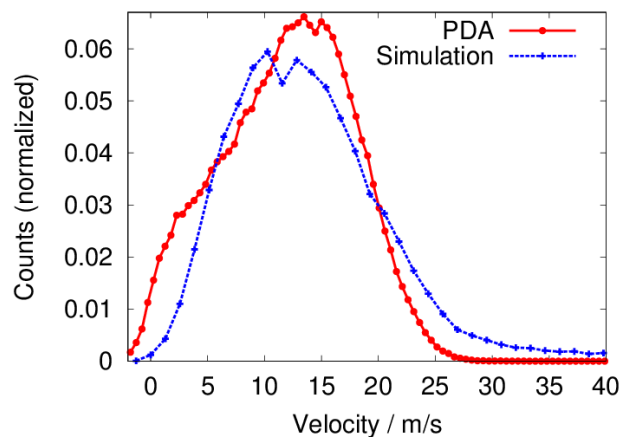


Figure 17: Number-weighted distribution of spray droplet velocities for experimental measurements (o) and CFD simulation (x). By increasing droplet starting velocity, the lack of atomizing air flow was compensated such that the curves show good agreement.

C-5.3 Simulation of the Air Flow inside the Coater

To a large extent, spray droplet movement and tablet film formation are governed by the drying air flow. Thus, it is critical to understand the air flow in the coater. In the following section, the drying air flow is studied in more detail. To depict the nature of the air flow, different properties of the air are shown in two-dimensional plots using cut planes through the coater geometry. Figure 18 shows the location of the cut planes: A) vertical through the nozzle position, B) vertical behind the air inlet, C) and D) are horizontal above and through the air inlet/outlet structure, respectively.

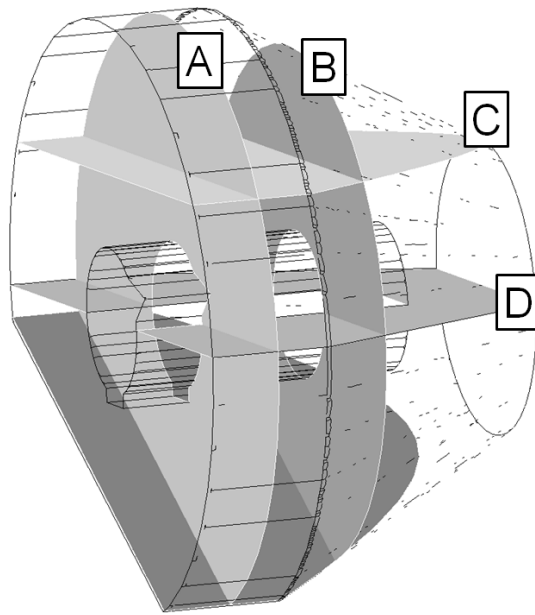


Figure 18: Location of the cut planes for the generation of two-dimensional plots inside the coater.

In Figure 19, the velocity of the drying air stream is shown for a cross-section through the coater, perpendicular to the rotational axis (plane A in Figure 18). As can be seen, the surface of the tablet bed was represented by a moving wall, i.e., the missing circle section in the lower left part.

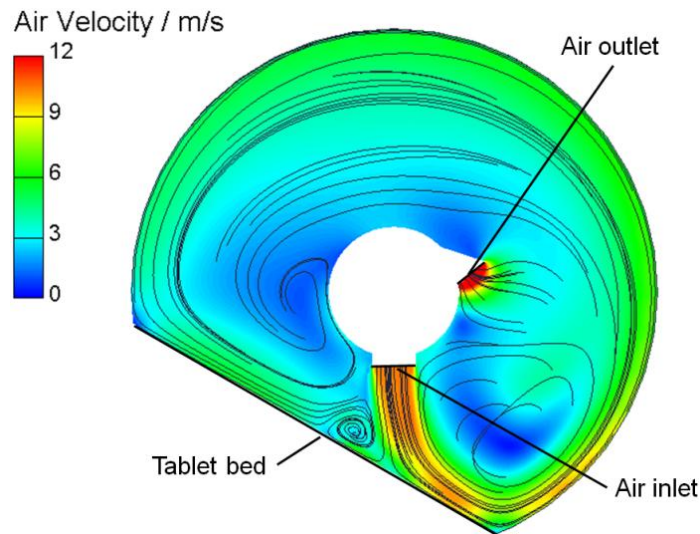


Figure 19: Air velocity for a cross-section through the location of the spray nozzle, perpendicular to the rotational axis. Streamlines are drawn in black.

As expected, zones with increased air velocity existed near the inlet and outlet. Starting from the inlet, the drying air streamed downwards and hit the tablet bed. After drying the tablets coming from the spray zone located upstream, the inlet air had increased humidity and should leave via the outlet. However, as Figure 19 shows, instead the majority of air moved along the drum wall (against the rotational direction). Furthermore, a smaller portion of the inlet stream was not following the main flow, but formed an undesirable eddy between the spray zone and the area where the inlet air impacts the tablet bed.

The results suggested that a more effective removal of the humid air would be desirable. If feasible, one option could be the reduction of the inlet air flow rate, while increasing the inlet air temperature. Other possibilities include increasing the pressure drop at the outlet or installing a well-designed baffle system for the air outlet.

Figure 20 shows that the counter-clockwise stream of the air that was seen above extended to the back section of the coater. As the air inlet and outlet did not cover the whole length of the coater, this section lied behind inlet and outlet. Without the direct air stream from the inlet to the tablet bed, the eddies near the tablet bed were not seen; however, eddy formation over the outlet region could be observed.

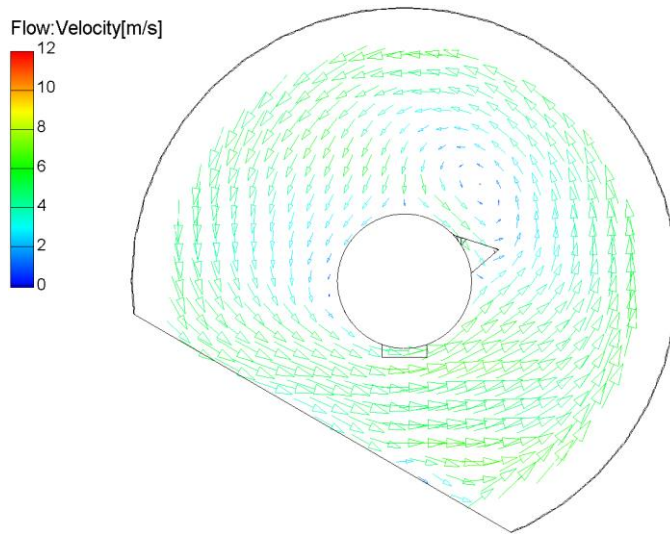


Figure 20: Vector plot of the air flow velocity inside cut plane B.

The lateral air movement is depicted in Figure 21 and Figure 22, the horizontal cuts through the coater. Note that the color scale has a maximum value of 6 m/s, compared to 12 m/s in the plots above. Overlaying the air flow against the coater rotation direction shown above, a rotational air flow in lateral direction took place. The air streamed from the middle of the coater to the end at the left side, and returned to the middle due to the lower pressure at the outlet.

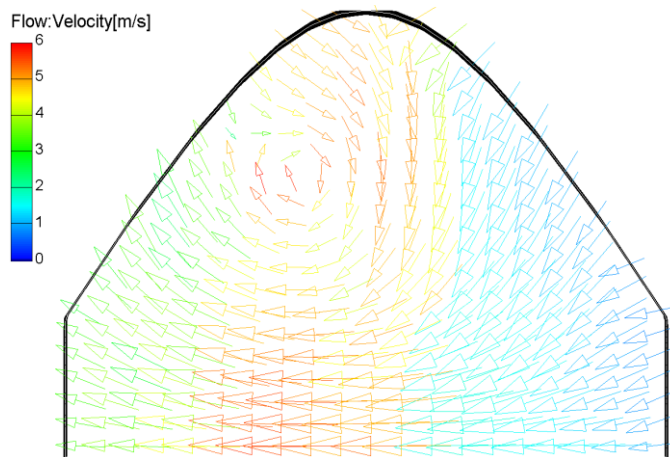


Figure 21: Vector plot of the air flow velocity inside cut plane C.

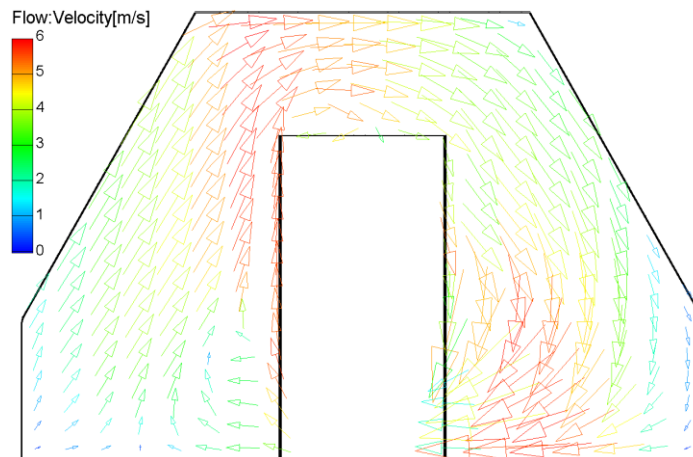


Figure 22: Vector plot of the air flow velocity inside cut plane D.

C-5.3.1 Water Content in the Coater

For the incoming air, the humidity was set to be 0.01, resembling a typical value of environmental air. At the start of the simulation, the water mass fraction inside the coater was set to 0.008 instead of 0.01, as it could be assumed that the dry and hygroscopic tablets will absorb some water from the environment. Without spray, in this setup the mean humidity would slowly rise from 0.008 to 0.01 with time, as the initial air was gradually replaced by fresh inlet air. If the additional water of the spray was included, the humidity would reach even higher values. Also, the humidity would be higher in areas directly affected by the spray, posing the risk of local over-wetting that could potentially damage the tablet cores. In Figure 23, the distribution of humidity, i.e., the mass fraction of water in the gas, at 0.5 seconds after the start of spraying is shown.

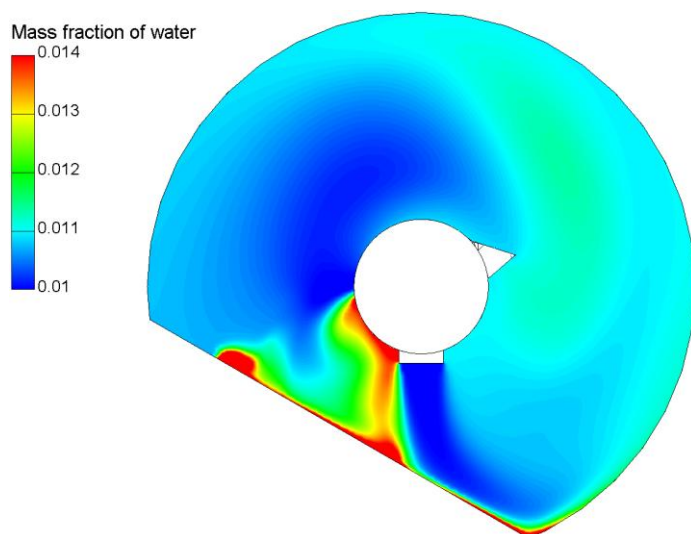


Figure 23: Mass fraction of water inside the coater.

Regions of high water content could be seen in the areas where the spray hit the tablet bed and along the tablet bed, but also in the area between the tablet bed and the inner cylinder. The latter region originated from direct water evaporation from relatively small spray droplets carried over from the primary spray zone by the air flow. The picture was qualitatively the same for other times, with increasingly higher maximum water content. In Figure 24, the time evolution of the average mass fraction of water in the coater over the simulated period is shown. While the water content increased steadily, it could be seen that the rate of increase slows down with time, as in the long term a dynamic equilibrium with a constant average level of humidity had to be obtained. While the *average* mass fraction of water was well inside typically acceptable limits, Figure 23 shows that the moisture near the tablet bed was approximately 1.6 times higher than the corresponding average value, meaning that local over-wetting could still occur.

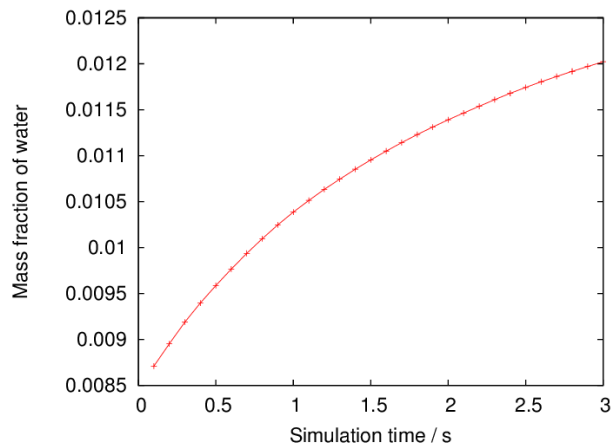


Figure 24: Average mass fraction of water in the coater as a function of time.

C-5.4 The Influence of Nozzle Placement on Spray Loss

In general, spray loss in drum coating occurs for two reasons. One part of the loss is made up of the spray droplets that are too dry to stick to a surface (spray drying phenomenon) or do not hit a surface at all. In both cases the droplets eventually leave the device with the exhaust air. The other contribution to spray loss is spray liquid that forms a film on surfaces other than the tablets and has to be removed during post-process cleaning.

In Figure 25, the spray inside the coater after 0.5 seconds spraying is shown. The color and size of the droplets is proportional to the water content. The big droplets close to the spray nozzle still had a water content close to the initial spray water fraction of 0.8. The small droplets at the right-hand side were already partially or completely dried. It could be seen that a fraction of the spray moves towards the tablet bed, but was then dragged upwards and impacts the air inlet/outlet cylinder. The dry droplets that came close to the outlet leave with exhaust air. The rest of the droplets followed the flow of drying air and either left after several rotations with a varying residence time, or stuck to the rotating coater wall.

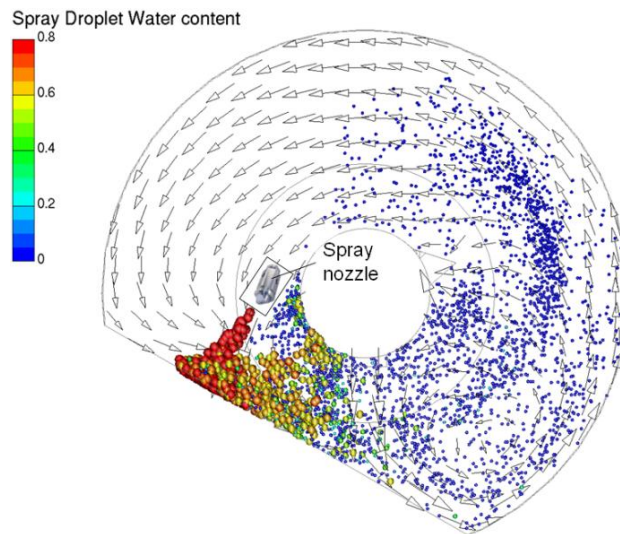


Figure 25: Spray after 0.4 seconds. The color of the spray droplets show the amount of water, ranging from the starting concentration of 0.8 (red) to 0 (blue). The droplet size is proportional to the water content as well. Additionally, the air flow velocity is shown as a vector plot.

The figures concerning the air and spray flow discussed above provide a qualitative picture of the dynamics of the process. In the following, more quantitative measures are described. While in a numerical simulation arbitrary values for the operating parameters may be selected, strict regulations and cost concerns limit the parameters that can be changed for an already established industrial process. In this work, the parameter chosen for variation was the spray gun placement, which may be changed both in simulation and reality. Thus, an investigation of the influence of the nozzle position on the coating process, especially on the amount of spray loss, was performed. These variations are shown in Figure 26. Starting from a base point (B), the spray nozzle was tilted away from (1) or towards (2) the air inlet. Additionally, a higher position (3) and two lower positions (4, 5) were selected.

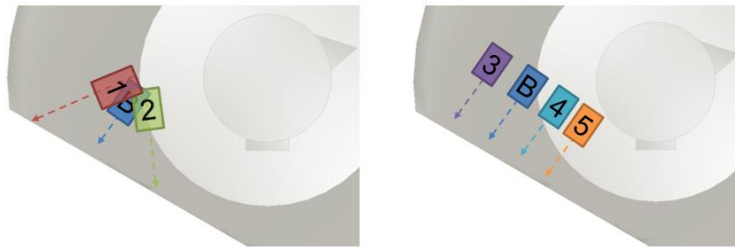


Figure 26: Variation of position and angle of the spray gun in the coating drum. Left: B denotes the standard position, 3-5 are variations translated parallel to the tablet bed. Right: Case 1 and 2 are a variation of the angle for basis position.

Concerning the numerical work, the gas flow simulation was first started without spray until convergence was reached. Then, the spray was activated, and a time span of three seconds was simulated. The following key parameters were computed by integration over all simulation time steps to arrive at quantitative conclusions for the amount of spray loss:

- **Spray mass leaving through outlet:** the fraction of total liquid mass that had left the coater with the exhaust air
- **Relative amount of film on the coater wall:** The relative amount of liquid that formed a film on a surface other than the tablets.

The results are shown in Figure 27 and Figure 17, respectively. When comparing the amount of spray loss for the different setups (Figure16), it can be seen that case 1 and case 3 performed better than the other cases, including the base case. “Better” in this case means that a larger percentage of the introduced spray stayed inside the coater instead of leaving with exhaust air. Taking the spray drying mentioned above into account, it can be concluded that the spray loss consisted largely of dried spray droplets.

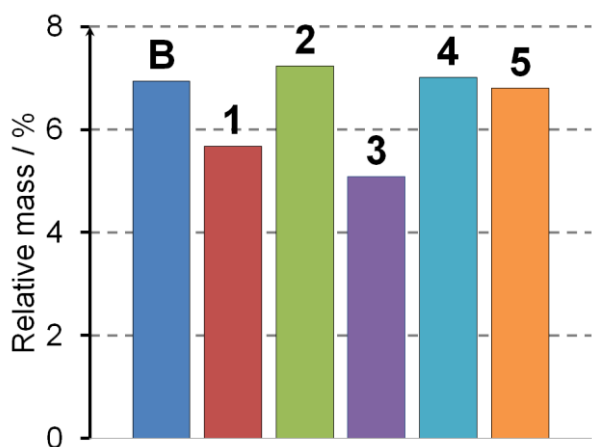


Figure 27: Total mass of the spray droplets leaving with the outlet air, relative to total introduced mass.

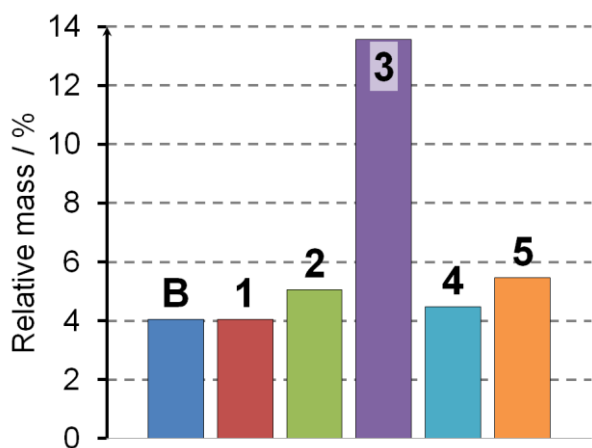


Figure 28: Total mass of spray droplets that hit a wall other than the tablet bed, relative to total introduced mass.

From this information on spray loss only, it can be concluded that case 1 and 3 should be preferred, as in these cases the largest amount of spray stayed in the coater. However, this would not take into account *where* the coating liquid is to be found in the coater. To get more information on the liquid distribution, we calculated the relative amount of film formation on coater surfaces other than the tablet bed (Figure 28). In case 3, a significant increase of unwanted material deposition was detected, showing that for this case, the low amount of spray droplets in the exhaust air comes with the price of increased deposition on coater surfaces. To examine this phenomenon in more detail, the distribution of the wall

film after three seconds of simulation time for case 3 was visualized, as shown in Figure 29.

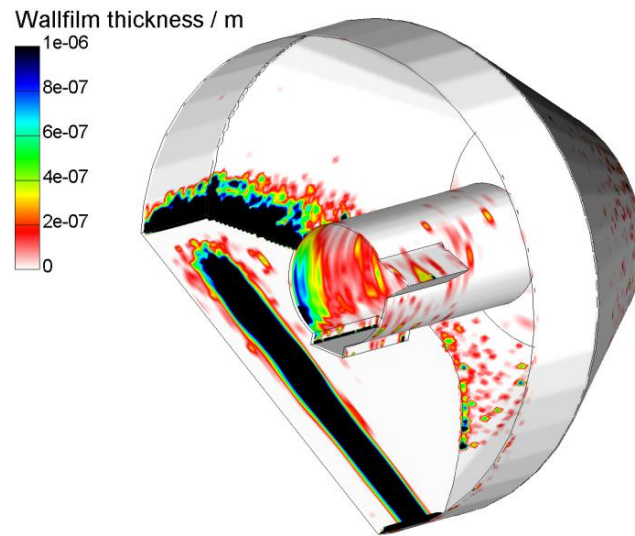


Figure 29: Wall film thickness on the coater wall, from no film (white) to a thickness above one micrometer (black). It can be seen that apart from the tablet bed, film liquid is also deposited on the rotating wall near the tablet bed top and the middle cylinder.

Apart from a coating of the tablet bed as expected, the rotating coater wall near the top of the tablet bed was showing film formation as well. In addition, a wall film was building up on the air inlet/outlet cylinder in the middle of the coater, on the side opposite of the outlet. Closer investigations showed that this phenomenon happened for all other nozzle positions, although to lesser extents. Film formation in the same locations has also been observed in industrial coating processes using the described coating equipment, underlining the predictive capability of the simulation model.

In summary, a reduction of spray losses compared to the standard operational conditions (B) was seen in case 1 and case 3. However, in case 3 the reduction occurred because a large portion of the spray ended up forming a highly undesirable film on the rotating coater wall. Therefore, making a nozzle arrangement according to case 1 was the optimum choice, where the spray loss was reduced without negative side effects by slightly tilting the spray nozzle away from the inlet.

C-6 Conclusions

In this work, we have presented the modeling of a pan coating process using Computational Fluid Dynamics (CFD). A hybrid mesh was generated mimicking the geometry of a full-scale industrial coater. The critical process parameters (e.g., inlet air temperature, flow rate, drum rotation speed) were selected according to standard operating conditions. A central part of each pan coater is the spray nozzle. In order to simulate the spray as realistically as possible, Phase-Doppler anemometry measurements were performed, using Eudragit L30D-55 filming solution to generate the basis for the “numerical” spray.

The results indicate that a detailed understanding of air flow inside a coater is necessary to optimize the dynamics of a coating process. As an important quantitative measure for the quality of the coating procedure, the spray loss was calculated. As variation parameters, different nozzle positions and directions were chosen. The rationale behind this choice was the fact that these parameters could be easily changed, even in an already validated process. Our results showed that the usual recommendation of placing the spray nozzle at a distance of one third of the total tablet bed length from the top of the tablet bed gave the best results. However, instead of orienting the spray strictly perpendicular to the tablet bed as is common practice, tilting the nozzle away from the inlet air showed a reduction in spray loss.

The model of the coater process described in this work was aimed to capture the fundamental phenomena leading to spray loss in an industrial coating process. Nevertheless, many aspects need to be further investigated. As a next step, the model will be expanded, e.g., by increasing the number of spray nozzles or accounting for the elliptical shape of the spray. A more detailed description of the turbulent air flow through the tablet bed is desirable as well. In the future we also intend to apply more sophisticated approaches, such as the LES-LPT model that we developed recently (Sungkorn & Khinast, 2010). The influence of a range of additional parameters, such as temperature, air flow boundary conditions or nozzle type, will be investigated in the future.

In addition, the validation of the numerical results represents an important step in our future work. Thermal imaging of the coater’s internal surfaces, or the quantification of the spray mass trapped inside the filters are some examples of our current activities. Furthermore, the coating efficiency on the tablet bed is to be quantified by means of Near-Infrared (NIR) spectroscopy online methods.

C-7 Notation

C-8 Latin Symbols

Symbol	SI Unit	Quantity
A	m^2	Area
$B_{M,j}, B_T$	-	Spalding mass and heat transfer number
c_p	$J/(kg\ K)$	Specific heat capacity at constant pressure
C	-	Drag coefficient
d	m	Particle diameter
D	m	Diffusion coefficient
F	N	Force
$F_{M,j}, F_T$	-	Mass and temperature correction
g	m/s^2	Gravitational acceleration
h	J/kg	Specific Enthalpy
m	kg	Mass
p	Pa	Pressure
\dot{Q}	W	Heat transfer rate
R	m	Pan radius
s_m	kg/m^2s	Area-specific mass source
t	s	Time
T	K	Temperature
u, v	m/s	Velocity
V	m^3	Volume
w	kg/kg	Mass fraction
x	mol/mol	Mole fraction
x_1, x_2	m	Cartesian coordinates
y	m	Space component normal to the wall
y^+	-	Non-dimensional wall distance

C-8.1 Dimensionless Numbers

Symbol	Quantity
Le	Lewis number ($=Sc/Pr$)
Nu	Nusselt number ($=\alpha L/k$)
Oh	Ohnesorge number ($=\mu/(\rho\sigma L)^{0.5}$)
Pr	Prandtl number ($=c_p\mu/k$)
Re	Reynolds number ($=uL/\nu$)

Sc	Schmidt number ($=\nu/\beta$)
Sh	Sherwood number ($=k_m L/b$)

C-8.2 Greek Symbols

Symbol	SI Unit	Quantity
γ	-	Activity coefficient
Δ	-	Variation
δ	m	Wall film thickness
ε	m^2/s^3	Turbulent dissipation
Φ	-	Exponent for heat transfer calculation
λ	$\text{W}/(\text{m}^2\text{K})$	Heat conductivity
μ	Pa s	Dynamic viscosity
ν	m^2/s	Kinematic viscosity
ρ	kg/m^3	Density
σ	N/m	Surface tension
ω	rad/s	Pan rotational speed

C-8.3 Subscripts and Superscripts

Symbol	Quantity
\dot{x}	Rate of change or flux of variable x
∞	Bulk
— (<i>overbar</i>)	at the reference point
d	Droplet
D	Drag
E	Evaporation
g	Gas
G	Gravity and buoyancy
i, j	Index
I	Interfacial
P	Pressure
<i>rel</i>	relative
S	Surface value
v	Vapor

Chapter D: Effect of tablet coating parameters: combining non-destructive measurements and dissolution testing

SUBMITTED as: Toschkoff, G., Schinwald, C., Markl, D., Koller, D. M., Scheideler, M., Leitner, M., & Khinast, J. G. (2013). Effect of Tablet Coating Parameters: Combining Non-Destructive Measurements and Dissolution Testing. European Journal of Pharmaceutics and Biopharmaceutics. Submitted.

The author of the thesis would like to stress that the description of the optical coherence tomography (section D-4.2) was written together with the co-authors Dipl.-Ing. Daniel Markl and Dr. Michael Leitner; as cited below. Figure 32 and Figure 33 were created by Dipl.-Ing. Daniel Markl. The experimental work described in this manuscript was done by co-author Dipl.-Ing. Christoph Schinwald in the scope of his diploma thesis (under the supervision of the author of this thesis).

D-1 Abstract

Pan coating is widely used in the pharmaceutical industry to cover tablets with a functional thin film. One of the most common types is enteric coating. Those films are resistant to gastric juice and dissolve in the gastrointestinal tract, providing a targeted release of the active pharmaceutical ingredient (API). To guarantee functionality, tablets are subjected to a standardized dissolution test (US Pharmacopeia Apparatus II, "USP II"). If they fail the test, the entire tablet batch may be rejected. Although reasons of failure are not always clear, no further investigations can be undertaken since USP II is a destructive test. This calls for an investigation of how different process conditions influence the outcome of the USP II test and a study of the USP II failure mode in more detail.

In this work, enteric-coated tablets were examined via a series of non-destructive measurements and finally subjected to the USP II dissolution test. By using non-destructive methods before dissolution, the same tablet can be subjected to all tests subsequently. We selected methods that can be readily applied in a production environment: direct length and weight determination, optical

coherence tomography (OCT) and near-infrared (NIR) spectroscopy. Each sample tablet was assessed using all of the above-mentioned methods and the results were compared. It was found that the influence of process parameters on the release characteristic was not as critical as previously assumed. Relatively fast and cheap methods (e.g., direct diameter measurement) were suitable for collecting basic information. OCT proved to be a flexible tool for in-depth coating quality validation.

D-1.1 Keywords:

tablet coating, dissolution, modified release, optical coherence tomography (OCT),

D-2 Introduction

Tablet coating is a common unit operation in the pharmaceutical industry. The applied coating layer has various functions, such as giving the tablet a certain color, adding an active pharmaceutical ingredient (API) or controlling the API release rate of the tablet. In today's industrial practice the most common coating process is pan coating. Here, tablets are placed in a pan rotating at moderate speeds and a coating liquid is sprayed onto them. Usually, the tablets are top-sprayed with a water-based coating using several spray guns. For drying, heated air is introduced into the coating pan; the exhaust air is extracted and filtered.

Coating is frequently applied to modify the release of the API from the tablet. One important type is enteric coating, providing an outer layer that dissolves in the alkaline environment of the intestinal tract but not in the low-pH environment of the stomach. Thus, the tablet can pass the stomach unharmed, and the API is released only once it reaches the intestinal tract. This can be applied to protect the stomach from certain types of API. Once a batch of enteric-coated tablets has been produced, it is subjected to a standardized dissolution test, typically following the US Pharmacopeia (<711> Dissolution, harmonized with the European and Japanese Pharmacopeia). During the test, the accuracy of the release behavior of the tablet is examined. If the film coating fails the dissolution test, the entire batch has to be reworked or rejected. This leads to significant time and financial losses, especially since coating is one of the last steps in the tablet production.

Therefore, understanding the influence of the coating process parameters on the quality of the final product and especially on the reliability of the coating layer is

important. A number of studies are described in literature. For example, an aqueous film coating process is investigated in (Porter, Verseput, & Cunningham, 1997) via a Design of Experiments (DoE) by varying the amount of suspension, the drying inlet air temperature, the spray rate, the atomizing air pressure, the pan speed and the number of spray guns. The output factors in question (i.e., the coating uniformity, the loss of weight during drying and the coating process efficiency) were determined by weight measurements. A similar DoE approach was applied in a study of the uniformity of a taste-masking coating (Dubey et al., 2012). The uniformity was quantified by laser-induced breakdown spectroscopy. In another study (Tobiska & Kleinebudde, 2003), the influence of parameters such as tablet size, fill level, and pan speed in a lab scale enteric coating process was investigated. After the process, tablets were subjected to a dissolution test. It was found that the rotation speed has a strong effect on the minimum amount of coating liquid needed for an enteric coating. A different approach that saw increased application in the pharmaceutical industry lately is computer simulation (Adam et al., 2011; Ketterhagen et al., 2009b). Where they are applicable, simulations can give information that is not accessible via experiment (Toschkoff et al., 2012), and were successfully applied to study quantities such as the batch coating mass variability (Dubey et al., 2011; Kalbag & Wassgren, 2009; Suzzi et al., 2012; Toschkoff et al., 2013). However, studies on the uniformity or quality of the coating layer are less common (Freireich, Ketterhagen, et al., 2011; Suzzi et al., 2010), and the prediction of coating dissolution is yet outside the scope.

A general challenge in the study of coating processes is to find a suitable method for the quantification of the coating quality. Various methods for analyzing the film are discussed in the literature. The coating morphology of enteric-coated tablets during the USP II dissolution test was analyzed using Scanning Electron Microscopy (SEM) and Confocal Laser Scanning Microscopy (CLSM) and compared to the release profile (F. Liu et al., 2009). The roughness of the film coating surface in batches prepared with varying spray gun pressures was analyzed using CLSM. (Ruotsalainen, Heinämäki, Guo, Laitinen, & Yliruusi, 2003). Another common method for analyzing the quality of a film coating is near-infrared (NIR) and/or Raman spectroscopy. Models predicting the film-coating thickness and the tablet hardness were developed using multivariate data analysis (MVDA). Moreover, the drug-release performance was studied (Kirsch & Drennen, 1995). Other studies investigated the influence of different tablet loads and plenum pressures in a fluidized bed coater on the coating thickness and compared various methods of analysis, such as X-ray fluorescence, Raman and

near-infrared spectroscopy (Cahyadi, Karande, Chan, & Heng, 2010). Raman spectroscopy was used to implement a PLS model that predicts the tablet's exposure time in a pan coater (Romero-Torres, Perez-Ramos, Morris, & Grant, 2005). A similar approach was used for predicting the tablets' film coating thickness by examining the Raman spectra of batches with varying weight gain and titanium dioxide concentration (Kauffman, Dellibovi, & Cunningham, 2007). One of the major drawbacks of using NIR or Raman spectroscopy for coating monitoring is that it does not provide an absolute value of the coating thickness, and thus, requires a complex calibration procedure based on primary measurements. This drawback could be overcome using optical coherence tomography (OCT) for the characterization of tablet coating, which allows the direct measurement of the coating thickness. OCT is increasingly applied to non-destructively evaluate the coating thickness and coating homogeneity of tablets with different shapes and formulations (Koller et al., 2011; Mauritz et al., 2010; Zhong et al., 2011). A comparison of different methods is given in (Brock et al., 2012).

Studies dealing with the coating process often investigate the coating quality of the finished product. However, the same level of attention is not paid to the actual outcome of a dissolution test, although often this will determine whether a tablet is deemed suitable for distribution or not. The aim of this work is to evaluate the influence of different process parameters on the film coating quality and directly relate this to the results of the applied dissolution test (USP <711> "Dissolution" Apparatus II, hereafter termed "USP II test"). The investigated process parameters are the tablet bed temperature, the spray rate and the supply air flow rate. In addition to the USP II dissolution test, the enteric coating layer quality was analyzed via a series of non-destructive methods. All measurements were done subsequently with the same tablet, the destructive USP II test obviously being the last step. This procedure makes it possible to directly see how the process settings influence the outcome of different coating quality tests, and to assess to what extent the data from non-destructive tests can be used to predict the result of the critical dissolution test.

D-3 Materials and methods

For this study, coated tablet batches were produced in a lab-scale coating apparatus with varying conditions. To obtain clear results, the batches were produced out of specification (OOS), i.e., on purpose the process parameters were chosen outside the range of the standard settings. One aim was to establish a

connection between the results of the different analytical methods and the dissolution test. For this purpose, a set of tablets was chosen from each batch. This tablet was then analyzed using the following non-destructive methods:

- length measurements with micrometer gauges to measure the coating thickness on the cap and band of the tablet,
- tablet weight measurements to determine the coating mass,
- OCT to validate the film coating thickness and quality, and
- NIR spectroscopy in order to give information on the moisture content.

Finally, the critical quality attributes “gastric-juice resistance” and “API release” were measured using the USP II test. The following sections discuss the tablet properties and the process parameters, followed by the details of the measurement methods (dissolution/disintegration test, mechanical size and weight measurement, OCT, NIR spectroscopy)

D-3.1 Tablet cores

The tablet cores were standard round bi-convex shape, with a diameter of 8 mm and a raw weight of 200 mg. They were made with a rotary press and contained an API, acetylsalicylic acid (ASA), and typical excipients.

D-3.2 Coating Process

An enteric coating layer was applied to the cores using a custom lab-scale non-perforated coating pan (Brucks Wabru Pan L10 GE, Heinrich Brucks GmbH, Alfeld, Germany); the apparatus is shown in Figure 30. To enhance drying, heated air was blown onto the tablet bed. The exhaust air was extracted from the pan. For coating, a standard preparation of Eudragit L30D (Evonik Industries AG, Essen, Germany) was produced according to manufacturer guidelines.

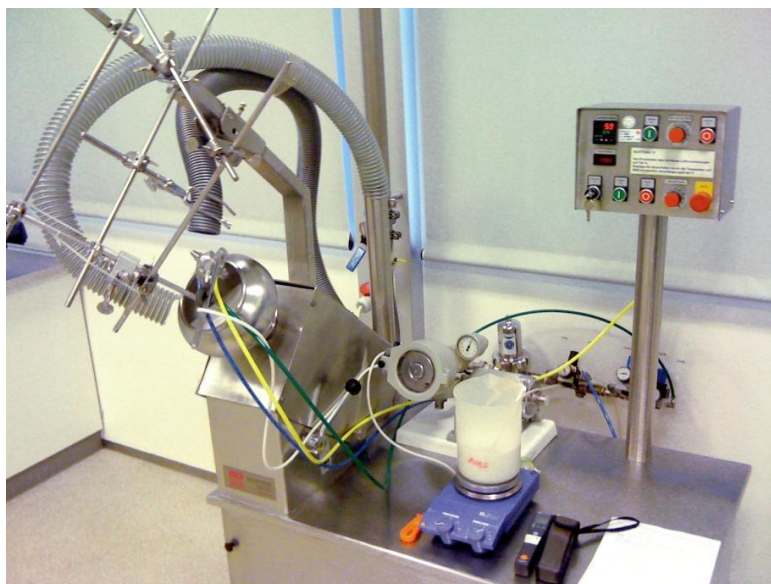


Figure 30: Laboratory coating apparatus, consisting of a coating pan, supply and exhaust air tubing, an atomization nozzle, a peristaltic pump, a coating suspension container and a control unit.

The coating parameters were adjusted according to the experimental plan described below. The spray rate was modified by increasing or decreasing the rotation velocity of the peristaltic pump. The supply air power was adjusted at the control unit and the tablet bed temperature was controlled by changing the supply air temperature. The process was terminated after a gain in weight of 15 mg and was monitored via at-line weight measurement of 20 tablets.

D-3.3 Experimental setup

The drying kinetics of the applied suspension is crucial for the formation of the film coating (Cole, Hogan, & Aulton, 1995). For this reason, three process parameters directly influencing the drying time were chosen, i.e.,

- the tablet bed temperature;
- the spray rate; and
- the drying air flow rate.

To validate the effect of each input parameter, one input factor at a time was changed. A base point was defined based on *a-priori* knowledge of the process (level 0). With regard to the base point, each parameter was increased and decreased (level 1 and level -1, respectively). This meant that all level 1 and level

-1 runs were considerably out of normal specifications for the coating process. For the base point, three replications were performed. A list of the experimental runs is given in Table 3.

Table 3: Experimental plan showing the parameter settings used for the coating runs. The numbers in brackets indicate the level, i.e., whether the setting is considered high (1), low (-1) or base (0).

Batch ID	Tablet bed temperature (°C)	Air flow rate (m ³ /min)	Spray rate (g/min)
B01	31 (0)	1.6 (0)	5.3 (0)
B02	42 (1)	1.6 (0)	4.4 (0)
B03	23 (-1)	1.6 (0)	4.9 (0)
B04	31 (0)	1.6 (0)	2.4 (-1)
B05	31 (0)	1.6 (0)	7.2 (1)
B06	31 (0)	2.4 (1)	4.7 (0)
B07	31 (0)	0.8 (-1)	3.8 (0)
B08	31 (0)	1.6 (0)	4.8 (0)
B09	31 (0)	1.6 (0)	4.7 (0)

During the experiments, the target spray rate could not be set as exactly as the other parameters. Therefore, a target spray rate was set but the actual spray rate was measured by weighing the loss of coating liquid. For the further evaluations and statistical models, the real (measured) spray rate was taken into account, as reported in Table 3.

D-3.4 Stress-tested tablets

From each batch (excluding repetition, B01 to B07), six tablets were sampled and subjected to a stress test. They were placed in 0.1 molar hydrochloric acid for two hours (equivalent to the first part of the combined test described in D-4.4) and then stored for over a month. The aim was to determine the long-term effects of the disintegration test. A visual inspection revealed no deviations from the non-stressed tablets. The stress-tested tablets were then subjected to the same measurement procedure as the regular (non-stressed) tablets. The results are presented separately below.

D-4 Measurement methods

In this study, two types of measurements were done. First, the quality of the coating, especially the thickness, was investigated using non-destructive

methods. Second, the release performance was quantified using a dissolution tester (USP apparatus II). The different measurement methods are described in the following sections.

D-4.1 Length and weight measurements

During the coating process, the gain in the coating thickness is often monitored by controlling the tablet's gain in weight. Although this is a convenient and straight-forward approach, the problem is that the uncoated tablet cores themselves show a significant variation in weight, which may be comparable to the (light) weight of the coating layer. Moreover, this method does not discriminate between the weight gain due to the coating material or to other factors, such as solvent (water) in the core.

In our study, the tablet weight was determined using a high-precision balance (SI-234A, Denver Instrument, Bohemia, US). For each measurement, ten tablets were selected from each batch. Ten uncoated tablet cores were measured as a reference. The coating weight gain was then calculated by subtracting the mean uncoated weight from the mean coated weight:

$$m_{\text{coat}} = \overline{m_{\text{total}}} - \overline{m_{\text{core}}} \quad (60)$$

The standard deviations connected with m_{total} and m_{coat} are in good approximation independent from each other. Therefore, accounting for the propagation of error, the standard deviation of the coating mass is given as:

$$\sigma_{m,\text{coat}} = \sqrt{\sigma_{m,\text{total}}^2 + \sigma_{m,\text{core}}^2} \quad (61)$$

where $\sigma_{m,\text{core}}$ and $\sigma_{m,\text{coat}}$ are the standard deviations of the weight measurements of the coated and uncoated tablets, respectively. Equation (2) shows that the uncertainties in the weight measurement of both coated and of uncoated tablets increase the total uncertainty of the coating mass.

The same problem arises when the film coating thickness is determined by comparing the height or diameter of uncoated and coated tablets: uncoated tablets do vary in size. Since the tablet cores are produced via compaction, and as such the die diameter is constant, the variation in diameter is lower than the variation in height (or weight). The tablet diameter can be measured with a micrometer screw gauge (Digimatic outside micrometer 293-821, Mitutoyo Inc., Japan). For the height of the tablet, a height gauge can be applied (Absolute

Digimatic dial gauge ID-S 543-690B, Mitutoyo Inc., Japan), measuring the distance between the outer-most points of the caps. This low-cost method can easily be applied at-line.

In our study, we measured the height and the diameter (along three different directions) on the ten tablets from each batch. The coating thickness was determined by subtracting the mean value of the uncoated tablets l_{core} from the mean value of the coated tablets l_{total} and by dividing the result by two to reflect that the coating was measured twice:

$$d_{\text{coat}} = \frac{1}{2}(\overline{l_{\text{total}}} - \overline{l_{\text{core}}}) \quad (62)$$

Similar to Eq. 2 the standard deviation is

$$\sigma_{d,\text{coat}} = \frac{1}{2}\sqrt{\sigma_{l,\text{total}}^2 + \sigma_{l,\text{core}}^2} \quad (63)$$

where $\sigma_{d,\text{total}}$, $\sigma_{l,\text{core}}$ and $\sigma_{l,\text{total}}$ are the standard deviations of the length measurements of the uncoated and coated tablets, respectively.

D-4.2 Optical Coherence Tomography (cited from Toschkoff, G. *et al.*, (2013). Effect of Tablet Coating Parameters: Combining Non-Destructive Measurements and Dissolution Testing.)

“OCT is a contact-free, non-destructive imaging method which can be used to investigate the internal structure of translucent and turbid materials. OCT allows the determination and localization of reflecting interfaces, separating media characterized by different refractive indices. The measurement principle is based on low-coherence interferometry (LCI), which uses near-infrared light sources with high spatial but low temporal coherence (i.e., a large bandwidth spectrum corresponding to coherence lengths of several microns). The short coherence length together with the interferometer acts as a temporal filter in terms of the arrival times of back-scattered and back-reflected photons from different sample structures (e.g., interfaces, pores, impurities). Comparing the arrival times of single scattered photons and a reference beam allows the acquisition of a depth or axial scan. Unlike other high-resolution microscopic techniques, in OCT axial

and lateral resolutions are decoupled. The axial resolution Δz is limited by the coherence length of the light source l_c :

$$\Delta z = \frac{l_c}{2} = \frac{2 \ln 2}{\pi n} \frac{\lambda_0^2}{\Delta \lambda_{FWHM}} \quad (64)$$

where λ_0 is the central wavelength, $\Delta \lambda_{FWHM}$ is the spectral bandwidth (i.e., the full-width of half maximum of the spectral profile) of the source and n is the refractive index of the sample (Wojtkowski, 2010).

The depth-resolved information can be acquired either in the time-domain (TD-OCT) by moving the reference mirror of the interferometer or in the frequency-domain (FD-OCT). In FD-OCT the depth-resolved data is obtained by detecting and processing the spectrum of the interfered signal. The main advantages of FD-OCT compared to TD-OCT are the higher acquisition speed (more than 10^5 depth scans per second) and the better sensitivity. The interference spectrum can be acquired in parallel (spectral-domain – SD-OCT) or sequentially (swept-source – SS-OCT). The images presented in this work were obtained with the SD-OCT approach.

Cross-sectional two-dimensional (2-D) images are generated by scanning laterally along the sample object. The lateral resolution is determined by the focused spot of the scanning beam:

$$\Delta x = \frac{4\lambda_0 f}{\pi n d} \quad (65)$$

where d is the spot size of the beam on the objective lens and f is the focal length (Fercher, 2010). An example of a 2-D OCT image of a film-coated tablet is shown in Figure 31. Furthermore, three-dimensional (3-D) volumetric data can be created by scanning the incident optical beam in a raster pattern.

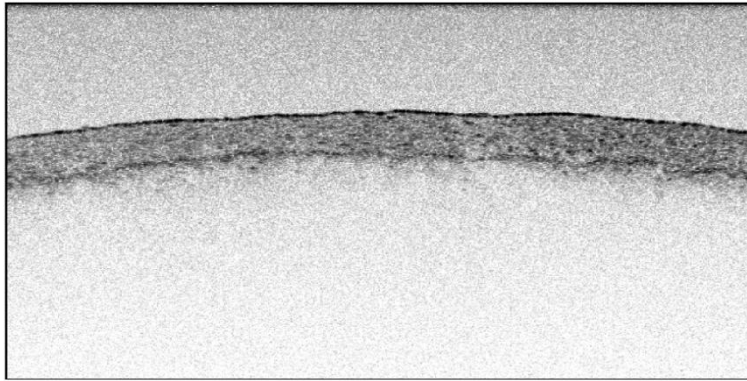


Figure 31: Two-dimensional OCT image of a film-coated tablet. Optical image dimensions (in air): 2 x 1 mm².

An in-house built OCT setup (Koller et al., 2011) with a supercontinuum white light laser source (Koheras SuperK Versa, NKT Photonics, Denmark, $\lambda_0 = 820$ nm, $\Delta\lambda_{FWHM} \lambda_0 = 820$ nm) was used. This setup provides an axial resolution Δz of 2.0 μm (in air) and a lateral resolution Δx of 6 μm . Moreover, this setup allows the visualization of 1.5 images per second using 1000 depth scans per image.

In order to measure the distance between layers in an OCT image, the pixel size must be determined. The optical image dimensions (in air) are 6 mm and 2.5 mm in the lateral and axial directions, respectively. Each OCT image consists of 1000 depth scans, where each scan corresponds to one measurement recorded by a CCD camera (Atmel Aviiva, 2048 pixel, 14 mm² pixel size, 12 bit resolution). The size of the corresponding digital image was thus 1000 x 1025 pixels. The pixel sizes (valid for a medium with a refractive index $n=1$) R_x in the lateral direction and R_y in the axial direction are given as

$$\begin{aligned} R_x &= \frac{6 \text{ mm}}{1000 \text{ px}} = 6 \mu\text{m/px}, \\ R_y &= \frac{2.5 \text{ mm}}{1025 \text{ px}} = 2.43 \mu\text{m/px}. \end{aligned} \tag{66}$$

The coating thickness was determined by measuring the distance on the OCT image in the units of pixel, multiplied by the pixel size and divided by the refractive index n of the coating. The refractive index of the used coating was taken as $n_{\text{Eudragit}} = 1.48$ (Koller et al., 2011). Due to the large number of images and the variation between images, two methods were implemented. First, the distance was measured semi-manually with appropriate software. Second, an automatic image analysis algorithm was developed and applied, which needed no

manual correction and was therefore suitable for comparison of larger image sets.”²

D-4.3 Near-Infrared (NIR) spectroscopy

The NIR measurements were performed using a FT-NIR spectrometer (FT-NIR Spectrum 400, Perkin Elmer, USA). The obtained spectra were analyzed using commercial software for multivariate data analysis (Unscrambler®, CAMO Software AS).

For the measurement, ten tablets from each batch were selected, and NIR spectra were recorded for both caps of each tablet using the NIR probe of the spectrometer. Different wavelength ranges were evaluated for their prediction ability. One of the models was based on the theory that dissolution performance is related to the moisture in the tablets. This model produced the best results when the spectra were limited to the wavelength range of 1786 - 2174 nm. The data were then preprocessed via a standard normal variate (SNV) transformation to remove multiplicative variations between the spectra, such as variations in the physical properties of the tablet.

Finally, a principal component analysis (PCA) was carried out to extract essential information from the large data set. The spectra were projected into a lower-dimensional space which is spanned by linearly uncorrelated variables (the principal components). The first principal component represents the most dominant source of variability in the data. Each succeeding component is defined such that the next dominant sources of variability is accounted for, under the condition that it has to be linearly uncorrelated to all previous components.

D-4.4 Disintegration and dissolution test

Following the non-destructive measurements, the same tablets were investigated in a dissolution tester (DT 800, ERWEKA R, Germany). The tests were performed according to the USP II dissolution test guidelines (United States Pharmacopeia 34/National Formulary 29, Chapter <711> Dissolution, 2011). It consisted of two parts, i.e., the disintegration test measuring the resistance to gastric juice, and the API-dissolution test, measuring the dissolution profile of the API.

² Toschkoff, G., Schinwald, C., Markl, D., Koller, D. M., Scheideler, M., Leitner, M., & Khinast, J. G. (2013). Effect of Tablet Coating Parameters: Combining Non-Destructive Measurements and Dissolution Testing. Submitted to Eur J Pharm Biopharm.

During the disintegration test, each tablet was placed in 0.1 molar hydrochloric acid (pH=1) and constantly kept in motion to simulate the stomach environment. A solution of hydrochloric acid containing 100 % dissolved API was prepared as a reference. After two hours, a sample was taken and the API concentrations in the sample and reference were compared in an UV-VIS spectrometer (Agilent 8453, Agilent Technologies Inc., USA). The characteristic absorption at 280 nm was measured to calculate the percentage of release according to the calibration curves. To pass the disintegration test, the API concentration in the sample had to be lower than 10%.

During the dissolution test, the hydrochloric acid was neutralized in-situ using a phosphate buffer of pH=6.8 to simulate the intestinal tract environment. The tablets were moved for 30 minutes in the buffer solution. Samples were taken every ten minutes and compared to a reference phosphate buffer with 100 % API in solution. The absorption at a characteristic wavelength of 265 nm was measured and the release percentage was determined. To pass the dissolution test, an API release of at least 75 % after 30 minutes (corresponding to an immediate release formulation) was necessary.

D-5 Results and discussion

As a first step, a larger number of tablets were investigated via NIR, the results are shown in the next subsection. Based on the NIR results, a number of tablets were chosen from each batch for closer investigation. The criteria for choosing the tablets are described below. These tablets were subjected to a series of non-destructive measurements (weight measurement, micrometer screw gauge, OCT imaging). The results for those tablets are discussed together with the outcome of the dissolution tests further down. Finally, the corresponding results for the stress-tested tablets are shown.

D-5.1 Near-infrared spectroscopy: moisture screening

Figure 32 depicts the score plot of the PCA analysis of the gathered spectra. Applying PCA to the data set may be viewed as a classification of the main events affecting the tablets.

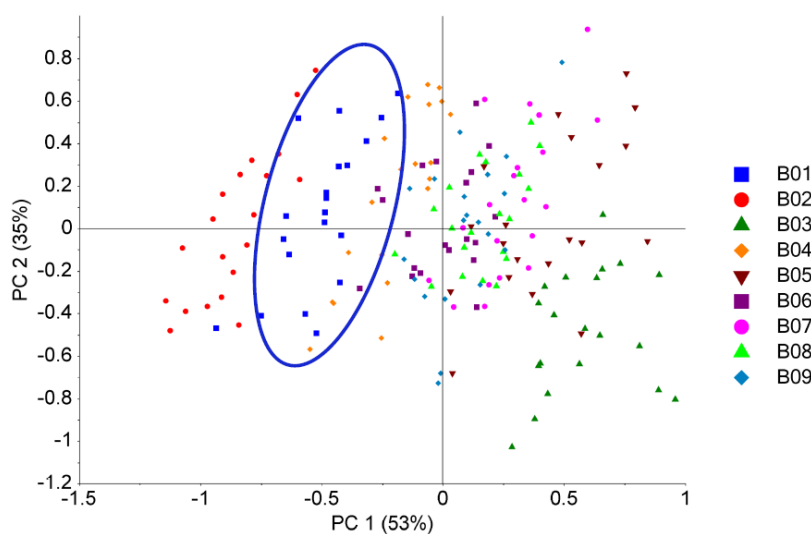


Figure 32: Score plot of the first and second principal components of the NIR spectra. The ellipse exemplarily indicates the clustering of batch B01. The values in parentheses of the PC 1 and PC 2 label state the percentage of total variance explained by each principal component. As example, batch 01 is highlighted by an ellipse.

It showed that the first two principal components described the main variations between the tablets from the different batches. Clustering of the batches was observed, especially for the first principal component (PC 1). For high drying rates, most of the resulting batches were located at lower values of PC 1. These were especially batches B02 (high tablet-bed temperature) and B04 (low spray rate). A high air flow rate (B06) did not show a strong effect. Values of PC 1 were higher for batches produced with slow drying (B03, B05, and B07). The replication runs B08 and B09 with medium settings were distributed around the PC 1 and PC 2 score center as expected. Surprisingly, batch B01 showed similar behavior to the batches produced at a high drying rate, although the spray rate was slightly higher than for B08 and B09. Apparently, the bed temperature was not changed by the higher spray rate, due to the relatively high inlet temperature. In this way, a first complete coating layer was formed rapidly and acted as a moisture barrier. Thus, subsequent spraying would not wet the core. This beneficial behavior of slightly higher spray rate together with a higher air temperature can also be seen in the corresponding industrial-scale process. In sum, it can be seen that the principal component PC 1 is connected to the moisture level of the coating process.

Tablets located at the center of the respective batch cluster were deemed representative of the whole batch and were further investigated, as described in the “Methods” section.

The same procedure was applied to the stress-tested tablets (Figure 33). The twelve measurement points per batch correspond to the two caps of the six tested tablets.

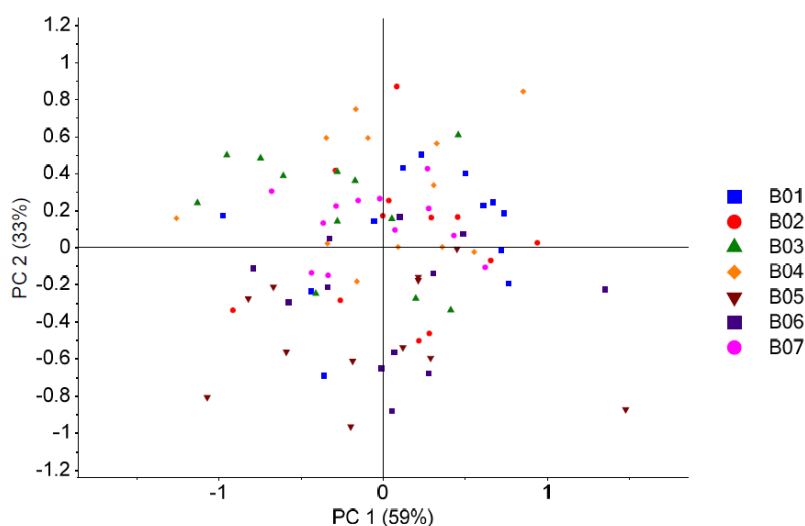


Figure 33: Score plot of the first and second principal components of the NIR spectra for the stress-tested tablets. The values in parentheses of the PC 1 and PC 2 label state the percentage of total variance explained by each principal component.

In this case, the spectra of the same batches did not form clusters and did not follow a discernible trend. The simulated gastric juice appeared to penetrate the tablets during the test, affecting their moisture content and making it impossible to distinguish one tablet from another. As before, one tablet per batch was chosen for further investigation.

The results suggest that performing combined NIR and PCA measurements are a suitable way to detect the tablets’ moisture content. To validate this and to develop a predictive model, a reference method for moisture measurement is required. However, this was beyond the scope of this work.

D-5.2 End point determination by tablet weight

For our process, the targeted end point of the coating was a mass increase of 15 mg. Table 4 shows the average weight before and after coating. While the values

were slightly higher than the target, a consistent end point requirement was met for all batches. The spread between the highest and lowest coating mass was less than 10% and in the order of the standard deviation of the weight measurement.

Table 4: Weight of tablet batches

Batch Id	m_{tablet} (mg)	σ_{tablet} (mg)	m_{coating} (mg)	σ_{coating} (mg)
Uncoated	199.9	0.7		
B01	215.3	0.5	15.3	0.9
B02	215.7	0.6	15.7	0.9
B03	216.4	0.9	16.5	1.1
B04	215.1	0.6	15.2	0.9
B05	216.2	0.7	16.2	1.0
B06	215.7	0.3	15.8	0.8
B07	215.4	1.0	15.4	1.2
B08	215.0	0.9	15.1	1.1
B09	216.0	0.3	16.0	0.7

Height and diameter measurements

The film coating thickness that was determined using the micrometer screw gauges is shown in Figure 34 for all batches. As expected, the error was greater for the coating thickness on the tablet's cap for the following two reasons. First, only one measurement direction per tablet was possible in the axial direction, while the radial measurements were performed for three positions (directions). Second, the uncoated cores already had a higher variation in height than in diameter: the diameter was determined by the fixed diameter of the die, while the height was influenced by variations in the pressure force curve during the compaction process.

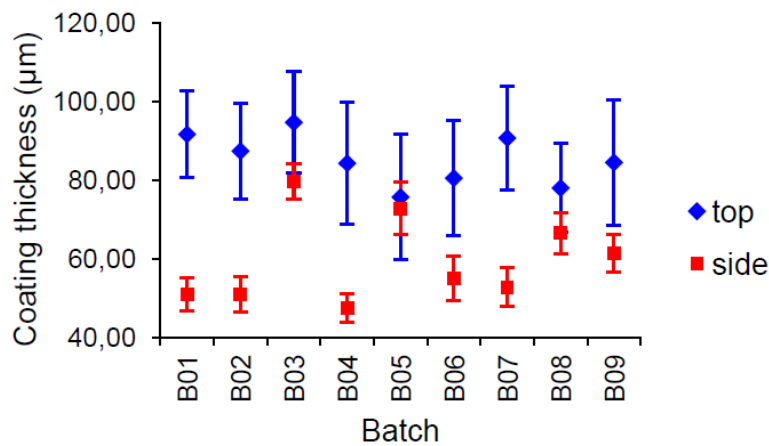


Figure 34: Film coating thickness for the different batches, determined with a micrometer screw gauge.

In Figure 34, the coating on the band is always thinner than on the cap, with the magnitude of the difference between cap and band changing from batch to batch. For the processes operated using “wet” settings (i.e., low tablet-bed temperature (B03) or a high spray rate (B05)), an almost equal thickness of the film on the cap and edge and therefore a higher inter-tablet coating uniformity were observed. The “dry” processes with high tablet-bed temperature (B02) or low spray rate (B04) resulted in higher coating thickness on the cap of the tablet compared to the band. A possible explanation is the longer drying time during the “wet” processes and the associated re-distribution of the coating liquid from freshly coated to surrounding tablets due to the tablet bed movement. In a “dry” environment, the applied coating solidifies almost immediately. Due to the preferred orientation of bi-convex tablets, the tablet’s cap is exposed to the spray more often than the band, and thus, receives more coating mass (Freireich, Ketterhagen, et al., 2011; Ho et al., 2007). Variations in the air flow rate (B06 and B07) did not affect the coating distribution significantly.

D-5.3 Optical Coherence Tomography

The coating thickness was determined based on the OCT images both semi-manually using image processing software (Image Processing Toolbox, MATLAB, Mathworks, Inc., Massachussets, USA) and automatically using an in-house developed algorithm. Although the results obtained via the algorithm and the manual evaluations generally correlated very well, for two batches distinct differences were observed (Figure 35). One reason is that on the OCT images the lower boundary (transition between coating and core) is not as defined as the

upper boundary (coating-air) due to a lower difference in the refractive index and because the coating solution fills pores on the core surface and to an extent diffuses into the core.

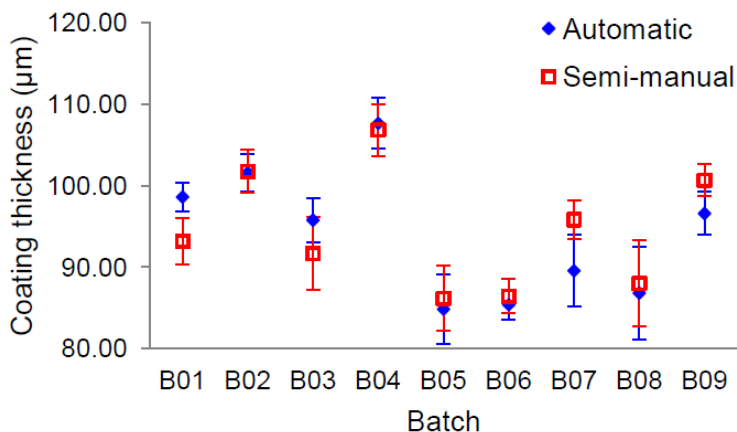


Figure 35: Film coating thickness determined manually and automatically from OCT images.

Figure 36 shows the film coating thickness on the tablet cap determined with a micrometer gauge and from OCT images. In most cases, the OCT results were above those obtained with the micrometer. However, the mechanical measurements showed higher standard deviations than those based on OCT images, to the extent that the differences between the two curves were not statistically significant. While the deviation of the micrometer gauge was low enough to determine significant differences between the cap and edge coating, the OCT method was a better choice for comparing more subtle differences between the batches.

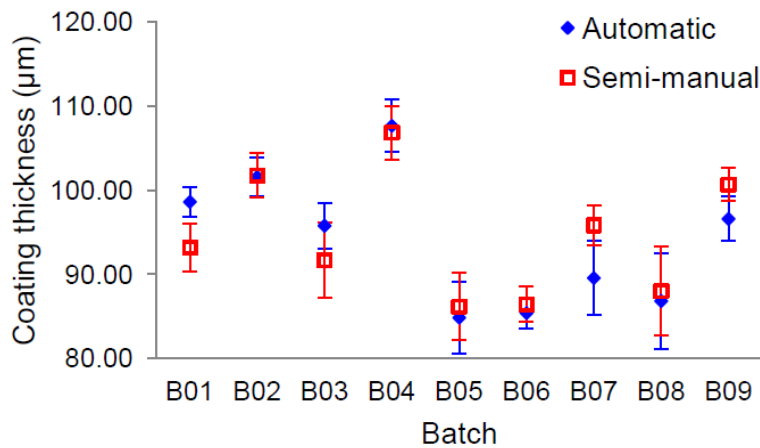


Figure 36: Film coating thickness as determined based on OCT images (semi-manual evaluation) and “direct” length measurement (micrometer gauge).

OCT images showed that one tablet had a damaged coating. For the damaged area, a three-dimensional image was assembled from the 2-dimensional scans (Figure 37), which demonstrated that coating was missing on an area of approximately 1 mm². Since this tablet was used for the replication experiment, it was decided not to replace it but to subject it to the disintegration/dissolution test.

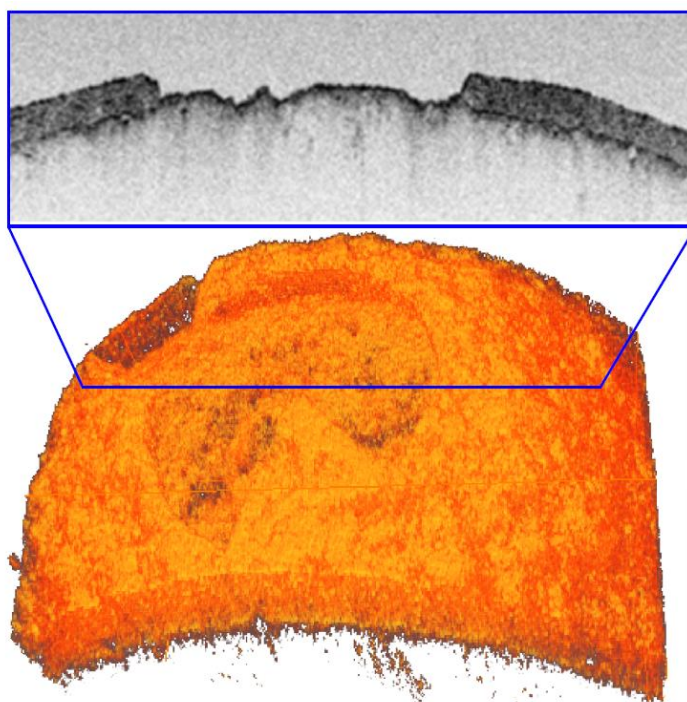


Figure 37: Three-dimensional image of the region with the missing coating from batch B08. Optical image dimension (in air): 6 x 0.5 x 2.5 mm³.

D-5.4 Dissolution and disintegration test

The results of the disintegration and dissolution tests are shown in Figure 38. Only one tablet (the one with the missing coating) failed the disintegration test. All tablets passed the dissolution test, i.e., the full amount of API was released from all tablets after less than 20 minutes. Despite the process parameters considerably out of specification and differences in the appearance of the coating surface, the intact coating layer was functional for all tablets.

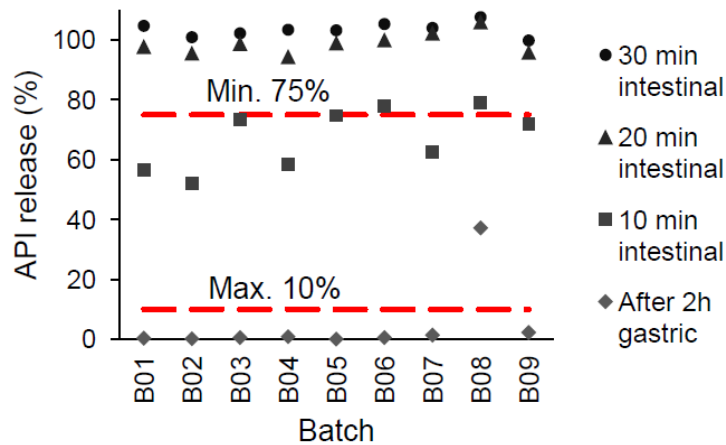


Figure 38: Dissolution performance in 0.1 m polar hydrochloric acid of pH = 1 (gastric) and phosphate buffer of pH = 6.8 (intestinal).

D-5.5 Stress-tested tablets

The seven stress-tested tablets were measured the same way as the regular tablets. The dimensions of the tablets were measured before and after the disintegration test, during which the coating thickness on the cap (Figure 39) and edge (Figure 40) of the tablets seemed to have increased by approximately 30 μm . However, the thickness was calculated based on the height/diameter measurements under the assumption that the size of the core was constant. An increase in the core size with the constant coating thickness would still register as a “coating thickness” increase. Thus, in this case the micrometer gauge measurements could only state a significant increase in volume without differentiating whether the coating or the tablet core changed in size.

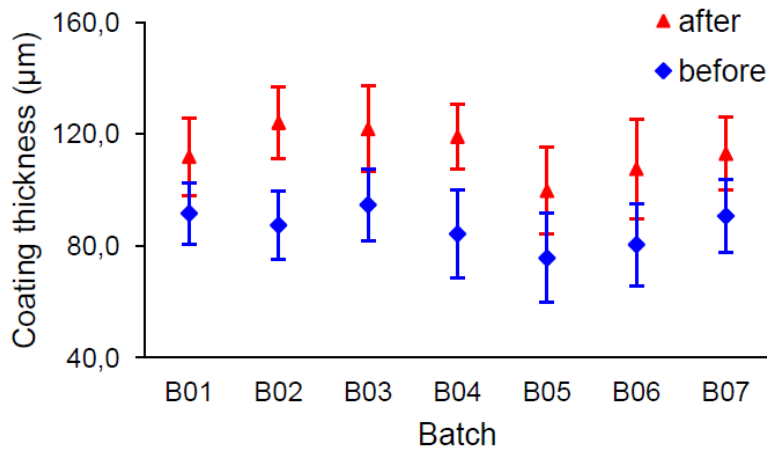


Figure 39: Film coating “thickness” (in fact a measure of total thickness, see text) on the caps for tablets from different batches determined with micrometer gauge before and after the disintegration test.

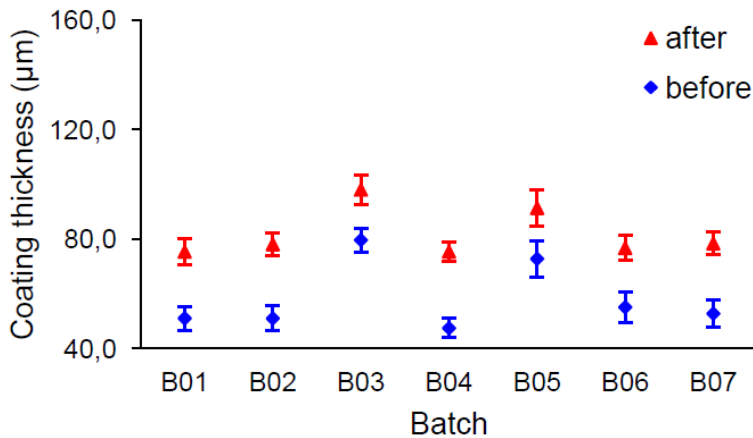


Figure 40: Film coating “thickness” (in fact a measure of total thickness, see text) on the band for tablets from different batches determined with micrometer gauge before and after the disintegration test.

The advantage of the OCT-based method is that the coating thickness is measured directly, regardless of the size changes in the core, and can therefore determine whether the coating or core size increased. Figure 41 shows the coating thickness of the tablets before and after the disintegration based on the OCT measurements.

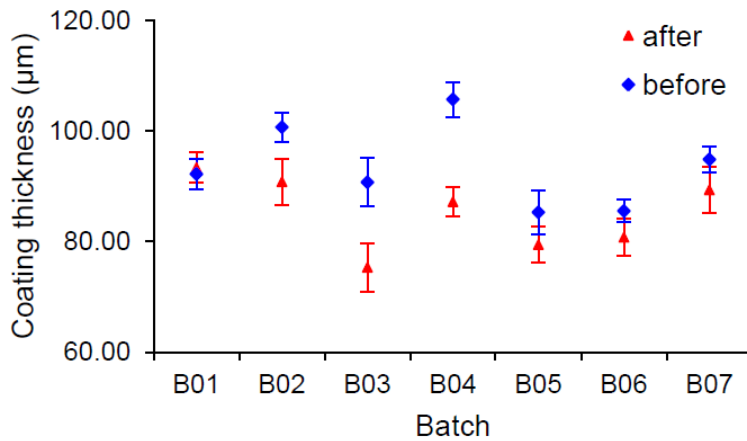


Figure 41: Film coating thickness determined from OCT images before and after the disintegration test.

Surprisingly, the coating thickness did not increase; for most batches it decreased slightly. However, since the total volume increased, the size of the tablet core must have increased. This swelling was most likely caused by the diffusion of the gastric juice into the tablet during the disintegration test. With the increase of volume, it also makes sense that the coating is stretched thinner; in addition, a small outer part of coating will most likely dissolve as well.

Additionally, the weight of the tablets was measured before and after the disintegration test. The average was calculated using 6 tablets from each batch (Figure 42). The tablets' weight increased significantly, which was in agreement with the observed swelling of the core.

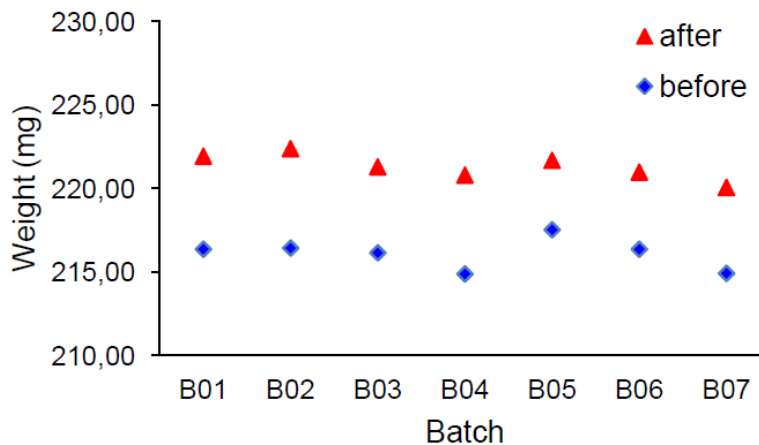


Figure 42: Weight of tablets before and after the disintegration test.

Although the dissolution test is known to increase the weight of tablets (Thoma & Bechtold, 1999), the exact mechanics are not clear. The results presented in this work indicate that the thickness of the coating layer decreases and, therefore, the increase in volume and weight must be due to the swelling of the core.

The seven tablets used for the disintegration testing were stored for over a month. Examining them showed that the coating thickness decreased, the core size increased and that moisture was present. Still, when these tablets were finally subjected to the API release test, they all had full API release after less than 20 minutes (Figure 43). Therefore, the moisture inside the film coating did not lead to the API degradation.

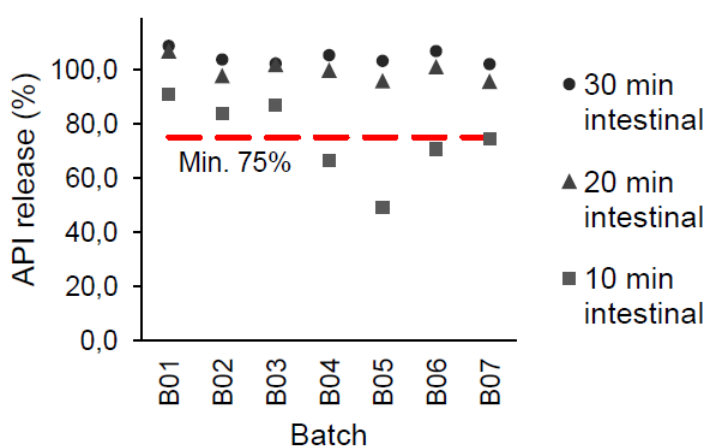


Figure 43: Release performance of the tablets used for the disintegration tested.

D-6 Conclusion

The main goal of this work was to study how varying process conditions influence the coating, and in further consequence the outcome of the USP II test. For this, the film coating of tablets produced with “out-of-spec” parameters was analyzed via different methods. Selected tablets were used in a series of non-destructive tests and a final destructive USP II disintegration/dissolution test. The coating thickness was determined with a micrometer screw gauge and OCT. The obtained results were compared and their relationship with the outcome of the final dissolution test was investigated.

The straight-forward measurement of the film coating thickness with the screw gauge had some limitations. The coating thickness on the band could be

measured with acceptable accuracy, but the thickness on the cap of the tablet was error-prone. Moreover, it was impossible to determine if the observed weight increase was due to the actual increase in the coating thickness or to the swelling of the core. In contrast, OCT imaging directly measured the tablets' coating thickness, regardless of the core size changes. Additionally, the images provided general information regarding the thickness distribution and the coating quality. Due to its fast processing time, the OCT method may potentially be used as an at-line or even in-line PAT tool for coating process monitoring.

All tablets (with one exception due to damage) tested in the USP II dissolution apparatus showed excellent gastric juice resistance and API release performance. Even the considerably out-of-spec process parameters did not lead to failure. The only exception was a tablet with damaged coating, which was detected based on OCT images prior to the dissolution.

It is known from the literature that coating on the tablet band tends to be thinner than on the cap (Freireich, Ketterhagen, et al., 2011; Ho et al., 2008). Our investigation confirmed this observation. However, the uniformity of the coating layer increased for the "wet" process conditions (i.e., high spray rate and/or low temperature).

During an additional investigation, the tablets were stress-tested (subjected to the simulated gastric juice for 2h without disintegrating and then stored for over a month) before being measured in the same manner as the regular tablets. The combination of different non-destructive measurements for the same tablet led to the conclusion that the coating thickness of the tablets actually decreased, while the tablet core volume and mass increased due to moisture uptake. However, the tablets showed a complete release of API, i.e., humidity in the core did not cause the API to degrade.

Acknowledgements

This work has been funded within the Austrian COMET Program under the auspices of the Austrian Federal Ministry of Transport, Innovation and Technology (bmvit), the Austrian Federal Ministry of Economy, Family and Youth (bmwfj) and by the State of Styria (Styrian Funding Agency SFG). COMET is managed by the Austrian Research Promotion Agency FFG.

Michael Leitner gratefully acknowledges support from the "K-Project for Non-Destructive Testing and Tomography (ZPT) within the COMET-program of the Austrian Research Promotion Agency (FFG), Grant No. 820492, the European

Regional Development Fund (EFRE) in the framework of the EU-program REGIO 13, and the federal state of Upper Austria.

We further gratefully thank G.L. Pharma GmbH (Lannach, Austria) for the support, for providing the coating apparatus and materials, and for the valuable discussions.

Chapter E: Spray Models for Discrete Element Simulations of Particle Coating Processes

Published as: Toschkoff, G., Just, S., Funke, A., Djuric, D., Knop, K., Kleinebudde, P., Scharrer, G., Khinast, J. G. (2013). Spray models for discrete element simulations of particle coating processes. *Chem Eng Sci*, 101, 603–614.

E-1 Abstract

In the pharmaceutical industry, drum coating is routinely used for the production of film tablets. In order to produce a high-quality product, it is important to understand this seemingly simple process in great detail. In our study we present the implementation of three different methods to include spray coating in DEM simulations: (1) an enhanced “spray zone approach” working during run-time, (2) the “discrete drop method”, a novel approach for tablet coating also applied at run-time, and (3) the “ray-tracing method”, which is applied after the DEM simulation using the saved data. Each method is described in detail. For evaluation purposes, the different models were applied to simulate the same coating process, and the comparability, advantages and limitations are discussed. In general, all three methods can give comparable results. However, the spray zone approach depended heavily on its model parameters; the discrete drop method was more reliable and versatile. While the time resolution is higher for the first two methods listed above, the third is faster and more flexible.

E-1.1 Keywords

Discrete Element Method, Spray coating, Granular materials, Particulate processes, Simulation

E-2 Introduction

Drum coating of tablets is a common unit operation in the pharmaceutical industry. During this process, a large number of tablet cores are placed in a cylindrical drum rotating around its horizontal axis. The rotational motion leads to radial and axial mixing of the tablets (Muliadi & Sojka, 2010). To enhance the

mixing and to achieve uniform coating, most commercially available systems have baffles mounted inside the drum. A coating layer is formed by spraying a coating liquid onto the moving tablet bed, typically consisting of an aqueous polymer dispersion. To prevent over-wetting of the tablets and to extract the solvent, an air flow through the coater is established, which may affect the tablets and the spray to a varying degree (Toschkoff et al., 2012). While the dominant factor globally is the movement of the tablet, locally it is the tablet-drop interaction (Bolleddula et al., 2010; Suzzi et al., 2010). When a tablet travels through the spray zone (that is, the region in the coating drum where the droplets hit the tablets), its exposed surface is covered with coating-liquid droplets that spread on the surface. The solvent evaporates and the remaining substances form a partial film on the tablet surface. In the course of a coating process, each tablet visits the spray zone multiple times. Each time, a partial coating is applied, and after a sufficient number of visits the tablet core is completely covered with a layer of a certain thickness. The relative effect of droplet size, impact and frequency, liquid spreading, drying and the ensuing solid-state transformations determine the morphology and quality of the coating.

While the tablet coating process itself is relatively simple, it is vital to understand it in detail, since the regulations in the pharmaceutical industry require a consistently high product quality. The main two criteria for adequate process performance are intra- and inter-tablet uniformities. Intra-tablet uniformity describes the variation of the coating thickness on one tablet. Inter-tablet uniformity describes the differences in total coating mass between individual tablets. An entire batch can be rejected if either or both of the required values are not met.

To achieve a deeper understanding of the coating process, a number of experimental investigations have been performed to study the influence of process parameters on the outcome (Mueller & Kleinebudde, 2007b; Sandadi et al., 2004). Both inter- and intra-tablet uniformities have been measured (Tobiska & Kleinebudde, 2003), with a trend towards novel non-destructive techniques, such as Terahertz-Pulse Imaging (Ho et al., 2007) or Optical Coherence Tomography (Koller et al., 2011; Mauritz et al., 2010; Zhong et al., 2011).

Along with experimental investigations, the Discrete Element Method (DEM) has gained interest as an additional tool for analyzing the process via simulation. In general, DEM has successfully been applied to many particulate processes (González-Montellano et al., 2011; Remy et al., 2010; Tsuji, 2000; Zhu, Zhou, Yang, & Yu, 2008), in the pharmaceutical industry (Ketterhagen, am Ende, &

Hancock, 2009c; Kuo et al., 2002; Turton, 2008) and especially to tablet coating (Yamane et al., 1995). DEM-based tools are particularly well-suited for tablet coating for two reasons. First, the movement of tablets in a coater is governed mostly by gravitational and inertial body forces, in combination with particle-particle and particle-wall collisions. Additional forces due to air flow or cohesion are mostly negligible. Second, although the number of tablets involved in the process is high enough for granular behavior, in many cases it is small enough to be processed with the available computational hardware. Pandey et al. (Pandey, Song, et al., 2006) investigated the movement of spherical particles in a pan coater both computationally via the DEM and experimentally via video-imaging and demonstrated that the results for the dynamic angle of repose and the cascading layer velocity were in good agreement. Sahni et al. (Sahni et al., 2011) used both simulations and experiments to study the influence of different parameters on mixing in a pan coater, with both methods showing the same qualitative behavior. In many cases, the investigated particles had a spherical shape or were approximated by spheres to reduce the computational effort. A few studies that focused on the influence of the shape itself (Ketterhagen, 2011; Suzzi et al., 2012) used the “glued sphere” approach to approximate arbitrary shapes by a number of spheres (Favier et al., 1999). An alternative new method is to apply a contact detection algorithm that models the bi-convex tablet shape using parts of intersecting spheres (M. a C. J. b H. B. c W. C. a d Kodam, 2012; Song et al., 2006). The shape is especially important for intra-tablet uniformity, since non-spherical tablets may not achieve perfect uniformity even for infinite coating times (Freireich & Wassgren, 2010).

A default DEM simulation provides limited data, such as the tablet position or velocity. To obtain additional attributes (e.g., coating uniformity), it must be established which tablets are in the spray region (i.e., being coated) at a given time and which are not. Different approaches to this problem have been proposed. Freireich et al. (Freireich & Wassgren, 2010) calculated intra-particle coating variability via Monte-Carlo simulations. To detect the spray zone, a two-dimensional grid was used. The dimension along the cylinder axis was neglected due to the small axial length of the cylinder. Another approach was presented in (Freireich, Li, et al., 2011) who combined DEM simulations with a population balance method in a compartment model. The spray zone was detected by projecting parallel rays in a rectangular region onto the tablets and detecting collisions. An experimental and computational study of the inter-tablet coating variability was performed in (Kalbag & Wassgren, 2009). Based on the results of the experiments the bi-convex tablets were approximated in a DEM simulation by

spheres of the same volume, which were reported to have nearly identical circulation times (Pandey & Turton, 2005). Using the output data of the DEM simulation, one proposed method to detect the spray zone is using the fill fraction of static cubical voxels. It is less accurate than a ray-tracing method, but needs less computational time (Kalbag et al., 2008). In an investigation of the influence of the particle shape on inter- and intra-coating uniformity, a top-detection algorithm to monitor residence time in a rectangular spray zone was used (Ketterhagen, 2011). The tablets on the top in each bin were detected each 20 ms. To evaluate single visit residence times, a threshold value of 100 ms was defined: if two visits to the spray zone are only separated by a short time span (shorter than the threshold), they are counted as one single, longer visit.

In our work, three different spray methods were implemented and integrated into a DEM simulation of a tablet coating process, namely:

1. using an enhanced static spray zone during the simulation,
2. including spray droplets directly into the DEM framework, and
3. applying a ray-tracing algorithm on saved data after the actual DEM runs.

The development was done with a focus on the simulation of tablet coating processes, but the models are applicable to general particle processing steps involving sprays.

E-3 Materials and Methods

E-3.1 Simulation of the Coating Process

The simulated tablet coating process was performed in a lab-scale drum coater (BFC5, L.B. Bohle, Germany), in which the drying air enters and leaves via a fully perforated drum. It is therefore assumed that the spray is not significantly affected by the air, and thus, the influence of the air stream was neglected in our work. To promote axial tablet mixing, two ribbon-shaped baffles were mounted inside the drum. The coater geometry used in the simulation was provided by the manufacturer and is shown in Figure 44.

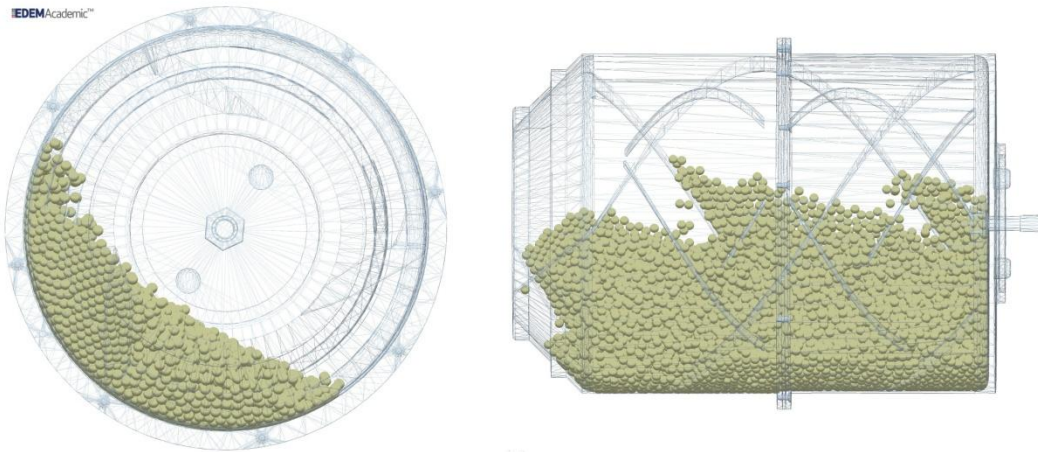


Figure 44: Geometry of the Bohle coating drum used for the investigation of spray modules. From left: front view, side view, and a perspective view.

DEM simulations were performed with the software package EDEM 2.3 (DEM Solutions Ltd., Edinburgh, UK). As tablets, spherical particles of a diameter of 4 mm were considered. This simplification (i.e., spherical tablets) was chosen as the implementation of spray models is the focus of the present work. The material parameters and simulation settings for the DEM simulations are given in Table 5.

Table 5 Parameters for the DEM simulation.

Material property Geometry (steel)	
Poisson's ratio	0.25
Shear Modulus	7.93×10^{10} Pa
Density	7850 kg/m^3
Material properties Particle (tablet)	
Poisson's ratio	0.3
Shear Modulus	1×10^6 Pa
Density	1200 kg/m^3
Interaction	
particle–steel = particle–particle	
Coefficient of Restitution	0.74
Static friction coefficient	0.16
Rolling friction coefficient	0.01
Simulation	
Time step length	6×10^{-5} s

Cell size	0.008 m
-----------	---------

For the initialization, 12446 particles were placed into the rotating drum, and the simulation was run until a dynamic equilibrium state of the tablet motion was reached after 2 seconds. This was then used as a starting point for all subsequent simulations including the spray model, running for 18 seconds each. Three different spray-modeling approaches were investigated in our work. An elliptical shape was chosen for the spray cross-section, approximating the shape produced by a typical spray nozzle. The size and location of the spray zone is shown in Figure 45.

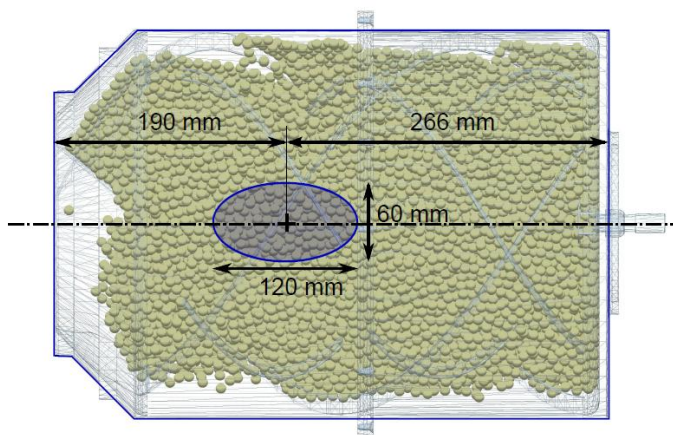


Figure 45: Size and position of the spray zone shown in a top view of the coater.

E-3.2 Spray Simulation Details

In general, spray simulations can be performed in two different ways, i.e., during the simulation along with other calculations for each time step (run-time), or after the simulation (post-processing). Due to the small time steps required by DEM simulations, data are typically not saved at every simulation time step. For example, a typical simulation time step is in the order of 50 μ s, while only each 10 ms data are written to the hard disc. Everything in between is lost after the DEM simulation, and therefore, only reduced data sets are available for post processing. Thus, a run-time method can, on one hand, take advantage of the small DEM time step and use the full data sets. On the other hand, the run-time spray simulation prolongs the already extensive simulation by up to 15%. This is the strength of the post-processing method: a typical run only takes a few minutes. However, a change of rotation speed or tablet shape still necessitates a

re-run of the DEM simulations. Nevertheless, when changing only the properties of the spray zone, such as position or size, this is not necessary.

In this work we developed and implemented two methods for the run-time spray simulation, and one post-processing algorithm. The run-time methods were realized using the programming interface provided by the software. The first one was based on an existing spray zone module but its functionality was significantly extended to better model a realistic spray. The second one was a method involving actual spray particles rather than the definition of a spray zone. The post-processing method was based on a ray-tracing algorithm and implemented in MATLAB. All three are detailed in the next sections.

E-3.2.1 Improved Spray Zone Approach

A common way of measuring for how long a particle is sprayed is to define a spray zone, i.e., a geometric region in which the particles “receive” a coating mass. At each time step, particles are detected to be (or not to be) in the spray zone. If they are in the spray zone the particle’s residence time is increased by the length of the time step. The most straightforward approach is to use the residence time in the zone as a measure of the coating mass received.

The DEM code used in our work already featured basic spray-zone detection features during run-time and post-processing. The run-time module only supports cubic spray zones, in which the faces are perpendicular to the coordinate axes. However in a realistic spraying process, only the tablets on and close to the top of the bed (i.e., tablets that are completely or partially exposed to the spray) receive coating mass. A very basic approach is to define a static spray zone around the top part of the tablet bed, i.e., only the upper layer of the tablets is in the zone. However, this only works if the tablet bed top is more or less stationary during the process. This is not the case for most coating drums, especially if baffles are present. In this case, either tablets in the second layer below may also receive coating, or tablets on the top do not receive coating.

To address these issues, we implemented an algorithm that uses a more general spray zone, and detects which tablets are on top of the bed so that only these received coating. This “improved spray zone approach” operated during run time and was implemented as a user module for the DEM software. The two components (generalized spray zone and top detection) are explained in the following two sections E-3.2.2 and E-3.2.3 .

E-3.2.2 Spray zone detection

To resemble a realistic spray, the spray zone is represented by a cylindrical zone with elliptical cross section (see Figure 46).

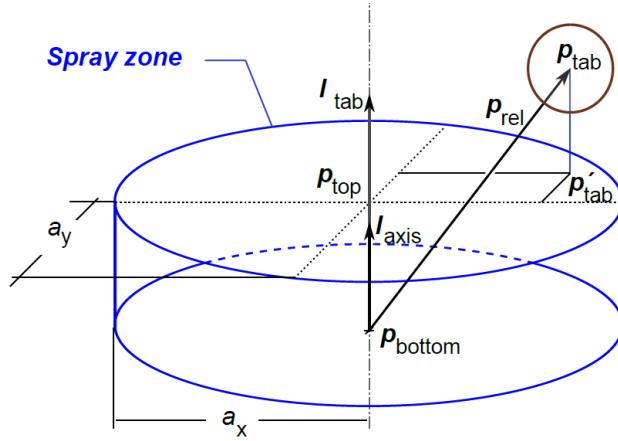


Figure 46: Schematic of the spray zone, showing the points and vectors governing the zone detection.

Position, orientation, and size of the zone are defined by stating the center points of the bottom and top faces of the cylinder ($\mathbf{p}_{\text{bottom}}$ and \mathbf{p}_{top} , respectively), and the major and minor ellipse axes normal to the cylinder axis. With this, the normalized axis vector \mathbf{l}_{axis} are defined as

$$\mathbf{l}_{\text{axis}} = (\mathbf{p}_{\text{top}} - \mathbf{p}_{\text{bottom}}) / |\mathbf{p}_{\text{top}} - \mathbf{p}_{\text{bottom}}| \quad (67)$$

For each tablet a check is performed if it is positioned within the zone. A scalar projection onto the axis vector gives a measure for the relative axial position of the tablet:

$$l_{\text{tab}} = \mathbf{p}_{\text{rel}} \cdot \mathbf{l}_{\text{axis}} = |\mathbf{p}_{\text{rel}}| |\mathbf{l}_{\text{axis}}| \cos(\alpha) = |\mathbf{p}_{\text{rel}}| \cos(\alpha) \quad (68)$$

with \mathbf{p}_{rel} being the vector from the bottom face to the particle center:

$\mathbf{p}_{\text{rel}} = \mathbf{p}_{\text{tab}} - \mathbf{p}_{\text{bottom}}$. For $l_{\text{tab}} < 0$, the tablet position is lower than the lower face. If

l_{tab} is larger than the cylinder's height, the particle is above the higher face. In

both cases, particles are not being coated. If l_{tab} is between 0 and the cylinder

height, the next step is to check if the particle is inside the cylinder's mantle. For

this purpose, a scalar projection of \mathbf{p}_{rel} onto the vectors of the ellipse axes a_x and

a_y is performed to obtain the tablet's positions $p'_{\text{tab},x}$ and $p'_{\text{tab},y}$ in the local coordinate system of the ellipse:

$$p'_{\text{tab},i} = \frac{\mathbf{p}_{\text{tab}} \cdot \mathbf{a}_i}{|\mathbf{a}_i|}, \quad i = x, y. \quad (69)$$

The inequality defining an ellipse can then be used:

$$\frac{p'^2_{\text{tab},x}}{|\mathbf{a}_x|^2} + \frac{p'^2_{\text{tab},y}}{|\mathbf{a}_y|^2} < 1 \quad (70)$$

If the inequality in Eq. (70) holds true, the tablet is within the spray zone. In this case, the residence time of the particle in the spray zone is increased by the length of the time step.

E-3.2.3 Top Detection

For reliable results with the spray-zone approach, only tablets at the top of the tablet bed should be included, since only these tablets receive spray mass. An additional algorithm was implemented that detects which tablets are on top at each time-step during the DEM simulation. This approach and its limitations are described in the following paragraphs.

For the detection, a static plane is defined that has to be approximately parallel to the top of the particle bed. For convenience, the direction of gravity is adjusted so that this plane can be chosen normal to the z-direction, see Figure 47.

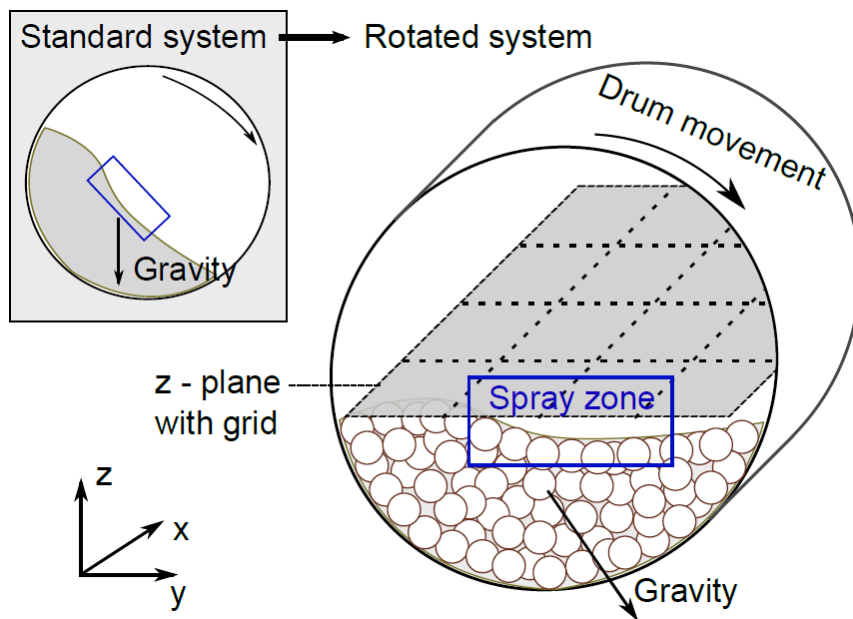


Figure 47: Schematic of the top detection by introducing a plane and dividing it into a detection grid.

The plane is divided into a regular grid with grid spacing Δ_g in both x- and y-direction. For each field of the grid, the particle that is the top-most in each field needs to be found. In other words, when looking from above through the grid, those particles that are seen as being the uppermost in each grid field are detected. The search for the top-most particle is done at each time step of the DEM simulation, and therefore, has to be efficient. Therefore, a fast algorithm using the center point of the spheres was developed.

Which particles are recognized as being on the top depends on the user-defined grid spacing. This is a consequence of the fact that normally particles are partially exposed rather than clearly “on top” or “not on top”. One has to define a threshold of exposure above which a particle is seen as being “on top”. Effectively, the grid spacing sets this threshold. An example is given in Figure 48, rather extreme grid spacing values are used to show the effect more clearly.

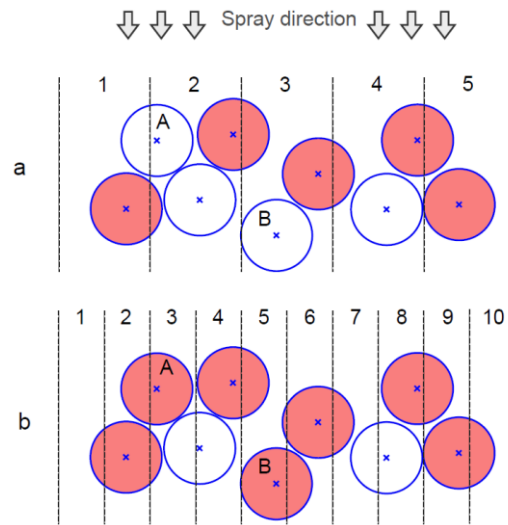


Figure 48: Influence of the grid spacing on the top detection algorithm for (a) wide and (b) narrow spacing. The filled circles denote particles that would be detected as being on the top of the tablet bed.

In Figure 48a, the larger grid spacing leads to some top particles not being detected (e.g., particle “A”). If a smaller grid spacing is chosen, Figure 48b, particle A is detected, but partially hidden particles (such as particle “B”) are detected as being on the top as well. In any case, choosing the grid spacing always implicitly sets a threshold, which should be chosen such that the most reliable results are achieved.

The *relative grid spacing*, that is, the spacing divided by the particle size is defined as:

$$\Delta_{g,rel} = \frac{\Delta_g}{r_{particle}} \quad (71)$$

The grid described above can be expressed as a grid *matrix*, where each field is represented by an element in the matrix. Each field is identified by its row index I_x and column index I_y . If the ranges of the tablet bed are $[x_{min}, x_{max}]$ and $[y_{min}, y_{max}]$ in the x and y directions, respectively, the grid matrix has $(x_{max} - x_{min}) / \Delta_g$ rows and $(y_{max} - y_{min}) / \Delta_g$ columns.

The algorithm needs to quickly find the grid field a certain particle can be found in. That is, for a given particle position \mathbf{p}_{tab} , the algorithm has to find I_x and I_y . As the plane was normal to the z -axis, only x - and y -position of the particle ($p_{\text{tab},x}$ and $p_{\text{tab},y}$) have to be considered, as those determine the location of the particle in the grid plane. With this, the assignment of a given particle of position \mathbf{p}_{tab} to the grid could be obtained efficiently by calculating row index I_x and column index I_y according to

$$I_x = \left\lfloor \frac{p_{\text{tab},x} - x_{\text{min}}}{d_x} \right\rfloor + 1, \quad (72)$$

$$I_y = \left\lfloor \frac{p_{\text{tab},y} - y_{\text{min}}}{d_y} \right\rfloor + 1. \quad (73)$$

(The expression inside the brackets is rounded down to the nearest integer). This assignment is done sequentially for all particles. At the start, all elements of the grid matrix are empty. For each particle, Eq. (72) and (73) give the corresponding matrix element. If it is the first particle to be assigned to this element, the height of the particle (the z -coordinate) is saved in the previously empty grid position (I_x, I_y) . If not, the array already contains the height level, which is compared to the height of the current particle. If the new value is higher, it replaces the old array value. This way, after all tablets looped through, the grid matrix contains the z -coordinates of the highest (top) particles.

E-3.3 Discrete Drop Method

Another approach to modeling the spray process is to directly account for the spray droplets as particles (i.e., “discrete drop method”). There are two reasons for doing this: first, the DEM software is designed for particle simulations, and thus, most of the needed framework is already implemented. Second, a spray description based on particles is closely aligned with the physical reality, i.e., size and speed distributions and the individual spray pattern may be implemented in a straightforward fashion. A typical illustration of the spray is shown in Figure 49.

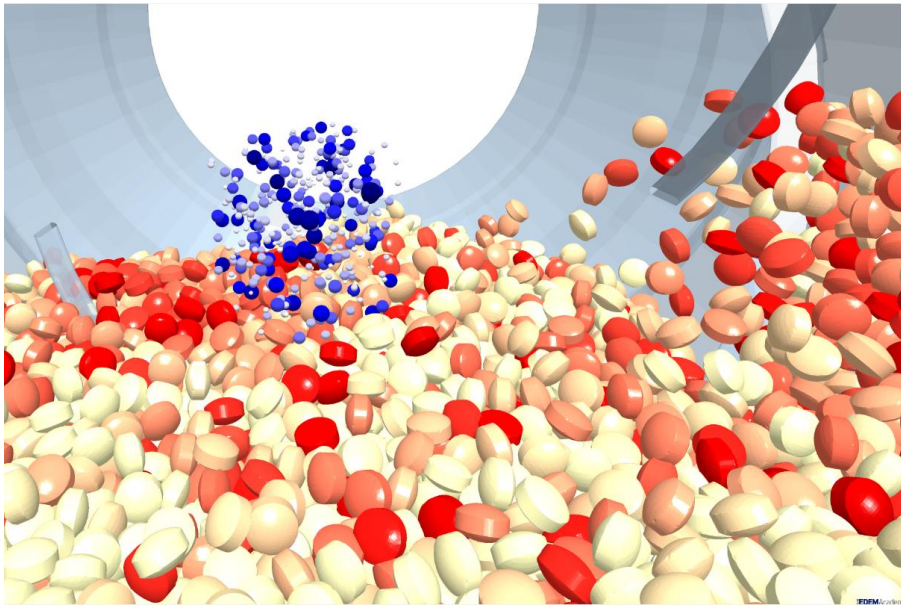


Figure 49: DEM simulation of a tablet coating process, including the coating spray. The spray droplets are colored blue, with darker shades indicating bigger droplets. The tablets are colored according to coating mass, from white (no coating mass) to red (high coating mass).

In most applications, it is neither feasible nor necessary to reproduce every single spray droplet with a corresponding DEM particle. Instead, a statistical approach is used, under which each particle is seen as a “package” that represents a certain number of identical droplets. This will obviously be inaccurate for a low number of packages. However, when averaged over a larger number, the spray pattern of the “package” statistically modeled the physical spray.

In our implementation, an additional property termed “coating mass” is added to the existing properties of every particle. Similarly, an additional global property “wall coating mass” is defined. “Drop” particles are treated as normal particles, with some exceptions that involve their behavior upon collision. Three types of collisions are possible:

- **Drop - drop:** the collision is ignored, the calculation proceeded immediately to the next particle.
- **Drop - non-drop particle** (i.e., the tablet): the mass of the drop package is added to the coating mass of the non-drop particle, and the drop is deleted.

- **Drop - wall:** when a drop particle collides with a wall, the mass of the particle is added to the global “wall-coating mass” and the drop is deleted. This way, the total amount of spray mass that would end up on the wall, accounting for the coating loss, is monitored.

Droplet collisions are neglected, as well as back-splashing effects and the generation of daughter droplets. This can be, however, easily implemented in future work, e.g., based on some of our previous work (Suzzi et al., 2010).

The spray itself consists of “drop-particles”, where at every time step a defined number of drops are introduced. Each particle is assigned the following properties:

- velocity magnitude and direction,
- size,
- location

The velocity is set to a (typical) mean velocity of 12 m/s. The size of each generated droplet is either constant (uniform drops) or may follow a prescribed size distribution (non-uniform drops). Both approaches were tested. In the latter case, the size of each drop is sampled randomly from the distribution shown in Figure 50. The volume-weighted mean drop size is the same as the constant size of the uniform drops, meaning that the spray had the same mass flow rate for both uniform and non-uniform drops.

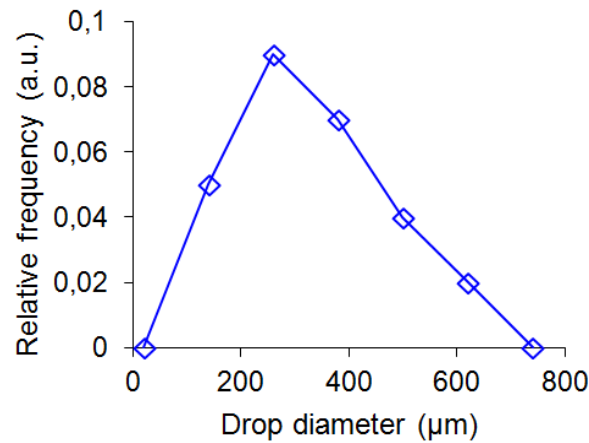


Figure 50: Drop diameter distribution from which sizes for the non-uniform case were sampled.

The most straight-forward location for drop initialization is the tip of the spray nozzle. However, this is not always the best choice. Often, the size distribution and the velocity profile of the used spray gun are known from phase-Doppler anemometry (PDA) measurements at some distance from the nozzle. In this case, it is convenient to initialize the drops at the location corresponding to the PDA measurement plane, so that the PDA results can be directly applied for drop creation. This mode of initialization is chosen here.

For this, the drops are randomly distributed over an elliptical area resembling the cross-sectional shape of the spray. For a random placement of each drop, two uniform random numbers, radius ρ and angle φ , are sampled from the range $(0,1]$ and $(0, 2\pi]$, respectively. From this, the location of the drop inside the ellipse is calculated according to:

$$\begin{aligned} x_{ell} &= \rho^u a \cos \varphi \\ y_{ell} &= \rho^u b \sin \varphi \end{aligned} \tag{74}$$

with a and b the semi-major and semi-minor axis of the ellipse, respectively. The Cartesian coordinates x_{ell} and y_{ell} are taken relative to the center of the ellipse, that is, the center has coordinates $x_{ell} = y_{ell} = 0$. The exponent u , termed *area uniformity exponent*, influences the radial distribution of drops inside the ellipse. For a value of $u = 0.5$, the drops are evenly distributed across the whole area. If it is larger, the drops show a concentration near the center of the ellipse. For a lower value, more drops are located closer to the border. Figure 51 compares the spray pattern for different values of the area uniformity exponent u .

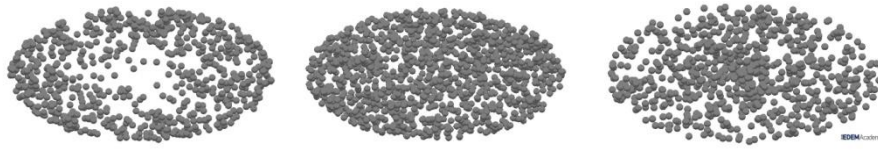


Figure 51: Spray pattern for different exponents of the radial sampling: 0.3 (left), 0.5 (middle, uniform) and 0.7 (right).

E-3.4 Post-Processing Ray-Tracing Approach

During a simulation, data are written to the hard disk at defined intervals, typically much larger than the simulation time steps. Data include the particle's

- position (x, y, and z components)
- velocity (x, y, and z components)
- angular velocity
- orientation (3x3 rotation matrix)

From the particle's position in the coater at a given time it can be determined whether the tablet is in the spray zone at that time. For that purpose, an algorithm based on ray-tracing was implemented. In a sense, the algorithm is similar to the spray module as it detected the intersection between a (virtual) drop trajectory and the tablet.

E-3.4.1 Ray-Tracing Detection Algorithm

Ray-tracing spray detection is based on the idea of representing the droplet trajectories as rays. The algorithm assumes that the particles are spherical (as was the case in this work). Particles of different shapes, e.g., biconvex tablets, would be treated using an enclosing sphere of a user-defined radius (Ketterhagen, 2011).

In the algorithm two main sets of information are needed: the positions of the tablets at each time step, and the rays that represented the spray zone. The positions of the tablets are exported from the DEM code and read in once at the beginning of each calculation. The set of rays is defined by choosing equally-spaced points on a defined ellipse and adding appropriate vectors normal to the ellipse pointing towards the tablet bed. As in the case of the run-time modules above, the size of the ellipse is taken from experimental measurements of the spray pattern at an appropriate distance (see Figure 52).

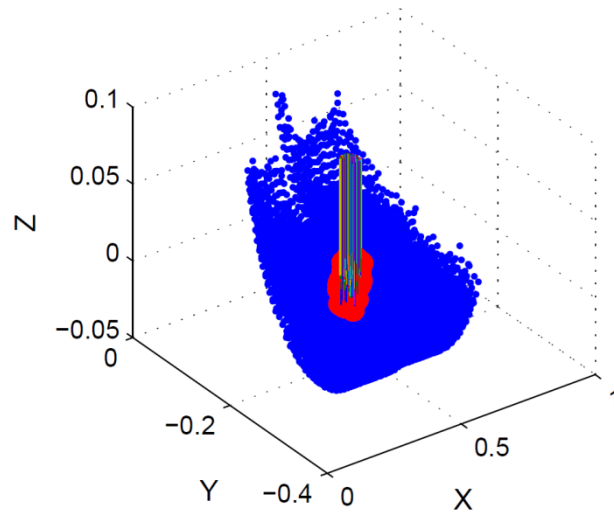


Figure 52: Principle of the ray-tracing method. The blue dots are the center positions of tablets as read in from the DEM simulation output. Tablets that are hit by a ray are colored red.

Using this approach, the rays represent the trajectory of a spray droplet. A particle coating event was detected if a ray terminated at the spherical particle (or at the enclosing sphere for non-spherical particles). Consider a sphere with a center \mathbf{c} and a radius r and a ray with an origin $\mathbf{0}$ and a unit-length direction vector \mathbf{a} . The distance between the ray origin and the intersecting point(s), d , is given as

$$d_{1,2} = (\mathbf{c} - \mathbf{o}) \cdot \mathbf{a} \pm \sqrt{D}, \quad (75)$$

with $D = [(\mathbf{c} - \mathbf{o}) \cdot \mathbf{a}]^2 - (\mathbf{c} - \mathbf{o}) \cdot (\mathbf{c} - \mathbf{o}) + r^2$. A determinant D of less than zero indicates that the ray and the sphere does not intersect. If D is zero, the sphere is touched tangentially, and the only solution for d is taken into account. For D greater than zero, two solutions exist: the points where the ray enters and leaves the sphere. Of these two, only the smaller distance is counted.

At each time-step, a loop over all rays in the defined set is performed. For each ray, Eq. (75) is solved for all particles. It should be noted that for larger systems (i.e., systems where the number of particles in the spray zone is very small compared to the total number), the computation time can be decreased by first excluding particles that cannot be hit due to some criteria, and then only solving Eq. (75) for the remaining particles. In any case, the particles that return the

smallest d (i.e., the particle closest to the nozzle) are detected as being coated. This is repeated for all time steps, and the following information is extracted:

- Total number of rays intersecting with a particle, representing the number of drops and thus the coating mass accumulated during the coating process. From this, coating mass distributions are obtained.
- Number of visits to the spray zone, regardless of the duration of the visit, for each particle and the corresponding distribution.
- Single-visit residence time (SVRT) distribution (Kalbag & Wassgren, 2009). Here, the duration of all visits in the spray zone is collected.

For the computation of the SVRT, a threshold time is defined: only when two visits are separated by a time longer than the threshold they are counted as two separate events. Otherwise, the two visits are considered as a single event. While similar, SVRT and coating mass distributions are conceptually different. For SVRT, *all* spray zone visits of any particle are equally taken into account, ignoring the identity of single particles. For coating mass distribution, all spray events *for a given particle* are added and attributed to the particle.

E-3.5 Simulation parameters

From the description of the three methods above, it can be seen that each method requires one or more parameters that need to be set. In this section, the parameter settings for the three different approaches are provided.

E-3.5.1 Spray zone approach

The parameter settings used are given in Table 6. Top detection “yes” means that the top detection is used (the default). Alternatively, all particles in the spray zone are coated, not only the ones on top. The column “relative detection grid spacing” provides the spacing of the top detection grid. For smaller values, i.e., a finer grid, the chance to detect all top particles increases, as well as the chance to falsely detect lower particles.

Table 6: Settings for the spray zone approach for the different simulation runs.

Case	Top detection	Relative detection grid spacing
1	Yes	1
2	Yes	1.25
3	Yes	1.5
4	Yes	2
5	No	-

E-3.5.2 Discrete drop method

The parameter settings used are given in Table 7. Uniform drops “yes” means that all drops have the same diameter. Alternatively, they follow the distribution in Figure 50 (“no”). The area uniformity exponent u describes the concentration of the spray at the center or the boundary of the spray zone; 0.5 gives a uniform distribution. Drops per event describes the number of drops introduced at every droplet-introduction event. Spray interval describes the time span between two spray drop introductions.

Table 7: Settings for the Discrete Drop method for the different simulation runs.

Case	Uniform drops	Area uniformity exponent u	#drops per event	Spray interval (ms)
1	Yes	0.5	10	1
2	Yes	0.5	50	1
3	Yes	0.5	100	1
4	Yes	0.5	200	1
5	Yes	0.5	400	1
6	Yes	0.5	200	0.5
7	Yes	0.5	200	2
8	Yes	0.3	200	1
9	Yes	0.7	200	1
10	No	0.5	200	1

E-3.5.3 Ray-tracing method

Table 8 provides the number of rays that are used to detect the spray zone, with higher values increasing the resolution of the method.

Table 8: Settings for the different cases using the post-processing ray-tracing method.

Case	Number of rays
1	24
2	70
3	128
4	217
5	308
6	442
7	572

E-4 Results and Discussion

The primary quality aspect of a coating process is the coating mass distribution (CMD). An optimal process should yield a narrow distribution, and thus, the goal of process optimization is to choose the design and operating parameters accordingly. The most comprehensive information is provided by reporting a histogram of the CMD itself. In addition, the Relative Standard Deviation (defined as $RSD = \sigma / \mu$, where μ is the mean coating mass and σ is the standard deviation of the coating mass over all tablets) can be used as a simple quantitative indicator. Moreover, an important parameter is the percentage of tablets that have zero coating.

It should be noted that the spray-zone approach provides only the residence time of the tablets. To calculate the actual coating mass, the residence time is multiplied by a factor that represents the coating a particle receives per unit time in the spray. Similar, the post-processing module gives the number of rays. This is then multiplied by the coating amount per ray to arrive at a coating mass. Here, these factors are chosen such that all three methods apply the same total coating mass, allowing a meaningful direct comparison of the methods.

E-4.1 Spray zone approach (SZA)

In Figure 53, the RSD and the fraction of zero mass tablets are shown for all cases (as defined in Table 6).

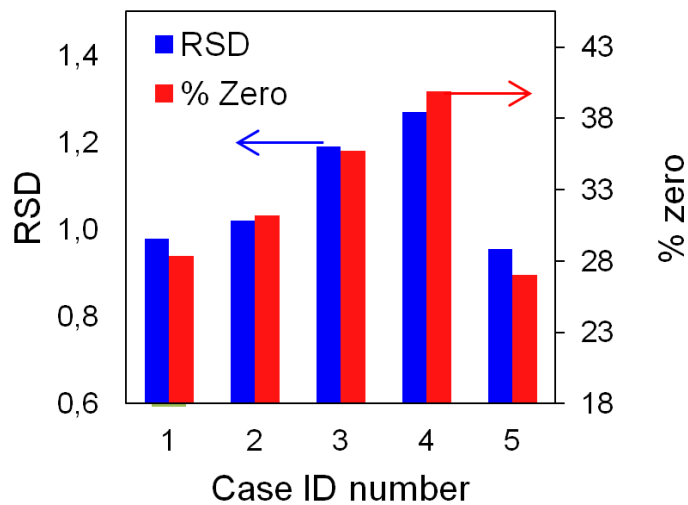


Figure 53: RSD and the amount of zero residence time tablets at the end of the simulated period for the investigated cases for the spray zone method.

In addition to the choice of using top detection or not (see below), the spray zone algorithm is based on a single parameter, i.e., the spacing of the detection grid. In the methods section E-3.2.3 it was pointed out how this influences the spray zone method. In cases 1 to 4, the grid spacing is increased from 1 to 2 with 0.25 intervals. As can be seen, both the RSD and the percentage of uncoated (zero-residence time) tablets increase significantly with increasing grid spacing. This is to be expected: an algorithm excluding a large number of particles from being detected in the spray zone will result in an uneven CMD. Still, it is notable that both values quantitatively follow a similar trend.

In Figure 54, the corresponding coating mass distributions are shown. For comparison, the result for case 4 of the discrete drop method is drawn as well (dashed line).

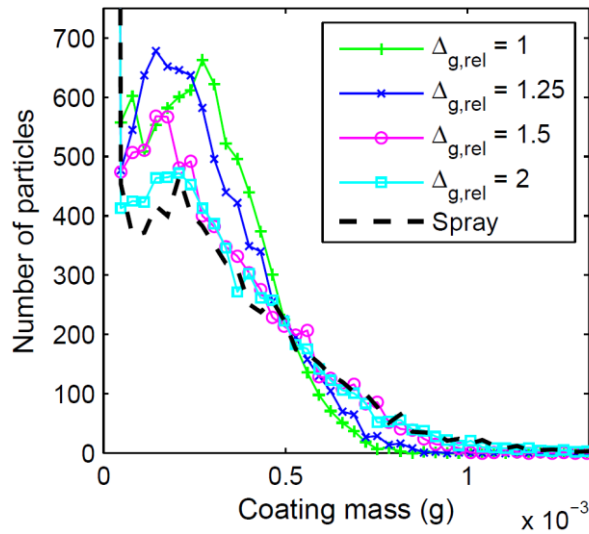


Figure 54: Comparison of the coating mass distribution for different settings of the relative grid spacing $\Delta_{g,rel}$. The result for the discrete drop method (case 4) is shown as reference (dashed line). Zero-coating mass data were omitted.

A high value of $\Delta_{g,rel}$ means that the algorithm misses any particle as being on top, if it is positioned slightly lower than the top particle, while in fact it still belongs to the top layer. Particles slightly lower than others and particles slightly covered by others will not be coated. Thus, values higher than 2 are not considered. Similarly, values below 1 result in coating of particles that are almost totally covered, and should be excluded. The curves in Figure 54 show a clear trend: the smaller the spacing, the broader is the computed distribution of the coating mass. This is because more particles are detected for small detection radii and therefore a relatively larger amount of the particles is coated. This influence on the distribution width can be clearly seen when plotting the relative standard deviation as a function of the grid spacing (Figure 55). It is evident that although the same spray process is simulated in all cases, the uniformity of the CMD strongly varies.

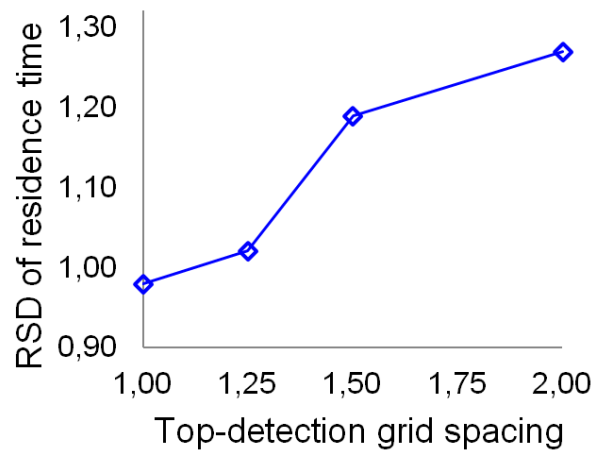


Figure 55: Relative standard deviation of coating as a function of top detection grid spacing.

For reference, the CMD obtained by the discrete drop method (DDM) is shown as well in Figure 54. The agreement between DDM and the spray-zone approach is best for $\Delta_{g,rel} = 2$, the highest value. As a consequence, it is clear the top detection grid spacing should be chosen carefully. Since a “correct value” is not known a priori this is not a trivial task. If possible, the “best” value should be determined by comparison with experiment or a reference method (such as DDM). Overall, it is evident that the spray zone method is sensitive to the choice of the grid spacing.

Coming back to Figure 53, case 5 is the same as case 2, but with top detection disabled. Thus, all particles in the spray zone receive mass rather than only those at the top. In this case, significantly more particles are coated at the same time. It is known that a large number of sprayed particles (relative to the total number of particles) leads to more uniform results (Kalbag et al., 2008). This can also be seen here: the RSD is far lower for case 5 compared to case 2. A comparison between the CMDs with and without top detection is shown in Figure 56. It is no surprise that the results differed significantly, clearly demonstrating the necessity of some form of top detection for this type of approach.

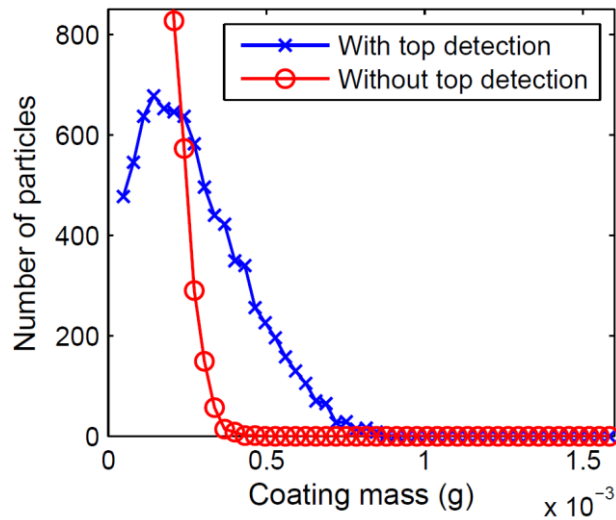


Figure 56: Comparison between the coating mass distribution with and without top detection (case 2 vs. 5).

E-4.2 Discrete drop method (DDM)

An overview of the RSD and the amount of uncoated particles is given in Figure 57 for all cases (see Table 7). In the case of the spray zone approach described above, the trends for RSD and uncoated particles are more or less the same. This is not the case here for the discrete drop method. Thus, there are not only changes in the RSD of the CMD, but those changes occur for different reasons. In the following sections the influences of different parameters are discussed.

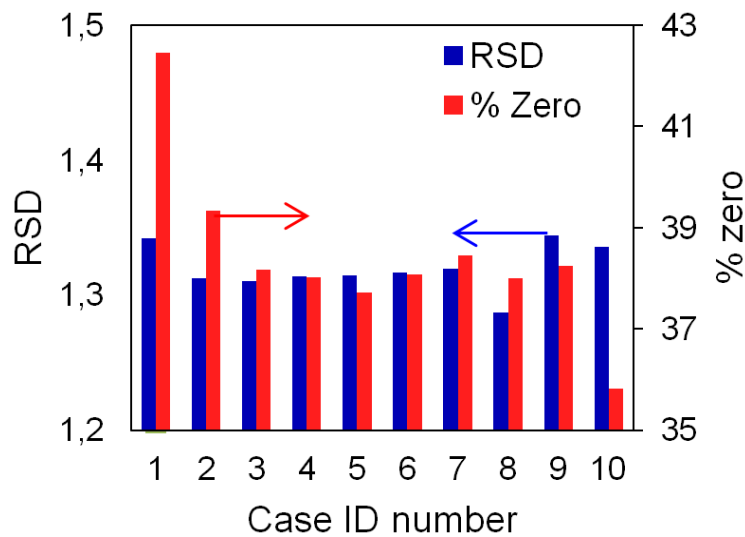


Figure 57: RSD and the amount of zero-mass at the end of the coating process for the discrete drop method.

E-4.3 Number of Drops and Spray Interval

As mentioned in section E-3.3, drops are not generated in every simulation time step. Rather, a user-defined number of drops is initialized at a given interval (the “spray interval”). Those two parameters, i.e., number of drops per spray event and spray interval between events, have a significant impact in the results.

In Figure 57, case 1-5 denote variations in the number of drops (from 10 to 400) per event and a spray interval of $\Delta t=1\text{ms}$. For case 1 (10 drops/step) and case 2 (50 drops/step), the percentage of uncoated particles is noticeably higher than for the cases with more drops. This shows that in case 1 and 2, there are not enough drops to provide statistically reliable results. Apparently not all particles that are in the spray zone are actually hit by a drop. However, above 100 drops/step with $\Delta t=1\text{ms}$ (cases 3-5), the results are consistent. Apart from the higher-than-normal number of uncoated particles, it is expected that a low number of drops also results in stronger overall fluctuations of the CMD. Yet, with an increasing number of drops, the results should converge. In Figure 58 it can be seen that this is indeed the case, as the curves are getting smoother and are converging with increasing number of drops per step.

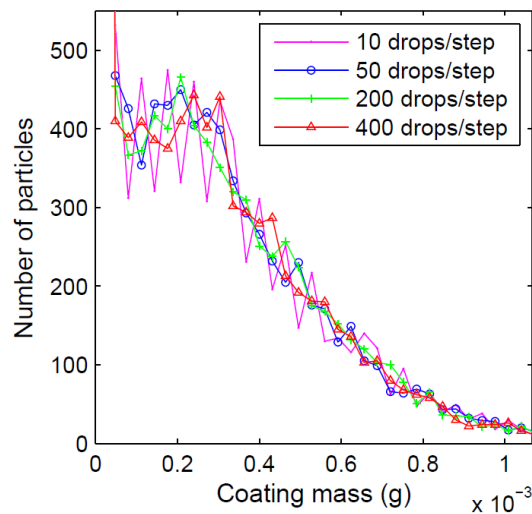


Figure 58: Influence of the number of drops per introduction step on the coating mass distribution

A similar result is seen for changes in the spray interval, with shorter intervals resulting in higher resolution. The results in Figure 57 for an interval of 0.5 ms (case 6), 1 ms (case 4) and 2 ms (case 7) are very close to each other, suggesting that even the longest step of 2 ms is sufficient, although the amount of zero-coated tablets slightly increases at higher intervals. A comparison of the distributions is presented in figure 16, showing consistent results for all spray interval times as well. This is understandable, considering that the average residence time in the spray zone is in the order of 100 ms (see below Fig. 23). This means that in the time it takes a tablet to cross the spray zone, even for 2 ms intervals some 50 introduction events occurred. However, longer intervals did not result in an appreciable speed-up of the code and were therefore not investigated.

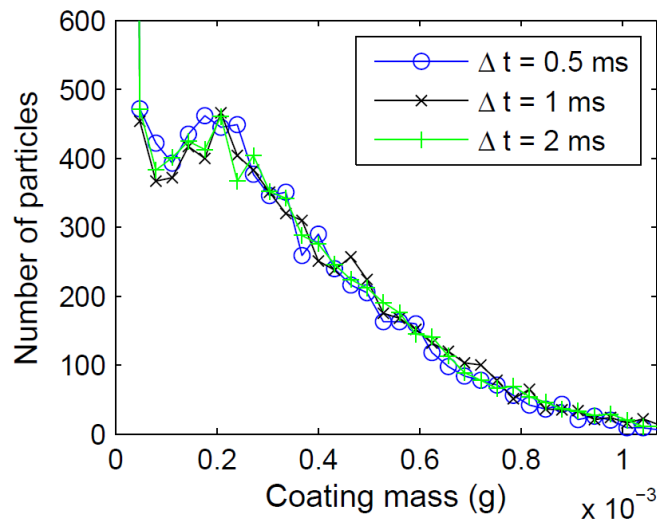


Figure 59: Influence of the drop introduction interval on the coating mass distribution.

As both the number of drops per spray event and the spray interval influence the number of drops, in Figure 60 both variations are shown in one plot, i.e., plotting the RSD and zero-mass fraction versus the amount of drops introduced per ms.

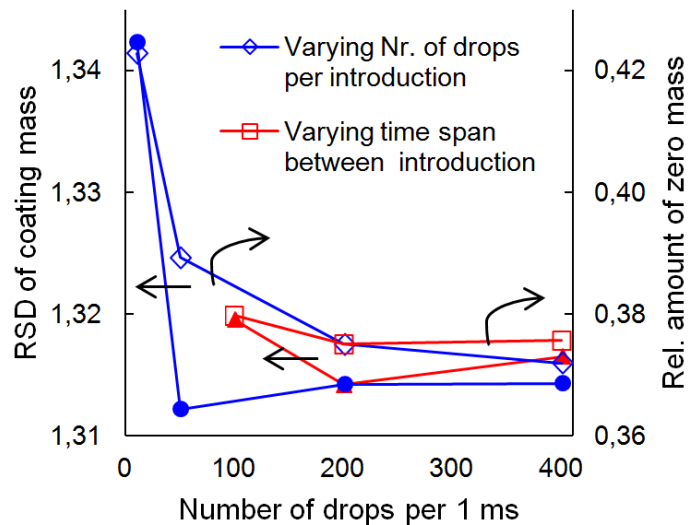


Figure 60: Relative standard deviation (left axis, filled symbols) and relative amount of zero mass particles (right axis, empty symbols) as a function of the drop number per time.

With increasing number of drops per time, the results converge to a constant value. While below 200 drops/ms, results seem unreliable, going from 200 drops/ms to 400 drops/ms does not change the outcome significantly. In conclusion, this means that cases 4, 5, and 6 provide a large enough number of drops and therefore sufficient resolution.

Furthermore, a rough estimate of the number of tablets sprayed at the same time can be made. For this, the area of the spray zone is divided by the area of a circle having the same radius as the particles, showing that the number of particles in the spray zone is in the order of 100. Therefore, at a rate of 200 drops / ms, about 2 drops per tablet are generated per millisecond. Keeping in mind that tablets stay approximately 100 ms in the spray zone, *on average* each tablet receives 200 drops per coating event. This is a large-enough number to provide sufficient statistics for the CMD, even for tablets deviating from this estimated mean.

E-4.3.1 Spray Area Uniformity

The spray module offers the option of using non-uniform area distribution of droplets by adjusting the area uniformity exponent. In cases 4, 8, and 9 the value of u is 0.5, 0.3 and 0.7, respectively (also see Figure 51). Other than that, the three cases are identical. Looking at the RSD in Figure 57 above, it follows that the boundary-heavy pattern ($u = 0.3$, case 8) produced a more uniform coating, while the centered spray pattern ($u = 0.7$, case 9) showed a considerable decrease in uniformity compared to the uniform area distribution (case 4). This can be explained by the fact that most of the particles move through the spray from top to bottom. For a uniform distribution, a tablet crossing the spray on the left or right side of the center receives less spray than a tablet travelling through the center. This effect can be counteracted by the border-heavy distribution, or exacerbated by the center-heavy distribution. However, the amount of zero coating is almost the same for all three. For all distributions, a droplet traversing the spray zone is very likely to receive at least a small amount of coating, explaining the identical amount of particles with zero coating in the three cases. The CMD in Figure 61 shows a similar behavior for the three different values of the area uniformity exponent.

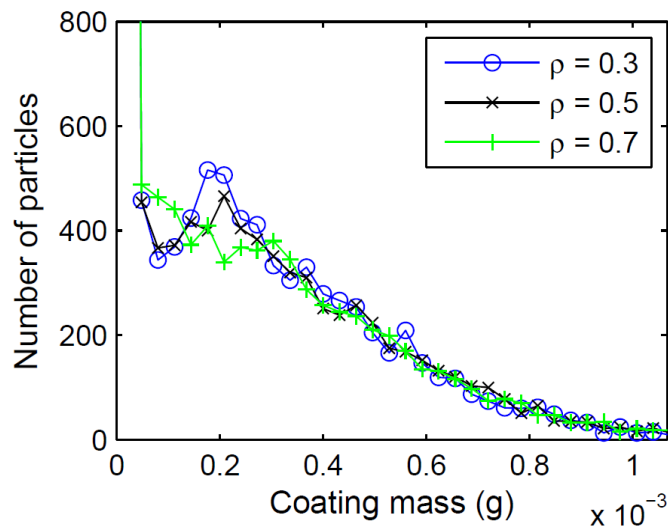


Figure 61: Influence of the spray cross-sectional area uniformity on the coating mass distribution.

Pronounced differences occur for small masses, below 0.3 mg. In this region (small mass), $\rho = 0.7$ does not show the fluctuations of the other cases, which decrease at ~ 0.08 mg and increase to a local maximum at ~ 0.2 mg. However, for $\rho = 0.7$ a higher number of particles with relatively high coating levels exist, strongly decreasing the RSD. This is in line with the practical experience that a center-heavy spray pattern negatively influences uniformity in a tablet coating process. On the contrast a boundary-heavy spray ($u=0.3$) should increase uniformity.

E-4.3.2 Drop size uniformity

In case 10, non-uniform drops are used. They were randomly sampled from the distribution in Figure 50, such that on average they have the same mass flow as the uniform drops. Case 4 has the same settings as case 10 (only with uniform drop size), and thus, is used as comparison. When comparing the two cases in Figure 57 it can be seen that the RSD is similar for both cases, while the number of uncoated particles is less for non-uniform drops. A result of the non-uniform size distribution is the presence of relatively small drops. Apparently they can reach particles in the lower layers of the bed, even when they are almost covered by other particles, thus leading to a higher absolute number of coated particles. (Here, the advantage of using a DEM approach for the drops becomes evident, as in this method the true size of a drop is considered, and drops are not assumed to be point sources). A comparison of the CMD for both cases is given in Figure 62.

The curves show differences, but are in general similar to each other. In summary, the drop size distribution does have an influence; however, drops of uniform size seem to be a reasonable approximation.

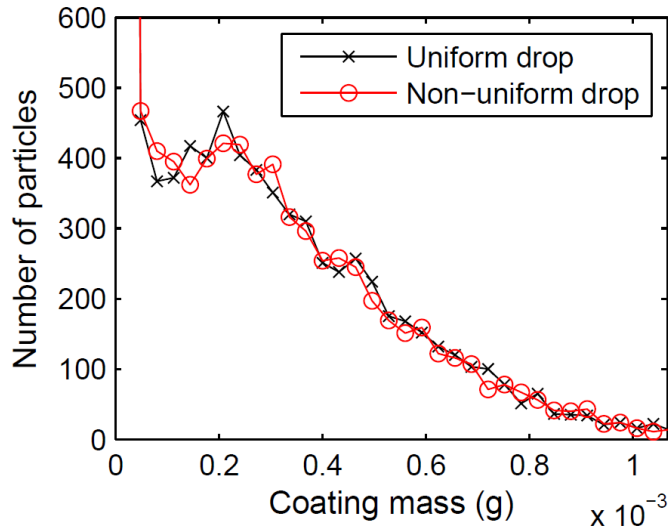


Figure 62: Comparison of the coating mass distribution for uniform and non-uniform drop size distributions (Cases 4 and 10 in Table 6, respectively)

E-4.4 Ray-tracing method

Just as the number of drops governs the performance of the drop algorithm, the number of rays is the most critical parameter in the ray-tracing method. Figure 63 shows the relative standard deviation as a function of the number of rays used. The curve quickly converges towards an asymptotic value, and is almost constant for more than 200 rays. In this study the highest number in this figure, i.e., 572 rays are used. In this case, the algorithm took approximately 10 minutes using a regular personal computer.

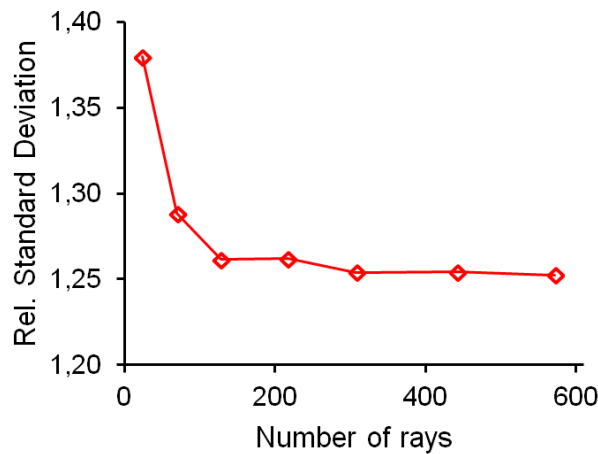


Figure 63: Relative standard deviation as a function of the number of rays.

As mentioned above, the evaluation in post-processing mode allowed a more comprehensive - though less accurate - method for the coating analysis. Similar to the other methods, the CMD is shown in Figure 64 (a bar plot is used for better comparison with the following plots). Particles with zero coating mass make up 32 % of all particles, and are omitted in the histogram.

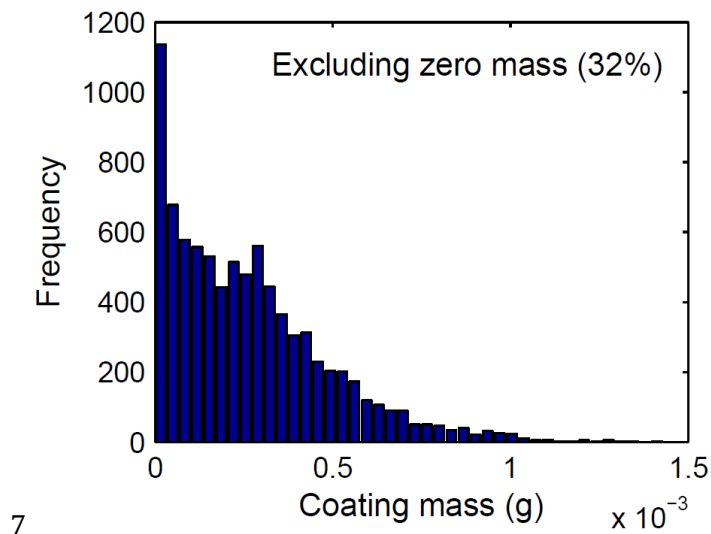


Figure 64: Coating mass distribution gathered after the DEM simulation using the ray-tracing method.

In addition, the algorithm also provides the number of visits for all tablets, and the single visit residence time. The number of visits, Figure 65 , provides basic information regarding the coating variability.

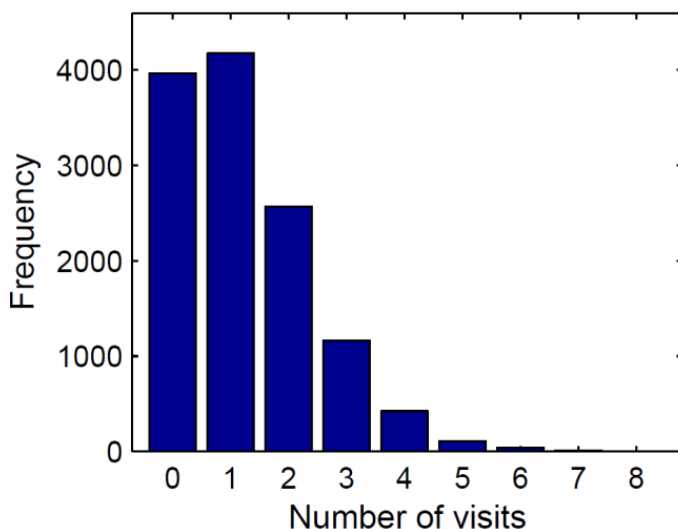


Figure 65: The number of visits to the spray zone for the total simulation time.

It does not take into account how long or how effective a single visit is, but it provides a first impression of the overall process performance. The significant amount of zero-visit particles can be seen, but most of the tablets have visited the spray zone at least once. The distribution also shows a tail towards high numbers, reaching up to eight visits in some cases, which is a considerable spread, and thus, a source of low coating uniformity.

The single-visit residence time (SVRT, figure 23) gives the average duration of a visit to the spray zone. It can be seen that durations from just over 0 seconds to approx. 0.1 seconds are about equally probable. Longer visits are increasingly rare, and no visit is longer than 0.3 seconds. The SVRT thus gives an important time-scale of the process and can be used as a basis for other coating models. In a coating process, the sources of variation can be roughly divided into two parts: variation in the number of visits and variation in a single coating event (Turton, 2008). Under the common assumption that the received coating is proportional to the time spent in the spray zone, the latter can be described by the variation in the number of visits and in SVRT, which can be determined from the presented simulations to be used in various generalized models.

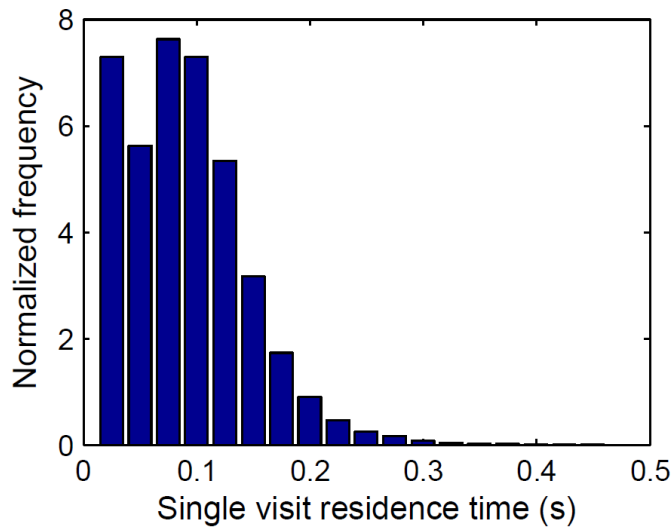


Figure 66: Histogram of the Single Visit Residence Time of all visits to the spray zone.

E-4.5 Comparison of the Approaches

Apart from the influence of the parameters on the same model, it is interesting to compare the results obtained for the three different methods. To do this, the most reliable parameter sets for each method were selected. The spray zone model depends on the top detection grid spacing and it was shown that the largest spacing (case 4) is most reliable. For the discrete drop method case 4 was chosen. In the ray-tracing method the maximum number of rays (case 7) was used.

shows the CMD for the selected cases of all methods. The three distributions show a very close match in terms of their qualitative behavior. This means that each method is able to capture the general process behavior, and one would arrive at similar predictions. However, there are deviations, especially for low coating masses. While the results for the two run-time methods are relatively similar, the ray-tracing approach shows more pronounced variations from these two. This can be expected, as the latter method is considered to be the least accurate method. It has to be noted however, than the deviation between the models is in many cases smaller than the variations of the same model, but with different parameters.

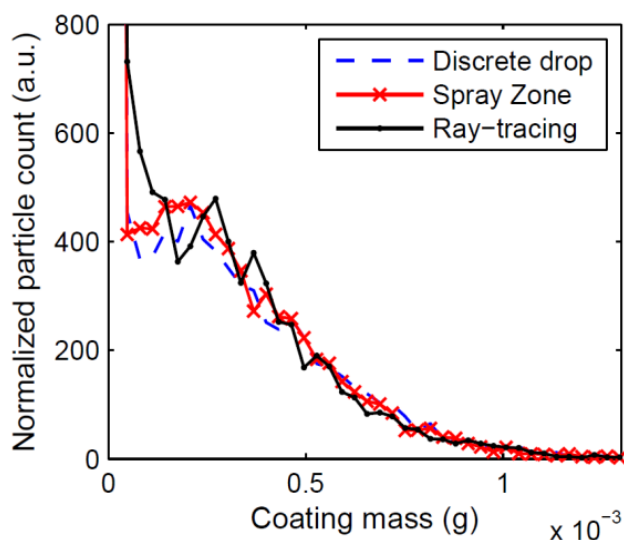


Figure 67: Comparison of the coating mass for the base settings of all three spray modules.

E-5 Conclusion

In this work, we investigated and compared three ways of simulating a coating process, and specifically the spraying event, using DEM. In two methods the calculations were performed during the DEM simulation run. The third approach was a ray-tracing algorithm that was applied after the DEM simulation using the position data output from the DEM runs.

All of the above methods had distinct advantages and disadvantages. Generally, the post-processing ray-tracing method was less accurate since it involves longer time steps. Nevertheless, this method was fast. Moreover, it requires only one DEM run for multiple spray simulations. The other two methods used all of the available data and the simulation time increased by approximately 15%, which may be significant for large-scale simulations.

The above spray simulation methods were applied to the same coating process. Any variations in the results were therefore due to the model assumptions. Comparing the models showed that they did not give identical results, as was expected, but gave the same qualitative outcome for reasonable settings. Comparing the results for different settings of a given model indicated that the performance strongly depended on the algorithm parameters, which is important for comparing simulation with experiments. The sensitivity of the models with

respect to the parameters was investigated, and the results show which parameters are critical. For most of them, the outcome converged to a constant value if chosen within an accurate range (e.g., number of droplets). However, for some parameters (such as the detection radius), there may be no obvious or “right” choice. Therefore, the validity of the model should be carefully checked.

The three methods are non-exclusive. If desired, all three can be applied to one simulation. However, since the spray-zone method showed inherent inaccuracies, it may be better to use the more versatile discrete-drop method during the DEM simulation. This can then be complemented by the ray-tracing post-processing method after the DEM simulation, if needed.

A typical industrial coating process may take a few hours. Nowadays, DEM simulations can only simulate a small fraction of the total time. From these limited DEM data, however, the final outcome can be predicted; this will be included in future work.

Acknowledgements

The Research Center Pharmaceutical Engineering is a K1 Competence Center initiated by the Federal Ministry of Transport, Innovation & Technology (BMVIT) and the Federal Ministry of Economy, Family & Youth (BMWFJ). We acknowledge funding by the Austrian Research Promotion Agency (FFG), Land Steiermark and the Styrian Business Promotion Agency (SFG).

Chapter F: Design-of-Experiment based DEM simulation of an active tablet coating process.

In preparation as: Toschkoff, G., Just, S., Funke, A., Djuric, D., Knop, K., Kleinebudde, P., Scharrer, G, Khinast, J. G. (2013). Design-of-Experiment based DEM simulation of an active tablet coating process.

F-1 Abstract

Tablet coating is a common unit operation in the pharmaceutical industry, where a coating layer is applied to tablet cores. A special subclass is active coating, that is, the coating itself contains an active pharmaceutical ingredient. In this case, the uniformity of coating mass between the different tablets of a batch is especially critical.

In recent years, discrete element method (DEM) simulations gained usage to investigate tablet coating. In this work, the DEM is applied to capture an active coating process as closely as possible, by e.g. using measured model parameters where possible, and using non-spherical particles. It is studied how the operational conditions (rotation speed, fill level, number of nozzles, and spray rate) influence the uniformity. For this, simulation runs are planned and interpreted according to a statistical design of (simulation) experiments. Further, it is sought to generally get a deeper understanding of the process in terms of residence times and dimensionless scaling laws. To this end, the results are interpreted in the light of analytical models.

Results are presented at different detail levels, going from an overview of all variations to in-depth considerations. It showed that the biggest uniformity improvement in a realistic setting can be achieved by increasing the number of spray nozzles, followed by increasing the rotation speed and decreasing the fill level.

F-2 Introduction

The coating of tablets is a common unit operation in the pharmaceutical industry. The target is to enclose the tablet core in one or more thin, solid layers. Most commonly, the coating is applied by constantly moving tablets in a rotating drum,

and spraying the coating liquid (containing solvent and film-forming solutants) onto them. Heated air is traveling through the system to enhance the evaporation of the solvent.

The coating layer may have different functions such as protection from environmental influences, taste masking, or release control. A special case is active coating, where the coating itself contains an active pharmaceutical ingredient (API). In each case, the coating layer has to fulfill strict quality expectations. A central topic is the uniformity of coating. The magnitude of coating typically is stated as the coefficient of variation (c_v), also termed relative standard deviation. Here, two categories can be defined: intra- and inter-tablet uniformity. Intra-tablet uniformity ($c_{v,intra}$) is the uniformity of coating layer thickness on each single tablet. Inter-tablet uniformity ($c_{v,inter}$) denotes the uniformity of the coating mass between different tablets. In an active coating process, the latter is more critical than the former: the tablets have to pass the test on uniformity of dosage units according to the regulations (Directorate for the Quality of Medicines of the Council of Europe, 2011; Ministry of Health Labour and Welfare, 2011; U. S. Pharmacopoeial Convention, 2011b). This applies to the amount of API, and with it to the directly related amount of coating mass. The actual regulatory threshold value for the uniformity depends on a number of factors: in this work, this amounts to a $c_{v,inter}$ that must not exceed 6.25%.

The challenge is therefore to design a coating process that will reliably yield tablets of high uniformity. For this, a high degree of understanding of the process is needed, in especial how the process parameter affect the outcome. To this end, various experimental studies have been performed (e.g. (Brock et al., 2012; Just, Toschkoff, Funke, Djuric, Khinast, et al., 2013; Koller et al., 2011; Mueller & Kleinebudde, 2007b; Pandey & Turton, 2005; Sandadi et al., 2004; Wang et al., 2012)). In recent years, this has been complemented by the use of computer simulations. While simulations have their downsides (e.g. the quality of the simulation depends on the input parameters), a valuable advantage of simulations is that they can provide a large amount of high-fidelity data, and enable to extract quantities which are hard or impossible to measure.

Different simulation approaches exist and were applied for coating processes depending on which part of it was to be looked at (Toschkoff & Khinast, 2013), ranging from detailed methods such as computational fluid dynamics (CFD) (Toschkoff et al., 2012) to quick analytic models such as renewal theory (Freireich & Li, 2013). For particulate processes, as are common in the pharmaceutical industry, the discrete element method (DEM) has seen increased application (Ketterhagen et al., 2009c). Tablet coating in special has shown to be

well suited for the DEM approach, and a number of studies were done, many of which include the investigation of the inter-tablet coating uniformity. Dubey et al. (Dubey et al., 2011) studied the influence of drum rotation speed, fill level on tablet mixing and coating uniformity. Different spray patterns were implemented in a post-processing step to gather the residence time of tablets in the spray zone. The result of one DEM simulation was compared to the laser-induced breakdown spectroscopy (LIBS) measurements, showing good agreement. A significant effect of spray pattern was seen. The coating uniformity was higher for higher rotation speed and higher fill levels. In two similar works, Sahni et al. (Sahni & Chaudhuri, 2011; Sahni et al., 2011) studied the coating of spherical particles in a lab-scale pan coater. The number of spray zone passings and the residence time distribution was gathered for different pan tilt, rotation speed and fill level. Simulation and experiment showed reasonable agreement for the mixing performance. Kalbag et al. (Kalbag et al., 2008) did experiments and DEM simulation for spherical particles. Particles in the spray zone were detected based on their solid fraction; for comparison a ray-tracing-based algorithm was used, with agreeing results. It was concluded that an increase in pan speed lead to a lower, narrower single-visit residence time distribution. Thus, a higher pan speed led to better coating uniformity, as was also found elsewhere (Chang & Leonzio, 1995; Denis et al., 2003; Sandadi et al., 2004). The results for different loads followed no simple trend. On the one hand, smaller loads with a higher sprayed-to-total-tablets ratio yielded better uniformity. On the other hand, as also Dubey et al. (2011) indicated, larger loads resulted in better mixing which in turn promoted uniformity as well. Suzzi et al. (Suzzi et al., 2012) investigated a cycled continuous coating process, with a cylindrical spray zone defined in post-processing. They found that an increased fill ratio resulted in a decreased uniformity (increased RSD of the fractional residence time) for round and oval tablets. Kalbag & Wassgren (Kalbag and Wassgren, 2009) compared DEM results with experiments and analytical models based on periodic random selection of tablets. An increase of uniformity was seen for decreasing the spray rate, increase the number of tablets in the spray zone, increasing the mixing efficiency, and decreasing the total number of tablets.

In this work, an active coating process was investigated, for which strict regulations apply with regard to the coating uniformity. To give reliable results, an effort was made to model the process as close to reality as possible, incorporating previous achievements and including new developments. The DEM simulations were done following a statistical design of (simulation) experiments (DoE), where process parameters are chosen according to an existing real-life coating process. Most material parameters for setting up the simulation were taken from measurements of the actual tablets, and the geometry of the coater

was provided by the manufacturer. An advanced post-processing algorithm is used for the spray modeling. The main aim of the study is to investigate how the inter-tablet coating mass uniformity, and with it the API uniformity, is directly affected by the process parameters. Further, it is sought to create a deeper understanding of the underlying principles of the coating process. Based on this, guidelines are given on how to consistently achieve a high coating uniformity in compliance with regulations.

F-3 Methods

F-3.1 Coating process

The considerations in this work are based on an active coating process for the production of tablets that contain two APIs: one of delayed release in the coating and one of immediate release in the core. In the process, gastrointestinal therapeutic systems (GITS) were used as starting material (Bayer Pharma AG, Leverkusen, Germany). The GITS are round biconvex two-layer tablets of approx. 9 mm diameter and approx. 5 mm height containing the API nifedipine. They were already coated with a layer of cellulose acetate and polyethylene glycol. The investigated process adds an additional coating layer containing the API candesartan cilexetil.

The coating is done in a lab coater (BFC 5, L.B. Bohle Maschinen + Verfahren GmbH, Ennigerloh, Germany). The geometry of the coating apparatus was provided by the manufacturer, and directly loaded into the DEM software (Figure 68). The operation settings used for the simulation runs are described in section F-3.3 and F-3.4.

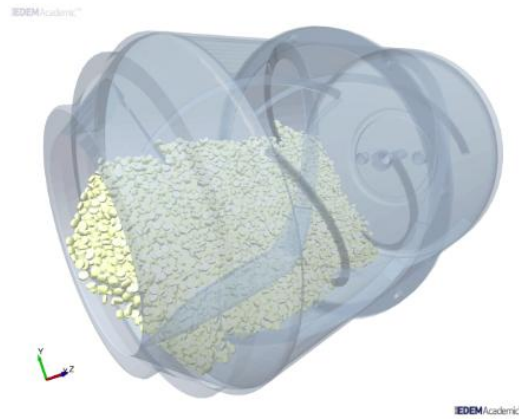


Figure 68: Coating drum geometry as used in the simulations, filled with 3.5 kg of tablets. (The front of the drum was covered by a non-rotating wall which is not shown here.)

To assess the quality of the coating for a given setting, the central quality attribute was the variation of coating mass between the tablets (inter-tablet uniformity). It was quantified as the coefficient of variation $c_{v,inter}$, defined as the standard deviation of coating mass divided by the mean mass:

$$c_{v,inter} = \frac{\sigma_{mc}}{\mu_{mc}} = \sqrt{\frac{1}{N} \sum_{i=1}^N (m_{c,i} - \overline{m_c})^2} / \overline{m_c}, \text{ with } \overline{m_c} = \frac{1}{N} \sum_{i=1}^N m_{c,i} \quad (76)$$

where N is the number of tablets, and $m_{c,i}$ is the coating mass of tablet i . The aim is to get consistently low values of $c_{v,inter}$. Note that in an experimental investigation, the total variation is estimated from the variation in a sample, while in the DEM simulation the coating of all tablets (the whole statistical population) is used for the calculation.

For an active coating on tablets, regulations define a maximum acceptable variation in coating mass (Directorate for the Quality of Medicines of the Council of Europe, 2011; Ministry of Health Labour and Welfare, 2011; U. S. Pharmacopoeial Convention, 2011b). The allowed value of variation depends on the exact application. For the application described in this work, and using a worst-case scenario, this amounts to an upper limit for the $c_{v,inter}$ of 0.625 (or 6.25 %).

F-3.2 Simulation setup

For the simulation, a commercial software (EDEM 2.4.4, DEM Solutions Ltd., Edinburgh, UK) was used. The round biconvex tablet shape is approximated by the “glued sphere” approach. Each particle was made up of eight intersecting spheres fixed relative to each other, such that the enclosed volume was equal to that of the bi-convex tablet (Figure 69). One tablet had a weight of 282 mg. The total number of tablets depended on the fill level, and was between 10638 (3 kg) and 14177 (4 kg).

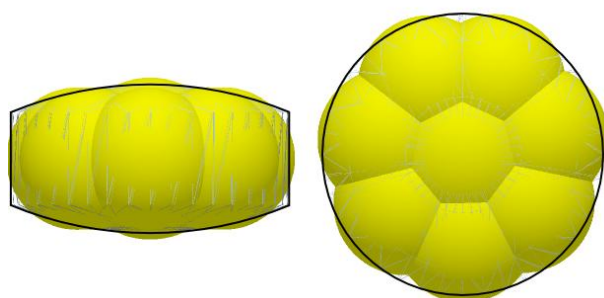


Figure 69: Top view and side view of the tablet created using the glued sphere approach. The bi-convex shape of the actual tablet is shown by the wire mesh and the black outline.

To set up a DEM simulation, material properties of the tablets are needed. The values were taken from measurements reported in (Just, Toschkoff, Funke, Djuric, Scharrer, et al., 2013). It is known that the friction parameter (between particle and wall as well as between two particles) has great influence on the outcome (Kalbag et al., 2008). At first, a direct measurement of the friction coefficients using a “pin-on-disk” tribometry setup was tried, which did not yield reliable results. A more useful approach (that sees increased application in literature as well) was to obtain the friction values from indirect calibration. For this, the dynamic angle of repose was measured experimentally, and the friction coefficients in simulation adjusted to get agreeing results. This was done for coated and uncoated tablets, giving two different friction coefficients (“coated” and “uncoated” here refers to tablets with and without the active coating layer; as mentioned above the “uncoated” tablets are in fact already pre-coated with another material). All simulation parameters are summarized in Table 9.

At the beginning of each simulation, the tablets are placed in the drum, and in an initial phase the drum is rotated for 6 seconds so that the tablet bed reaches a stable state. After that, the simulation that is actually used for further evaluation

is started. For each set of process parameters, a process time of 90 seconds is simulated.

F-3.2.1 Spray modeling

A standard DEM simulation gives values such as the position and velocity of tablets, but does not yield information on the coating. For this, additional methods are needed (Toschkoff et al., 2013). Here, a post-processing algorithm is used. During the simulation, the position data of all tablets is written out every 0.02 seconds. These positions are then read in by an in-house algorithm to simulate the application of coating. The spray is simulated by a set of rays that are oriented normal to the tablet bed surface. For each time step, the algorithm determines at which particle each ray is terminating (if any). By assigning each ray a certain amount of coating mass based on the targeted total spray rate, the coating mass on each tablet was then calculated. The whole algorithm is repeated for each nozzle in the setup. The outcome is the modeled coating mass on each tablet for each time step, both per nozzle and total.

One additional input for the simulation is the shape of the spray zone. This was taken from measurement: the spray nozzle was mounted above a piece of card in the same distance as used in the active coating process (approx. 10 cm) and the resulting spray pattern was measured. Its shape could be approximated by an ellipse, with major and minor axes of 6.5 cm and 3.2 cm, respectively. This was then used for the simulation. A drawing of size and position of the nozzles is shown in Figure 70.

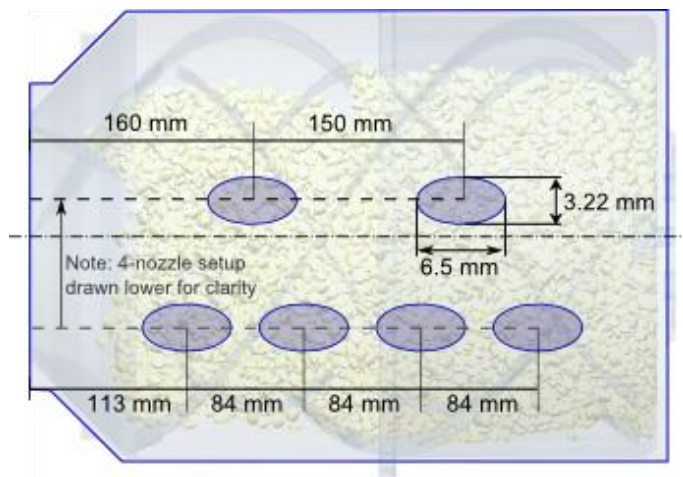


Figure 70: Position and shape of the spray zones in the coating drum (view from top, normal to the tablet bed surface). Note that the four-nozzle setup is drawn lower for clarity; its actual vertical position is the same as for the two-nozzle setup.

Table 9:

Geometry material property (steel)	
Poisson's ratio	0.25
Shear Modulus	7.93×10^{10} Pa
Density	7850 kg/m ³
Tablet material properties	
Poisson's ratio	0.29
Shear Modulus	2.92 MPa
Density	1150 kg/m ³
Interaction tablet–wall	
Coefficient of Restitution	0.78
Static friction coefficient	0.15 / 0.45
Rolling friction coefficient	0.01
Interaction tablet–tablet	
Coefficient of Restitution	0.78
Static friction coefficient	0.39 / 0.13 (core / coated)
Rolling friction coefficient	0.01
Simulation	
Time step length	4×10^{-5} s
Cell size	0.006 m

F-3.3 Investigated parameters and quality criteria.

To investigate the influence of input parameters, the simulation was run with varying parameter settings. The parameters were chosen according to two criteria: the anticipated magnitude of their influence (from literature and prior experience), and their actual potential to be changed in a real-world coating process. The selected parameters were rotation speed, fill level, number of spray nozzles, spray rate, and strictly speaking also tablet-tablet friction.

In the list above, the tablet-tablet friction has a special role. It cannot be adjusted for a given formulation, but changes over the duration of the process, and has a known potential to critically influence the simulation. To see whether results are strongly affected here, two values were used, corresponding to coated and uncoated tablets, as explained in section F-3.2

For each variation in rotation speed, fill level, or friction, a dedicated DEM run was performed. The number of nozzles was considered in the post-processing spray modeling using the data from the DEM runs. The spray rate is modeled indirectly via the coating time as follows. For the purpose of DEM simulation, the

effect of a change in spray rate can be divided into two classes. First, it changes the total coating time (in the active coating process, a fixed amount of coating has to be applied). Second, it changes the properties of the spray, such as droplet size or spray zone shape, and influences the humidity of the process if the setting for the drying air is not changed accordingly. The second effect (or group of effects) is intricate, and was anticipated to be small compared to the effects of a change in total spray time for the spray settings used in the investigated active coating. It was therefore not taken into account here. The first effect was included indirectly. It is reported (Kalbag & Wassgren, 2009; Kandela et al., 2010; Pandey, Katakdaunde, et al., 2006; Shi & McCarthy, 2008) that the coefficient of variation of coating mass, $c_{v,inter}$, decreases as the inverse of the square root of coating time t :

$$c_{v,inter} \propto 1/\sqrt{t} \quad (77)$$

For all the actual DEM simulations, a spray rate of 12 g/min (center point setting) was assumed and all values calculated accordingly. To get results for another spray rate setting, an extrapolation to shorter or longer process times according to Eq. (77) was done. From the given $c_{v,1}$ at a certain time (e.g. at the coating end) and for the base spray rate \dot{V}_1 , the $c_{v,2}$ for another spray rate \dot{V}_2 is thus calculated as:

$$c_{v,2} = c_{v,1} \sqrt{\frac{\dot{V}_2}{\dot{V}_1}} \quad (78)$$

F-3.4 Design of (simulation) experiments

The simulation runs were set up following a statistical design. The approach is commonly known as Design of Experiments (DoE), even if the “experimental runs” are in fact simulations as is the case here. For each parameter, an upper and lower limit was defined. While the simulation would accept almost arbitrary and unrealistic settings, the ranges were chosen such that all values within them would be feasible in a real process. Rotation speed was varied between 16 rpm and 20 rpm, fill level between 3 kg and 4 kg. Either two or four spray nozzles were used.

Two statistical designs were made, one for each friction value, as shown in Table 10 and Table 11. Note that for convenience, the tables already list the final result

for $C_{v,inter}$ as well. No replication runs were included, because the simulation would give very close results each time. Strictly speaking, results would not be identical each time, because the generation of the initial tablet position in the filling of the drum was a random process. The influence of this was tested, and it showed that the variation was negligible. Still, to give a rough idea of the model quality relative to some variation, two pseudo replication runs were created by increasing and decreasing the value of the center run by 15%, respectively. A full factorial design was used for the uncoated tablets. In this way, a larger number of non-linear dependencies could be captured. However, it showed that the resulting model in fact only included linear terms, and a fractional factorial design was used for the coated tablets (which would still capture possible non-linear dependencies).

Table 10: Statistical design of simulation runs for uncoated tablets. For the sake of completeness, the last two columns already contain the results of the runs; a detailed description is given in the results section.

Drum speed	Drum load	Spray rate	CoV (%) 2 nozzles	CoV (%) 4 nozzles
16	3	8	6,68	2,61
18	3	8	6,05	2,4
20	3	8	5,67	2,21
16	3,5	8	7,21	2,71
18	3,5	8	6,67	2,57
20	3,5	8	6,12	2,32
16	4	8	8,34	3,02
18	4	8	7,47	2,75
20	4	8	6,97	2,56
16	3	12	8,19	3,19
18	3	12	7,41	2,94
20	3	12	6,94	2,71
16	3,5	12	8,82	3,32
18	3,5	12	8,17	3,15
20	3,5	12	7,5	2,84
16	4	12	10,22	3,7
18	4	12	9,15	3,37
20	4	12	8,53	3,13
16	3	16	9,45	3,69
18	3	16	8,56	3,4
20	3	16	8,02	3,13
16	3,5	16	10,19	3,84
18	3,5	16	9,43	3,64
20	3,5	16	8,66	3,28
16	4	16	11,8	4,27
18	4	16	10,56	3,89
20	4	16	9,85	3,62

Table 11: Statistical design of simulation runs for coated tablets. For the sake of completeness, the last two columns already contain the results of the runs; a detailed description is given in the results section.

Drum speed	Drum load	Spray rate	CoV (%) 2 nozzles	CoV (%) 4 nozzles
16	3	8	6,97	2,74
20	3	8	6,1	2,3
18	3,5	8	6,66	2,57
16	4	8	7,8	3,05
20	4	8	6,74	2,55
16	3	12	8,53	3,36
20	3	12	7,47	2,82
18	3,5	12	8,15	3,15
16	4	12	9,56	3,73
20	4	12	8,25	3,12
16	3	16	9,85	3,88
20	3	16	8,62	3,26
18	3,5	16	9,42	3,63
16	4	16	11,04	4,31
20	4	16	9,53	3,6

F-4 Results & Discussion

For active coating, the central question is the magnitude of the coefficient of variation of the coating mass, $c_{v,inter}$, and how it is influenced by changes in the operation conditions. First, results that directly relate to the coefficient of variation are given. After that, investigations that give a general insight into the investigated tablet coating process are detailed.

F-4.1 Time dependence of the uniformity

In literature, it is reported that the $c_{v,inter}$ decreases with the inverse of the square root of time, Eq. (77). To see if this holds true for the process investigated here, the decrease of $c_{v,inter}$ over time is shown in Figure 71. As a non-dimensional measure of time, the number of revolutions was used; this facilitates the comparison of different rotation speeds. The results are shown for six representative simulation runs (omitting the cases with 18 rpm for clarity). A logarithmic scale is used for both axes, such that a result following the power law in Eq. (77) would give a straight line of slope $-1/2$ (shown by the solid line in Figure 71).

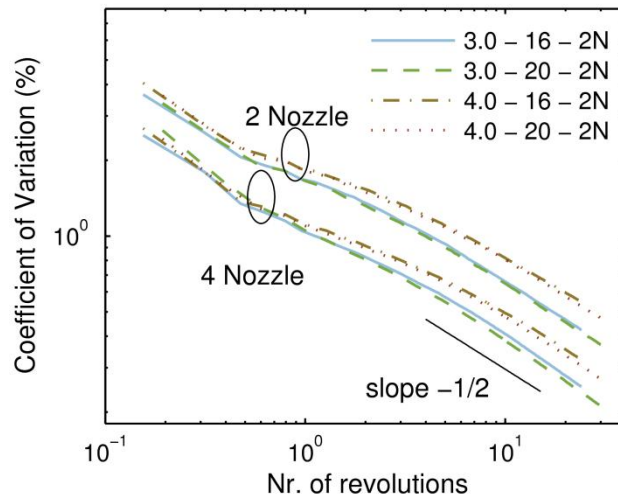


Figure 71: Decrease of the coefficient of variation of coating mass over time. The four highest curves correspond to a process using two nozzles, the four lowest ones to four nozzles. The line shows the slope predicted by analytical models according to Eq.(77).

At first (below ~ 0.5 revolutions), the curve already shows a slope close to -0.5 . This is to be expected: if each tablet would be coated one after the other with the same mass, the decrease would follow the “ $t^{-0.5}$ behavior”. However, after this there is a region ($\sim 0.5 - 10$ revolutions) where the decrease is slower than predicted. The analytic model is based on the assumption of random mixing of the tablets. In this assumption, the fact that a tablet is in the spray zone at a given time does not influence its probability to be in the spray zone at future times. However, this is not true: a tablet passing through the spray has a highly increased probability to travel along the drum wall, emerge at the top, and pass a second time. At the very beginning, the time is too short for a tablet to actually visit the spray zone twice, and the analytic prediction holds. After that, there is a time where many already coated tablets get a second coating, while the majority has no coating at all. The system “recognizes” that the mixing is not random, that in fact tablets are yet in a correlated state, and the less-than-predicted decrease in $C_{v,inter}$ is seen. Once the investigated time is noticeably larger than the correlation time span, the graphs finally shows the predicted decrease parallel to the model line again. This is in accordance with literature results for spherical tablets (Dubey et al., 2011; Kalbag & Wassgren, 2009). It can be concluded that it is viable to apply Eq. (77) for this type of coater (as long as coating times are not extremely short).

Curves differing only in rotation speed lie almost on top of each other in Figure 68. Higher rotation speed gives slightly lower variation (better uniformity) at the

same number of revolutions. The larger benefit is that for a given coating time, a higher rotation speed also gives more rotations in this time, and therefore higher uniformity in all cases. For a constant rotation speed, the $c_{v,inter}$ is decreased with decreasing fill.

F-4.2 DoE model of the uniformity as a function of process parameters

For each process parameter setting (or factor setting), the coating mass uniformity $c_{v,inter}$ (the response) after 90s process time, was calculated as described above. The response was then entered into the statistical design, and a model was build. A second-order model is applied, including all possible linear and quadratic terms, and the data is fitted to the model using multiple linear regression. Starting from this, it is determined which terms are actually needed for the model by backward regression. The whole model building was done twice, for the designs of coated and uncoated tablets, respectively. It should be noted that it was also tried to combine both designs into one, and having the friction coefficient as an additional level. However, more valuable insights could be gathered by treating the two sets separately.

It showed that for both, only linear terms contribute significantly. The general model for both for coated and uncoated tablets was:

$$c_v = a_1 x_{Rot} + a_2 x_{Load} + a_3 x_{Spray} + a_4 x_{Noz}, \quad (79)$$

where x_{Rot} is the rotation velocity, x_{Load} the total mass of tablets, x_{Spray} the spray rate, and x_{Noz} the number of nozzles. The corresponding coefficients a_i were determined by fitting to the known data points. The model showed a good fit ($R^2 = 0.997$) and good predictive capability ($Q^2 = 0.996$). The centered and scaled coefficients are shown in Figure 72 for both coated and uncoated tablets.

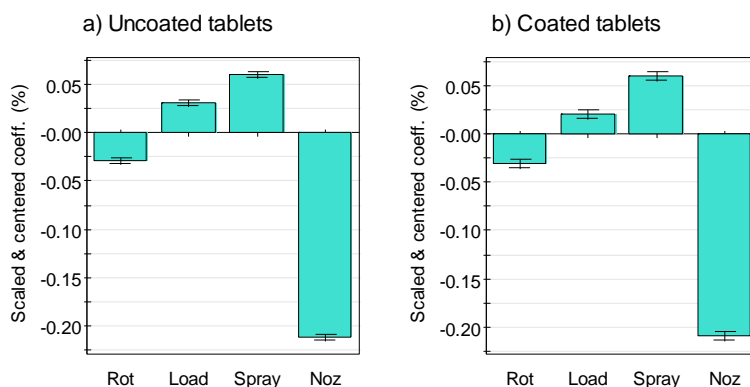


Figure 72: Centered and scaled coefficient plot of the statistical model.

A high absolute value in Figure 72 means that a change in this variable strongly afflicts $c_{v,inter}$. Positive values mean that an increase in the variable increases $c_{v,inter}$; negative values that it is decreased. Figure 72 shows that the largest decrease of $c_{v,inter}$ (the largest increase in uniformity) is achieved for an increase in the number of nozzles, followed by a decrease in spray rate, increase in rotation speed, and decrease in load. The result is nearly the same for coated and uncoated tablets, even though more data points were available for the coated tablets.

Now that a mathematical model is found, it can be investigated in detail how changing the process conditions influences the uniformity. An overview of all results in a very dense form can be presented in a “4D” contour plot (Figure 73). The “4D” plot is a matrix of contour plots, where the location of the contour plot in the matrix shows the values of spray rate and number of nozzles chosen in the creation of this plot, and the contour plot itself shows the dependence on rotation speed and fill level. The scale is the same for all plots. This makes it possible to quickly assess which setting is better, and also how much it is better. In this way, the benefit of a setting can be weighed against its estimated cost. The main conclusions are as follows. From a global perspective, best results (lowest values) are obtained in the upper left part, that is, with 4 nozzles and lowest spray rate, and worst results in the lower right, for 2 nozzles and highest spray rate. In Figure 73, the whole upper row (four nozzles) is better than the regulatory limit of 6.25% by a large margin, irrespective of other settings. This is also true for three nozzles and sprayrates of 8 g/min and 12 g/min (the two left-most contour plots in the middle row), although the $c_{v,inter}$ gets close to the limit for some settings. There are certainly more detailed ways to look at the results (see below), but in a sense Figure 71 contains the main information of this work, already allowing for informed decisions. For example, one can assess whether the benefit of additional spray nozzles is large enough to justify the investment, or whether the increased efficiency of higher fill levels outweighs the slight decrease in uniformity (or the increase in coating time to keep the same uniformity as lower fill levels).

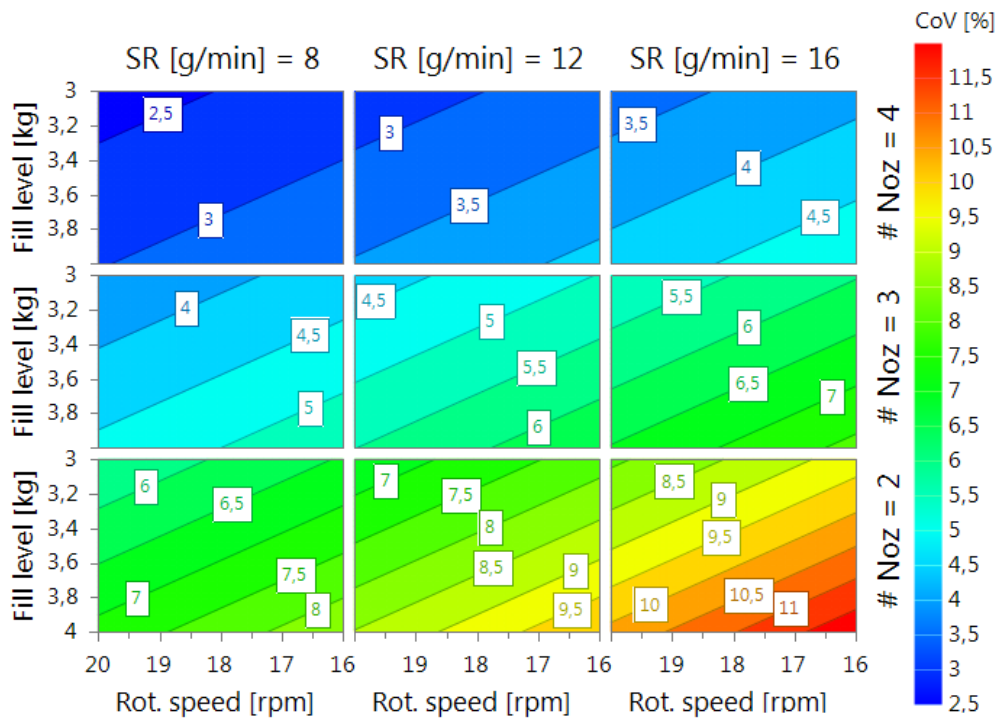


Figure 73: „4D“ contour plot, showing the influence of number of nozzles, spray rate (g/min), rotation speed and fill level on the coefficient of variation of coating mass (CoV). In each of the 9 subplots, the abscissa is rotation speed (rpm), the ordinate is fill level (kg).

F-4.3 Coating mass distribution

The spray simulation gave information on the amount of coating mass on each tablet in each time step. In the DoE above, this distribution was characterized by a single number: the coefficient of variation at the coating end point. In other words, the width of the coating distribution over all tablets at the last simulation time step was considered. A deeper level of information can be shown by plotting the actual distribution, Figure 74.

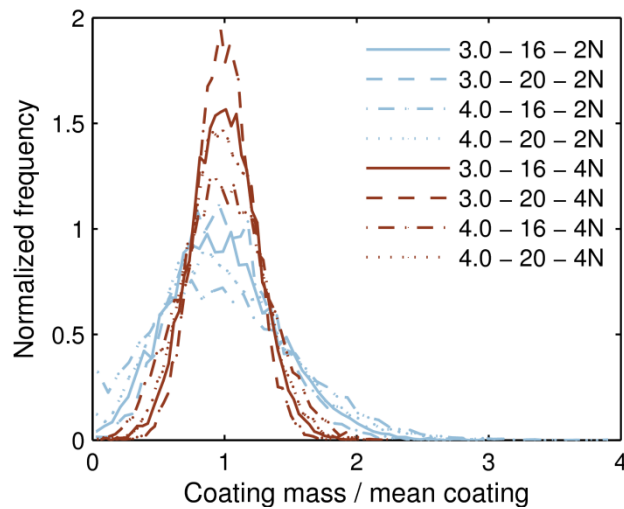


Figure 74: Distribution of the coating mass gathered over all tablets for different simulation runs.

Shown are the results for coated tablets for the different settings of rotation speed and fill level for two and four nozzles (“corners” in the DoE). The relative coating mass, i.e., the coating mass divided by the mean mass is used; for direct comparison all curves are normalized such that the area under each curve is one. The data is from the last simulation step, therefore all curves show the situation after the same coating time (90 s). As explained above, the spray rate would only enter via a change in simulation time, and has no influence here. On one hand, if a constant spray rate is assumed, depending on fill level a different mean mass is achieved. On the other hand, if a constant mean mass is to be achieved in all cases, the spray rates have to be assigned accordingly. In both cases, the relative results are the same. It should be noted that the DoE results above differ insofar as they are calculated for given spray rates and constant mass increase, and thus different coating times, as this is the approach typically chosen in the real process.

Looking not only at the $c_{v,inter}$ values, but at the whole distribution would give the possibility to detect additional characteristics that would hint at additional underlying effects such as bi-modal distribution or skewness. This is not the case here, all distributions have a symmetric, Gaussian shape, originating in the random nature of the coating process. The narrower the curves, the higher the positions of the maximum value due to the constant area, and the higher the uniformity. The results for four nozzle are distinctly better compared to two nozzles. For constant nozzle number, lower rotation speed and lower fill level give better (narrower) distributions.

The results for uncoated tablets are too similar to give different insights, and are omitted here.

F-4.4 Spray residence time

The spray residence time t_{spray} is the time a tablet spends in the spray zone for a single spray event. By assuming that the time in the spray zone is proportional to the received coating, t_{spray} can be used to approximate the coating mass a tablet receives. Note that in this work, a more detailed approach to simulate the coating was used; the spray residence time is monitored in addition. It is collected in the post-processing algorithm for each spray zone visit of each tablet. Only complete visits are included: if the last visit is not finished before the end of the simulation, the true end time is not known and it is therefore not considered to avoid a slight bias. Likewise, events starting at (or potentially before) the beginning of simulation are excluded.

In Figure 75, the distributions of the residence times are shown for all “corner” cases for coated tablets. For each curve, the data of all tablets over the simulated 90 seconds enters. Results for two and four nozzles are shown. However, it is to be expected that for otherwise same conditions, the number of nozzles plays little role; this is confirmed here. The spray residence time is mainly governed by the spray zone shape and determined on a per-nozzle basis, and only to a little extent on the actual position of the nozzles.

Most tablets take a relatively short time to traverse the spray, and not too many tablets stay considerably longer than the mean residence time. This also means that the tablet velocity at the spraying location is relatively uniform. In general, it can be stated that a typical visit takes about 0.1 seconds, giving a useful time scale of the coating process. When comparing the curves, it can be seen that residence times are shorter and the distributions narrower for faster rotation speed and for higher fill level. Thus the lowest and narrowest distribution is seen for a fill of 4 kg and a rotation speed of 20 rpm, and the highest and broadest distribution for 3 kg and 16 rpm.

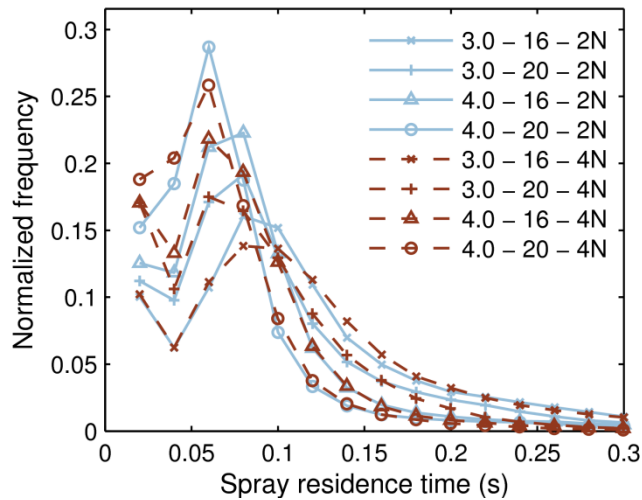


Figure 75: Distribution of spray residence times of a single visit, gathered from all complete spray events for all tablets in the simulation time span.

F-4.5 Bed cycle time

The bed cycle time is the time a tablet spends in the bed between two spray events. The distributions of the bed cycle times are shown in Figure 76 (top and bottom) for different rotation speed and fill level. The data for coated tablets is used. The distribution shows a high first peak after approx. 1.8 seconds, followed by smaller peaks at regular intervals (Figure 76 top). This pattern can be explained by the flow behavior in the drum. After a tablet has crossed the spray zone of one nozzle, it is very likely that it rolls down the tablet bed top, emerges into the bed, is transported back up to the top by the drum wall, and crosses the same spray zone again. The time span this takes is more or less constant (for a given drum rotation speed), and will therefore be commonly seen in the distribution, leading to the first peak. If for some reason the tablet by-passes the spray zone, chances are that it makes the same cycle a second time and crosses the zone during this second try. This is much less likely, and leads to the smaller second peak, and so on for the next peaks.

The higher the rotation speed, the more the peaks are shifted to shorter cycle times, as is to be expected. To investigate this further, Figure 76 also shows a semi-logarithmic, scaled (dimensionless) representation (bottom). The logarithmic y-axis serves to pronounce the periodically repeating peaks. For scaling, the time is divided by the time span one revolution takes at the used rotation speed. With this scaling, the curves for different rotation velocities almost collapse. This means that for the parameter ranges investigated here, bed cycle time is in good approximation directly dependent on the rotation speed,

and not so much on fill level. It also means that the bed time is always the same in terms of fractions (or multiples) of total revolutions, irrespective of the rotation speed (again, in the investigated range). For example, the high first peak at 0.5 means that the most common time between two spray events is 0.5 times the amount a total revolution takes. The actual value in seconds then directly depends on the applied rotation speed. This also implies that for one revolution of the drum, it is common that a tablet can cycle through the bed twice.

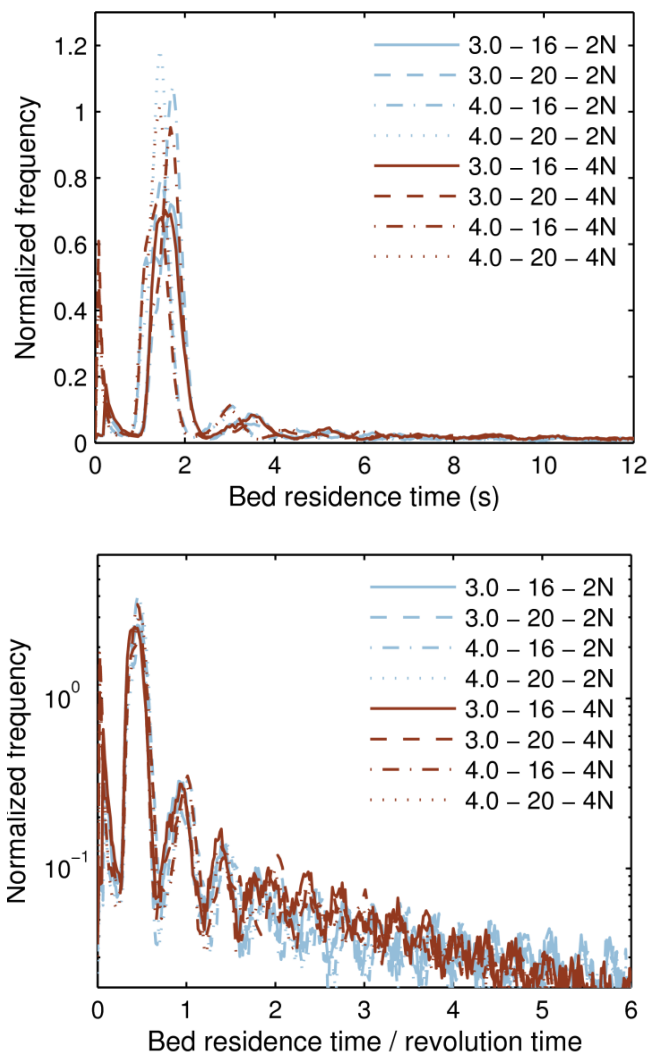


Figure 76: Distribution of bed residence time (time between single spray events of one tablet), gathered from all complete spray events for all tablets in the simulation time span. Top: unscaled plot, bottom: semi-logarithmic, dimensionless plot (please refer to the text for details).

Due to the described mechanic, the first peak should correspond to the time it takes a just-sprayed tablet to move down the rest of the tablet bed top, move back up at the wall, and roll down to the spray zone again. A rough approximation can show whether this is plausible. One bed cycle leading to the first peak can be divided into two segments: transportation along the wall, and rolling down the tablet bed surface. At the fill levels used here, about a third of the drum circumference is in contact with tablets. Due to the presence of baffles, it can be assumed that those tablets move with approximately the same speed as the wall. For the given drum and a rotation speed of 18 rpm, the circumferential velocity (velocity of the drum wall) is 0.3 m/s. With this, the first segment takes approx. 1.1 seconds. For the second segment, the velocity is not as uniform, but from the DEM results a mean velocity of 0.5 m/s can be estimated. Assuming that the tablet follows a straight line along the bed surface, this takes approx. 0.55 seconds. In sum, this rough estimate gives a cycle time of 1.65 seconds, which is in the vicinity of the first peak.

F-4.6 Considerations on analytic uniformity calculation

A commonly found relationship to estimate the variation in total coating (c_v) as a function of the cycle time and coating per pass is given as (Ketterhagen, 2011; Mann, 1983):

$$c_v = \sqrt{\frac{\mu_{ct}}{T_0} \left[\left(\frac{\sigma_{cpp}}{\mu_{cpp}} \right)^2 + \left(\frac{\sigma_{ct}}{\mu_{ct}} \right)^2 \right]} \quad (80)$$

T_0 is the total coating time. The distributions are quantified by their mean and standard deviation (μ_{cpp} and σ_{cpp} for the coating per pass; μ_{ct} and σ_{ct} for the cycle time). Often, the coating per pass is not known, and is assumed to be proportional to the spray residence time. With this reasonable assumption, μ_{cpp} and σ_{cpp} can be directly replaced by the corresponding values of the residence time distribution. Note that Eq. (80) traditionally is formulated in terms of total cycle time (bed plus spray time), while throughout this work, the bed cycle time is used. The bed cycle time is the preferred choice, as it is independent of the spray time, which obviously is not true for the total time. Still, the difference (namely, adding or not adding the spray time) is small, and for the sake of the following estimations, the bed cycle time was seen as a good approximation to the total cycle time.

In any case, looking at Figure 76, the question arises how well the nature of the curve can be captured by stating mean value and standard deviation. The form can be approximated by a normal distribution, but this may under-estimate the tail towards high bed residence times. To investigate this further, the coefficient of variation $c_{v, \text{inter}}$ was calculated in two ways from Eq. (80). First, the needed mean and standard deviation values were calculated from the distributions as shown in Figure 75 (μ_{cpp} and σ_{cpp}) and Figure 76 (μ_{ct} and σ_{ct}), respectively. Second, the same calculation is done, but bed cycle times larger than 5 are neglected (the tail of the distribution is truncated). The investigation includes all eight cases (that is, all curves that are present in the spray residence time and cycle time figures as well). The resulting values are shown in Figure 77. The values taken directly from the DEM simulation (that is, the results that were reported above) are shown as a benchmark.

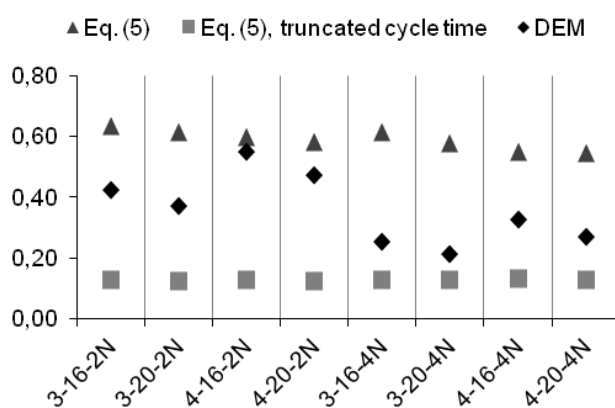


Figure 77: Comparison of results directly from the DEM simulation, and indirectly using the analytic expression Eq. (80) with and without very high values for the cycle time. The naming scheme of cases is as follows: Fill level (kg) – Rotation speed (rpm) – Number of nozzles.

First of all, it can be seen that the prediction of Eq. (80) highly depends whether the tail of the bed cycle distribution is included (triangles in Figure 77) or not included (squares in Figure 77), differing more than a factor 4 for all cases. It is not surprising that truncating the distribution will have an influence, but it is informative to see the magnitude of the influence. This has two immediate consequences. First, even a low number of tablets with a very high cycle time (that is, tablets that spend an extraordinary long duration in the coating drum without seeing any spray) have the potential to seriously impact the uniformity. Second, Eq. (80) seems to have some room for interpretation, and one at least has to be careful in the choice of values that enter the calculation. If the values are extracted from DEM simulation as was done here, this also means that the

simulations have to be long enough, such that even long cycle times are captured. The benchmark results (diamonds in Figure 77) lie in between the “tail” and “no tail” results, and show much more pronounced variation for different process setting. One thing that all evaluations agree upon is that for otherwise same settings, the $C_{v,inter}$ is lower for higher rotation speed. This is apparent when comparing the first two cases with 3 kg fill and 2 nozzles but 16 rpm and 20 rpm rotation speed (named “3-16-2N” and “3-20-2N”, respectively). Apart from that, both the behavior for fill level and number of nozzles is different. Higher fill level lead to a higher $C_{v,inter}$ in the benchmark DEM results, but to a lower value when using the equation. The number of nozzles decreases the $C_{v,inter}$ in all cases, but much more so in the DEM results. It should be pointed out that the number of nozzles had little influence on the spray residence time, as was to be expected. According to Eq. (80), this means that most influence of the number of nozzles on $C_{v,inter}$ is due to a change in the cycle time. In other words, one main reason why a high number of nozzles greatly improved the uniformity is that it reduced the risk of extremely long times between spray events is strongly reduced. This can also be seen in Figure 76b, where the curves for four nozzles are below the curves for two nozzles for high times.

F-4.7 Uniformity per nozzle

The post-processing algorithm gathers the data for each nozzle separately. In this way, it is possible to compare the different nozzles with respect to the quality of coating they provide due to their location in the coater (cf. Figure 70 for the nozzle position). For the comparison, the $C_{v,inter}$ for coated tablets at the end time of the DEM simulation is taken, both for the two nozzle and for four nozzle cases.

Figure 78 shows the result for two nozzles, stating values for each nozzle separately and for the total coating mass. The two nozzles give very similar results, and the total RSD is roughly half the single nozzle RSD.

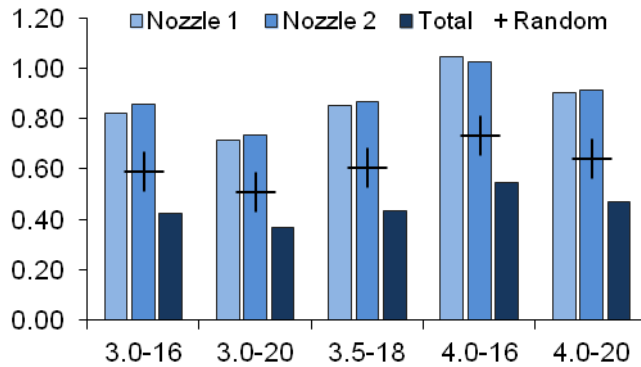


Figure 78: Comparison of the uniformity for each nozzle and total, for cases using the two-nozzle setup. Nozzle numbering starts at the drum opening (i.e., “Nozzle 1” is closest to the front). The naming scheme of the cases is “fill level (kg) – rotation speed (rpm)”.

To put this into perspective, it is useful to consider two limiting cases. First, it could be assumed that both nozzles are operating totally independent of each other. The fact of a tablet currently being in one spray has no influence on its probability to be in the other spray zone. This is similar to coating the tablets using regular settings, but one nozzle only, then coating the same tablets using the other nozzle. The resulting “random” $c_{v,\text{rand}}$ follows from the standard deviations and means of the single nozzles:

$$c_{v,\text{rand}} = \sqrt{\sigma_1^2 + \sigma_2^2} / (\mu_1 + \mu_2) \approx \frac{c_{v,1}}{\sqrt{2}} \quad (81)$$

Where σ_i and μ_i is the standard deviation and mean value for nozzle i ; $c_{v,i}$ is the corresponding coefficient of variation given as σ_i / μ_i . The approximation in the last step assumes that the mean and variation of the distribution of each nozzle is similar.

The second limiting case is a worst case scenario of nozzle placement: both nozzles are located at the exact same position and operate at the same time. Assuming again that the nozzles are identical, both have the same variation, and the total coefficient of variation is simply:

$$c_{v,\text{same}} = c_{v,1} = c_{v,2}. \quad (82)$$

In Figure 78, $c_{v,rand}$ from Eq. (81) is shown by the cross-shaped marker; $c_{v,same}$ from Eq. (81) is already given by the single nozzle values. The actual total RSD value is lower than $c_{v,rand}$, meaning that going from one to two nozzles brings more benefit than a random mixing scenario would predict. This is because spray zones are in fact not independent; tablets that have just been in one spray zone have a decreased probability of turning up in the other spray zone (which would further increase their coating).

Similar, the result for four nozzles (Figure 79) also shows a total RSD that is lower than a perfectly random mixing would predict. In addition, a new phenomenon arises: not all single nozzles show the same RSD, with the front- and backmost locations performing worse than the center positions. When four nozzles are inserted, the first and last nozzle is relatively close to the inlet and back wall, respectively. The mixing in the front and back regions is less effective. The difference is not so drastic as to necessitate a change in the positioning, but there may be potential for improvement by placing the nozzles closer to each other. On the other hand, one has to be careful not to create overlapping spray zones, as this decreases uniformity and has high potential for coating defects caused by local over-wetting.

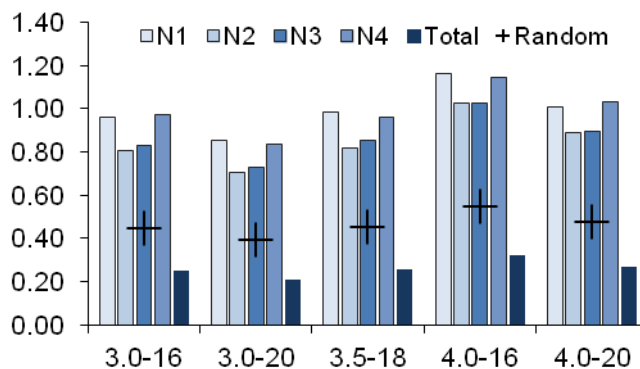


Figure 79: Comparison of the uniformity for each nozzle and total, for cases using the four-nozzle setup. Nozzle numbering starts at the drum opening (i.e., “N1” is the nozzle closest to the front). The naming scheme of the cases is “fill level (kg) – rotation speed (rpm)”.

The topic of nozzle numbers is connected to the speed of mixing in axial direction. While it is relatively fast with the spiral-shaped baffles of the used coating drum it is slow relative to the radial mixing, as is inevitable in useful

rotating drum setups. Therefore, in a sense, the marked improvement with nozzle number that was seen above is a consequence of the “slow” axial mixing vs. “fast” radial mixing. The more nozzles there are, the closer the system gets to the limiting case of a coating zone that is running across the whole axial extent of the coater. In this case, each slice of the coating drum would look the same, and each axial position would be (almost) equivalent, making axial mixing irrelevant.

F-5 Conclusion

The scope of this work was to closely investigate an active coating process using Discrete Element Method simulations, aiming for a setup that is as close to the real process as possible. This includes the use of the actual coater geometry and measured material properties, process conditions following experimental runs, and modeling the actual tablet shape by the glued sphere approach.

The process parameter variations for different simulation runs were chosen according to a statistical design of experiments, and the influence of process parameters on the inter-tablet uniformity was studied in this framework. In addition, different aspects were investigated in detail to get a deeper mechanistic understanding.

Summarizing, the following can be said on factors influencing the coating uniformity. In the investigated range of 16 to 20 rpm, the uniformity increases as a function of the number of revolutions of the coating drum. For the same number of revolutions, very similar results were seen, independent on the rotation speed. A higher rotation speed has then the benefit of more revolutions in a given time or a shorter process, but no additional influences such as a change in the movement pattern regime were seen.

The theoretical model of a decrease inverse to the square root of time that is described throughout literature was in very good agreement with the presented results. In this work, spray rate enters via the change in simulation time for a constant coating mass end point. Therefore, it influences the coating uniformity following the same dependence with the inverse of the square root.

An increase in fill level led, on the one hand, to a decrease in coating uniformity, as is expected due to the lower ratio of sprayed to total particles. On the other hand, higher fill may mean a more efficient utilization of the equipment. The presented quantitative comparison can guide in the decision at which fill level the optimum is reached.

Increasing the number of nozzles led to the largest increase in uniformity. Of course, going from two to four nozzles means a large relative change by doubling this parameter. On the other hand, like the variations in the other parameters it is a change that can be realistically made. It may necessitate to update existing equipment, but the expected increase in uniformity may well justify this.

For each of the summarized points mentioned above, deeper considerations are given in the text. Finally, for most of the investigated process conditions, the uniformity was below 6.25%, thus fulfilling the regulatory requirements for active coating. For four nozzles, this was true irrespective of the other settings. In conclusion, the presented results help to optimize the uniformity such that the quality criteria are consistently met and the process time is minimized.

Chapter G: Conclusion

In one respect, tablet coating is similar to the board game “Go”: both are simple to describe, but difficult to master. In other words, the coating process may not be the most spectacular, but the devil, so to speak, lies in the detail.

This is the reason why, in this work, different approaches and simulation tools were used for different details of the process. The main parts are: modeling of the air flow and spray droplets inside the drum using Computational Fluid Dynamics, investigation of the tablet movement behavior using Discrete Element Method, and based on the last, description of the actual spraying in terms of coating mass distribution and residence times. Results are presented and compared to findings in literature inside the respective fields. It should be noted that other details, such as the impact of drops on the tablets or the influence of particle shape, were studied at the Research Center Pharmaceutical Engineering as well; the interested reader is referred to the respective publications (some of them mentioned in Chapter I:).

All aspects can be found in any coating process, but are not equally important in all. The importance of air flow heavily depends on the location of air inlet and outlet, with great impact in cases where the drying air comes into immediate contact with the spray. It showed that in those cases, one should choose the position and also orientation with great care, as this has potential in reducing spray drying and thus increasing the yield.

At its core, all tablet coating processes follow the same schematic: a tablet receives coating in the spray zone, moves inside the tablet bed for some time while it is being dried, until it re-enters the spray zone again. The question that arises is: how is this related to the coating uniformity? With the even more important follow-up question: how does this relate to the actual (critical) process parameters? The presented work tried to give answers to both questions. Summarizing, the following results were found:

- The uniformity increases as a function of the number of revolutions of the coating drum. For the same number of revolutions, very similar results were seen, independent on the rotation speed. A higher rotation speed has then the benefit of more revolutions in a given time or a shorter process.
- An increase in fill level led, on one hand, to a decrease in coating uniformity, as is expected due to the lower ratio of sprayed to total

particles. On the other hand, mixing may be more effective for higher fills, which in some cases may prevail. In addition, a higher fill level most likely means a more efficient utilization of the equipment.

- Increasing the number of nozzles led to the largest increase in uniformity. It may necessitate updating existing equipment, but the expected increase in uniformity argues in favor.
- The theoretical model of a decrease inverse to the square root of time that is described in literature was in very good agreement with the presented results.
- In this work, spray rate enters via the change in process time that is needed to keep the mean coating mass constant; therefore, the findings for the coating time above apply.

The real strength of simulations is that it not only yields the dependencies as described above, but also provides means to gather a mechanistic understanding of the underlying principles. In general, throughout this work it was aimed to include this detailed investigations, ranging from the influence of model parameters on the spray considerations to the contrasting of different levels of detail (such as highly resolved DEM results in comparison with global statistical considerations). To give an example, one factor that showed potential to decrease the uniformity were very high bed residence times (times between two spraying events) of some tablets. This is one way to explain the good performance when using a higher number of spray nozzles: when there are spray zones all along the axial direction, the possibility to escape all spray zones for a long time is limited.

The state-of-the-are at the time this work started was such that it was if not impossible, then at least not very feasible to simulate the large number of tablets that are present in a full-scale coating apparatus, let alone coupled to the air flow. However, technology progresses fast, and modern computer simulations can continue where there were limitations previously. For example, the coupled CFD-DEM code "XPS FIRE" that is developed in-house (XPS: Research Center Pharmaceutical Engineering GmbH, Austria; FIRE: AVL List GmbH, Austria) can now be applied for this kind of complex large-scale processes (Jajcevic et al., 2013; Radeke et al., 2010). Next steps would therefore be to build onto the insights that where gathered here and move on to larger systems that capture even more of the underlying mechanics. Simulation of larger scales gives exciting new possibilities for the study of scale-up effects. An enhanced coupling of CFD and DEM can resolve the interplay of air stream and moving tablets in more detail, showing even subtle effects.

Chapter H: References

- Abe, E., Yamada, N., Hirose, H., & Nakamura, H. (1998). Coating mass distributions of seed particles in a tumbling fluidized bed coater. *Powder Technology*, 97(1), 85–90. doi:10.1016/S0032-5910(98)00004-7
- Abedi, S., & Mirghasemi, A. A. (2011). Particle shape consideration in numerical simulation of assemblies of irregularly shaped particles. *Particuology*, 9(4), 387–397. doi:10.1016/j.partic.2010.11.005
- Abramzon, B., & Sirignano, W. A. (1989). Droplet vaporization model for spray combustion calculations. *INTERNATIONAL JOURNAL OF HEAT AND MASS TRANSFER*, 32(9), 1605–1618.
- Adam, S., Suzzi, D., Radeke, C., & Khinast, J. G. (2011). An integrated Quality by Design (QbD) approach towards design space definition of a blending unit operation by Discrete Element Method (DEM) simulation. *Eur J Pharm Sci*, 42(1-2), 106–15. doi:10.1016/j.ejps.2010.10.013
- Agrdria, E. S., Apoldnia, Q. D. S., Engineering, R., Engenharia, F. De, Peres, A. M., & Macedo, E. A. (1997). A modified UNIFAC model for the calculation of thermodynamic properties of aqueous and non-aqueous solutions containing sugars. *Fluid Phase Equilibria*, 139(1-2), 47–74.
- Ahmadian, H., Hassanpour, A., & Ghadiri, M. (2011). Analysis of granule breakage in a rotary mixing drum: Experimental study and distinct element analysis. *Powder Technology*, 210(2), 175–180. doi:10.1016/j.powtec.2011.03.013
- Alexander, A., Shinbrot, T., & Muzzio, F. J. (2002). Scaling surface velocities in rotating cylinders as a function of vessel radius, rotation rate, and particle size. *Powder Technology*, 126(2), 174–190. doi:10.1016/S0032-5910(02)00010-4
- Aliseda, A., Hopfinger, E. J., Lasheras, J. C., Kremer, D. M., Berchielli, A., & Connolly, E. K. (2008). Atomization of viscous and non-newtonian liquids by a coaxial, high-speed gas jet. Experiments and droplet size modeling. *International Journal of Multiphase Flow*, 34(2), 161–175. doi:10.1016/j.ijmultiphaseflow.2007.09.003
- Alleborn, N., & Raszillier, H. (2004). Spreading and sorption of droplets on layered porous substrates. *Journal of colloid and interface science*, 280(2), 449–64. doi:10.1016/j.jcis.2004.08.003

- Attarakih, M., Abu Fara, D., & Sayed, S. (2001). Dynamic modeling of a packed-bed glycerol-water distillation column. *Industrial & Engineering Chemistry Research*, 40(22), 4857–4865.
- Bolleddula, D. A., Berchielli, A., & Aliseda, A. (2010). Impact of a heterogeneous liquid droplet on a dry surface: application to the pharmaceutical industry. *Advances in colloid and interface science*, 159(2), 144–59. doi:10.1016/j.cis.2010.06.003
- Bradley Eldredge, H., & Drown, D. C. (1999). Solids flow and mixing model for a fluidized bed coating and calcination process. *Chemical Engineering Science*, 54(9), 1253–1264. doi:10.1016/S0009-2509(98)00498-9
- Brenn, G., Deviprasath, L. J., Durst, F., & Fink, C. (2007). Evaporation of acoustically levitated multi-component liquid droplets. *International Journal of Heat and Mass Transfer*, 50(25-26), 5073–5086.
- Brock, D., Zeitler, J. A., Funke, A., Knop, K., & Kleinebudde, P. (2012). A comparison of quality control methods for active coating processes. *Int J Pharm*, 439(1-2), 289–95. doi:10.1016/j.ijpharm.2012.09.021
- Cahn, D. S., & Fuerstenau, D. W. (1969). A probabilistic model of the diffusional mixing of particulate solids. *Powder Technology*, 2(4), 215–222. doi:10.1016/0032-5910(69)80015-X
- Cahyadi, C., Karande, A. D., Chan, L. W., & Heng, P. W. S. (2010). Comparative study of non-destructive methods to quantify thickness of tablet coatings. *International Journal of Pharmaceutics*, 398(1-2), 39–49. doi:10.1016/j.ijpharm.2010.07.020
- Chang, R.-K., & Leonzio, M. (1995). The Effect of Run Time on the Inter-Unit Uniformity of Aqueous Film Coating Applied to Glass Beads in a Hi-Coater. *Drug Development and Industrial Pharmacy*, 21(16), 1895–1899. doi:10.3109/03639049509070865
- Cheng, X. X., & Turton, R. (2000a). The prediction of variability occurring in fluidized bed coating equipment. I. The measurement of particle circulation rates in a bottom-spray fluidized bed coater. *Pharmaceutical development and technology*, 5(3), 311–22. doi:10.1081/PDT-100100546
- Cheng, X. X., & Turton, R. (2000b). The prediction of variability occurring in fluidized bed coating equipment. II. The role of nonuniform particle coverage as particles pass through the spray zone. *Pharmaceutical development and technology*, 5(3), 323–32. doi:10.1081/PDT-100100547

- Choi, M. M. S., & Meisen, A. (1997). Sulfur coating of urea in shallow spouted beds. *Chemical Engineering Science*, 52(7), 1073–1086. doi:10.1016/S0009-2509(96)00377-6
- Cole, G., Hogan, J., & Aulton, M. E. (1995). *Pharmaceutical coating technology*. Informa Healthcare.
- Cole, G., Hogan, J., Aulton, M. E., & Twitchell, A. M. (2002). *Pharmaceutical Coating Technology*. (Graham Cole, Ed.). London: Taylor & Francis.
- Couroyer, C., Ning, Z., Ghadiri, M., Brunard, N., Kolenda, F., Bortzmeyer, D., & Laval, P. (1999). Breakage of macroporous alumina beads under compressive loading: simulation and experimental validation. *Powder Technology*, 105(1-3), 57–65. doi:10.1016/S0032-5910(99)00118-7
- Cox, D. C., Wells, C. E., Furman, W. B., Savage, T. S., & King, A. C. (1982). SYSTEMATIC-ERROR ASSOCIATED WITH APPARATUS-2 OF THE USP DISSOLUTION TEST-II - EFFECTS OF DEVIATIONS IN VESSEL CURVATURE FROM THAT OF A SPHERE. *Journal of Pharmaceutical Sciences*, 71, 395–399. doi:10.1002/jps.2600710405
- Cundall, P. A., & Strack, O. D. L. (1979). A discrete numerical model for granular assemblies. *Géotechnique*, 29(1), 47–65. doi:10.1680/geot.1979.29.1.47
- Davis, J. R. (2004). *Handbook of Thermal Spray Technology*. ASM International.
- Deen, N. G., Annaland, M. V. S., der Hoef, M. A. Van, & Kuipers, J. A. M. (2007). Review of discrete particle modeling of fluidized beds. *Chemical Engineering Science*, 62(1-2), 28–44.
- Denis, C., Hemati, M., Chulia, D., Lanne, J.-Y., Buisson, B., Daste, G., & Elbaz, F. (2003). A model of surface renewal with application to the coating of pharmaceutical tablets in rotary drums. *Powder Technology*, 130(1-3), 174–180. doi:10.1016/S0032-5910(02)00262-0
- Ding, Y. L., Forster, R. N., Seville, J. P. K., & Parker, D. J. (2001). Scaling relationships for rotating drums. *Chemical Engineering Science*, 56(12), 3737–3750. doi:10.1016/S0009-2509(01)00092-6
- Directorate for the Quality of Medicines of the Council of Europe. (2011). Monograph 2.9.40. Uniformity of dosage units. In *European Pharmacopoeia* (7th ed.). Strasbourg.
- Dubey, A., Boukouvala, F., Keyvan, G., Hsia, R., Saranteas, K., Brone, D., ... Muzzio, F. J. (2012). Improvement of tablet coating uniformity using a quality by

- design approach. *AAPS PharmSciTech*, 13(1), 231–46. doi:10.1208/s12249-011-9723-x
- Dubey, A., Hsia, R., Saranteas, K., Brone, D., Misra, T., & Muzzio, F. J. (2011). Effect of speed, loading and spray pattern on coating variability in a pan coater. *Chem Eng Sci*, 66(21), 5107–5115. doi:10.1016/j.ces.2011.07.010
- Dukowicz, J. K. (1980). A particle-fluid numerical model for liquid sprays. *Journal of Computational Physics*, 35(2), 229–253. doi:10.1016/0021-9991(80)90087-X
- Ende, M. T. am, & Berchielli, A. (2005). A Thermodynamic Model for Organic and Aqueous Tablet Film Coating. *Pharmaceutical Development and Technology*, 10(1), 47–58. doi:10.1081/PDT-200035915
- EVONIK Röhm GmbH. (2007). Specifications and test methods for EUDRAGIT® L 30 D-55.
- Favier, J. F., Abbaspour-Fard, M. H., Kremmer, M., & Raji, A. O. (1999). Shape representation of axi-symmetrical, non-spherical particles in discrete element simulation using multi-element model particles. *Engineering Computations*, 16(4), 467–480. doi:10.1108/02644409910271894
- Fercher, A. F. (2010). Optical coherence tomography - development, principles, applications. *Z Med Phys*, 20(4), 251–76. doi:10.1016/j.zemedi.2009.11.002
- Freireich, B., Ketterhagen, W. R., & Wassgren, C. (2011). Intra-tablet coating variability for several pharmaceutical tablet shapes. *Chem Eng Sci*, 66(12), 2535–2544. doi:10.1016/j.ces.2011.02.052
- Freireich, B., & Li, J. (2012). A Renewal Theory Approach to Understanding Inter-Particle Coating Variability. In *AICHE Annual Meeting*. Pittsburgh, PA.
- Freireich, B., & Li, J. (2013). A renewal theory approach to understanding interparticle coating variability. *Powder Technology*, 249, 330–338. doi:10.1016/j.powtec.2013.08.040
- Freireich, B., Li, J., Litster, J., & Wassgren, C. (2011). Incorporating particle flow information from discrete element simulations in population balance models of mixer-coaters. *Chemical Engineering Science*, 66(16), 3592–3604. doi:10.1016/j.ces.2011.04.015
- Freireich, B., Litster, J., & Wassgren, C. (2009). Using the discrete element method to predict collision-scale behavior: A sensitivity analysis. *Chemical Engineering Science*, 64(15), 3407–3416. doi:10.1016/j.ces.2009.04.019

- Freireich, B., & Wassgren, C. (2010). Intra-particle coating variability: Analysis and Monte-Carlo simulations. *Chemical Engineering Science*, 65(3), 1117–1124. doi:10.1016/j.ces.2009.09.066
- Fries, L., Antonyuk, S., Heinrich, S., & Palzer, S. (2011). DEM–CFD modeling of a fluidized bed spray granulator. *Chemical Engineering Science*, 66(11), 2340–2355. doi:10.1016/j.ces.2011.02.038
- Ganser, G. H. (1993). A rational approach to drag prediction of spherical and nonspherical particles. *Powder Technology*, 77(2), 143–152. doi:10.1016/0032-5910(93)80051-B
- González-Montellano, C., Ramírez, Á., Gallego, E., & Ayuga, F. (2011). Validation and experimental calibration of 3D discrete element models for the simulation of the discharge flow in silos. *Chemical Engineering Science*, 66(21), 5116–5126. doi:10.1016/j.ces.2011.07.009
- Gorham, D. A., & Kharaz, A. H. (2000). The measurement of particle rebound characteristics. *Powder Technology*, 112(3), 193–202. doi:10.1016/S0032-5910(00)00293-X
- Hall, H. S. (1990). Chapter 11. In K. L. Karam (Ed.), *Granulation Technology for Bioproducts*. Boca Raton, FL, USA: CRC Press.
- Hancock, B. C., Mojica, N., St John-Green, K., Elliott, J. A., & Bharadwaj, R. (2010). An investigation into the kinetic (sliding) friction of some tablets and capsules. *International journal of pharmaceutics*, 384(1-2), 39–45. doi:10.1016/j.ijpharm.2009.09.038
- Hirleman, E. D. (1996). History of Development of the Phase-Doppler Particle-Sizing Velocimeter. *Particle and Particle Systems Characterization*, 13(2), 59–67.
- Ho, L., Müller, R., Gordon, K. C., Kleinebudde, P., Pepper, M., Rades, T., ... Zeitler, J. A. (2008). Applications of terahertz pulsed imaging to sustained-release tablet film coating quality assessment and dissolution performance. *J Control Release*, 127(1), 79–87. doi:10.1016/j.jconrel.2008.01.002
- Ho, L., Müller, R., Römer, M., Gordon, K. C., Heinämäki, J., Kleinebudde, P., ... Zeitler, J. A. (2007). Analysis of sustained-release tablet film coats using terahertz pulsed imaging. *J Control Release*, 119(3), 253–61. doi:10.1016/j.jconrel.2007.03.011
- Jajcevic, D., Radeke, C., Scharrer, G., & Khinast, J. G. (2012). Coupled CFD and DEM Simulation of Fluid-Granular Systems. In *AIChE Annual Meeting*. Pittsburgh, PA.

- Jajcevic, D., Siegmann, E., Radeke, C., & Khinast, J. G. (2013). Large-scale CFD–DEM simulations of fluidized granular systems. *Chemical Engineering Science*, *98*, 298–310. doi:10.1016/j.ces.2013.05.014
- Joglekar, A., Joshi, N., Song, Y., & Ergun, J. (2007). Mathematical model to predict coat weight variability in a pan coating process. *Pharmaceutical development and technology*, *12*(3), 297–306. doi:10.1080/10837450701247442
- Just, S., Toschkoff, G., Funke, A., Djuric, D., Khinast, J. G., Knop, K., & Kleinebudde, P. (2013). Optimization of Inter-Tablet Coating Uniformity for an Active Coating Process at the Lab and Pilot Scale. *International Journal of Pharmaceutics*, *30*(11).
- Just, S., Toschkoff, G., Funke, A., Djuric, D., Scharrer, G., Khinast, J., ... Kleinebudde, P. (2013). Experimental analysis of tablet properties for discrete element modeling of an active coating process. *AAPS PharmSciTech*, *14*(1), 402–11. doi:10.1208/s12249-013-9925-5
- Kalbag, A., & Wassgren, C. (2009). Inter-tablet coating variability: Tablet residence time variability. *Chem Eng Sci*, *64*(11), 2705–2717. doi:10.1016/j.ces.2009.02.037
- Kalbag, A., Wassgren, C., Sumana Penumetcha, S., & Pérez-Ramos, J. D. (2008). Inter-tablet coating variability: Residence times in a horizontal pan coater. *Chem Eng Sci*, *63*(11), 2881–2894. doi:10.1016/j.ces.2008.03.009
- Kandela, B., Sheorey, U., Banerjee, A., & Bellare, J. (2010). Study of tablet-coating parameters for a pan coater through video imaging and Monte Carlo simulation. *Powder Technology*, *204*(1), 103–112. doi:10.1016/j.powtec.2010.07.024
- Kauffman, J. F., Dellibovi, M., & Cunningham, C. R. (2007). Raman spectroscopy of coated pharmaceutical tablets and physical models for multivariate calibration to tablet coating thickness. *J Pharm Biomed Anal*, *43*, 39–48. doi:10.1016/j.jpba.2006.06.017
- Ketterhagen, W. R. (2011). Modeling the motion and orientation of various pharmaceutical tablet shapes in a film coating pan using DEM. *International journal of pharmaceutics*, *409*(1-2), 137–49. doi:10.1016/j.ijpharm.2011.02.045
- Ketterhagen, W. R., am Ende, M. T., & Hancock, B. C. (2009a). Process modeling in the pharmaceutical industry using the discrete element method. *Journal of Pharmaceutical Sciences*, *98*(2), 442–470. doi:10.1002/jps.21466

- Ketterhagen, W. R., am Ende, M. T., & Hancock, B. C. (2009b). Process modeling in the pharmaceutical industry using the discrete element method. *Journal of pharmaceutical sciences*, *98*(2), 442–70. doi:10.1002/jps.21466
- Ketterhagen, W. R., am Ende, M. T., & Hancock, B. C. (2009c). Process modeling in the pharmaceutical industry using the discrete element method. *Journal of pharmaceutical sciences*, *98*(2), 442–70. doi:10.1002/jps.21466
- Ketterhagen, W. R., Bharadwaj, R., & Hancock, B. C. (2010). The coefficient of rolling resistance (CoRR) of some pharmaceutical tablets. *International journal of pharmaceutics*, *392*(1-2), 107–10. doi:10.1016/j.ijpharm.2010.03.039
- Kim, J., & Kim, J. (2009). A Characterization of the Spray Evolution by Dual-mode Phase Doppler Anemometry in an Injector of Liquid-propellant Thruster. *Journal of Mechanical Science and Technology*, *23*(6), 1637–1649.
- Kirsch, J. D., & Drennen, J. K. (1995). Determination of film-coated tablet parameters by near-infrared spectroscopy. *J Pharm Biomed Anal*, *13*, 1273–1281. doi:10.1016/0731-7085(95)01562-y
- Kodam, M. a C. J. b H. B. c W. C. a d. (2012). Discrete element method modeling of bi-convex pharmaceutical tablets: Contact detection algorithms and validation. *Chemical Engineering Science*, *69*, 587–601.
- Kodam, M., Bharadwaj, R., Curtis, J., Hancock, B., & Wassgren, C. (2009). Force model considerations for glued-sphere discrete element method simulations. *Chemical Engineering Science*, *64*(15), 3466–3475. doi:10.1016/j.ces.2009.04.025
- Kodam, M., Curtis, J., Hancock, B., & Wassgren, C. (2012). Discrete element method modeling of bi-convex pharmaceutical tablets: Contact detection algorithms and validation. *Chemical Engineering Science*, *69*(1), 587–601. doi:10.1016/j.ces.2011.11.011
- Kohav, T., Richardson, J. T., & Luss, D. (1995). Axial dispersion of solid particles in a continuous rotary kiln. *AIChE Journal*, *41*(11), 2465–2475. doi:10.1002/aic.690411112
- Koller, D. M., Hanneschläger, G., Leitner, M., & Khinast, J. G. (2011). Non-destructive analysis of tablet coatings with optical coherence tomography. *European journal of pharmaceutical sciences : official journal of the European Federation for Pharmaceutical Sciences*, *44*(1-2), 142–8. doi:10.1016/j.ejps.2011.06.017

- Krugger-Emden, H., Rickelt, S., Wirtz, S., & Scherer, V. (2008). A study on the validity of the multi-sphere Discrete Element Method. *Powder Technology*, *188*(2), 153–165. doi:10.1016/j.powtec.2008.04.037
- Kuo, H. P. P., Knight, P. C. C., Parker, D. J. J., Tsuji, Y., Adams, M. J. J., & Seville, J. P. K. P. K. (2002). The influence of DEM simulation parameters on the particle behaviour in a V-mixer. *Chemical Engineering Science*, *57*(17), 3621–3638. doi:10.1016/S0009-2509(02)00086-6
- KuShaari, K., Pandey, P., Song, Y., & Turton, R. (2006). Monte Carlo simulations to determine coating uniformity in a Wurster fluidized bed coating process. *Powder Technology*, *166*(2), 81–90. doi:10.1016/j.powtec.2006.05.001
- Lekhal, A., Conway, S. L., Glasser, B. J., & Khinast, J. G. (2006). Characterization of granular flow of wet solids in a bladed mixer. *AIChE Journal*, *52*(8), 2757–2766. doi:10.1002/aic.10868
- Levin, M. (2005). Scaling up manufacturing: How to Scale Up Scientifically. *Pharmaceutical Technology*, *3*, s4–s13.
- Li, Y., Xu, Y., & Thornton, C. (2005). A comparison of discrete element simulations and experiments for “sandpiles” composed of spherical particles. *Powder Technology*, *160*(3), 219–228. doi:10.1016/j.powtec.2005.09.002
- Liu, F., Lizio, R., Schneider, U. J., Petereit, H.-U., Blakey, P., & Basit, A. W. (2009). SEM/EDX and confocal microscopy analysis of novel and conventional enteric-coated systems. *Int J Pharm*, *369*(1-2), 72–8. doi:10.1016/j.ijpharm.2008.10.035
- Liu, L. X., & Litster, J. D. (1993). Coating mass distribution from a spouted bed seed coater: Experimental and modelling studies. *Powder Technology*, *74*(3), 259–270. doi:10.1016/0032-5910(93)85034-7
- Liu, X. Y., Xu, X., & Zhang, Y. Y. (2011). Experimental Study on Time Features of Particle Motion in Rotating Drums. *Chemical Engineering & Technology*, *34*(6), 997–1002. doi:10.1002/ceat.201000483
- Mann, U. (1983). Analysis of spouted-bed coating and granulation. 1. Batch operation. *Industrial & Engineering Chemistry Process Design and Development*, *22*(2), 288–292. doi:10.1021/i200021a019
- Mann, U., & Crosby, E. J. (1975). Cycle time distribution measurements in spouted beds. *The Canadian Journal of Chemical Engineering*, *53*(5), 579–581. doi:10.1002/cjce.5450530522

- Mann, U., Rubinovitch, M., & Crosby, E. J. (1979). Characterization and analysis of continuous recycle systems. *AIChE Journal*, 25(5), 873–882. doi:10.1002/aic.690250516
- Mansour, A., & Chigier, N. (1995). Air-blast atomization of non-Newtonian liquids. *Journal of Non-Newtonian Fluid Mechanics*, 58(2-3), 161–194. doi:10.1016/0377-0257(95)01356-Z
- Maronga, S. J., & Wnukowski, P. (1997). Modelling of the three-domain fluidized-bed particulate coating process. *Chemical Engineering Science*, 52(17), 2915–2925. doi:10.1016/S0009-2509(97)00112-7
- Masters, K. (1985). *Spray Drying Handbook. Chemical and Process Engineering Series* (4th ed.). London: Halsted Press.
- Mauritz, J. M. A., Morrisby, R. S., Hutton, R. S., Legge, C. H., & Kaminski, C. F. (2010). Imaging pharmaceutical tablets with optical coherence tomography. *J Pharm Sci*, 99(1), 385–91. doi:10.1002/jps.21844
- Ministry of Health Labour and Welfare. (2011). Monograph 6.02 Uniformity of Dosage Units. In *Japanese Pharmacopoeia* (16th ed.). Tokyo.
- Mueller, R., & Kleinebudde, P. (2006). Influence of scale-up on the abrasion of tablets in a pan coater. *European journal of pharmaceutics and biopharmaceutics: official journal of Arbeitsgemeinschaft für Pharmazeutische Verfahrenstechnik e.V*, 64(3), 388–92. doi:10.1016/j.ejpb.2006.05.016
- Mueller, R., & Kleinebudde, P. (2007a). Comparison of a laboratory and a production coating spray gun with respect to scale-up. *AAPS PharmSciTech*, 8(1), 3. doi:10.1208/pt0801003
- Mueller, R., & Kleinebudde, P. (2007b). Prediction of tablet velocity in pan coaters for scale-up. *Powder Technology*, 173(1), 51–58. doi:10.1016/j.powtec.2006.11.016
- Muguruma, Y., Tanaka, T., & Tsuji, Y. (2000). Numerical simulation of particulate flow with liquid bridge between particles (simulation of centrifugal tumbling granulator). *Powder Technology*, 109(1-3), 49–57. doi:10.1016/S0032-5910(99)00226-0
- Muliadi, A. R., & Sojka, P. (2009). Implementation of Quality-by-Design Principles: Modeling of Spray Tablet Coating Using a CFD Approach. In *AIChE Annual Meeting*. Nashville.

- Muliadi, A. R., & Sojka, P. E. (2010). A REVIEW OF PHARMACEUTICAL TABLET SPRAY COATING. *Atomization and Sprays*, 20(7), 611–638. doi:10.1615/AtomizSpr.v20.i7.40
- Mundo, C., Sommerfeld, M., & Tropea, C. (1995). Droplet-wall collisions: Experimental studies of the deformation and breakup process. *International Journal of Multiphase Flow*, 21(2), 151–173. doi:10.1016/0301-9322(94)00069-V
- Nakamura, H., Abe, E., & Yamada, N. (1998). Coating mass distributions of seed particles in a tumbling fluidized bed coater Part II. A Monte Carlo simulation of particle coating. *Powder Technology*, 99(2), 140–146. doi:10.1016/S0032-5910(98)00097-7
- Nase, S. T., Vargas, W. L., Abatan, A. A., & McCarthy, J. J. (2001). Discrete characterization tools for cohesive granular material. *Powder Technology*, 116(2-3), 214–223. doi:10.1016/S0032-5910(00)00398-3
- Nukiyama, S., & Tanasawa, Y. (1939). Experiments on the atomization of liquids in an airstream. *Trans Soc Mech Eng Japan*, 68–75.
- Orpe, A., & Khakhar, D. (2001). Scaling relations for granular flow in quasi-two-dimensional rotating cylinders. *Physical Review E*, 64(3), 031302. doi:10.1103/PhysRevE.64.031302
- Page, S., Baumann, K.-H., & Kleinebudde, P. (2006a). Mathematical modeling of an aqueous film coating process in a Bohle Lab-Coater, part 1: development of the model. *AAPS PharmSciTech*, 7(2), E42. doi:10.1208/pt070242
- Page, S., Baumann, K.-H., & Kleinebudde, P. (2006b). Mathematical modeling of an aqueous film coating process in a Bohle Lab-Coater: part 2: application of the model. *AAPS PharmSciTech*, 7(2), E43. doi:10.1208/pt070243
- Pandey, P., Katakdaunde, M., & Turton, R. (2006). Modeling weight variability in a pan coating process using Monte Carlo simulations. *AAPS PharmSciTech*, 7(4), 83. doi:10.1208/pt070483
- Pandey, P., Song, Y., Kayihan, F., & Turton, R. (2006). Simulation of particle movement in a pan coating device using discrete element modeling and its comparison with video-imaging experiments. *Powder Technology*, 161(2), 79–88. doi:10.1016/j.powtec.2005.09.003
- Pandey, P., & Turton, R. (2005). Movement of different-shaped particles in a pan-coating device using novel video-imaging techniques. *AAPS PharmSciTech*, 6(2), E237–44. doi:10.1208/pt060234

- Pandey, P., Turton, R., Joshi, N., Hammerman, E., & Ergun, J. (2006). Scale-up of a pan-coating process. *AAPS PharmSciTech*, 7(4), E125–E132. doi:10.1208/pt0704102
- Parker, D. J., Dijkstra, A. E., Martin, T. W., & Seville, J. P. K. (1997). Positron emission particle tracking studies of spherical particle motion in rotating drums. *Chemical Engineering Science*, 52(13), 2011–2022. doi:10.1016/S0009-2509(97)00030-4
- Patel, J. K., Shah, A. M., & Sheth, N. R. (2009). Aqueous-based film coating of tablets: Study the effect of critical process parameters. *International Journal of PharmTech Research*, 1(2), 235–240.
- Patel, V. C., Rodi, W., & Scheuerer, G. (1985). Turbulence Models for Near-wall and Low Reynolds-number Flows - A Review. *AIAA Journal*, 23(9), 1308–1319.
- Payri, R., Tormos, B., Salvador, F. J., & Araneo, L. (2008). Spray Droplet Velocity Characterization for Convergent Nozzles with Three Different Diameters. *Fuel*, 87(15-16), 3176–3182.
- Piccioli, R. (2006). *Injection and Combustion of Water / Diesel Fuel Emulsions. Analysis and CFD Modelling Based on FIRE 8.5*. Università di Bologna.
- Podczeck, F., Drake, K. R., Newton, J. M., & Haririan, I. (2006). The strength of bilayered tablets. *European journal of pharmaceutical sciences: official journal of the European Federation for Pharmaceutical Sciences*, 29(5), 361–6. doi:10.1016/j.ejps.2006.07.005
- Pohlman, N., Ottino, J., & Lueptow, R. (2006). End-wall effects in granular tumblers: From quasi-two-dimensional flow to three-dimensional flow. *Physical Review E*, 74(3), 31305. doi:10.1103/PhysRevE.74.031305
- Porter, S. C. (2012). Scale-up of film coating. In M. Levin (Ed.), *Pharmaceutical Process Scale-Up* (pp. 444–489). Marcel Dekker, Inc.
- Porter, S. C., Verseput, R. P., & Cunningham, C. R. (1997). Process Optimization Using Design of Experiments. *Pharm. Technol.*, 1, 1–7.
- Prpich, A., am Ende, M. T., Katzschner, T., Lubczyk, V., Weyhers, H., & Bernhard, G. (2010). Drug product modeling predictions for scale-up of tablet film coating—A quality by design approach. *Computers & Chemical Engineering*, 34(7), 1092–1097. doi:10.1016/j.compchemeng.2010.03.006

- Radeke, C. A., Glasser, B. J., & Khinast, J. G. (2010). Large-scale powder mixer simulations using massively parallel GPU architectures. *Chemical Engineering Science*, 65(24), 6435–6442. doi:10.1016/j.ces.2010.09.035
- Radl, S., Kalvoda, E., Glasser, B. J., & Khinast, J. G. (2010). Mixing characteristics of wet granular matter in a bladed mixer. *Powder Technology*, 200(3), 171–189. doi:10.1016/j.powtec.2010.02.022
- Rafai, S., Bonn, D., & Boudaoud, A. (2004). Spreading of non-Newtonian fluids on hydrophilic surfaces. *Journal of Fluid Mechanics*, 513. doi:10.1017/s0022112004000278
- Rähse, W. (2009). Produktdesign disperser Stoffe: Industrielles Partikelcoating. *Chemie Ingenieur Technik*, 81(3), 225–240. doi:10.1002/cite.200800103
- Ranz, W. E., & Marshall, W. R. (1952a). Evaporation From Drops .1. *Chemical Engineering Progress*, 48(3), 141–146.
- Ranz, W. E., & Marshall, W. R. (1952b). Evaporation From Drops .2. *Chemical Engineering Progress*, 48(4), 173–180.
- Remy, B., Canty, T. M., Khinast, J. G., & Glasser, B. J. (2010). Experiments and simulations of cohesionless particles with varying roughness in a bladed mixer. *Chemical Engineering Science*, 65, 4557–4571. doi:10.1016/j.ces.2010.04.034
- Romero-Torres, S., Perez-Ramos, J. D., Morris, K. R., & Grant, E. R. (2005). Raman spectroscopic measurement of tablet-to-tablet coating variability. *J Pharm Biomed Anal*, 38, 270–274. doi:10.1016/j.jpba.2005.01.007
- Ruotsalainen, M., Heinämäki, J., Guo, H., Laitinen, N., & Yliruusi, J. (2003). A novel technique for imaging film coating defects in the film-core interface and surface of coated tablets. *European journal of pharmaceuticals and biopharmaceutics: official journal of Arbeitsgemeinschaft für Pharmazeutische Verfahrenstechnik e.V*, 56(3), 381–8.
- Ruotsalainen, M., Heinämäki, J., Rantanen, J., & Yliruusi, J. (2002). Development of an automation system for a tablet coater. *AAPS PharmSciTech*, 3(2), E14. doi:10.1208/pt030214
- Sahni, E., & Chaudhuri, B. (2011). Experiments and numerical modeling to estimate the coating variability in a pan coater. *International journal of pharmaceuticals*, 418(2), 286–96. doi:10.1016/j.ijpharm.2011.05.041
- Sahni, E., & Chaudhuri, B. (2012). Experimental and modeling approaches in characterizing coating uniformity in a pan coater: a literature review.

- Pharmaceutical development and technology*, 17(2), 134–47.
doi:10.3109/10837450.2011.649852
- Sahni, E., Yau, R., & Chaudhuri, B. (2011). Understanding granular mixing to enhance coating performance in a pan coater: Experiments and simulations. *Powder Technology*, 205(1-3), 231–241. doi:10.1016/j.powtec.2010.09.019
- Sandadi, S., Pandey, P., & Turton, R. (2004). In situ, near real-time acquisition of particle motion in rotating pan coating equipment using imaging techniques. *Chemical Engineering Science*, 59(24), 5807–5817. doi:10.1016/j.ces.2004.06.036
- Schreiber, R., Vogt, C., Werther, J., & Brunner, G. (2002). Fluidized Bed Coating at Supercritical Fluid Conditions. *The Journal of Supercritical Fluids*, 24(2), 137–151.
- Shelukar, S., Ho, J., Zega, J., Roland, E., Yeh, N., Quiram, D., ... Reynolds, S. (2000). Identification and characterization of factors controlling tablet coating uniformity in a Wurster coating process. *Powder Technology*, 110(1-2), 29–36. doi:10.1016/S0032-5910(99)00265-X
- Shen, Y.-C. (2011). Terahertz pulsed spectroscopy and imaging for pharmaceutical applications: A review. *International Journal of Pharmaceutics, In Press*, -.
- Sherony, D. F. (1981). A model of surface renewal with application to fluid bed coating of particles. *Chemical Engineering Science*, 36(5), 845–848. doi:10.1016/0009-2509(81)85037-3
- Shi, D., & McCarthy, J. J. (2008). Numerical simulation of liquid transfer between particles. *Powder Technology*, 184(1), 64–75. doi:10.1016/j.powtec.2007.08.011
- Song, Y., & Turton, R. (2007). Study of the effect of liquid bridges on the dynamic behavior of two colliding tablets using DEM. *Powder Technology*, 178(2), 99–108. doi:10.1016/j.powtec.2007.04.010
- Song, Y., Turton, R., & Kayihan, F. (2006). Contact detection algorithms for DEM simulations of tablet-shaped particles. *Powder Technology*, 161(1), 32–40. doi:10.1016/j.powtec.2005.07.004
- Subramanian, G., Turton, R., Shelukar, S., & Flemmer, L. (2003). Effect of Tablet Deflectors in the Draft Tube of Fluidized/Spouted Bed Coaters. *Industrial & Engineering Chemistry Research*, 42(12), 2470–2478. doi:10.1021/ie020577k

- Sungkorn, R., & Khinast, J. G. (2010). Euler-Lagrange Modeling of Large-Scale Gas-Liquid Bubbly Flows.
- Suzzi, D., Radl, S., & Khinast, J. G. (2010). Local analysis of the tablet coating process: Impact of operation conditions on film quality. *Chem Eng Sci*, 65(21), 5699–5715. doi:10.1016/j.ces.2010.07.007
- Suzzi, D., Toschkoff, G., Radl, S., Machold, D., Fraser, S. D., Glasser, B. J., & Khinast, J. G. (2012). DEM simulation of continuous tablet coating: Effects of tablet shape and fill level on inter-tablet coating variability. *Chem Eng Sci*, 69(1), 107–121. doi:10.1016/j.ces.2011.10.009
- Terashita, K., Natsuyama, S., Nishimura, T., & Sakamoto, H. (2000). Design for Fluidized Bed with Draft Tube by DEM Analysis. *Journal of the Japan Society of Powder and Powder Metallurgy*, 42(12), 1306–1311.
- Teunou, E., & Poncelet, D. (2002). Batch and continuous fluid bed coating – review and state of the art. *Journal of Food Engineering*, 53(4), 325–340. doi:10.1016/S0260-8774(01)00173-X
- Thoma, K., & Bechtold, K. (1999). Influence of aqueous coatings on the stability of enteric coated pellets and tablets. *Eur J Pharm Biopharm*, 47(1), 39–50. doi:10.1016/S0939-6411(98)00086-1
- Tobiska, S., & Kleinebudde, P. (2003). Coating uniformity and coating efficiency in a Bohle Lab-Coater using oval tablets. *Eur J Pharm Biopharm*, 56(1), 3–9.
- Toschkoff, G., Just, S., Funke, A., Djuric, D., Knop, K., Kleinebudde, P., ... Khinast, J. G. (2013). Spray models for discrete element simulations of particle coating processes. *Chem Eng Sci*, 101, 603–614. doi:10.1016/j.ces.2013.06.051
- Toschkoff, G., & Khinast, J. G. (2013). Mathematical modeling of the coating process. *Int J Pharm*. doi:10.1016/j.ijpharm.2013.08.022
- Toschkoff, G., Suzzi, D., Tritthart, W., Reiter, F., Schlingmann, M., & Khinast, J. G. (2012). Detailed Analysis of Air Flow and Spray Loss in a Pharmaceutical Coating Process. *Aiche Journal*, 58(2), 399–411. doi:10.1002/aic.12681
- Tran-Cong, S., Gay, M., & Michaelides, E. E. (2004). Drag coefficients of irregularly shaped particles. *Powder Technology*, 139(1), 21–32. doi:10.1016/j.powtec.2003.10.002
- Tropea, C., Xu, T.-H., Onofri, F., Géhan, G., Haugen, P., & Stieglmeier, M. (1996). Dual-Mode Phase-Doppler Anemometer. *Particle & Particle Systems Characterization*, 13(2), 165–170. doi:10.1002/ppsc.19960130216

- Tsuji, Y. (2000). Activities in discrete particle simulation in Japan. *Powder Technology*, 113(3), 278–286.
- Turton, R. (2008). Challenges in the modeling and prediction of coating of pharmaceutical dosage forms. *Powder Technology*, 181(2), 186–194. doi:10.1016/j.powtec.2006.12.006
- Turton, R., & Cheng, X. X. (2005). The scale-up of spray coating processes for granular solids and tablets. *Powder Technology*, 150(2), 78–85. doi:10.1016/j.powtec.2004.11.021
- U. S. Pharmacopoeial Convention. (2011a). Monograph 711 Dissolution. In *United States Pharmacopoeia*.
- U. S. Pharmacopoeial Convention. (2011b). Monograph 905 Uniformity of Dosage Units. In *United States Pharmacopoeia* (35th ed.). Rockville.
- Varga, C. M., Lasheras, J. C., & Hopfinger, E. J. (2003). Initial breakup of a small-diameter liquid jet by a high-speed gas stream. *Journal of Fluid Mechanics*, 497, 405–434. doi:10.1017/S0022112003006724
- W. Chan, C., Seville, J. P. K., Parker, D. J., & Baeyens, J. (2010). Particle velocities and their residence time distribution in the riser of a CFB. *Powder Technology*, 203(2), 187–197. doi:10.1016/j.powtec.2010.05.008
- Waldie, B., & Wilkinson, D. (1986). Measurement of particle movement in a spouted bed using a new microprocessor based technique. *The Canadian Journal of Chemical Engineering*, 64(6), 944–949. doi:10.1002/cjce.5450640609
- Wang, J., Hemenway, J., Chen, W., Desai, D., Early, W., Paruchuri, S., ... Varia, S. (2012). An evaluation of process parameters to improve coating efficiency of an active tablet film-coating process. *International journal of pharmaceutics*, 427(2), 163–9. doi:10.1016/j.ijpharm.2012.01.033
- Wilcox, D. C. (1998). *Turbulence Modeling for CFD* (2nd ed.). DCW Industries La Canada, CA.
- Wnukowski, P., & Setterwall, F. (1989). The coating of particles in a fluidized bed (residence time distribution in a system of two coupled perfect mixers). *Chemical Engineering Science*, 44(3), 493–505. doi:10.1016/0009-2509(89)85027-4
- Wojtkowski, M. (2010). High-speed optical coherence tomography: basics and applications. *Appl Opt*, 49(16), D30–61.

- Wong, C. X., Daniel, M. C., & Rongong, J. a. (2009). Energy dissipation prediction of particle dampers. *Journal of Sound and Vibration*, 319(1-2), 91–118. doi:10.1016/j.jsv.2008.06.027
- Yamane, K., Sato, T., Tanaka, T., & Tsuji, Y. (1995). Computer simulation of tablet motion in coating drum. *Pharmaceutical research*, 12(9), 1264–8.
- Zaidi, S. H., Altunbas, A., & Azzopardi, B. J. (1998). A Comparative Study of Phase Doppler and Laser Diffraction Techniques to Investigate Drop Sizes in Annular Two-phase Flow. *Chemical Engineering Journal*, 71(2), 135–143.
- Zhong, S., Shen, Y.-C., Ho, L., May, R. K., Zeitler, J. A., Evans, M., ... Kleinebudde, P. (2011). Non-destructive quantification of pharmaceutical tablet coatings using terahertz pulsed imaging and optical coherence tomography. *Optics and Lasers in Engineering*, 49(3), 361–365. doi:10.1016/j.optlaseng.2010.11.003
- Zhou, Y. C., Xu, B. H., Yu, A. B., & Zulli, P. (2002). An experimental and numerical study of the angle of repose of coarse spheres. *Powder Technology*, 125(1), 45–54. doi:10.1016/S0032-5910(01)00520-4
- Zhou, Z. Y., Yu, A. B., Nakagawa, M., & Luding, S. (2009). Simulation of the Flow and Segregation of Particle Mixtures in Liquid Fluidization. In U. Twente & M. Colorado Sch (Eds.), *AIP Conference Proceedings* (Vol. 1145, pp. 993–996). Golden, CO: AIP. doi:10.1063/1.3180099
- Zhu, H. P. P., Zhou, Z. Y. Y., Yang, R. Y. Y., & Yu, A. B. B. (2008). Discrete particle simulation of particulate systems: A review of major applications and findings. *Chemical Engineering Science*, 63(23), 5728–5770. doi:10.1016/j.ces.2008.08.006

Chapter I: List of publications

I-1 Publications in Peer-reviewed journals

I-1.1 As main author

- Toschkoff, G., Just, S., Funke, A., Djuric, D., Knop, K., Kleinebudde, P., Scharrer, G., Khinast, J. G. (2013). Spray models for discrete element simulations of particle coating processes. *Chem Eng Sci*, *101*, 603–614.
- Toschkoff, G., Suzzi, D., Tritthart, W., Reiter, F., Schlingmann, M., & Khinast, J. G. (2012). Detailed Analysis of Air Flow and Spray Loss in a Pharmaceutical Coating Process. *Aiche Journal*, *58*(2), 399–411.
- Toschkoff, G., & Khinast, J. G. (2013). Mathematical modeling of the coating process. *Int J Pharm*.
- Toschkoff, G., Suzzi, D., Adam, S., & Khinast, J. G. (2012). Numerical simulation of tablet coating: First Steps Towards an in-silico Design Space. *Pharmaceutical Technology*, *36*(9), 52–55.
- Toschkoff, G., Schinwald, C., Markl, D., Koller, D. M., Scheideler, M., Leitner, M., & Khinast, J. G. (2013). Effect of Tablet Coating Parameters: Combining Non-Destructive Measurements and Dissolution Testing. *European Journal of Pharmaceutics and Biopharmaceutics*, *submitted*.
- Toschkoff, G., Just, S., Funke, A., Djuric, D., Knop, K., Kleinebudde, P., Scharrer, G., Khinast, J. G. (2014). Design-of-Experiment based DEM simulation of an active tablet coating process, *in preparation*.

I-1.2 As co-author

- Just, S., Toschkoff, G., Funke, A., Djuric, D., Scharrer, G., Khinast, J., ... Kleinebudde, P. (2013). Experimental analysis of tablet properties for discrete element modeling of an active coating process. *AAPS PharmSciTech*, *14*(1), 402–11.
- Just, S., Toschkoff, G., Funke, A., Djuric, D., Khinast, J. G., Knop, K., & Kleinebudde, P. (2013). Optimization of Inter-Tablet Coating Uniformity for an Active Coating Process at the Lab and Pilot Scale. *International Journal of Pharmaceutics*, *30*(11).
- Suzzi, D., Toschkoff, G., Radl, S., Machold, D., Fraser, S. D., Glasser, B. J., & Khinast, J. G. (2012). DEM simulation of continuous tablet coating: Effects of tablet shape and fill level on inter-tablet coating variability. *Chem Eng Sci*, *69*(1), 107–121.

Adam S., Suzzi D., Toschkoff G., Khinast J.G. (2011). Application of Advanced Simulation Tools for Establishing Process Design Spaces within the Quality-by-Design Framework. *Submitted as book chapter.*

I-2 Conference contributions

I-2.1 Oral presentation (main author)

Toschkoff G, Böhling P, Johnson D, Sun J, Silverman A, Scharrer G, Khinast JG, Rajniak P
Experimental and theoretical study of tablet flow in a lab scale pan coater AICHe 2013, San Francisco (USA)

Toschkoff G, Just S, Knop K, Kleinebudde P, Funke A, Djuric D, Scharrer G, Khinast JG
Application of DEM Simulations and Experimental Studies to Improve the Uniformity of An Active Coating Process AICHe 2013, San Francisco (USA)

Toschkoff, G.; Just, S.; Funke, A.; Djuric, D.; Knop, K.; Kleinebudde, P.; Scharrer, G.; Khinast, J.
Application of enhanced DEM simulations for the improvement of a tablet coating process. AICHe Meeting, Pittsburgh, 2012

Toschkoff, G.; Suzzi, D.; Just, S.; Knop, K.; Kleinebudde, P.; Altmeyer, A.; Khinast, J.:
Investigation of Tablet Coating Processes using Discrete Element Method Simulations. AICHe Annual Meeting, Minneapolis, 2011.

Toschkoff, G.; Suzzi, D.; Khinast, J.: A deeper understanding of tablet coating processes through Discrete Element Method simulations. EDEM User Conference 2011, Edinburgh.

Toschkoff, G.; Suzzi, D.; Adam, S.; Khinast, J.: Multi-Scale Simulation of Tablet Coating Processes. 8th European Congress of Chemical Engineering, Berlin, 2011

Toschkoff, G.; Suzzi, D.; Machold, D.; Radl, S.; Khinast, J.: Investigation of a Tablet Coating Processes using Multi-Model Simulation Approach. AICHe Annual Meeting, Salt Lake City, 2010.

I-2.2 Oral presentation (co-author)

Suzzi, D.; Toschkoff, G.; Hörmann, T.; Schaffer, M.; Machold, D.; Radeke, C.; Khinast, J.
SIMNET days 2010, Graz (A) Modeling and Simulation of Complex Multiphase Flows in the Pharmaceutical Industry 2010

Suzzi, D., Toschkoff, G., Tritthart, W., Reiter, F., Radl, S., Khinast, J. Detailed Numerical Simulations of Tablet Coating Processes, PBP World Meeting, Valletta (MT), 2010

Suzzi, D., Toschkoff, G., Hörmann, T., Radl, S., Radeke, C., Eitzlmayr, A., Machold, D., Khinast, J. Multiphase Simulation in the Pharmaceutical Industry 11th ERCOFTAC Alpe Danube Adria PC Meeting, Graz (A) 2010

- Suzzi, D., Radl, S., Toschkoff, G., Adam, S., Radeke, C., Koller D., Khinast, J. Numerical Simulation of Pharmaceutical Production Processes: towards Model Predictive Control (MPC) and QbD-based Simulation Design Space EuPAT4 - Fourth pan-European Science Conference on Process Analytical Technology, Kuopio (FI) 2010
- Suzzi, D.; Toschkoff, G.; Adam, S.; Radl, S.; Khinast, J. Development of a QbD-based Simulation Design Space for Online PAT Control of Spray Coating Processes EuPAT4 - Fourth pan-European Science Conference on Process Analytical Technology, Kuopio (FI) 2010
- Suzzi, D.; Toschkoff, G.; Machold, D; Radl, S.; Khinast, J. Combined Numerical Method for Multi-Scale Analysis of Tablet Coating Processes CESPT 2010, Graz (A) 2010
- Adam, S., Suzzi, D., Radl, S. Toschkoff, G., Hörmann, T., Khinast, J. Quality-by-Design Based Characterization of Pharmaceutical Processes by Means of Numerical Simulations CESPT 2010, Graz (A) 2010
- Heigl, N.; Hörl, G.; Koller, D.; Toschkoff, G.; Fraser, S.D.; Khinast, J. Raman Chemical Mapping vs. NIR Spectroscopy for Assessing the API Distribution and Coating Thickness of Tablets AIChE 2010, Salt Lake City (USA) 2010
- Suzzi, D.; Adam, S.; Iannuccelli, M.; Toschkoff, G.; Radeke, C.; Khinast, J. G. Use of Computer Simulations as Process Characterization Tool for Generation of Mechanistic Process Understanding within the Quality by Design Environment 2nd European Conference on Process Analytics and Control Technology (EuroPact 2011), Glasgow (UK) 2011

I-2.3 Poster Presentation (main author)

- Toschkoff, G.; Suzzi, D.; Tritthart, W Reiter, F.; Fraser, S.D.; Khinast, J. . Computational Analysis and Experimental Evaluation of a Drum Coating Process International Congress for Pharmaceutical Engineering, Graz (A) 2009
- Toschkoff G.; Suzzi D.; Just S.; Khinast J. Optimization of Tablet Coating Processes using Discrete Element Method Simulations 5th International Congress for Pharmaceutical Engineering, Graz (A) 2011
- Toschkoff, G.; Just, S.; Funke, A.; Djuric, D.; Knop, K.; Kleinebudde, P.; Scharrer, G.; Khinast, J.: Application of DEM spray models for the optimization of tablet coating processes. CHISA , Prague, 2012
- Toschkoff, G.; Suzzi, D.; Khinast, J. GL Pharma. Schlingmann, M.; GL Pharma: Reiter, F.; GL Pharma: Tritthart, W. Numerical simulation of film formation in tablet coating CESPT 2010, Graz (A) 2010

Toschkoff G, Just S, Scharrer G, Knop K, Kleinebudde P, Djuric D, Altmeyer A, Funke A, Khinast J DoE investigation of tablet coating simulations using the Discrete Element Method: uniformity improvement JG PARTEC 2013, Nuremberg (DE)

I-2.4 Poster presentation (co-author)

Schinwald C.; Toschkoff G.; Koller D.; Khinast J. DoE Investigation of Tablet Coating using Non-invasive Methods and Dissolution Testing 5th International Congress for Pharmaceutical Engineering, Graz (A) 2011

Just S, Toschkoff G, Funke A, Djuric D, Scharrer G, Khinast JG, Knop K, Kleinebudde P Optimization of Inter-Tablet Coating Uniformity in an Active Coating Process 6th International Symposium on Solid Oral Dosage Forms, Malmö (SE)

Just S, Toschkoff G, Funke A, Djuric D, Scharrer G, Khinast JG, Knop K, Kleinebudde P Optimization of Inter-Tablet Coating Uniformity in an Active Coating Process AAPS Annual Meeting 2012, Chicago (USA)

Just S, Toschkoff G, Funke A, Djuric D, Scharrer G, Khinast J, Knop K, Kleinebudde P Der dynamische Böschungswinkel zur Bestimmung von Reibungskoeffizienten für DEM Simulationen von Überzugsprozessen Jahrestreffen der Fachgruppen Agglomerations- und Schüttguttechnik, Weimar (DE)

Just S, Toschkoff G, Funke A, Djuric D, Khinast JG, Knop K, Kleinebudde P Optimization of Inter-Tablet Coating Uniformity in an Active Coating Process Polish-German Symposium on Pharmaceutical Sciences, Danzig (PL)

Chapter J: List of figures and tables

J-1 Figure captions

Figure 1: Schematic description of the representation of coating in a simplified statistical model based on consecutive single tablet coating and mixing. _____	23
Figure 2: Decrease of the coefficient of variation of coating time over time, gathered from statistical simulations. (a): whole time range, (b): Detail showing the first 28 coating events. _____	24
Figure 3: Increase of the standard deviation of coating mass over time, gathered from statistical simulations. A: whole time range, b: Detail showing the first 28 coating events. _____	25
Figure 4 _____	25
Figure 5: General principle of a particle coating process. This cycle (Coating in the spray zone – transportation and drying - re-enter the spray) appears in most types of coating apparatus. Modified from (Turton, 2008). _____	28
Figure 6: Schematic representation of a typical drum coating apparatus. Modified from (Turton and Cheng, 2005) _____	29
Figure 7: Schematic representation of a top spray fluid bed granulator or coater. Modified from (Teunou & Poncelet, 2002) _____	31
Figure 8: Different forms of fluid bed coating: (a) top spray or granulator, (b) bottom spray, (c) “Wurster” type, (d) side spray with rotating disk. From (Teunou & Poncelet, 2002) _____	32
Figure 9: Schematic explanation of the dependence of the total coefficient of variation on the distribution of cycle time and coating per pass. After (Turton, 2008). _____	37
Figure 10: Deposition model of impacting droplets: critical curve. From (Suzzi et al., 2010) _____	44
Figure 11: Relationship of the tablet orientation indices predicted based on the DEM data and the tablet sphericity (a) or aspect ratio (b). Taken from (Ketterhagen, 2011). _____	58
Figure 12: Schematic representation of a coating process in a drum coater. A tablet emerging on the top enters the spray zone and the drying air zone before re-entering the bed. _____	73
Figure 13: Picture of the experimental setup, showing the spray gun on the right and the receiver unit at the bottom. The laser beams are entering from the left, the beam crossing area (measurement zone) can be seen at position -40. _____	76
Figure 14: Three-dimensional graphic of the back half of the coating drum. The cylinder along the rotation axis in the middle holds the air inlet and outlet. The tablet bed is approximated by a moving (straight) wall at the lower left. _____	77
Figure 15: Ohnesorge number Oh as a function of Reynolds number Re . The splashing region and the deposition region are separated by the critical splashing curve. _____	85
Figure 16: Number-weighted spray droplet size distribution in μm , as a mean of all positions in the PDA spray measurement at a distance of 20 cm. _____	86
Figure 17: Number-weighted distribution of spray droplet velocities for experimental measurements (o) and CFD simulation (x). By increasing droplet starting velocity, the lack of atomizing air flow was compensated such that the curves show good agreement. _____	87

Figure 18: Location of the cut planes for the generation of two-dimensional plots inside the coater. _____	88
Figure 19: Air velocity for a cross-section through the location of the spray nozzle, perpendicular to the rotational axis. Streamlines are drawn in black. _____	89
Figure 20: Vector plot of the air flow velocity inside cut plane B. _____	90
Figure 21: Vector plot of the air flow velocity inside cut plane C. _____	90
Figure 22: Vector plot of the air flow velocity inside cut plane D. _____	91
Figure 23: Mass fraction of water inside the coater. _____	92
Figure 24: Average mass fraction of water in the coater as a function of time. _____	93
Figure 25: Spray after 0.4 seconds. The color of the spray droplets show the amount of water, ranging from the starting concentration of 0.8 (red) to 0 (blue). The droplet size is proportional to the water content as well. Additionally, the air flow velocity is shown as a vector plot. _____	94
Figure 26: Variation of position and angle of the spray gun in the coating drum. Left: B denotes the standard position, 3-5 are variations translated parallel to the tablet bed. Right: Case 1 and 2 are a variation of the angle for basis position. _____	95
Figure 27: Total mass of the spray droplets leaving with the outlet air, relative to total introduced mass. _____	96
Figure 28: Total mass of spray droplets that hit a wall other than the tablet bed, relative to total introduced mass. _____	96
Figure 29: Wall film thickness on the coater wall, from no film (white) to a thickness above one micrometer (black). It can be seen that apart from the tablet bed, film liquid is also deposited on the rotating wall near the tablet bed top and the middle cylinder. _____	97
Figure 30: Laboratory coating apparatus, consisting of a coating pan, supply and exhaust air tubing, an atomization nozzle, a peristaltic pump, a coating suspension container and a control unit. _____	106
Figure 31: Two-dimensional OCT image of a film-coated tablet. Optical image dimensions (in air): 2 x 1 mm ² . _____	111
Figure 32: Score plot of the first and second principal components of the NIR spectra. The ellipse exemplarily indicates the clustering of batch B01. The values in parentheses of the PC 1 and PC 2 label state the percentage of total variance explained by each principal component. As example, batch 01 is highlighted by an ellipse. _____	114
Figure 33: Score plot of the first and second principal components of the NIR spectra for the stress-tested tablets. The values in parentheses of the PC 1 and PC 2 label state the percentage of total variance explained by each principal component. _____	115
Figure 34: Film coating thickness for the different batches, determined with a micrometer screw gauge. _____	117
Figure 35: Film coating thickness determined manually and automatically from OCT images. _____	118
Figure 36: Film coating thickness as determined based on OCT images (semi-manual evaluation) and “direct” length measurement (micrometer gauge). _____	119
Figure 37: Three-dimensional image of the region with the missing coating from batch B08. Optical image dimension (in air): 6 x 0.5 x 2.5 mm ³ . _____	120
Figure 38: Dissolution performance in 0.1 M polar hydrochloric acid of pH = 1 (gastric) and phosphate buffer of pH = 6.8 (intestinal). _____	121

Figure 39: Film coating “thickness” (in fact a measure of total thickness, see text) on the caps for tablets from different batches determined with micrometer gauge before and after the disintegration test. _____	122
Figure 40: Film coating “thickness” (in fact a measure of total thickness, see text) on the band for tablets from different batches determined with micrometer gauge before and after the disintegration test. _____	122
Figure 41: Film coating thickness determined from OCT images before and after the disintegration test. _____	123
Figure 42: Weight of tablets before and after the disintegration test. _____	123
Figure 43: Release performance of the tablets used for the disintegration tested. _____	124
Figure 44: Geometry of the Bohle coating drum used for the investigation of spray modules. From left: front view, side view, and a perspective view. _____	131
Figure 45: Size and position of the spray zone shown in a top view of the coater. _____	132
Figure 46: Schematic of the spray zone, showing the points and vectors governing the zone detection. _____	134
Figure 47: Schematic of the top detection by introducing a plane and dividing it into a detection grid. _____	136
Figure 48: Influence of the grid spacing on the top detection algorithm for (a) wide and (b) narrow spacing. The filled circles denote particles that would be detected as being on the top of the tablet bed. _____	137
Figure 49: DEM simulation of a tablet coating process, including the coating spray. The spray droplets are colored blue, with darker shades indicating bigger droplets. The tablets are colored according to coating mass, from white (no coating mass) to red (high coating mass). _____	139
Figure 50: Drop diameter distribution from which sizes for the non-uniform case were sampled. _____	141
Figure 51: Spray pattern for different exponents of the radial sampling: 0.3 (left), 0.5 (middle, uniform) and 0.7 (right). _____	142
Figure 52: Principle of the ray-tracing method. The blue dots are the center positions of tablets as read in from the DEM simulation output. Tablets that are hit by a ray are colored red. _____	143
Figure 53: RSD and the amount of zero residence time tablets at the end of the simulated period for the investigated cases for the spray zone method. _____	147
Figure 54: Comparison of the coating mass distribution for different settings of the relative grid spacing $\Delta_{g,rel}$. The result for the discrete drop method (case 4) is shown as reference (dashed line). Zero-coating mass data were omitted. _____	148
Figure 55: Relative standard deviation of coating as a function of top detection grid spacing. _____	149
Figure 56: Comparison between the coating mass distribution with and without top detection (case 2 vs. 5). _____	150
Figure 57: RSD and the amount of zero-mass at the end of the coating process for the discrete drop method. _____	151
Figure 58: Influence of the number of drops per introduction step on the coating mass distribution _____	152
Figure 59: Influence of the drop introduction interval on the coating mass distribution. _____	153

Figure 60: Relative standard deviation (left axis, filled symbols) and relative amount of zero mass particles (right axis, empty symbols) as a function of the drop number per time.	153
Figure 61: Influence of the spray cross-sectional area uniformity on the coating mass distribution.	155
Figure 62: Comparison of the coating mass distribution for uniform and non-uniform drop size distributions (Cases 4 and 10 in Table 5, respectively)	156
Figure 63: Relative standard deviation as a function of the number of rays.	157
Figure 64: Coating mass distribution gathered after the DEM simulation using the ray-tracing method.	157
Figure 65: The number of visits to the spray zone for the total simulation time.	158
Figure 66: Histogram of the Single Visit Residence Time of all visits to the spray zone.	159
Figure 67: Comparison of the coating mass for the base settings of all three spray modules.	160
Figure 68: Coating drum geometry as used in the simulations, filled with 3.5 kg of tablets. (The front of the drum was covered by a non-rotating wall which is not shown here.)	167
Figure 69: Top view and side view of the tablet created using the glued sphere approach. The bi-convex shape of the actual tablet is shown by the wire mesh and the black outline.	168
Figure 70: Position and shape of the spray zones in the coating drum (view from top, normal to the tablet bed surface). Note that the four-nozzle setup is drawn lower for clarity; its actual vertical position is the same as for the two-nozzle setup.	169
Figure 71: Decrease of the coefficient of variation of coating mass over time. The four highest curves correspond to a process using two nozzles, the four lowest ones to four nozzles. The line shows the slope predicted by analytical models according to Eq.(74).	175
Figure 72: Centered and scaled coefficient plot of the statistical model.	176
Figure 73: „4D“ contour plot, showing the influence of number of nozzles, spray rate (g/min), rotation speed and fill level on the coefficient of variation of coating mass (CoV). In each of the 9 subplots, the abscissa is rotation speed (rpm), the ordinate is fill level (kg).	178
Figure 74: Distribution of the coating mass gathered over all tablets for different simulation runs.	179
Figure 75: Distribution of spray residence times of a single visit, gathered from all complete spray events for all tablets in the simulation time span.	181
Figure 76: Distribution of bed residence time (time between single spray events of one tablet), gathered from all complete spray events for all tablets in the simulation time span. Top: unscaled plot, bottom: semi-logarithmic, dimensionless plot (please refer to the text for details).	182
Figure 77: Comparison of results directly from the DEM simulation, and indirectly using the analytic expression Eq. (77) with and without very high values for the cycle time. The naming scheme of cases is as follows: Fill level (kg) – Rotation speed (rpm) – Number of nozzles.	184
Figure 78: Comparison of the uniformity for each nozzle and total, for cases using the two-nozzle setup. Nozzle numbering starts at the drum opening (i.e., “Nozzle 1” is closest to the front). The naming scheme of the cases is “fill level (kg) – rotation speed (rpm)”.	186
Figure 79: Comparison of the uniformity for each nozzle and total, for cases using the four-nozzle setup. Nozzle numbering starts at the drum opening (i.e., “N1” is the nozzle closest to the front). The naming scheme of the cases is “fill level (kg) – rotation speed (rpm)”.	187

J-2 Table captions

Table 1: Development of the number of simulated particles and the particle shapes in DEM simulations over the recent years for selected references. _____	50
Table 8: Parameters defining the coating process. _____	73
Table 2: Experimental plan showing the parameter settings used for the coating runs. The numbers in brackets indicate the level, i.e., whether the setting is considered high (1), low (-1) or base (0). _____	107
Table 3: Weight of tablet batches _____	116
Table 4 Parameters for the DEM simulation. _____	131
Table 5: Settings for the spray zone approach for the different simulation runs. _____	145
Table 6: Settings for the Discrete Drop method for the different simulation runs. _____	145
Table 7: Settings for the different cases using the post-processing ray-tracing method. _____	146
Table 9: _____	170
Table 10: Statistical design of simulation runs for uncoated tablets. For the sake of completeness, the last two columns already contain the results of the runs; a detailed description is given in the results section. _____	173
Table 11: Statistical design of simulation runs for coated tablets. For the sake of completeness, the last two columns already contain the results of the runs; a detailed description is given in the results section. _____	174

Acknowledgements

First of all, I would like to thank my supervisor, Prof. Johannes G. Khinast, who has not only provided scientific guidance during my first academic steps, but is also a personal inspiration.

My thanks go to all my colleagues both at the RCPE and the IPPT, please excuse that I cannot list you all. It seems impossible that such an enjoyable and most optimal surrounding still counts as “being at work”. I would like to give special thanks to Dr. Daniele Suzzi, who helped me during my first steps in this field that was new in many respects, and to Dipl.-Ing. Georg Scharrer, who has motivated both by being the person he is, and by forging an awesome modeling & simulation team. Further, I would like to thank all persons involved in the projects that I and with me this thesis was part of for the pleasant and fruitful collaboration.

My deepest gratitude goes to my parents, who have supported and encouraged me throughout my life, giving me both roots and wings.

The last spot is reserved for the person that holds it all together, without her nothing would fit together. My eternal love goes to Kathrin Toschkoff, who had to endure me throughout this work with its ups and downs, but amazingly even married me in the middle of it.

This work was funded through the Austrian COMET Program by the Austrian Federal Ministry of Transport, Innovation and Technology (BMVIT), the Austrian Federal Ministry of Economy, Family and Youth (BMWFJ) and by the State of Styria (Styrian Funding Agency SFG)